Human T cell responses to bone regenerating biomaterials

Jessica Roberts BSc (Hons), MBBS, MRCS

A thesis submitted in fulfilment of the requirements of the University of Glasgow for the degree of Doctor of Philosophy

School of Infection & Immunology
College of Medical, Veterinary and Life Sciences
University of Glasgow

February 2025

Engineering and Physical Sciences Research Council
eTIME Engineering Underpinning Medicine
BlondMcIndoe RESEARCH FOUNDATION
Canniesburn PLASTIC SURGERY UNIT

Abstract

Enhanced bone healing and bone provision are fundamental therapeutic orthoplastic strategies for complex fracture management, and for post-oncological or traumatic composite wounds with critical bone loss. Such surgery remains highly challenging and potentially morbid, such that synthetic bone provision would have particular appeal. It could also be indicated to enhance prosthetic fitment after blast injury, and for restoration after digit or limb loss or congenital absence.

Regenerative medicine aims to improve the body's inherent regenerative capacity after injury, or to replace damaged or lost tissues with fully functional, engineered ones, to address unmet clinical need. Bone requires both scaffold and cellular therapy options. Bioengineered tissues come in many forms, with allogenic mesenchymal stem cell (MSC) based biomaterials achieving successful osteogenesis *in vitro,* and in animal models *in vivo*.

Despite these advances, the T cell immune reactivity of a human host towards bone biomaterials remains unknown yet may present a critical barrier to the clinical translation of these promising therapies. Ethical investigation has been precluded through lack of a human *in vitro* model. Here, a novel, human, multicellular, *in vitro*, T cell response model was established. Host responses to osseoreconstructive fibronectin and laminin MSC biomaterials were defined across their differentiation into osteoblasts, for the first time. Subsequent, T cell responses to engineered immunomodulation of the allogenic biomaterial were examined.

These data demonstrate successful *in vitro* T cell modelling. MSC biomaterials triggered human T cell activation responses that increased with osteogenic differentiation. These responses were mixed encompassing regulatory, Thelper (Th) 1 and Th17 associated responses that were detectable by 5 days *in vitro*. Furthermore, manipulation of the biomaterial glycoprotein did not change the surface activation marker expression of T cells but revealed differences in the cytokine response. Less osteogenic differentiation of MSCs occurred on laminin biomaterials, highlighting the importance of fibronectin for functional presentation of bone morphogenic protein 2 (BMP-2) to guide successful osteogenesis. Finally, manipulation of the immune microenvironment, towards pro-inflammation, appeared to reduce the viability of the allogenic MSCs within the biomaterial, which may have consequences for biomaterial engraftment, longevity and function *in vivo*.

Table of Contents

List of Abbreviations

aCD	Anti-cluster of differentiation
ACTH	Adrenocorticotropic hormone
ALP	Alkaline phosphatase
a-MSH	Alpha melanocyte-stimulating hormone
APCs	Antigen presenting cells
BCA-1	B cell attracting chemokine 1
BMPs	Bone morphogenic proteins
BMDMs	Bone marrow-derived macrophages
C3	Complement protein 3
CAR T	Chimeric antigen receptor T-cell
CCL17	C-C Motif Chemokine Ligand 17
CCR4	C-C chemokine receptor type 4
CD	Cluster of differentiation
CO_2	Carbon dioxide
CTLA-4	Cytotoxic T lymphocyte associated protein 4
CCR	Chemokine receptor
CXCL	C-X-C motif ligand
D3	Day 3
D28	Day 28
D35	Day 35
D	Diversity region
DAMPs	Damage-associated molecular patterns
DCs	Dendritic cells
DKK1	Dickkopf-1
DMEM	Dulbecco's Modified Eagle Medium
DMSO	Dimethyl sulfoxide
DN	Double negative
DP	Double positive
E	Young’s modulus
ECM	Extra-cellular matrix
EDC/NHS	1-ethyl-3-(3-dimethylaminopropyl)-carbodiimide/N-hydroxysuccinimide
EDTA	Ethylenediaminetetraacetic acid
EGF	Epidermal growth factor

ELISA	Enzyme-linked immunosorbent assay
ETP	Early thymic progenitor
FACS	Flow cytometry staining buffer
FBR	Foreign body response
FDA	Food and Drug Administration
FGF	Fibroblast growth factor
FLT-3L	FMS-like tyrosine kinase 3 ligand
FN	Fibronectin
FOXP3	Forkhead box protein P3
GAG	Glycosaminoglycans
GATA	GATA binding protein
G-CSF	Granulocyte-colony stimulating factor
GelMA	Gelatin methacryloyl
GF	Growth factor
GM-CSF	Granulocyte-macrophage colony-stimulating factor
GvHD	Graft versus host disease
H	Histamine receptor
HMGB1	High mobility group box 1
ICOS	Inducible co-stimulator
IF	Immunofluorescence
IFN	Interferon
Ig	Immunoglobulin
IL	Interleukin
ILCs	Innate lymphoid cells
iNOS	Inducible nitric oxide synthase
J	Joining region
KIT^{hi}	Kit-high
KO	Knockout
LT-α	Lymphotoxin alpha
MFI	Mean fluorescent intensity
MHC	Major histocompatibility class
MHRA	Medicines and Healthcare products Regulatory Agency
MMPs	Matrix metalloproteinases
MSCs	Mesenchymal stem cells
MW	Molecular weight
NK	Natural killer
NKT	Natural killer T cells

iNOS	Inducible nitric oxide synthase
LPS	Liposaccharide
MSCs	Mesenchymal stem cells
NF-κB	Nuclear factor-kappa B
NLRs	Nod-like receptors
+ Obs	With osteoblasts
OCN	Osteocalcin
OPG	Osteoprotegerin
OPN	Osteopontin
OSM	Oncostatin-M
P	Passage
PA	Polyacrylamide
PAMPs	Pathogen-associated molecular patterns
PBMCs	Peripheral blood mononuclear cells
PBS	Phosphate-buffered saline
PD1	Programmed cell death protein 1
PDGF	Platelet-derived growth factor
PEA	Poly(ethyl) acrylate
PEG	Polyethylene glycol
PEGDA	Polyethylene glycol acrylate derivatised
PEGDAA	Polyethylene glycol Diacrylate
PEO	Polyethylene oxide
PFA	Paraformaldehyde
PGLA	Polylactic-co-glycolic acid
PMNs	Polymorphonuclear leukocytes
PRRs	Pattern recognition receptors
PTH	Parathyroid hormone
qPCR	Quantitative polymerase chain reaction
RANK	Receptor activator of NF-κB
RANKL	Receptor activator of NF-κB ligand
RGD	Arginylglycylaspartic acid
RORγt	RAR-related orphan receptor gamma type receptor
RPMI	Roswell Park Memorial Institute media
RUNX2	Runt-related transcription factor 2
sCD	Soluble Cluster of Differentiation
sFas	Soluble Fas
SOST	Sclerostin

T-bet	T-box transcription factor TBX21
TCF	T cell factor
TCR	T cell receptor
TGF	Transforming growth factor
Th	T effector type
Tc	T cytotoxic type
TLRs	Toll-like receptors
TNF	Tumour necrosis factor
Tregs	Regulatory T cells
tTregs	Thymic T regulatory cells
TSLP	Thymic stromal lymphopoietin
UV	Ultraviolet
V	Variable region
VEGF	Vascular endothelial growth factor
2D	Two dimensional
3D	Three dimensional

List of Figures

Chapter 1 Figures

Chapter 2 Figures

Chapter 3 Figures

Chapter 4 Figures

Chapter 5 Figures

List of Tables

Acknowledgements

I would like to firstly acknowledge the unwavering support of my husband, Rob. Thank you for keeping me fed and watered with both sustenance and support. Appropriate fuelling and encouragement were required to survive 3 years of 50% research, 50% clinical practice with on calls throughout and weekends in the lab. Never has anyone labelled as part time, worked 100hr weeks so frequently. I'm grateful for the confidence when I had none, the belief in my capabilities and the 'can do' attitude you have on my behalf for every task I set out to achieve. There were many obstacles to completing this PhD and you championed each and every one, pausing my clinical career, application for grants, fellowships and subsequent national selection for Plastic Surgery higher training.

To my family, Mum, Dad, Frankie and Sam. Thank you for listening to my complaints, frustrations, the PhD highs and lows. Thank you for sending gifts, care packages, cards and the occasional pep talk text message. Thank you for celebrating my successes and being an ear for my failures. To my friends, I am grateful for the distractions and for the years of friendship, 4 of which you have endured with my PhD and my inability to switch off. I look forward to rediscovering my life, personality and hobbies.

To my supervisors Megan, Manuel and Andy. Thank you for your guidance, mentorship and support over the years. To Megan, thank you for your patience with my terrible maths, my initial trials and tribulations at flow cytometry and for being a hands-on supervisor who was always available to sound-board science and trouble shoot problems. Thank you for welcoming me into your lab and for helping me to navigate my way from clinician to academic with all the challenges

that brought. To the MacLeod lab and LIVE lab groups, thank you for the laughs, the jokes, the trips, the meals and the pints. To Manuel, thank you to the Salmeron-Sanchez group for all your support and guidance, especially in the final year of my PhD. It was lovely to be a small part of CeMi for the year. To Andy you have been my colleague and academic mentor for 6 years already and long do I hope that guidance continues. Thank you for having faith in me and my abilities beyond what I feel is ever reasonable, we will never agree that I am worthy of the support, but I appreciate it nonetheless. Thank you for pushing me, encouraging me to aim higher and being such a good role model both personally and professionally. I aspire to live up to your expectations and hope to pay forward your mentorship in future to support others as you have me.

Finally, I'd like to acknowledge my own hard work. I sacrificed a lot to undertake and then complete this PhD. I delayed career and spent 4 years of my life either in a hospital or in a lab, with not much life in-between. There were times I never thought finishing would be possible due to the need for full time research time and funding, I am proud of myself for securing the Blond McIndoe Fellowship and completing this PhD thesis for submission. I've had many lows and highs throughout and look forward to looking back on this experience fondly. I'd like to acknowledge being proud of myself for future referential purposes.

Author’s Declaration

All experiments are the work of the author unless specifically stated otherwise.

Jessica Roberts
BSc (Hons), MBBS, MRCS
University of Glasgow
November 2024

Chapter 1 Introduction

1.1 The unmet clinical need

The primary challenge for reconstructive surgeons is that of tissue loss and the desire to restore both form and function. Whilst autologous tissues have for some time been used for the reconstruction of lost tissues, surgeons are limited by a lack of available donor tissue options for larger defects (1-3). Regenerative medicine was born out of the need to combat this problem, aiming to improve the body's inherent regenerative capacity after an injury or to replace damaged tissues with fully functional, reproducible engineered ones (4). Since its beginnings, tissue engineering has sought to combine the ingenuity of an engineering approach, with advances in other disciplines, including stem cell biology, materials science and medicine, to drive the development of scaffolds and other biomaterials to address this unmet need (5).

Bioengineered tissues can come in many forms and historically are comprised of scaffolds, cells and biochemical cues (4, 6). The scaffolds provide both the physical support in a 3D structure onto which the cells adhere, whilst also providing a safe place to proliferate and secrete extracellular matrix (ECM) to rebuild the desired tissue (4, 6). Endogenous cells are recruited from the local environment or migrate into the scaffold from distant sites. Exogenous cells are either expanded in culture and redelivered back to the patient as autologous cells, or they are harvested from healthy donors as allogenic cells. The scaffolds provide an opportunity for the incorporation of biochemical cues that can enhance cellular function, tissue production and potentially modulate a more favourable immune response.

Modern biomaterials have included the use of 3D scaffolds with the application of polymers as hydrogels, metals and ceramics to augment, repair or replace damaged, diseased or lost tissues. Advances in this field have revolutionised surgical practices with orthopaedic joint replacements, vascular grafts, bone fixation and use of skin substitutes (5, 7, 8). Due to the ever-increasing demands for smarter and more creative healthcare solutions, the potential clinical applicability of modern biomaterials has been propelled into the more recent research space (6). Recent developments have focussed on the optimisation of the biomaterial delivery system used, aiming for robust, scalable and reliable constructs that are also safe, sterile and cost-efficient.

Current limitations with progress in the use of biomaterials are centred on vascularisation and host tissue integration (9). A cornerstone for the applicability and clinical translatability of bioengineered tissues will be developing a thorough understanding of the interplay between the biomaterial and the host immune system. Scaffolds, despite a lack of cellular components, are not immunologically inert and activate a foreign body response (FBR) soon after implantation, resulting in the formation of granulation tissue (4). Extensive in *vivo* animal studies have shown promise for biomaterial applications in regenerative medicine; however, obstacles persist with translation and applicability to humans (10-13).

Furthermore, the landscape of pre-clinical trials testing is changing. In the United States, the testing of drug candidates on non-relevant animals is no longer a requirement for United States Food and Drug Association (FDA) approval since the FDA Modernization Act 2.0 in 2022 (14). Non-animal-based models, such as *in vitro* humanised studies, are to be increasingly utilised in pre-clinical trial phase testing, establishing a paradigm shift for regulators and researchers within the industry. Biomaterials are classed as medical devices which covet a $457 billion

industry(15). Within the United Kingdom, biomaterials currently reside within the umbrella of the Medicines and Healthcare products Regulatory Agency (MHRA), for whom pre-clinical trial safety and efficacy studies using animal models are still required (16). Historically, immune response testing has relied heavily upon *in vivo* mouse models due to the interconnected nature and complexity of the immune system (17-20). With increasingly complex, cellularised and functional biomaterials, the regulation of such and need for pre-clinical trial human data is of paramount importance to ensure only the most suitable biomaterials translate to clinical trial.

Despite advances defining the innate immune response to biomaterials, a clear understanding of the adaptive immune reactivity of the human host against biomaterials remains elusive (9, 21-29). Defining the role of the adaptive human immune system and its interplay with biomaterials is crucial for tolerance, incorporation, and clinical utility.

1.2 Bone Injury

Trauma to bone can result in a bone fracture, with or without bone loss. In 2019 the Lancet reported a global incidence of 178 million fractures with 25.8 million years lived with disability as a result of a fracture over a 29-year period (30). Worldwide, lower limb fractures are both the most common and the most burdensome (30). The study furthermore evidenced that delayed or non-union rates were highest for lower limb fractures and contributed to the longest duration of years lived with disability (30). For unstable or displaced fractures and in cases of unstable non-union, operative management is required. For unstable or displaced fractures, operative management involves reduction followed by either internal or external fixation to stabilise the fracture using metalwork such as pins, plates, screws or combination approaches.

1.2.1 Fracture healing

After a bone breaks the process of fracture healing consists of haematoma formation, granulation tissue formation, bony callus formation and finally, bone remodelling. The mechanical stability and strain at the fracture site will govern the mode of fracture healing (31). Primary bone healing occurs with mechanical strain below 2% and is dictated by intramembranous bone healing through Haversian remodelling (32). Secondary bone healing occurs when a strain exceeds 2% but is less than 10% and occurs by endochondral bone healing (33). Bone healing can occur through a mixture of primary or secondary healing and strains >10% usually result in a non-union or delayed healing malunion of bone (32, 34).

1.2.1.1 Haematoma formation

Fracture haematoma formation occurs immediately after injury due to the disruption of blood vessels within the fracture environment forming a haematoma. The fracture haematoma is rich in haematopoietic cells and the clots form a temporary framework for subsequent healing. Mesenchymal stem cells (MSCs) are recruited to the site and express matrix metalloproteinases (MMPs) to influence the further migration of MSCs (35-37). As part of recruitment of haematopoietic cells, macrophages, neutrophils and platelets release TNFα, bone morphogenic proteins (BMPs) and vascular endothelial growth factor (VEGF), platelet-derived growth factor (PDGF) and various interleukins known to stimulate various key mechanism for healing at the fracture site (38).

1.2.1.2 Granulation tissue formation

Within 2 weeks the formation of primary or fibrocartilaginous callus provides provisional stability at the fracture site. Platelets recruited secrete fibronectin and PDGF triggering local immune responses to recruit further immune cells (38).

Fibroblasts and epithelial cells will lay down fibrin-rich granulation tissue and VEGF begins to support angiogenesis (39).

1.2.1.3 Bony callus formation

If the bone ends are in contact, then the endosteum and periosteum source periosteum-derived fibroblasts which play a pivotal role in secretion of matrix components needed for bone callus formation. These include collagen, elastin, glycoproteins and mesh fibres (40). If the bone ends are not in contact, in the context of a bone gap then a soft bridging callus forms (38). Ultimately, fibroblasts differentiate into osteoblasts under the direction of BMPs and fibroblast growth factors (FGFs) at the fracture site (41, 42). This leads to increased alkaline phosphatase (ALP), total calcium and osteogenic marker genes such as runt-related transcription factor 2 (RUNX2) and osteoblast-associated transcription factors and associated proteins; osteopontin (OPN) and osteocalcin (OCN) (43).

1.2.1.4 Bone remodelling

This process continues from months to years after clinical fracture union and involves complex signalling pathways and a balance of osteogenesis and resorption processes (38). Osteoclasts can resorb bone matrix however their differentiation and activity are coordinated by osteoblasts, whose primary job is new bone formation (44, 45). Osteoblasts produce osteoprotegerin (OPG) and express the receptor activator of nuclear factor-B ligand (RANKL) (46, 47). Osteoclasts express receptor activator of nuclear factor-B (RANK) which interacts with the RANKL on osteoblasts resulting in osteoclastic differentiation (47). With ongoing recruitment and migration of cells, osteoblasts and osteoclasts work to repeatedly remodel the hard callus in a process called ‘coupled remodelling’. This

process results in a bone callus whose centre is formed by compact bone and its edges formed from lamellar bone (38, 48).

1.2.2 Bone loss

The aforementioned depiction of bone healing refers to the most common scenario, in which fracture management achieves bone apposition. ‘Segmental’ bone loss and ‘critical’ bone gap management is an increasing clinical problem given demographic and morbidity changes within Western civilian populations that promote non-union (whose management necessitates addressing small bone gaps), in the management of osteomyelitis (wherein debridement creates larger gaps), and as we face the current international major trauma epidemic resulting from military grade weapons (whether injuring armed combatants, or civilians) (49-51).

A bone gap or defect implies a lack of osseoconductive matrix between bone ends which imposes limitations on how far osseoconduction can be carried by attempts at innate healing across the gap. The resulting concept is the “critical bone gap”, the exact size of this will relate to patient co-morbidities and inter-individual variance. Bone loss/gaps can be subclassified based on the amount of ‘missing’ or ‘lost’ bone: <2cm is usually considered a small bone defect, 2-5cm is a ‘critical’ bone defect and >5cm is a ‘segmental’ bone defect (50, 52). Massive ‘segmental’ bone defects present one of the most challenging problems for orthoplastic reconstructive surgeons to manage.

Where a bone defect is classified as small (<2cm), surgical management will often involve bone shortening with the use of either autologous or allogenic bone graft. Autologous bone grafting (often from the patient’s rib or iliac crest as donor sites) provides both matrix and cells to the patient, that may or may not survive.

Allogeneic bone grafting, from cadaveric bone donors delivers just decellularised matrix only that can be either non-structural (cancellous) or structural (cortico-cancellous) (53). Finally, an alternative would be to use one of many bone graft substitutes that are commercially available or combination approaches (54). In cases of ‘critical’ or ‘segmental’ bone loss, surgical treatment options vary and there remains equipoise within the orthoplastic surgical community as to best approach due to the requirement for more complex reconstruction (52). In these cases, the bone defect size will ultimately affect structural stability and functional outcomes so shortening is not an option, as spontaneous healing will not occur (54). For these larger bone defects, often resulting from major trauma, cancer or osteomyelitis, the currently available surgical treatment options include distraction osteogenesis (bone transport), combination approaches using implants (customised or non-customised) or cement spacers and allografts. Bone transport is effective but a laborious process for the patient to endure, taking on average 14.9 months (range 6-62 months) for the acquisition of lower limb bone healing (55).

A more complex autologous reconstruction option for patients with large ‘segmental’ bone defects are bone flaps (matrix and viable cells) or periosteal flaps and vascularised bone graft (56-58). Microvascular free flap for lower leg reconstruction of a ‘critical’ or ‘segmental’ bone defect often involves the free transfer of a pedicled fibular graft from the contralateral, uninjured leg, with maintenance of its circulation through microvascular anastomoses (58). Another notable flap used for the purpose of bone gap treatment, is the periosteal medial femoral condyle free flap (59). For massive ‘segmental’ defects (>6-9cm), reconstruction with autogenous vascularised bone free flaps is associated with a higher union rate (49, 60). Furthermore, the use of vascularised over non-vascularised autografts improves bone graft survival, union, mechanical strength

and is associated with lower infection rates (61-64). The potential issues with these existing strategies for management of ‘segmental’ bone loss include a lack of available donor sites, significant donor site morbidity and need for specialist microvascular reconstructive services. Additionally, the surgery requires extensive operative time, closely monitored inpatient stay and rehabilitation. Therefore, a tissue engineered solution for the “bone gap problem” would ideally replicate these existing strategies, but without the associated donor morbidity or need for prolonged bone transport intervention. Furthermore, additional applications for a bone regenerative tissue engineered solution, would be to provide scope to address the limb length deficiency in amputees, to optimise prosthetic options. Being able to increase proximal tibial length for example, could facilitate a below versus and above knee amputation by facilitation of prosthesis fit to a longer length of proximal tibia. Above knee amputation is well-documented to be associated with poorer clinical and functional outcomes than below knee amputations (65).

In this thesis I address one previously unexamined challenge to the *in-vivo* therapeutic efficacy and bioincorporation of a promising tissue engineered bone substitute.

1.2.3 Osteogenic biomaterials for bone regeneration

Biomaterials have captivated the bone regenerative medicine space for many years now as research attempts to bridge the ‘bone gap’ with these promising technologies. Within the Salmeron-Sanchez group at the University of Glasgow there is a rich 10-year experience with both two-dimensional (2D) and three-dimensional (3D) biomaterial models for engineering material-based strategies for tissue repair and regeneration. A well described biomaterial pioneered by the group and well characterised over this time is poly(ethyl) acrylate (PEA) with

fibronectin adsorption for efficient presentation of bone morphogenic protein 2 (BMP-2) and I will introduce this particular biomaterial in more depth.

1.2.3.1 The role of BMP-2

BMP-2 is an osteoinductive growth factor that has been used for over a decade for the promotion of osteogenic differentiation within *in vitro* and more recently, *in vivo* models (66-70). BMP-2 is a member of the transforming growth factor-β (TGFβ) superfamily and directs MSCs to differentiate into osteoblasts and osteocytes (70, 71). Despite promising applications for human BMP-2, challenges remain with its short half-life and rapid clearance *in vivo* often leading to large initial dosing in biomaterial applications (71, 72). In high concentrations recognised side effects include oedema, ectopic bone formation and irritation to local nerves (71-73).

To address this, the Salmeron-Sanchez group pioneered an ultralow-dose growth factor technology that yielded high bioactivity of BMP-2 (67). This technology uses PEA coatings with fibronectin adsorbed for efficient growth factor presentation.

1.2.3.2 PEA and fibronectin for efficient presentation of BMP-2

PEA is a simple, bioactive polymer (67). It has been shown that although fibronectin usually adsorbs onto polymers in a globular confirmation, PEA promotes the spontaneous organisation of fibronectin into more physiological networks (67). Assembled networks of fibronectin on PEA consequently present integrin-binding (III_{9-10}) and growth factor (GF) binding (III_{12-14}) regions to cells (74, 75). BMP-2 can bind stably to this GF-binding site in ultralow-doses (74).

1.2.3.3 PEA coatings and degradation for clinical purposes

Major drawbacks to PEA use clinically have included its usual application by spin coating which is difficult to apply to a 3D surface and furthermore, it is nonbiodegradable (76). Spin coatings usually require PEA to be dissolved in an organic solvent and result in PEA coatings with a thickness of approximately 1μm on a flat surface which is too thick for clinical applications, would not biodegrade and would leave traces of harmful substances (67). PEA applied as a coating with a thin enough layer (<10s of nm) to a degradable polymeric scaffold would allow metabolism after the scaffold degradation (77, 78).

As such, the Salmeron-Sanchez group developed a solvent-free coating method with nanoscale PEA coating depth that can be applied to a variety of 3D surfaces (67). This coating method involved development of a plasma-polymerisation strategy for thin PEA coating, that resulted in successful fibronectin assembly and BMP-2 binding leading to osteogenesis achieved *in vitro* and also *in vivo* in a veterinary canine clinical trial (67).

1.2.4 Osteoblast roles in immune responses

Osteoblasts are known primarily for their bone forming function in the physiology of bone turnover, however, an increasing role is being explored in the literature for subsections of osteoblasts to act as modified antigen presenting cells (79). Osteoblasts have been shown to not only play a role in antigen presentation to activate T cells but they have been shown to help promote differentiation and maturation of T cells (80).

Osteoblast maturity is heavily regulated by immune cells. CD4+ T cells secreting IFNγ can promote the differentiation of MSCs in bone marrow into osteoblasts,

whereas release of TGFβ can inhibit osteoblast differentiation. Furthermore IL-17A and IL-17F when released by Th17 T cells or regulatory T cells (Tregs) and in combination with BMP -2 can promote MSCs to differentiation into osteoblasts (81).

1.3 T cells

1.3.1 T cell development

T cells are the major cells of the adaptive immune response and undertake cell-based immune responses to keep the host safe from threats (82). Maintenance of homeostasis, immunological cell memory and self-tolerance depends on T cells (83). T cells express a receptor, the T cell receptor (TCR), that recognises a diverse array of antigens from pathogens, tumours and the environment (83). As such, T cells have been implicated as the drivers of a wide range of autoimmune and inflammatory diseases (83, 84).

T cells develop in the thymus from migrating bone marrow-derived thymocyte progenitors (82). Within the thymus, T cells undergo maturation before subsequent peripheral exportation. Low numbers of progenitors migrate to the thymus each day, however they rapidly proliferate whilst initiating the T cell differentiation program (85, 86). The developmental stages of a T cell within the thymus involve the acquisition of T cell characteristics with the associated loss of cellular multipotentiality (87). In the T cell differentiation programme, thymocytes begin the process as double negative (CD4-CD8-, DN) cells that initiate differentiation by becoming firstly, double positive (CD4+CD8+, DP) through the acquisition of T cell markers, before finally becoming single positive for either CD4 (CD4+CD8-) or CD8 (CD4-CD8+)(87-89).

Overall T cell development occurs in 3 stages that I shall introduce: T cell commitment, positive selection to ensure the TCR can recognise self-peptide major histocompatibility complexes (MHC) and negative selection to remove autoreactive T cells and generate Tregs.

1.3.1.1 T cell commitment

The earliest T cell precursor is called an early thymic progenitor (ETP) cell or a Kit-high double-negative 1 (KIT^{hi}DN1) cell. At this early stage of development they are not restricted to the T cell lineage and retain potential to access non-T cell fates (87, 88). Phase 1 of T cell development is notch-dependent, which switches on canonical Notch target genes and initiates the expression of T cell transcription factor coding genes: GATA binding protein 3 (GATA3) and T cell factor 1 (TCF1) (90). This process is reliant on various cytokines including IL-7 to drive KIT^{hi}DN1 cells into KIT^{hi}IL-$7R^{hi}$ DN2a cells. During the next stage, these KIT^{hi}IL-$7R^{hi}$ DN2a cells begin to express T cell markers and through a series of positive and negative gene regulation changes, T cell lineage commitment occurs (91). The key transcriptional repressor, turned on late in the DN2a stage by Notch signalling, is Bcl11b whose role excludes cells from any further commitment to a non-T cell fate (92). Bcl11b does this through downregulation of KIT expression creating the DN2b phenotype which have slower proliferation (88). The DN3a stage is the peak of Notch-dependent gene expression, and these cells are then committed to T cell fate, even in the absence of TCR on their surface. DN3a cells undergo TCR rearrangements to ultimately generate either $\alpha\beta$TCR-expressing ($\alpha\beta$ T cells) or $\gamma\sigma$TCR-expressing ($\gamma\sigma$ T cells) T cells (82, 87). The $\alpha\beta$ T cells form different sublineages including CD4, CD8, Tregs and natural killer T (NKT) cells (87). The

process transitions to a Notch-independent one at this point as cells become DN3b and then DN4 cells (88, 93).

1.3.1.2 Positive selection of functional T cells

In order to differentiate between self and nonself, the T cells must recognise peptide-MHC complexes (94). In the thymus, positive selection of developing T cells ensures the survival of $\alpha\beta$T cells that are capable of this immune recognition when exposed to human peptides on thymic epithelial cells (94). T cell fate is therefore marshalled by the selection of only functional and self-tolerant T cells (95).

1.3.1.3 Negative selection of autoreactive T cells

After the developing T cells are positively selected based upon their ability to recognise self, they are then committed to either a CD4+ or CD8+ lineage (95). However, an ability to identify self can also commit T cells to alternative fates, with either death via negative selection to remove autoreactive cells or Treg differentiation to promote self-tolerance (95).

1.3.2 T cell receptor (TCR) gene rearrangement

T cells recognise their antigen as peptides presented on MHC molecules via the TCR. Each T cell has a unique TCR generated by gene re-arrangement of Variable (V), Diversity (D), and Joining (J) regions during T cell development in the thymus. TCR diversity is achieved by the random combination of different VDJ regions and the pairing of different alpha and beta chains. It is estimated that there is a possibility of over 10^{15} different TCRs, though studies suggest that in humans there are around 10^{11} different T cell clones: (96).

1.3.3 T cell activation

T cell activation relies on multiple signals *in vivo* and in the majority of cases leads to successful host defence (97). Alternative *in vitro* methods for T cell activation have also been developed [Figure 1-1]. Adaptive immune responses do not happen immediately at the site of insult but are initiated in the peripheral lymphoid tissues by exposure to migrating naïve T cells. Naïve T cells then become activated via several mechanisms, leading to proliferation, differentiation into effector subsets of T cells, and migration to promote pathogen clearance (83). Once a naïve T cell is activated its effector cell duration is short-lived, but a small pool persists as memory T cells (83). Memory T cells have had prior T cell antigen priming and retain immunological memory.

1.3.3.1 Peptide-MHCII complex activation

The first interaction (signal 1) required for successful T cell activation is through contact with antigen presenting cells (APCs) carrying complexes of MHC protein and peptide antigen that the T cell recognises (98, 99). In this context, the T cell recognises the MHC-peptide complex by clonotypic TCR subunits. The TCR complex consists of TCRα/β chains and associated CD3γ/δ/ε/ζ subunits (100, 101). The binding of the TCR on either a CD4+ or CD8+ T cell to the antigen on the APCs MHC complex triggers downstream signalling pathways that lead to specific transcriptional activation which leads to T cell proliferation and cytokine secretion (98, 102, 103).

1.3.3.2 Co-stimulatory molecules activation

In addition to TCR binding to APC MHC complexes, both CD4+ and CD8+ T cells also recognise adhesion molecules and cell surface receptors on APCs in an

antigen-independent fashion (98, 99). These are usually required in addition to TCR-MHC recognition as secondary signals (signal 2) to enable T cell activation (104). CD4+ T cells express CD28 which is a molecule on T cells that binds to CD80 or CD86 molecules on the APCs cell surface and initiates T cell proliferation (105). CD8+ T cells require signals from CD70 or CD137 to initiate activation and rely less so on CD28 (106, 107).

During the coronavirus pandemic, vaccine trials described flow cytometry activation-induced marker assays looking for T cell expression of OX40+CD137+ or OX40+CD40 ligand (CD40L)+ T cells. They combined this approach with intracellular staining for cytokines TNFα, IL-2 and IFNγ to identify responding T cell populations to the vaccines (108). OX40 (also known as CD134) is expressed by activated CD4+ and CD8+ T cells and is part of the tumour necrosis factor (TNF) family of costimulatory molecules (109). It leads to increased T cell proliferation and effector function when engaged by dendritic cell ligands. CD137 (also known as 4-1BB) is also a member of the TNF family of costimulatory molecules and is a type 1 transmembrane protein expressed on the surface of activated T and natural killer (NK) cells (110). CD40L is a membrane glycoprotein expressed on activated CD4+ T cells shortly after activation. CD40 is the ligand for CD40L which is present on B cells, follicular dendritic cells (DCs) and macrophages (111).

Inducible co-stimulator (ICOS) is a protein found on the T cell surface and is a member of the CD28 superfamily that is stimulated by ligands (ICOSL) found on APCs following antigen recognition only (112). Naïve T cells express ICOS at low levels but can rapidly upregulate ICOS after TCR and CD28 stimulation, to promote proliferation and T helper (Th) 2, Th1 and Th17 differentiation depending on the inflammatory context (112, 113).

The CD28 superfamily also includes molecules programmed cell death 1 (PD1) and cytotoxic T lymphocyte-associated protein 4 (CTLA-4) (112). The PD1 axis acts as an immune checkpoint to negatively regulate T cell activation and limit tissue damage by reducing the T cell response (114). PD-L1 is the ligand which APCs express in response to IFNγ that binds to PD1 to restrain the immune response and prevent hyperactivation (114, 115).

CD25 is part of the trimeric IL-2 receptor and is often used to identify T cells activated through their TCR (116). CD25 is expressed in high amounts early on in activated T cells and, also in Tregs, which are dependent on IL-2 for survival (116, 117). Despite its reliability in identifying murine Tregs, caution is advised for reliance on CD25 expression alone to identify Tregs in humans (117). It has been suggested that *in vitro* discrimination of CD4+CD25+ Tregs from CD4+CD25+ activated T cells can be achieved based on proportionately higher CD25+ expression in true Tregs (117). This assumption was based on the discovery that 2-4% of human CD4+ T cells expressing high levels of CD25+ exhibited potent immunosuppressive activity *in vitro* (118-120).

1.3.3.3 Cytokine mediated activation

A TCR-MHC, costimulatory signal activated T cell will further respond to cytokines. The presence of specific cytokines determines what effector type of T cell differentiates. The different T cell subsets differentiate from exposure to different cytokines e.g. Th2 cells from IL-4 exposure. The activated, differentiated Teffector cells then migrate out to the peripheral sites of infection, insult or inflammation for their downstream response (121).

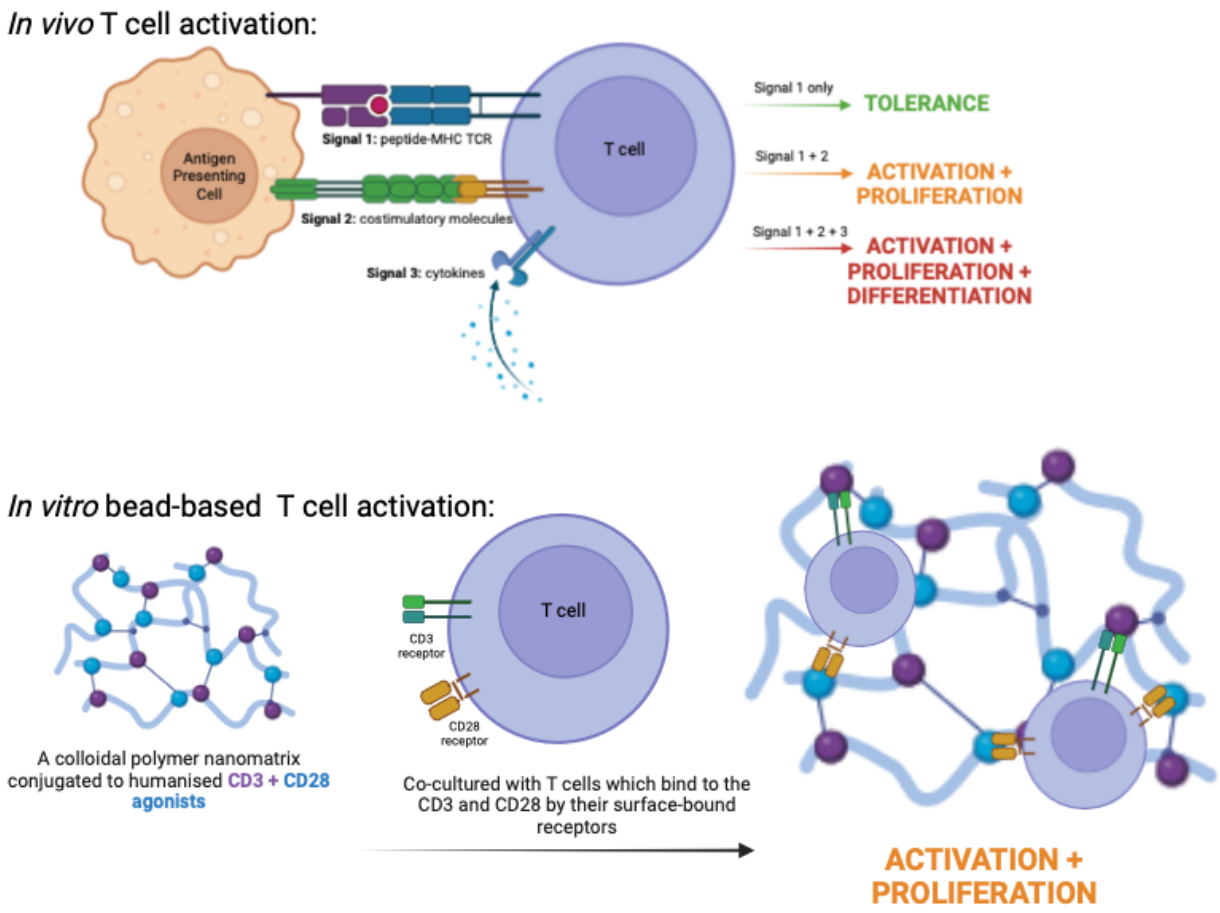

Figure 1-1: Summary of three signal in vivo T cell activation versus in vitro bead-based T cell activation methods. Created with BioRender.com

1.3.3.4 Dendritic cell maturation

DCs are crucial to the balance of immunity and tolerance through their role as sentinels of the immune system, to capture, process and present antigens to T cells (122). Essentially pre-DCs exit the bone marrow pre-committed to lineages to seed the peripheral or lymphoid organs (123, 124), here they differentiation into chemokine receptor-expressing type 1 or type 2 DCs and behave as phagocytes, sampling tissue antigens in search for pathogens (122). Once they encounter a pathogen, this triggers their pathogen recognition receptors (PRRs) and they rapidly undergo DC maturation with functional and morphological changes (122).

As part of this maturation process, DCs upregulate and express MHC molecules (signal 1), costimulatory molecules CD80, CD86 and CD40 (known as signal 2) and finally secrete cytokines and chemokines (signal 3) (125, 126). Expression of CC-chemokine receptor (CCR) 7 hallmarks DC maturation and guides DC migration to T cell zones in the draining lymph nodes or in the spleen (122).

Historically, it was believed that DC maturation was, by default, immunogenic leading to the activation of T cells. However, the presence of MHC molecules (signal 1) in the absence of costimulatory molecules (signal 2), has been linked to tolerance fates as opposed to activation of T cells (122). Current perspectives view two distinct DC maturation modes: homeostatic or immunogenic. The expression of DC maturation markers cannot in isolation be used to predict immunogenicity (122). Furthermore, how DCs become activated in homeostatic conditions to maintain and promote immune tolerance is an area of ongoing intense debate in the immunology literature (122).

1.3.4 CD4 T cell classification

CD4+ T cells differentiate into heterogenous subsets, including Th1, Th2, Treg, follicular helper T (Tfh), Th17, Th9, Th22 and CD4+ cytotoxic T cells (127). I will focus on introducing the most established subsets, Th1, Th2, Th17 and Treg and describe their roles in health and disease.

Th1 cells protect the host against intracellular bacteria and viruses and their differentiation is driven by the expression of T-box transcription factor (T-bet), which is the major transcription factor associated with pro-Th1 differentiation (128). T-bet directly binds to the Ifng gene promoter resulting in increased expression of the pro-inflammatory cytokine IFN-γ, which along with IL-12 make up the key cytokines essential for Th1 responses (129).

Th2 cells act to protect the host from helminth infections as well as being key mediators of chronic inflammation in conditions such as, asthma and allergy responses (130). Th2 cells are formed through the expression of GATA3 and express a range of cytokines including IL-4, IL-5 and IL-13. A number of cells types including DCs and innate lymphoid cells 2 (ILC2) can express IL-4 and IL-13 that drive Th2 responses (131).

Th17 cells with their master transcription factor, receptor-type nuclear receptor (RORγt), play crucial roles for protection against extracellular pathogens, as well as a key part in chronic inflammation with regards to autoimmune diseases (132). Cytokines IL-1, IL-6 and TGFβ drive differentiation of Th17 cells leading to upregulation of RORγt and suppression of forkhead box protein 3 (FOXP3) (133). Th17 cells secrete IL-17A-F, IL-21, IL-10, IL-23 and IL-22 to enact Th17 mediated immune responses (134, 135). Th17 cells have gained notoriety for their plasticity based on the presence or absence of TGFβ. IL-6 and TGFβ induce the classical Th17 cells that produce IL-17, IL-21 and IL-10. In the absence of TGFβ, IL-6, IL-1β and IL-23 induce more pathogenic Th17 cells that lead to increased secretion of IFNγ, GM-CSF and IL-22 (136-138).

Tregs are important for immune regulation and promotion of immune tolerance (82, 139). Tregs maintain immune tolerance through immunosuppressive actions and are characterised by increased expression of IL-2 receptor alpha chain (IL-2Rα, also known as CD25), IL-10, TGFβ and IL-35, driven by transcription factor expression of FOXP3 (140, 141). Tregs can be classified based on developmental origin. Those that developed in the thymus are known as thymic Treg (tTreg) cells and those that differentiate from CD4+ T cells in the periphery, in the presence of tolerogenic signals, including IL-10, TGFβ or retinoic acid, are known as induced

Treg (iTreg) cells (82). Tregs have been shown to play an important role in tissue immune homeostasis and contribute to tissue regeneration via crosstalk with M2 macrophages (21). Tregs can push the local immune response to a pro-regenerative state with the secretion of anti-inflammatory cytokines such as IL-10 and the induction of an M2 macrophage response (21).

1.3.5 CD8 T cell classification

CD8+ T cells when activated by antigen stimulation, give rise to effector and memory T cells that play crucial roles in elimination of malignant cancer cells or fights against intracellular pathogens (82). CD8+ T cells can differentiate into various Teffector cells and can be grouped as classical cytotoxic CD8+ T cells (Tc1 cells), non-Tc1, Tc2 , Tc9, Tc17, Tc22, follicular cytotoxic T cells (Tfcs) and CD8+ Tregs (142).

Tc1 cells are the major population of CD8+ T cells and are thought to primarily be responsible for elimination of tumour or infected cells and do this through production of perforin, granzyme B, IFNγ and TNFα. Tc1 cells can be differentiated under IL-12 conditions and produce IFNγ in response to activation of transcription factor STAT4, Eomes and T-bet (142). Tc1 cells also have roles in viral diseases including, human immunodeficiency virus, hepatitis C and measles (143-145).

Non-Tc1 cells make up the minority of CD8+ T cell subsets and share common signalling cytokines, transcription factors and effector cytokines to their CD4+ Teffector cell equivalents. For example, Tc2 cells are differentiated by IL-4 producing further IL-4 in a positive feedback loop, IL-5 and IL-13 through GATA3 and STAT6 signalling (142). Tc9 cells also differentiate under IL-4 conditions and TGFβ conditions and produce IL-9 through IRF-4 and STAT6 (142). Tc17 cells are differentiated by IL-6 and TGFβ through RoRγt and STAT3 signalling (142).

Finally, CD8+ Tregs are differentiated by TGFβ conditions and produce IL-10 and further TGFβ through activation of FOXP3 (142). Regulatory T cells maintain immune homeostasis and can play immunosuppressive roles in humans (146-148).

1.4 Overview of the innate immune response to biomaterials

The immune system functions to quickly detect and eliminate pathogens. It does this via relatively rapid, innate immunity or by the process of acquired, adaptive immunity over time (149). The innate immune response is driven by fast recognition of pathogen-associated molecular patterns (PAMPs) and danger-associated molecular patterns (DAMPs) often by pattern-recognition receptors (PRRs). PRRs are present on many cell types including APCs such as DCs and macrophages and trigger signalling pathways that result in the clearance of the pathogen or danger (9, 150). Example PRRs include toll-like receptors (TLRs), as well as cytoplasmic Nod-like receptors (NLRs) (151). Activation of PRRs on sentinel APCs leads to production of proinflammatory associated cytokines IL-1 and TNFα, as well as vasoactive amines like histamine and serotonin that lead to early responses to injury (152).

1.4.1 PAMPs, DAMPs and TLRs

PAMPs are usually conserved microbial products, for e.g. lipopolysaccharide or bacterial endotoxin, and molecular motifs from some viruses that activate PRRs (151, 153). DAMPs are vital to inflammation responses in sterile inflammation. The system that responds is based on the same innate pattern recognition system as for detecting microbes, but the immunostimulatory molecular patterns differ and are associated with damage (151). The proinflammatory environment of surgical

wounding induced by implantation of biomaterials encourages an enrichment of endogenous DAMPs including apoptotic cells and their byproducts, fibronectin (FN) and heat shock proteins which adsorb to the biomaterial causing ongoing irritation (23, 153, 154). TLRs are transmembrane proteins that play critical roles in bone metabolism and regeneration and may therefore be crucial to biomaterial incorporation (155). Furthermore, TLRs are widely expressed on MSCs, haematopoietic and immune cells in the osteogenic microenvironment and have been shown to impact MSC osteogenic differentiation and subsequent bone remodelling (155, 156).

1.4.2 Complement

Other components of the innate immune response include the activation of the complement system, which is triggered by extracellular pathogens, to assemble serum proteins capable of forming complexes that destroy the pathogen (9). It is well-established that biomaterial surfaces can also activate complement, usually via the classical and the alternative pathways (9, 22, 24) [Figure 1-2]. The alternative pathway of complement activation is triggered directly by foreign surfaces, such as biomaterials, that do not provide acceptable down regulation of the complement protein 3 (C3) convertase (24). C3 deposition, generated by the alternative pathway was found on both glass and plastic surfaces leading to neutrophil adhesion to non-biologic prosthetic surfaces (22). Furthermore, it is well accepted that physical biomaterial properties such as hydrophobicity can be more prolific activators of the complement system (24).

The classical pathway is triggered by formation of antigen-antibody complexes or alternatively by C-reactive protein released by damaged cells (24). A limited activation of the classical pathway at biomaterial surfaces has been reported, but this is short lived. A proposed method for this is that C3b binds because of

adsorbed proteins (fibrinogen, human serum albumin, immunoglobulins) in a film on the biomaterial surface (24). Adsorbed IgG to biomaterial surfaces has been shown to initiate the classical pathway (157, 158). It remains unclear the exact mechanism by which complement is activated, given all biomaterial complement activation assays have been performed *in vitro* with diluted sera and non-physiological conditions (24).

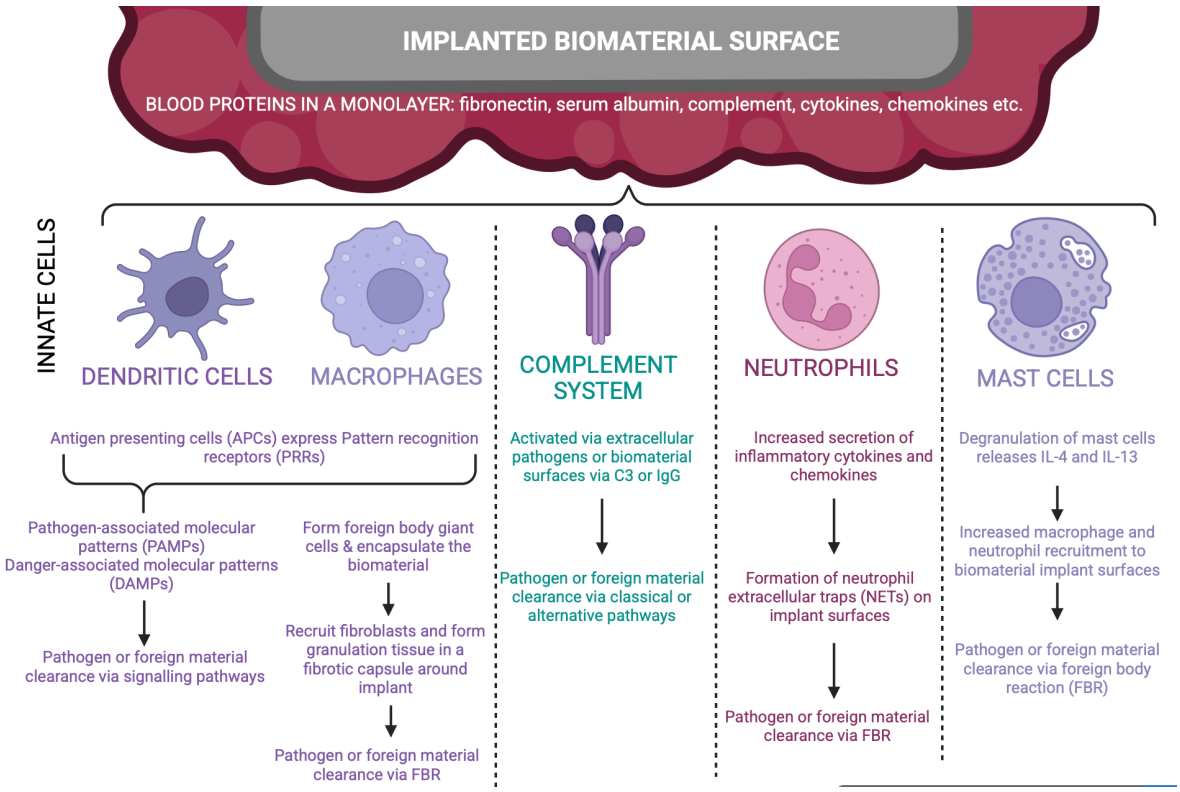

Figure 1-2: Summary of the innate immune response to biomaterials. Figure demonstrates the key responding innate immune cells that are the first responders at biomaterial implantation sites. A summary of each cell's initial response and downstream actions is provided by cell type. FBR= foreign body response. Created with BioRender.com

1.4.3 Foreign body response to biomaterials

Immediately following the implantation of a biomaterial, the host reacts at the blood-material interface, with rapid formation of a provisional matrix that encompasses structural, biochemical and cellular processes all intrinsically interlinked with wound healing and macrophage activation (26). The biomaterial recruits plasma proteins when exposed to blood, and the provisional matrix formed is effectively a monolayer formed on its surface (159). This can be passive or can result in conformational changes in the individual proteins in the layer. For example, C3 and the antibody immunoglobulin G (IgG) are particularly prone to changes that can then activate the complement system on the biomaterial surface (27, 160). Recognition of these by APCs will trigger attempts to phagocytose the biomaterial, and the provisional matrix also provides the foundation for the accumulation of chemoattractants, cytokines, and growth factors that can modulate local wound healing and immune responses (23, 26, 161) [Figure 1-3].

Polymorphonuclear leukocytes (PMNs), such as neutrophils, characterise the acute inflammatory response to biomaterials, alongside mast cell degranulation with histamine release and fibrinogen adsorption (26). During the degranulation of mast cells, IL-4 and IL-13 are released, affecting the extent of the development of the subsequent foreign body reaction to the biomaterial (26, 162). Consequently, ways to alter the cytokine milieu or to reduce the availability of histamine, have been explored as potential immunomodulatory targets to reduced foreign body responses. H1 and H2 histamine receptor antagonists, have been shown to reduce the recruitment of macrophages and neutrophils to implant surfaces (26). Macrophages are a key player in the response to an implanted biomaterial, forming foreign body giant cells and helping to encapsulate the biomaterial in a fibrotic capsule [Figure 1-3]. Through ongoing macrophage recruitment, infiltration

of fibroblasts and formation of granulation tissues as a precursor, the fibrotic capsule is separated from the biomaterial by a one or two cell layer of inflammatory cells (26). This encapsulation separates the biomaterial from the local environment and has been shown to affect local functionality (163-165) [Figure 1-3].

The innate immune response is multifaceted and plays a pivotal role in the response to injury or implantation of allogenic biomaterials (149). As described, neutrophils migrate to the site of injury to secrete cytokines and chemokines that recruit further immune cells such as macrophages (6, 26, 149). Focus of recent research has been on macrophage phenotype polarisation, crudely that resting primary macrophages (M0) can be polarized toward pro-inflammatory (M1) or anti-inflammatory (M2) phenotypes, however studies have shown they can be reprogrammed and have their phenotypes reversed (28, 166). M1 macrophages are known to phagocytose pathogens and produce inflammatory factors such as TNF-α, IL-8, IL-12 and inducible nitic oxide synthase (iNOS) for usually the first 2-3 days following injury (9, 149, 167). Following this, the macrophage may shift from a M1 to M2 phenotype, with a preponderance for wound healing and tissue repair via cytokine and growth factor secretion and the deposition of ECM (149) [Figure 1-3].

Given the different macrophage phenotypes, much interest has centred on this spectrum of macrophage behaviour, with recent focus on controlling the transition from a pro-inflammatory to a pro-repair state (167). Interactions between immune cells at the biomaterial interface, result in the release of profibrogenic factors such

as, platelet-derived growth factor (PDGF), VEGF and TGF-β which recruit fibroblasts (168-170). These activated fibroblasts deposit type I and III collagen and excessive secretion can result in fibrotic deposition of ECM which encapsulates the biomaterial, isolating it from the tissue microenvironment and limiting the functionality of the implant (163-165).

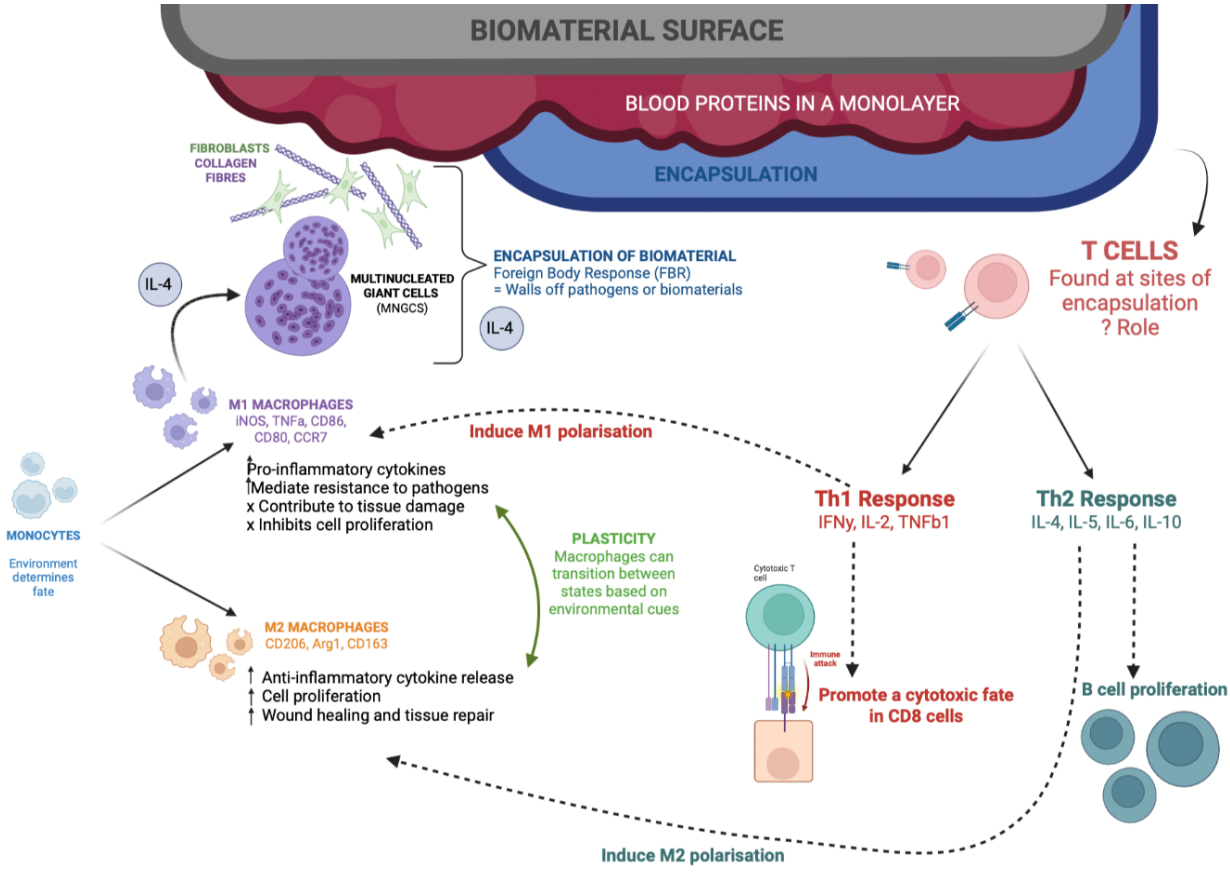

Figure 1-3: Role of macrophage M1 vs M2 response to implanted biomaterials. Interactions with T cells demonstrated and interplay of the innate and adaptive arms of the immune response. Created with BioRender.com

1.5 Overview of the adaptive immune response to biomaterials

The adaptive immune system is a slower but more specific response that leads to the generation of immunological memory. The adaptive immune system relies on cell-mediated or antibody-mediated responses to specific, foreign antigens. The

adaptive response contains T and B lymphocytes that have antigen receptors capable of responding specifically to pathogens. T cells can act as helper (CD4), or cytotoxic (CD8) T cells and cell-mediated immunity encompasses the activation, recruitment and differentiation of T cells able to destroy intracellular pathogens. Subtypes of CD4 T cells include Th17 cells, Th1 cells, Th2 cells and Tregs which all help to carry out specific helper adaptive immune responses that are differentiated by the cytokines they produce (171) [introduction 1.3.4].

Allogenic cells are nonself cells provided by a donor that are biologically distinct from the recipient. In biomaterials containing allogenic cells, through antigen presentation by DCs and macrophages to T cells in secondary lymphoid organs, the adaptive immune response may be triggered, and will regulate long term immune interactions with implanted biomaterials (172). Antibody-mediated immunity, in contrast, relies on the activation of B lymphocytes to secrete antibodies that can bind to pathogens, and their roles in biomaterial incorporation is conflicting in the literature (149, 173). B cells are a minority population of cells resident at biomaterial implantation sites. B cell knockout mouse models have demonstrated reduced fibrosis and wound healing whereas alginate biomaterials, polymer derived from alginic acid, have correlated B cell presence to fibrotic microenvironments mediated by macrophage recruitment (25, 174, 175).

Historically, it was hypothesised that synthetic biomaterials (ceramics, polymers, metallic materials), were immunologically inert and believed not to initiate an adaptive immune response due to a lack of perceived antigen (9). Lymphocytes have however since been found at sites of synthetic biomaterial implants and multiple studies have shown a role for adaptive immunity with biomaterial integration (26, 176, 177). Studies have shown indirect inflammatory T cell effects through DC antigen presentation from allogenic cells within biomaterials as well as

more direct T cell responses due to their attraction to implanted biomaterials (23, 178). One of these studies used *in vivo* Balb/c mice as hosts in receipt of both xenogeneic Chinese hamster skin grafts and implanted biomaterials simultaneously (179). The authors then rechallenged these primed splenocytes *in vitro* and observed that those receiving both biomaterial and xenogeneic skin grafts had a transient suppression of the second set response (23, 179). The authors summarised that their work contradicted the paradigm that biomaterials should be designed to minimise inflammation and that inflammatory responses may be beneficial to tolerance (23). However, a lack of human cell *in vitro* or i*n vivo* studies remains a challenge within the current literature.

Researchers have begun to address the relative lack of T cell studies in the biomaterial research space and hypothesise that T cells play a key role in the infiltration of MSCs around bone biomaterials in *vivo* (180). MSC infiltration is critical for ectopic osteogenesis (the laying down of new bone via a process called endochondral ossification), and therefore they are frequently incorporated within biomaterials (181, 182). MSC migration is triggered by pro-inflammatory cytokines, growth factors and angiogenic factors, specifically inflammatory mediators released by macrophages and NK cells (183, 184). The number of MSCs rise significantly between day 7 to 14 post implantation around a bone biomaterial and this coincides with T cell presence as part of the delayed response to the material (180). When modelled in a T cell depleted mouse, almost no osteogenic MSCs were found, demonstrating T cells are critical to MSC recruitment to bone biomaterials in *vivo* (180). The authors recognised a positive correlation between T cell recruitment to an implantable osteoinductive material (biphasic calcium phosphate) and the infiltration and osteogenic differentiation of MSCs (180). Further studies have explored the role of T cells as regulators, demonstrating an increase in pro-inflammatory macrophages, decrease in anti-inflammatory

macrophages and reduced MSC recruitment in response to titanium implants in T cell deplete mice (185). The authors concluded that an absence of T cells compromises new bone formation at the implantation site (185).

Despite their established role in immune responses, T cells are poorly characterised as to their role in the response to biomaterials. Studying T cell activation and differentiation and defining the roles of their subsets poses significant challenges (149, 185). The role of T cells and their subsets in the response to implantation remain unknown and delineation of specific T cell roles within the biomaterial microenvironment are currently highly understudied.

1.6 Biomaterials property-associated immune responses

Implanted biomaterials will interact with both the innate and adaptive arms of the host immune system in ways that determine the biological functionality and performance of the implant over time (21, 26, 186). The quest for biomaterial longevity *in vivo* has led to a greater understanding of degradation time frames, interaction with cells at the biomaterial surface and the formation of foreign body giant cells at implantation sites (186, 187). An emerging strategy in tissue engineering is immunomodulation of the materials themselves to control the local immune interaction over time to reduce chronic inflammation (172). It has been shown that macrophages play distinct roles in different tissues niches and can trigger tissue-specific innate responses (188). Understanding the properties of the biomaterial constructs, its degradation products, and the local tissue microenvironment, is therefore crucial to favourably tune the immune interplay between the biomaterial and the host [Figure 1-4].

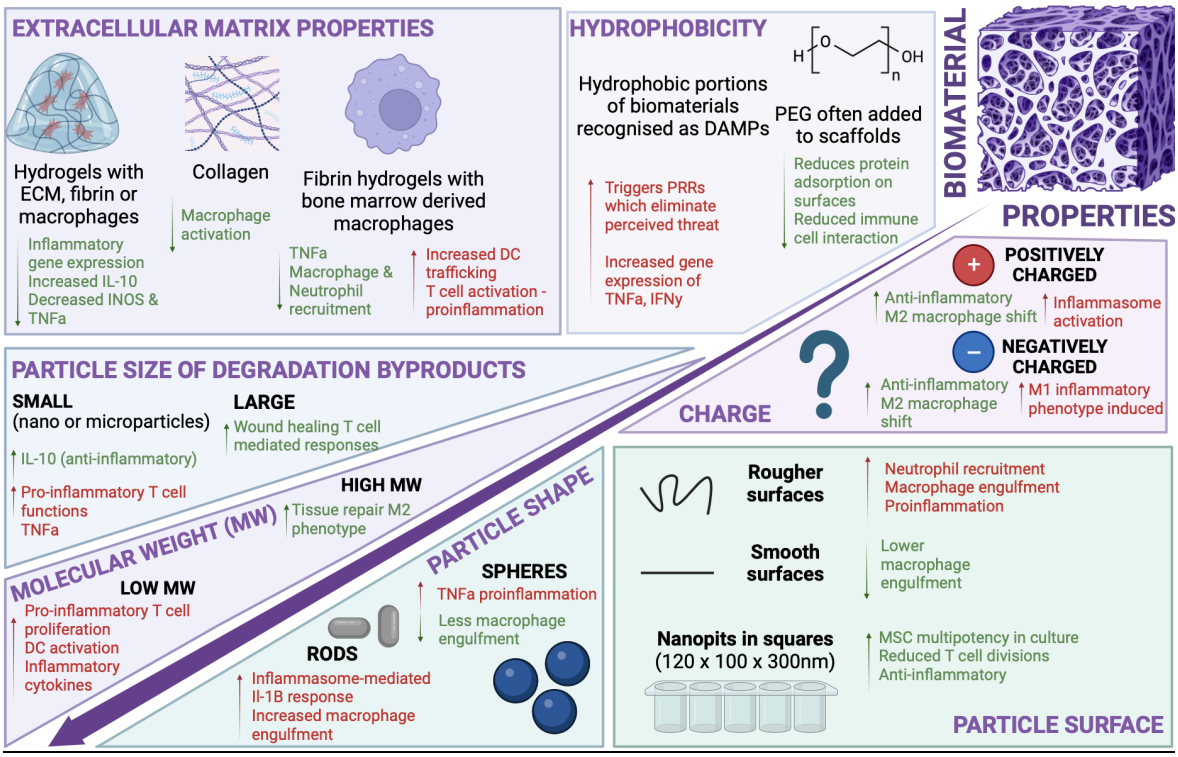

Figure 1-4: Summary of biomaterials properties and their associated immune interactions. Detailed discussion within introduction section 1.6. Created with BioRender.com

1.6.1 Extracellular matrix

One way to immunomodulate a biomaterial is to take advantage of its natural ECM properties, which have been shown to have immune regulatory effects. Collagen chemically crosslinked with 1-ethyl-3-(3-dimethylaminopropyl)-carbodiimide and N-hydroxysuccinimide (EDC/NHS) has been shown to modulate the innate immune component with an effect on macrophage activation (172). Hydrogels made of gelatin methacrylooyl (GelMA) cultured with human monocytes were shown to have lower inflammatory gene expression when compared to cells cultured on plastic (172). Furthermore, macrophages cultured on GelMA showed higher expression of IL-10, an anti-inflammatory cytokine, as well as lower expression of INOS and TNF-α, a pro-inflammatory cytokine, compared to those cultured on PEGDA (172). A study in wild type mice treated with either collagen, bone or cardiac extracellular matrix scaffolds showed that those mice exposed to the

scaffolds inserted subcutaneously had increased CD4 T cells numbers, expression of Th2-associated genes and associated tissue repair (189). Transcriptome analysis of CD3 T cells removed from the local microenvironment one week post biomaterial scaffold treatment revealed increased messenger RNA associated with T helper type 2 (Th2) responses which are pro-repair. These experiments were repeated in B and T cell deficient mice demonstrating an IL-4 gene expression decrease to levels comparable with saline control treatments (189). These data suggest that adaptive immune cells are central to the Th2-asssociated tissue repair response in mouse models.

Fibrin also plays a key role in the immune modulation of biomaterials. Bone marrow-derived macrophages (BMDMs) cultured *in vitro* on fibrin hydrogels showed a reduced soluble, inflammatory TNF-α cytokine secretion compared to those cultured on tissue culture plastic (172). This was replicated *in vivo* with porcine burn wounds treated with fibrin hydrogels demonstrating reduced macrophage and neutrophil recruitment and a more pro-repair, anti-inflammatory phenotype (190). However, fibrin has also been associated with a pro-inflammatory adaptive immune activation of DC trafficking and sequestration of growth factors. T cells, macrophages and monocytes express protease activated receptor 1 (PAR-1), which is activated by fibrin and been shown to be required for DC trafficking and subsequent T cell activation demonstrating a pro-inflammatory, adaptive immune response to fibrin (172, 191).

1.6.2 Particle size & degradation

Changing the physical properties of the biomaterials to reduce immunogenicity has included altering: particle size; shape; hydrophobicity; surface features; and the effects of degradation by-products (4). The size of these degradation products has been shown to have an effect on the subsequent inflammatory response (149).

Smaller nano or microparticles are associated with increased proinflammatory T cell function as well as production of TNF-α and within the same study, also an increase in, classically anti-inflammatory, IL-10 (149, 192). This demonstrates that anti-inflammatory and pro-inflammatory signalling can often occur in parallel and the shift between the two is dependent on the local microenvironment. In contrast, larger degradation particles have shown association with a more favourable, increased wound healing, T-cell mediated immune response (149, 193). A study demonstrated that gold nanoparticles with diameters of 3nm caused higher activation levels and greater IL-12 and IFN-γ secretion than particles with 12nm diameters, and these effects translated to increased proinflammatory T cell function (193).

Biomaterial chemistry can be altered to promote more stability *in vivo*, as acrylate-derivatised PEG (PEGDA) hydrogels are well known to slowly degrade leaving them unsuitable for long term implantation, but with amide linkages in the place of acrylate esters, forming PEG diacrylamide (PEGDAA), stability was shown *in vivo* over 12 weeks (187). The complexity of the biomaterial degradation profile is not fully understood and studies have found distinct subpopulations of tissue-resident macrophages that undertake the majority of the biomaterial degradation (194). Furthermore, studies suggest that scaffold architecture can affect the mechanotransduction and activity of these macrophage subpopulations leading to differences in degradation rate *in vivo* (194).

Control of precise biomaterial degradation is a challenge within the field of materials science, too slow and the biomaterial may be rejected by the host or encapsulated preventing satisfactory incorporation, too fast and the intended regeneration of tissues may not be complete (195). It is known that biomaterial porosity and particle dimensionality play critical roles in regulating the degradation

process and in biomaterials used as delivery mechanisms, the release kinetics for any molecules adsorbed to the biomaterial are critically dependent on the surrounding environmental cues (196).

1.6.3 Particle shape

The inflammasome is a multiprotein complex responsible for the activation of caspases and the secretion of pro-inflammatory cytokines (197). Micro and nanoscale shape changes can alter the immune cell interactions and promote either pro-inflammatory or pro-repair niches (149). Studies showed that a rod particle shape triggered an inflammasome-mediated IL-1β response compared to sphere particle shape, which led to cytokine-mediated, proinflammatory response through release of TNF-α (198). Additionally, nanorods were internalised more by macrophages than were nanospheres (199). Overall, studies have demonstrated shape-dependent cytokine secretion, production of reactive oxygen species and DC maturation, with nanotubes shown to exhibit the largest immunogenic effects (200). In terms of T cell activation, ellipsoidal biomimetic APCs were shown to significantly enhance *in vitro* and *in vivo* activity of CD8 T cells over spherical APCs, indicating particle geometry is a critical design criterion in artificial APC generation (201).

However, the shape needs to be considered alongside the size of the biomaterial particles. Longer rods were shown to be less readily phagocytosed by macrophages than shorter ones and induced greater levels of TNF-α in a process known as ‘frustrated phagocytic interactions’ (202). Failure to phagocytose larger-scale objects led to increased production of reactive oxygen species and inflammatory cytokines leading to chronic inflammation and fibrosis (149, 202). This process bears relevance as biomaterial scaffolds are often too large for engulfment, relying on a process in which longer fibres are shed and further

degraded over the duration of the lifespan of the biomaterial, which may lead to a greater activation of the inflammasome, and downstream pro-inflammatory signalling. Tissue engineering uses materials enabling a variety of different shapes and topographies, a thorough understanding of the impact of shape on inflammasome activation will enable immune tuneability through materials science.

1.6.4 Particle surface

The surface topography of the biomaterial also can tune the immune response. Rougher surface morphology has been shown to increase neutrophil recruitment and IL-1β, TNF-α and IL-6 secretion compared to smoother surfaces (203, 204). Biomaterials with particles with rougher surfaces were also preferentially engulfed by macrophages leading to increased activation of the immune system (198). Furthermore, Th2 cells and Tregs are upregulated in response to rough, hydrophilic titanium implants due to increased anti-inflammatory macrophages exhibiting local anti-inflammatory effects (185, 205). Th1 and Th17 cells were reduced in response to rough, hydrophilic implants demonstrating a proinflammatory phenotype (205).

Biomaterials that have been well-described in the literature are implanted silicone breast implants. With time, patients may develop capsular contracture as a consequence of chronic inflammation and require surgical removal of the implants and their capsule. Immunohistochemical analysis of fibrous capsules removed from patients with capsular contracture around silicone biomaterial breast implant sites demonstrated a preponderance for macrophages, DCs, fibroblasts and activated CD4+ T cells expressing CD25 and CD45RO markers at biomaterial interfaces (186). Analysis by flow cytometry demonstrated greater numbers of effector Th17 cells, known to increase production of IL-17, as well as less Tregs implying a pro-inflammatory interface.

The surface roughness of bone is around 32nm and nanotopography can be used to maintain immunomodulatory capacity (206). Nanopits of 120nm diameter, 100nm depth and 300nm centre-to-centre spacing within a square arrangement led to MSC multipotency in culture (207). Furthermore, the square arranged nanopits were shown to promote immunomodulation of the MSCs evidenced by reduced T cell division in a proliferation assay when compared to increased division found with flat and near-square topographies (207). Over 28 days of culture, MSC immunomodulation was maintained, driven exclusively by the material properties alone which the authors attributed to a shift in MSC respiration towards oxidative glycolysis driven by the changes evoked in cytoskeletal tension rather than by a hypoxic mechanism (173). Micro and nanoscale shape changes can significantly alter the immune material interface with downstream proinflammatory or pro-repair responses. Consequently, whilst trying to mimic the architecture of the desired reconstructive tissue for better biomaterial functionality, tissue engineers also need to account for and prioritise conformations that provoke a pro-repair niche.

1.6.5 Molecular weight

In addition to the shape and size of the degradation products, the molecular weight (MW) has been shown to influence the immune response to the biomaterial. Low MW hyaluronic acid, weighing 1500-5300Da, increased DC activation, inflammatory cytokine secretion and T cell proliferation by triggering TLR-2 and TLR-4 signalling (192, 193, 196). Additionally, low MW hyaluronic acid polarised macrophages towards the pro-inflammation M1 phenotype compared with high MW hyaluronic acid which promoted the tissue repair M2 phenotype (208, 209).

1.6.6 Hydrophobicity

The immune system recognises hydrophobic portions of biomaterials as DAMPs, and this triggers PRRs which attempt to eliminate it to remove the perceived threat. Additionally, particles with greater hydrophobicity have been shown to increase the gene expression of pro-inflammatory cytokines, including TNF-α and IFN-γ and they undergo increased phagocytosis with clearance by the reticuloendothelial system (210-212). Hydrophilic molecules like polyethylene oxide (PEO) and polyethylene glycol (PEG) are often added to scaffolds to reduce protein adsorption on the surface, this leads to reduced interactions with immune cells (213-215).

A study showed hydrophilic carbon nanofibers generated the smallest inflammatory response from macrophages compared to hydrophobic ones(216). Furthermore, hydrophobic carbon nanofibers led to increased macrophage pro-inflammatory cytokines including TNF- and IL-6, as well as expression of co-stimulatory markers CD80 and CD86 which may ultimately lead to increased T cell activation. This study suggested that the wettability of carbon nanostructured materials could be linked to macrophage behaviour to induce or minimise inflammatory responses and interaction with T cells (216).

1.6.7 Stiffness

The mechanical properties of a biomaterial can alter the T cell activation (217). However, as with a lot of the literature around immune responses to biomaterials, there are differences between mouse and human T cell responses and contrasting results to substrate stiffness effect (217). O'Conner *et al.* demonstrated primary human T cells activated on polydimethylsiloxane elastomer surfaces presenting anti-CD3 and anti-CD28 antibodies exhibited increased T cell expansion to soft (Young's modulus E ~100 kPa) vs stiff (E ~2 MPa) surfaces (218, 219). However,

the suggested mechanosensing of T cells is not a behaviour that is well defined or understood. In a study of mouse CD4+ T cells responding to polyacrylamide (PA) gels of varying stiffness, higher T cell activation was found with stiffer gels (E ~200 kPa) (220). A suggestion for the varied *in vitro* findings in human T cells are that the elastic moduli of the materials used are far higher than physiological tissues and that therefore T cells are mechanosensitive in nominally super-physiological ranges (221). Shi *et al.* demonstrated that stiffness can induce Tregs on PA gels within the Young's modulus range of 7.5kPa to 140kPa (chosen to mimic physiological stiffness ranges from liver to bone) (222). Tregs within this study were defined as those expressing FOXP3+ at day 3 culture (222).

1.6.8 Charge

Different exposed functional groups on nanorods were able to change surface activation markers and gene expression on immune cells (199). For example, amine-terminated nanorods became positively charged and shifted macrophages to an anti-inflammatory M2 phenotype. In contrast, positively charged particles were shown to cause greater activation of the inflammasome than negatively charged ones (199, 223). However, there appears to be conflicting evidence in the literature with regards to the effect of charge on the immune response. Carboxylic acid-terminated nanorods with a negative charge induced an M1 inflammatory phenotype, which is in contrast to other reports where carboxylated polylacticcoglycolic acid (PGLA), polystyrene or microdiamonds all with a negative charge, were able to suppress inflammatory macrophages (199, 224).

Two of the most commonly used, naturally-derived biomaterial scaffolds are alginate and hyaluronic acid, which is an ECM glycosaminoglycan, and they are both negatively charged at their surfaces (223). The naturally-derived polymers tend not to induce the typical FBR but a more favourable immune remodelling

reaction that has been associated with the adaptive immune response (225). It is difficult to uncouple related properties like hydrophobicity and chemical functionality, and the effect of negatively charged surfaces on immune activation is yet to be fully clarified.

1.6.9 Porosity

Porous biomaterials have been extensively investigated with uses in dental and bone implants (226). A study investigated the effects of fibrinogen as a porous scaffold in a bone injury model in mice, after implantation, the more porous fibrinogen scaffold promoted bone regrowth through altered cytokine gene expression and changes in local and systemic immune cell responses (227). A further study investigated varying pore size of electrospun polydioxanone, revealing a shift to M2 phenotype and function with increasing pore size (228). Many reports comment on optimal pore size in their modelling but this is conflicting across the literature and pores ranging from 20-1500μm have been successfully used for cartilage and bone formation (21, 229). Furthermore, pore size diameters of 300-400μm have been shown to provide the optimum dimension for bone formation in porous hydroxyapatite (230).

Immune cells crucially act as regulators of osteogenesis in order to progress bone regeneration (231). Optimal porosity of biomaterial structures is required to ensure these cells can infiltrate and interact with bone biomaterial constructs to achieve osteogenesis. Osteoprotegerin (OPG), a decoy receptor, interrupts receptor activation of receptor activator of NF-κB ligand (RANKL) inhibiting differentiation and function of osteoclasts (232). B cells are a major source of bone marrow-derived OPG, preventing osteoclastogenesis in normal physiological conditions (232, 233). In CD40/CD40L knock out mice, T cells were shown to work cooperatively with B cells to increase OPG production by CD40/CD40L co-

stimulation, and the mice were ultimately osteoporotic (233). Exposure to persistent excess inflammation with continuous pro-inflammatory cytokines (TNF-α, IL1-α, IL-1ß, IL-6) is associated with an increased RANKL/OPG ratio, increased osteoclast activity and a resultant bone loss effect (234).

Bone mineralisation has been shown to be dependent on the activity and availability of cytokines (231). TNF-α increased ALP activity and mineralisation by MSCs in a dose-dependent manner through activation of the NF-κB signalling pathway (235). Furthermore, knockout of IL-6 and oncostatin M (OSM) in the early stages of fracture healing causes reduced new bone deposition (236, 237). However, increased TNF-α has led to the differentiation of osteoblasts with pro-apoptotic effects due a suppression in BMP2 release (238). The effects of inflammatory cytokines may be dose and timing specific in their effect on osteogenesis aiming to reduce bone resorption and promote optimal bone formation (231).

Bone fracture healing is reliant on resident macrophages promoting osteoblast mineralisation and studies have shown a loss of bone formation in vivo with macrophage depletion (239). However, other studies using T and B cell knockout mice have shown significantly enhanced fracture healing in their absence implying the dual roles of immune cells in osteogenesis and evidencing the need for greater elucidation (240, 241).

Another consideration for bone biomaterial development is the requirement for the induction of vascular structure development. Porous structures allow for tissue integration, vascularisation and nutrient transport and have been associated with induction of iNOS representing an activation of the pro-inflammatory pathways. Pore sizes greater than 20μm have been associated with increased neovascularisation and a reduction in iNOS expression, representing a shift away

from the inflammatory M1 phenotype (230, 242). Whilst a larger pore size may have a beneficial effect on macrophage polarity and FBR, it is important to consider porosity within the perspective of structural integrity needed for the implanted bone biomaterial so that this is not compromised.

1.7 The role of Mesenchymal Stem Cells (MSCs) in biomaterials

For over 20 years the potential therapeutic use of MSCs has been investigated as an approach for several clinical regenerative strategies (243, 244). However, even after extensive clinical research, the question still remains if MSCs will live up to their foreshadowed therapeutic promise or whether they will fail to emulate pre-clinical animal research (244).

1.7.1 MSCs Properties

MSCs act on a number of immune cells and have immunomodulatory properties (245). Furthermore they can self-renew and differentiate into a number of cell types including, adipocytes, chondrocytes, osteoblasts and myofibroblasts in the presence of the appropriate molecular cues (243). Due to MSCs properties of immunomodulation, multilineage differentiation potential and relative ease at culture *in vitro* they have been regarded as the ideal source for the future of therapeutics for tissue regeneration (243). MSCs can be generated from either mesoderm or ectoderm and the most common source of MSCs in clinical trials is adult bone marrow (244). The first-in-human clinical trials involved MSC transfusion for haematopoietic recovery after high-dose myeloablative chemotherapy and successful treatment of graft versus host disease (GvHD)(246, 247). Following successful clinical translation it led to the use of both autologous and allogenic MSCs for acute tissue injury, chronic degenerative diseases and

inflammatory diseases (244). The use of allogenic MSCs has many advantages, they can be manufactured in high number (up to 1 million doses per donor for mass deployment), batch to batch consistency, availability for patients otherwise unsuitable for bone marrow aspiration, as well as facilitating the possibility of 'off the shelf' therapies for reconstruction at times of injury. To date, MSC therapies are largely available through clinical trials, with very few translational clinical treatments available due to regulatory issues and a lack of published clinical trial results (244).

1.7.2 MSCs immune properties

MSCs have been shown to effectively suppress T cell activation, proliferation and shift stimulated macrophages from an M1 to an M2 phenotype (245, 248-250). What is understood about MSCs action and properties has been identified largely through animal studies in murine systems, or in *in vitro* analysis of human MSCs (244). What has been identified is that under certain inflammatory conditions MSCs can release more TGFβ and suppress activated T cells by enhancing FOXP3 expression in Tregs (251-253). However, gaps in our understanding of the exact mechanism of MSC immunosuppression persist. MSCs can express a wide range of surface markers and common characterisation markers include CD73, CD105, CD90 and a lack of expression of CD45, CD34, CD14, CD19 and HLA-DR (245, 254, 255). However, differences exist between mouse and human clinical outcomes resulting in poor clinical translation at human phase III clinical trials (244).

A lack of clinical success at phase III trials versus promising animal pre-clinical trials may be attributed to differences in immune compatibility. MSCs have been hallmarked as being immune privileged for many years with the promise of

permissive adoptive transfer in allogenic immune-competent recipients without risk of rejection. However, this narrative is based upon pre-clinical animal models of MHC-matched syngeneic cells when assessing efficacy endpoints (244). It has been established subsequently that MSCs do express MHC class I molecules constitutively and can rarely express MHC class II molecules when exposed to cues from the inflammatory microenvironment (244, 256). A potential challenge for MSC therapy clinical translation may be to balance the need for 'off the shelf' pre-banked, donor, allogenic MSCs for time-critical conditions, with the need for the treatment to be immune tolerated by the recipient. It has been shown that measurable humoral alloimmunisation in human subjects receiving mismatched MSCs can be detected (257). The exact reason for the failure to meet endpoints in the phase III clinical trials remains largely unknown and very few studies have published their results.

1.8 Immunomodulation of biomaterials

A rapidly growing field of research is the design of biomaterials to modulate the immune response. A greater understanding of immune cell activation as well as receptor-ligand interactions has led to the development of materials-based strategies for treating disease (258). MSCs have been incorporated within biomaterials for several proposed clinical applications, from biomaterial-based wound dressings to bone or nerve regenerative materials (180, 259-261). The synergistic effects stems from MSCs' shelter within the protection of the material scaffold and ability to respond to biochemical or biophysical cues that alter their ultimate differentiation and potential for clinical utility (259).

An important concept for future immunomodulation of biomaterials is the interconnected nature of biomaterial physiochemical properties and an

appreciation that changes to any component will alter the immune responses. For example, changing the shape of the particle may also change the size, whilst altering a functional group on the surface has an impact on the surface charge and hydrophobicity (149, 201, 262, 263). Future biomaterials will need to understand the relative contributions of the different properties in modulating immune cell functions and interactions.

1.8.1 Biomaterials as immune signal delivery systems

In addition to the immunomodulation of the biomaterial physiochemical properties, an alternative approach to immunobioengineering is to design functional biomaterials with anti-inflammatory factors within the biomaterial construct for the purpose of orchestrating host immune cell responses. Polymeric scaffolds and hydrogels have been widely used for controlled release of therapeutic proteins, peptides, drugs and nucleic acids (264-267). Using anti-inflammatory factors to immunomodulate biomaterials could represent a new avenue to explore ways to control the local microenvironment and favourably tune interactions with the host immune system.

Previous *in vitro* studies have trialled different surface treatments for implant coatings with a view to exploring options for future surface immunomodulation at sites of implantation *in vivo*. Research groups have tested the passive release of dexamethasone (268-271), alpha melanocyte-stimulating hormone (α-MSH) (272-274), curcumin (275, 276) and vitamin E (277) *in vitro*, and the surface immobilisation of heparin (278, 279) and α-MSH (280). The results vary with many of these coatings eliciting reduced protein adsorption and leukocyte adhesion within *in vitro* models using human cells but with inconsistent translation to *in vivo* findings in mouse models where acute and chronic inflammatory responses still occurred (281, 282). No *in vivo* human trials have occurred.

Use of anti-inflammatory cytokines, immobilised within biomaterials, for sustained cytokine release is an emerging concept trialled for several potential medical applications (283-286). A gelatin hydrogel with polymer poly(amidoamine) functionalised with IL-10 *in vitro* exhibited sustained release of IL-10 reducing the inflammatory response of macrophages and microglia alongside the enhanced neurogenic differentiation of neural stem cells in a model of neural regeneration (286). Titanium oxide nanotubes functionalised with RGD peptide to release IL-4 were shown to drive macrophages to a predominantly anti-inflammatory state in an osteogenic environment (283).

DCs play a crucial role in initiating the adaptive immune responses to biomaterials and studies have shown reduced DC maturation when functionalised PEG hydrogels primed with immunosuppressive factors (TGF-β1 and IL-10) have been used (287). TGF-β1 and IL-10 are commonly used as soluble factors to program DCs in *vitro* and when immobilised in hydrogels, have been shown to retain bioactivity (287). Whilst promising, the focus of this work to date has been on macrophage polarisation and modulation of the innate immune response to biomaterials, using mouse models.

Biomaterials have also been used to model cancer *in vitro* to recapitulate key elements of the tumour microenvironment and have led to a greater understanding of cancer biology (288). These models have led to the development of cancer vaccines that have moved into the clinical trial phase but have also provided a wealth of knowledge and understanding of biomaterial T cell interactions (288). One such study reported delivery of C-C Motif Chemokine Ligand (CCL) 17 on a polyglyconate and gelatin scaffold to act as a chemoattractant for C-C chemokine receptor type 4 (CCR4) positive and CD8 positive T cells to pancreatic cells *in vivo*. Mice with these scaffolds demonstrated inhibited tumour growth and the

prevention of pancreatic cancer cells metastasising to the liver (289). Further work on this concept has shown promise for biomaterials as drug delivery systems that influence immune responses and cell behaviour. When used in conjunction with key immune checkpoint inhibitors such as anti-PD1 and anti-CTLA-4 therapies, the potential is for improved *in vivo* retention of antibodies at local tumour sites (290).

1.8.2 Biomaterials as T cell delivery systems

Biomaterials have been used to deliver the T cells themselves using scaffolds to increase the efficacy and longevity of T cell anti-cancer therapies. Additional benefits are controlled delivery of the T cells within a target area, negating the toxicity associated with large intravenous dosage of T cell therapies. The commonly used biomaterials for cancer immunotherapies are hydrogels composed of chitosan, polymerised alginate or hyaluronic acid. Recently, there has been a recent rise in the use of hydrogels for immunomodulation with a focus on enhancing the outcomes of cancer vaccines (258). Chimeric antigen receptor (CAR) T cell therapy is a type of immunotherapy which involves collection of patient T cells, subsequent engineering of those T cells to recognise and target a specific protein on cancer cells and readministration of these T cells back into the patient as a treatment (291). CAR T cell therapy has seen remarkable success in treating haematological malignancies but comes with significant limitations including on-target off-tumour effects, and toxicity, all of which could be potentially addressed through biomaterials research (292-294). Studies have further immune modulated CAR T cells to secrete cytokines into the tumour microenvironment including IL-2, IL-7, IL-15 and IL-18 (295-298). The majority of this work has been undertaken in immunodeficient mouse models, however, promising anti-tumour results were shown in *in vitro* trials using human cells taken from patients with chronic lymphocytic leukaemia (297). With the ability for biomaterials to deliver

both the cells and immune signals to local microenvironments, the potential applications beyond cancer therapies are only in beginning to be explored.

1.8.3 Biomaterials as MSCs delivery systems

Cell therapy holds promise as an alternative to autologous bone grafting for promotion of bone repair and fracture healing (260). Local factors that influence bone union include the defect size, the site of injury, the quality of the overlying skin and muscle and availability of an adequate blood supply (260). Use of biomaterials matrices with bone morphogenic protein (BMP2 or BMP4) has been shown to differentiate MSCs to an osteoblastic lineage in mouse models but translation to humans remains limited (260, 299). Another potential advantage for the development of bone biomaterials for large defect healing, is that MSCs lack major histocompatibility complex class II molecules (300). These cells have been shown to induce no T cell proliferation, even in allogenic conditions and may have immunosuppressive properties owing to an immune privileged phenotype (300-302). The possibility of successful MSC allogenic transplantation without immunosuppressive therapy makes MSCs the focus of a lot of regenerative medicine applications (207, 260). A number of material-based strategies have been explored for bone healing, including MSC culture *in vitro* on biomaterials prior to implantation into the injury site and use of growth factor adjuncts to promote vascularisation and osteoblast differentiation (67, 182). Despite extensive research on the functionality of MSCs incorporated into scaffolds or biomaterials, gaps persist in our understanding of how they then interact with both the innate and adaptive immune cells within the implantation microenvironment.

The next chapter in the development of regenerative bone biomaterials will involve improving the survival of implanted cells, ensuring vasculature ingrowth and the use of cytokines and growth factors to modulate the local microenvironment to

promote repair phenotypes to improve biomaterial functionality and outcomes. The next frontier for regenerative medicine is the design of biomaterials capable of tuning the local immune response at the implantation site. Control of the local immune response that is tailored to a specific biomaterial, in a specific tissue, for a specific local environment offers the potential to engineer biocompatible biomaterials that will integrate with the host. Despite recent advances, inconsistencies remain in the applicability of experimental findings *in vitro* compared with *in vivo* results for many biomaterials. Biomaterial interactions with both innate and adaptive immune responses need further elucidation to facilitate their optimisation. Additionally, the immunogenicity of biomaterials over time, throughout the degradation process also needs to be characterised. This will provide the knowledge to assess how material properties change and the impact of degradation by-products on the immune response to the biomaterial.

1.9 Hypothesis and aims

The hypothesis of this PhD was that functionalised allogenic MSC biomaterials will trigger human T cell activation responses *in vitro* that could affect their clinical utility. I aimed therefore to:

1. Establish an *in vitro* model to test human T cell activation responses to allogenic biomaterials

2. Define human T cell activation responses to allogenic MSC-based PEA+ fibronectin (FN) biomaterials in both their undifferentiated MSC and differentiated osteoblast condition

3. Trial altering the constituent biomaterial components and utilise the model to assess for altered T cell response

4. Trial modification of the local immune microenvironment to assess for altered MSC differentiation potential and altered T cell response

Chapter 2 Materials and Methods

2.1 Biomaterial preparation

2.1.1 Plasma polymerisation of nanoscale coatings

Tissue culture treated 24 well plates (*Corning*) or circular 12mm microscopy glass cover slips (*borosilicate glass D263^{TM} M, Marienfeld GmbH & Co. KG, Germany*) were prepared to be polymerised with ethyl acrylate (*Sigma, St. Louis, MO*) using a standardised plasma polymerisation protocol using a custom-built plasma reactor. The glass coverslips were cleaned by sonication in ethanol for 30 minutes and dried in a lab oven prior to use. The surfaces were cleaned using air plasma for 5 minutes at a controlled pressure of around 1.5-2.2 x 10^{-1} mbar. Subsequently, a second stage of plasma was run with monomer flow, to allow polymerisation of the surfaces. Inlet valves were used to control the chamber pressure, maintaining 1.5-2.3 x 10^{-1} mbar, whilst the plasma was running. After 60 minutes the process was complete with poly(ethyl) acrylate (PEA) nanoscale coatings applied to the tissue culture wells or glass cover slips.

2.1.2 Fibronectin and BMP2 adsorption to PEA coatings

The PEA-coated tissue wells or coverslips were sterilised under ultraviolet (UV) light for 20 minutes before functionalisation by adding a 200μl working concentration 20μg/ml fibronectin (FN) droplet onto the surface of a cover slip or 300μl droplet onto the surface of a 24 well. After one hour at room temperature, the unbound FN was removed, and the coverslips or tissue culture wells were washed with 300μl of phosphate-buffered saline (PBS) before adding 300μl of working concentration 50ng/ml bone morphogenic protein 2 (BMP-2). After one hour at room temperature, the growth factor was removed, and the cover slips or

wells were further washed with 300μl of PBS. The glass or PEA-coated cover slips or tissue culture wells with FN and BMP-2 adsorbed, were deemed to be functionalised and then immediately used for downstream experiments.

2.1.3 Laminin and BMP-2 adsorption to PEA coatings

The PEA-coated tissue wells were sterilised under UV light for 20 minutes before functionalisation by adding 300μl of working concentration 10μg/ml laminin onto the surface. After one hour at room temperature, the unbound laminin was removed, and the tissue culture wells were washed with 300μl of PBS before adding 300μl of working concentration 50ng/ml of BMP-2. After one hour at room temperature, the growth factor was removed, and the wells were further washed with 300μl of PBS. The PEA-coated tissue culture wells with laminin and BMP-2 adsorbed, were deemed to be functionalised and then immediately used for downstream experiments.

2.1.4 MSC culture with functionalised PEA biomaterials

MSCs were bought as primary cells (*Promocell, C-12974*) at passage (P) 0 and expanded in cell culture using mesenchymal stem cell (MSC) culture media [Appendix 1, 7.1] at P2 before storage in liquid nitrogen in 10% dimethyl sulfoxide (DMSO). For experiments, the P2 MSCs were defrosted by adding them to a 50ml falcon tube filled with MSC culture media and centrifuged at 400g for 5 minutes to remove the DMSO. The supernatant was then aspirated and MSCs resuspended in MSC culture media for cell counting using a haemocytometer. The MSCs were then used for the downstream experiments immediately by adding 100,000 MSCs to a T75 culture flask with 7.5ml of 'fast' MSC growth media *(Promocell, C-28009)* and 7.5ml of normal MSC growth media [Appendix 1, 7.1]. The MSCs in T75 flask were left in the 37°C with 5% CO_2 incubator for 2 days before aspirating the

supernatant and changing the media to 15ml of fresh normal MSC growth media per flask and returning them to the incubator for 3 further days. On day 5, trypsin with 1% ethylenediaminetetraacetic acid (EDTA) was used to release the cell bonds and free the adherent MSCs from the tissue culture flask so that they could be harvested. MSCs were added to the functionalised glass or biomaterial cover slip/wells at a concentration of 10,000 per slip for short term cultures of up to one week in duration or 2500 per cover slip/wells for longer cultures. The biomaterial and MSC co-culture were left for 3 days in the 37°C with 5% CO_2 incubator to allow them to form a monolayer on the biomaterial surface.

2.2 Cell Donors

Human MSCs were bought from Promocell, and donor information recorded from the company [Appendix 1, 7.1]. The purchased MSCs had come from the bone marrow of a femoral head and had been extensively quality control checked by the company. The donor MSCs exhibited 99% expression of stemness markers CD73, CD90, CD105 as well as 0% expression for differentiation markers CD14, CD34, CD45 , CD19 and HLA-DR. They had also been found negative for bacteria, fungi, mycoplasma, Human Immunodeficiency Virus (HIV-1 and HIV-2) as well as negative for hepatitis B and C viruses.

Healthy human blood volunteers were sought through word of mouth under University of Glasgow Research Ethics (*application ID: 300200112*). Volunteers were consented per ethical permissions and their consent forms stored. The thesis contains samples from 15 different donors (8 female: 7 male).

2.3 Cells

2.3.1 Cell culture

All cell culture was undertaken in a tissue culture hood under sterile conditions. Cells were incubated in a 37°C with 5% CO_2 incubator dedicated for human cell use.

2.3.2 PBMC isolation

The whole blood of healthy volunteers was obtained via venepuncture under ethics granted by the University of Glasgow (*application ID: 300200112*). Whole blood was layered in 3ml volumes on to 3ml of Histopaque (*Sigma-Aldrich, 11191*) in 15ml test tubes. These were then centrifuged at 400g for 30 minutes at room temperature to generate a density gradient, from which the opaque layer of mononuclear cells was aspirated from each 15ml tube and placed into a new 50ml tube. The cells were washed in 10ml of PBS and centrifuged for a further 300g for 10 minutes. The wash step was repeated twice. The PBMCs were then ready for use in downstream experiments.

2.3.3 Monocyte isolation

Whole blood was taken from healthy volunteers and PBMCs isolated per previous methodology [2.2]. The PBMCs were then added to a 50ml falcon tube and diluted using serum-free Roswell Park Memorial Institute (RPMI) media [7.1] and centrifuged at 400g for 5 minutes. The cells were diluted with media and placed in the 5% CO_2 incubator for 2-3 hours. This allowed the monocytes to adhere to the bottom of the wells. Each well was then washed with culture media leaving only the adherent monocytes (that comprised 10% of the total PBMCs). Approximately 10^6 monocytes were retrieved from 10 x 10^6 PBMCs added per well. A solution containing 50ng/ml of research grade human GM-CSF (*Miltenyi Biotech, 130-093-*

862) in RPMI complete medium [Appendix 1, 7.1] was added per in a 6 well flat-bottomed plate. The cells were placed in the 5% CO_2 incubator at 37 degrees for 3 days.

2.3.4 Macrophage differentiation

On day 3 of monocyte culture, 1ml of cell culture media was removed from each well and replaced with 1ml of fresh complete RPMI media supplemented 50ng/ml with GM-CSF and added back into the 37 degree/5% CO_2 incubator for a further 3 days. On day 6, IFNγ (*Stemcell, 78020.1*) and lipopolysaccharide (LPS) (*Merck, L2880*) was added for the last 18 hours of cell differentiation to obtain fully polarised and mature M1 macrophages. A 1ml volume of fresh complete media was added to the wells to obtain a final concentration of 50ng/ml IFNγ and 10ng/ml LPS in the culture and then the cultures were placed back in the 5% CO_2 /37°C incubator overnight.

To harvest the macrophages off the 6 well culture plates, cells were trypsinized in 1ml of trypsin per well for at least 5 mins in the 5% CO_2 /37°C incubator and harvested into a fresh 15ml tube. A cell scraper was used to help free the macrophages off the bottom of the tissue culture plate. The trypsin containing macrophages were centrifuged at 400g for 5 minutes and resuspended in fresh culture media. Macrophages were added to a 24 well plate by plating at 300,000 cells/well for downstream applications.

2.3.5 PBMC storage and thawing

PBMCs for storage were suspended in freezing media [7.1] at a concentration of 1-5 x 10^6 cells per 1ml. The cells are stored in liquid nitrogen appropriate freezing Eppendorfs and labelled with date, concentration of cells, anonymised donor identification number and the cell type, i.e. PBMCs. The samples were frozen

slowly at -80° in a Styrofoam box before being transferred to a storage box after 24hrs.

PBMC samples were defrosted quickly in a water bath and added to a 50ml tube of PBS or culture media, depending on if for cell culture or flow cytometry antibody staining. They were centrifuged at 400g for 5 minutes to remove the DMSO freezing media from the cells. The cell supernatant was discarded, the cells were resuspended in culture media or PBS for cell counting [2.3.9] and used in downstream applications.

2.3.6 T cell priming by bead activation

Isolated PBMCs were activated using T cell TransAct anti-cluster of differentiation 3 and 8 (aCD3/aCD28) activator [*Miltenyi Biotech, cat 130-128-758*]. A series of optimisation experiments were undertaken to ascertain the optimum dose of the activator to use and the duration of culture with the activator [3.3.3, 0, 0, 3.3.9, 3.3.10].

Stock aCD3/aCD28 activator was recommended to be used at 1:100 where 10μl was added to a 48 well with 990μl of culture media containing 2 million PBMCs. Ultimately, this protocol was optimised, and stock was diluted 1 in 5 to prepare a working stock. From which 10μl of working stock was then added to 990μl of culture media per 48 well containing 2 million PBMCs (an ultimate 1:500 dilution of stock). The PBMCs were incubated with the reduced dose of TransAct T cell aCD3/aCD28 activator for 24 hours at 37°C with 5% CO_2.

2.3.7 T cell activator removal and cell rest

After 24 hours of T cell aCD3/aCD28 activator culture, the cells were harvested into a 50ml tube containing at least 10ml of culture media before centrifugation at 300g for 10 minutes. The supernatant was then aspirated and discarded, and the

cells were then resuspended in a further 10ml of culture media. The washes were undertaken 3 times. After this, the cells were counted [2.3.9] and plated in a new 48 well plate at a density of 1-2 x 10^6 PBMCs per well in culture media and allowed to rest in the 37°C with 5% CO_2 incubator for 24 hours. These PBMCs were now considered to contain primed T cells ready for downstream experiments.

2.3.8 T cell reactivation

Where experiments necessitated positive controls consisting of reactivated T cells, T cell reactivation was undertaken using the activator. After T cell priming and subsequent rest [2.3.6-2.3.7], the positive controls were exposed to a further 10μl of a working stock (1:5 dilution of stock activator) in 990μl of T cell culture media (ultimate 1:500 dilution of stock) [7.1]. They were then cultured for 3 days in the 37°C with 5% CO_2 incubator until flow cytometry analysis.

2.3.9 Cell counting

For each sample, 10μL was mixed with 10μL of 0.04% Trypan blue. 10μL of this solution was added add to a haemocytometer with a glass cover slip. Routinely, five haemocytometer squares were counted. If <100 cells were counted, then all 25 haemocytometer squares were counted to increase the accuracy of the cell number calculation. Total cell numbers were calculated using the following formula:

Cell count x (25/Number of squares counted) x Dilution factor (2) x 10^4 x Sample Volume = Total number of cells in the sample

2.4 Co-culture conditions

2.4.1 Co-culture of MSC biomaterials with T cells

The biomaterial and MSC co-cultures were incubated for 3 days at 37°C with 5% CO_2 to allow the MSCs to form a monolayer on the biomaterial surface. During this time, human PBMCs were isolated, and the T cells were activated ('primed') and subsequently rested for 24 hours [3.3.1, 3.3.4]. Once rested, the T cells were then harvested, counted and 1 x 10^6 cells added into the co-culture with the functionalised biomaterial and the established MSC monolayer for 24 to 48 hours. T cells in the supernatant were then removed and a series of wash steps with PBS, were undertaken to release as many T cells from the surface as possible for analysis [7.1].

2.4.2 Co-culture of MSC biomaterials, T cells and macrophages

The biomaterial MSC co-cultures, as well as the priming of the T cells were established as per previous methods [2.3.1]. A different biological donor PBMC isolation was undertaken to isolate monocytes and differentiate these into macrophages as per previous methods [2.2.3 - 2.2.4]. The macrophages were then harvested, counted and added to the MSC biomaterials in 24 well plates at a density of 300,000 macrophages per well. The primed T cells were then added at a density of 1 x10^6 per well. The three-cell co-culture was incubated for 24-48hrs at 37°C with 5% CO_2. Following this, the T cells in the supernatant were then removed and a series of wash steps with PBS were undertaken to release the T cells from the surface of the biomaterial into the supernatant for analysis.

2.4.3 Co-culture of T cells and macrophages

T cells were primed and rested as per previous methods [2.3.6-2.3.7]. A different biological donor PBMC isolation was undertaken to isolate monocytes and

differentiate these into macrophages as per previous methods [2.3.3-2.3.4]. The macrophages were then harvested, counted and added to 24 well plates at a density of 300,000 per well. The primed T cells were then added to the macrophages at 1 x10^6 per well. The co-culture was incubated for 72-120hrs at 37°C with 5% CO_2. Following this, the supernatant was harvested, and the T cells stained for flow cytometry analysis.

2.4.4 Conditioned 'proinflammatory' media

For experiments involving the use of conditioned 'proinflammatory' media this was made in advance in a larger batch from the supernatant of proinflammatory M1 macrophages. Due to the volume of monocytes needed to create enough media, a leukocyte cone was sourced from the Non-Clinical Issue Department at NHS Blood & Transplant. A PBMC isolation was undertaken as per previous methods [2.3.2]. The PBMCs were then diluted to 50ml in a falcon tube using serum-free Dulbecco's Modified Eagle Medium (DMEM) media containing 5ml of L-glutamine and 5ml of penicillin-streptomycin and centrifuged at 500g for 5 minutes. The cells were then resuspended in 20ml of serum-free DMEM for counting. The cells were then diluted to 15 x 10^6 PBMCs per T150 flask in 30ml of serum-free culture media and placed in the 5% CO_2 at 37°C incubator for 3 hours.

After the monocytes had had time to settle and adhere to the bottom of the T150 flasks, the culture media was removed from each flask and the flasks were washed gently with 15ml of serum-free media 3 times. The remaining adhered cells were predominantly monocytes and 30ml of complete DMEM media containing a working concentration of 50ng/ml human GM-CSF was added to each T150 flask. The flasks were all returned to the 5% CO_2 at 37°C incubator for 3 days.

On day 3 of the monocyte culture, 15ml of supernatant was removed from each T150 flask and replaced with 15ml of fresh complete DMEM media supplemented with a 50ng/ml working concentration of GM-CSF. The flasks were all returned to the 5% CO_2 at 37°C incubator for 3 further days.

On day 6 of the macrophage differentiation, 15ml of supernatant was carefully removed from each T150 flask and replaced with 30ml of fresh DMEM complete media supplemented with 50ng/ml IFNγ and 10ng/ml LPS. This increased the total volume of culture media per T150 to 45ml. The flasks were then placed back in the 5% CO_2 at 37°C incubator for 48 hours. The supernatant from each T150 flask was then aspirated being careful to not disturb the adhered macrophage cell layer and centrifuged at 3000g for 30 minutes to remove any cells or debris. The supernatant was then removed and placed into a sterile culture media bottle before aliquoting and freezing at -20°C for storage, until use in downstream experiments. The conditioned proinflammatory media was characterised using the Luminex plates [Appendix 2, 7.2] and the cytokines and chemokines found within [Appendix 4, 7.4].

2.4.5 Culture with conditioned ‘proinflammatory’ media

When conditioned ‘proinflammatory’ media was required, an aliquoted frozen falcon tube was defrosted in a water bath. This was then prepared at a ratio of 50:50 with freshly prepared MSC culture media that was prepared with double concentration of media additives to account for the deficits in the pro-inflammatory media and to increase the glucose concentration to the 8g/L high glucose required to culture with MSCs [Appendix 1, 7.1].

2.5 Preparation of cells for flow cytometry

2.5.1 Surface antibody staining of cells

Samples were first incubated with 50μl of 1:200 solution of FC receptor blocking solution [Table 1] and flow cytometry staining (FACS) buffer (PBS, 2% FCS, 1mM EDTA) for 15 minutes at 4°C [Appendix 1, 7.1]. Subsequently, 50μl of surface antibody mix [Table 1] made up to 2X concentration was added to each sample and incubated for 20 minutes. Cells were then washed twice in PBS.

2.5.2 Viability staining

Viability staining differentiates between live and dead cells. Following surface antibody staining and subsequent wash steps, 100μl of eFluor 506 or eFluor 780 viability dye was added at 1:1000 diluted in PBS for 20 minutes at 4°C. The choice of viability dye depended on the flow cytometry antibody panel used for the independent experiments. Cells were then washed in FACS buffer twice before being resuspended in a final volume of 200μl of FACS buffer. Samples were then fixed using 4% paraformaldehyde (PFA) solution with 100ul added to each well and incubated at 4°C for 20 – 30 minutes. Samples were then transferred to FACS tubes through nitex and acquired on either the LSR Fortessa II or Celesta flow cytometers (*both BD Biosciences*) depending on panel.

2.5.3 Intranuclear antibody staining for transcription factors

Following surface antibody and viability staining [section 2.4.1 – 2.4.2] the cells were fixed in 200μl of True-Nuclear fixing solution (*Miltenyi Biotech, cat 424401*) for 45 minutes at room temperature. The cells are then washed three times with 200μl of perm buffer (1X) at 400g for 5 minutes centrifugation. The cells are then stained for 60 minutes in a volume of 50μl of 1:100 dilution of antibody mix with

perm buffer at 4°C [Table 1]. Following staining, the cells are washed three further times with perm buffer at 400g for 5 minutes before being resuspended in 200μl of FACS buffer for flow cytometry.

2.5.4 List of antibodies used for flow cytometry

Antibody	Fluorochrome	Clone	Dilution or Concentration	Manufacturer
Human TruStain FcX™ (Fc Receptor Blocking Solution)	-	-	1/200	Biolegend Cat 422302 AB_2818986
Viability	efluor 506	-	1/1000	eBioscience Cat 65-0866-14
Viability	efluor 780	-	1/1000	eBioscience Cat 65-0865-14
CD3	BV 785	OKT3	1/100	Biolegend Cat 317330 RRID: AB_2563507
CD4	BV 711	OKT4	1/100	Biolegend Cat 317440 RRID: AB_11219404
CD8	PerCP/Cy5.5	SK1	1/100	Biolegend Cat 344710 RRID: AB_2044010
CD19	PE/Cy7	HIB19	1/200	Biolegend Cat 302216 RRID: AB_314245
CD25	FITC	BC96	1/100	Biolegend Cat 302604 RRID: AB_314273
ICOS	PE/Cy7	C398.48	1/100	Biolegend Cat 313520 RRID: AB_10641839
PD1	PE	A17188A	1/100	Biolegend Cat 379210 RRID: AB_2922607

CD14	BV421	HCD14	1/200	Biolegend Cat 325628 RRID: AB_2561342
CD16	FITC	3G8	1/200	Biolegend Cat 302006 RRID: AB_314205
HLA-DR	Pe-Cy7	L243	1/200	Biolegend Cat 307616 RRID: AB_493588
ALP	APC	B4-78	1/100	R&D Systems Cat FAB1448A RRID: AB_357039
HLA-DR	BV785	L243	1/200	Biolegend Cat 307641 RRID: AB_2561360
FOXP3	PE	QA18A03	1/200	Biolegend Cat 364704 RRID: AB_2892441
GATA-3	BV 421	16E10A23	1/200	Biolegend Cat 653814 RRID: AB_2563221
T-bet	PE-Cy7	eBio4B10	1/200	eBioscience Cat 25-5825-82 RRID: 11042699
RoRyt	APC	AFKJS-9	1/200	eBioscience Cat 17-6988-82 RRID: AB_10609207

Table 1: List of antibodies used for flow cytometry

2.6 Biomaterial preparation for imaging analysis

2.6.1 Immunofluorescence staining

Tissue culture 24 well plates containing functionalised FN PEA biomaterials with MSCs were allowed to culture until 28 and 35 days. At these time points, the plates were fixed using 300μL of a 4% formaldehyde fixative, per 24 well, for 5 minutes in the 37°C with 5% CO_2 incubator. The fixative was then removed from each well and the cells washed with 1X PBS. The wells were then incubated at 4°C with 400μL of permeabilisation buffer for 5 minutes. The permeabilization buffer was removed and 400μL of PBS with 1% BSA was added to each well and incubated for 5 minutes at 37°C as a blocking step. The blocking buffer was then removed, and the primary antibodies added at a total volume of 300μL per well at the appropriate concentrations [Table 2]. The plates were then wrapped in foil and incubated at 37°C for one hour. After the hour, the antibodies were removed, and the wells washed with PBS with 0.5% tween on a slow swirl plate shaker three times. For those only needing a primary antibody stain, these were then stored in 500ml of PBS per 24 well, wrapped in foil at 4°C until the day of imaging. For antibody stains requiring a secondary antibody incubation, these were added in a total volume of 300μl and incubated at 37°C for a further hour, before removal of antibody and a subsequent three PBS with 0.5% tween plate shaker washes. These were then stored in 500ml of PBS per 24 well, wrapped in foil at 4°C until the day of imaging. On the day of imaging, the PBS was removed from each well and 20μL of vectorshield DAPI was added to each well with a glass cover slip placed on the top. Imaging was undertaken on a Nikon Eclipse Ti2 Confocal microscope and analysed using Fiji, Image J software (303).

2.6.2 List of antibodies used for immunofluorescence staining

Antibody	Fluorochrome	Clone	Dilution or Concentration	Manufacturer
Osteopontin	Unconjugated	Ag19216	1/100	Proteintech Cat 22952-1-AP RRID: AB_2783651
Osteocalcin	Unconjugated	Ag20065	1/100	Proteintech Cat 23418-1-AP RRID: AB_2879275
Secondary anti-rabbit	568 red	Polyclonal	1/500	Thermo Fischer Cat A-11011 RRID: AB_143157
Phalloidin Green	-	-	1/200	Proteintech Cat PF00001
Phalloidin Red	-	-	1/1000	Abcam Cat ab235138 RRID: unknown
HLA-DR	FITC	AC122	1/50	Miltenyi Biotech Cat 130-113-401 RRID: AB_2726157
HLA-DR isotype	FITC	AC122	1/50	Miltenyi Biotech cat 130-113-271 RRID: AB_2733685

Table 2: List of antibodies used for immunofluorescent staining of cells for microscopy

2.6.3 Quantification of immunofluorescence

Images were analysed in Fiji by Image J (303). Colour thresholds were set using appropriate controls and maintained the same for all compared images. Multiple images were taken per well and after setting the colour threshold, used to calculate an average image intensity for that well normalised to the cell number within the well. All averages were a mean of 6 images per well.

2.6.4 Alkaline phosphatase assay

The 24 well culture plates containing day 35 (D35) aged osteoblasts on the fibronectin biomaterials were fixed using 4% paraformaldehyde for 30 minutes at room temperature. The assay was then performed using the Alkaline Phosphatase Kit (*Sigma-Aldrich, Cat. 86C-1KT*) and performed per manufacturer's instructions. The plates were then immediately imaged on an EVOS microscope (*Thermofisher*).

2.6.5 Alizarin red staining

The 24 well culture plates containing D35 aged osteoblasts on the fibronectin biomaterials were fixed using 4% paraformaldehyde for 30 minutes at room temperature. The cells within the wells were then stained using 2% alizarin red monosodium salt (*Sigma, cat. 130-22-3, pH 4.2*). The extracellular matrix was stained for 30 minutes using 1% Alcian blue in 3% acetic acid (*Sigma, cat. B8438, pH 2.5*). The wells were then washed twice in 3% acetic acid. The plates were then immediately imaged on an EVOS microscope (*Thermofisher*).

2.7 Quantitative polymerase chain reaction (qPCR)

2.7.1 RNA purification

RNA purification from the cells within the biomaterial was undertaken using RNeasy Micro Kits (*Qiagen, cat. 74004*). Cells were harvested from the 24 well biomaterial coated plates in 350μl of 'Buffer RLT' that had been added to each well to homogenize them. The lysate was centrifuged for 3 minutes at maximum speed before the supernatant was removed by pipetting. The manufacturer's standard protocol was then followed to purify the RNA; however, centrifugation steps were optimised, and full procedure was as follows. One volume of 70% ethanol was added to the aspirated lysate supernatant and mixed well by pipetting up and down. The sample was transferred to the 'RNeasy MinElute' spin column placed in a 2ml collection tube. The lid to the spin column was closed and it was centrifuged for 1 minute at >8000g. The flow through was discarded and 350μl of 'Buffer RW1' was added to the 'RNeasy MinElute' spin column. The lid was closed, and the sample was centrifuged for another 1 minute at >8000g. The flow through was again discarded and 10μl of 'DNase I stock solution' was added to 70μl of 'Buffer RDD' and mixed by inverting the tube. This mix (80μl) was then added to the 'RNeasy MinElute' spin column membrane. The samples were then placed on the benchtop and incubated at room temperature for 15 minutes.

A further 350μl of 'Buffer RW1' was then added to the columns before centrifugation for 1 minute at >8000g. The collection tubes were then discarded, and the spin columns placed into new 2ml collection tubes. 500μl of 80% ethanol was then added to the spin column, the lids were closed and centrifuged for a further 2 minutes at >8000g. The spin columns were placed into fresh collection tubes and the lids were opened before centrifugation at full speed for 5 minutes to

dry the membrane. The flow through and collection tubes were all discarded keeping only the spin columns. These spin columns were placed into one final fresh collection tube and 14μl of RNase-free water was added directly to the centre of the column membrane, the lids were closed, and the columns centrifuged for 1 minute at full speed, to elute the RNA. The RNA concentration was quantified by nanodrop before progressing with reverse transcription.

2.7.2 cDNA synthesis

The reverse transcription process was carried out on the extracted RNA to synthesis cDNA using QuantiTect Reverse Transcription Kit *(Qiagen, Cat. 205311)*. A total 12μl of quantified RNA sample and 2μl of gDNA wipeout was added to a 0.2ml PCR tube to cleave any remaining DNA. The samples were then placed in a PCR block on a ProFLex PCR System (*Applied biosystems*) for 2 minutes at 42°C followed by an infinite hold at 0°C, to enable gDNA elimination. A master mix was made on ice for the number of reactions required (1μl reverse transcriptase, 4μl RT buffer and 1μl RT primer mix per reaction). Once gDNA elimination was complete, 6μl of the master mix was added per sample before transferring them back into the PCR block for the reverse transcription reaction (30 minutes at 42°C, then 3 minutes at 95°C and finally a 0°C infinite hold). Reverse-transcription samples were stored at -20°C until the following morning when they were used for the qPCR reaction.

2.7.3 RT-qPCR

For qPCR, all sample concentrations were normalised to 2ng/μl. Per sample, 20μl aliquots were prepared with the amount of cDNA volume (guided by quantified RNA concentration values) and the UltraPure water (Invitrogen) was added to make the volume up to 20μl per sample. A master mix was made for the total

number of samples using the QuantiNova SYBR Green PCR Kit (*Qiagen, cat. 208054*). A total 10μl of SYBR Green mix was added to 7.7μl of DNase-free water, 0.1μl of Rox dye, 0.1μl of forward primer and 0.1μl of reverse primer [Appendix 5, 7.5]. A 96 well qPCR reaction plate (*Applied biosystems*) had 2μl of previously prepared sample aliquots, with 18μl of the SYBR green qPCR master mix loaded into each of the wells. Each sample was conducted in duplicate. The plate was sealed and gently spun down before being placed in a 7500 Fast Real-Time PCR System (*Applied biosystems*). The program consisted of a 20 second holding stage at 95°C before 40 cycle stages (3 seconds at 95°C , then 30 seconds at 60°C). After the 40th cycle, a melt curve analysis of qPCR was conducted and the data exported to excel for analysis. The ΔCT value was generated by subtraction of the housekeeping gene (GAPDH) from the CT value generated per sample. An average was taken of each sample's technical replicates and the ΔΔCT value was determined by taking the sample ΔCT value from the control ΔCT value.

2.8 Luminex

2.8.1 Luminex plate design

5 different Luminex plates were bought to assess 74 analytes in 74 samples with appropriate controls [Appendix 2, 7.2]. The plate design for samples is shown in

Figure 2-1.

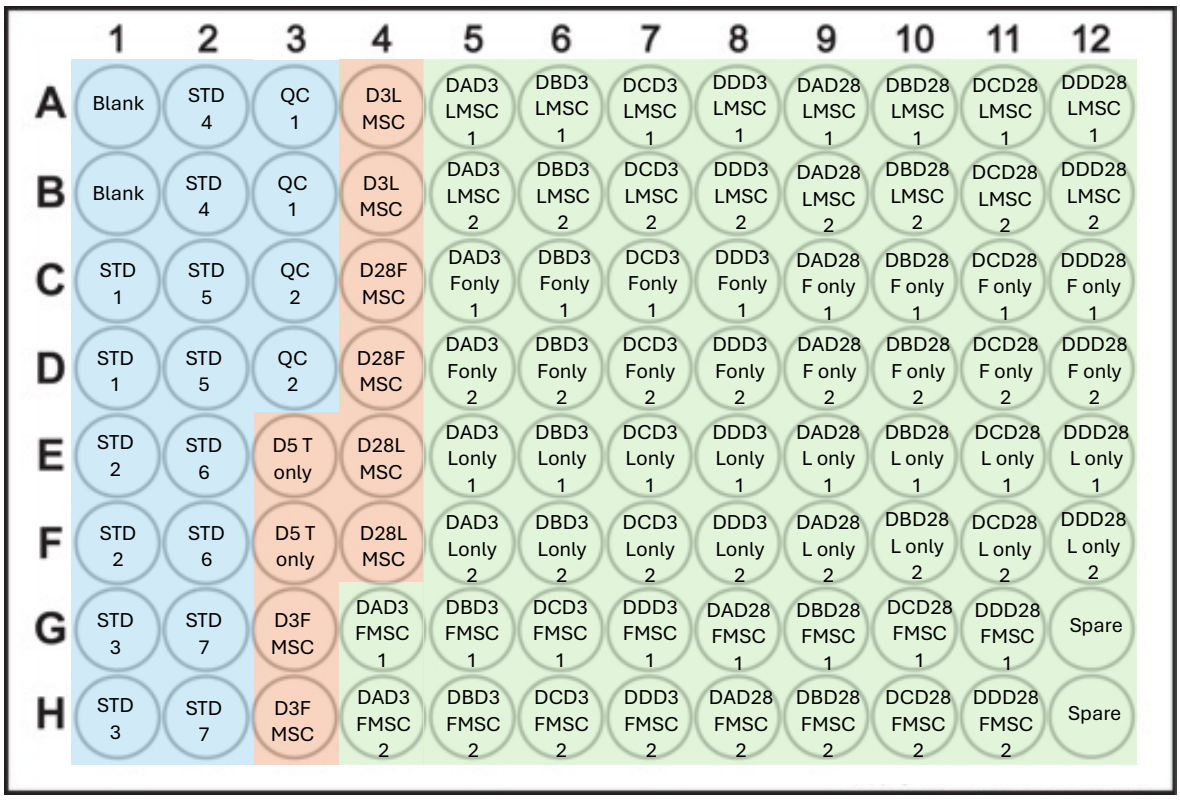

Figure 2-1: Plate set up for the analysing 3 co-culture supernatant samples. Blank, standard (STD) and quality control (QC) shown in blue are Luminex technical controls. Experimental biological controls are shown in orange including day 5 (D5) T cell only supernatant, day 3 FN with MSC biomaterials only (D3F MSC) or laminin (D3L MSC), day 28 FN with MSC biomaterials only (D28F MSC) or laminin (D28L MSC). The 64 samples are shown in green. Labelled as donor (D) with donor A, B, C or D, followed by day 3 or 28 (D3 or D28). Fibronectin (F) or laminin (L) only or with MSCs. All samples analysed in replicate. Biological n=4 in technical duplicate.

2.8.2 Sample preparation

Tissue culture supernatant samples were removed from the various MSC biomaterial-T cell co-culture wells and placed into pre-labelled Eppendorfs. These were centrifuged at 8000g for 10 minutes to remove any debris or cells. From these the supernatant was harvested into fresh Eppendorfs for freezing and stored at -80°C until sample preparation for Luminex assay.

2.8.3 Immunoassay procedure

All reagents were warmed to room temperature before use. 200μl of 'Assay Buffer' was added into each well of the 96 well custom-made Luminex plates [Appendix 2, 7.2]. Manufacturer's standard protocol was then followed as detailed. The plate was sealed and mixed on a plate shaker for 10 minutes at room temperature. The assay buffer was then decanted and removed from all wells by inverting the plate and tapping it onto absorbent towels several times.

Each standard or control was added in 25μl volumes into the appropriate wells and 25μl of 'Assay Buffer' was added to the background well and sample wells. A further 25μl volume was added of 'matrix solution' to the background, standards and control wells. Each sample was added to the sample wells in 25μl per well volumes. The premixed beads bottle was vortexed and added in 25μl volumes to each sample well. The plate was sealed and then wrapped in foil and incubated with agitation on a plate shaker overnight for 20 hours at 4°C.

The following day the contents of each well were gently removed, and the plate was washed 3 times using a magnetic plate washer. After washing, 50μl of room temperature 'Detection Antibodies' were added into each well. The plate was sealed, recovered with foil and incubated on a plate shaker for 1 hour at room temperature. The 'Detection Antibodies' were subsequently left in the wells and

50μl of streptavidin-phycoerythrin was also added to each well. The plate was sealed, covered in foil and incubated with agitation on a plate shaker for 30 further minutes at room temperature. Following incubation, the well contents were gently removed, and the plate was washed 3 times using the magnetic plate washer. 'Sheath Fluid PLUS' was added at 100μl to each well and the plate was placed on a plate shaker for 5 minutes to resuspend the beads.

2.8.4 Data analysis

The plates were run on a Luminex® 200™ instrument and the mean fluorescent intensity (MFI) data was saved and analysed using a 5-parameter logistic method for calculating analyte concentrations in samples.

2.8.5 GraphPad Prism statistical analysis

All data are expressed as mean plus standard error of mean. All statistical tests were undertaken on GraphPad Prism software, version 9.4.1 (*GraphPad software, San Diego, CA, USA*). All data was tested for normality using the Shapiro-Wilk normality test. In data that was normally distributed, significance was calculated using paired t-tests for comparison between two groups and a one-way ANOVA with Šídák's multiple comparisons test when more than two groups were compared. In data not normally distributed, a Wilcoxon matched pairs signed rank test was undertaken to compare two groups. P values = *p<0.05, **p<0.01, ***p<0.001, ****p<0.0001.

Chapter 3 Building an in *vitro* model of primed T cells

3.1 Introduction

The literature demonstrates ever-advancing biomaterials capable of promoting bone regeneration (67, 181, 227, 299). The possibilities for reconstructive surgery if bone regeneration can be assisted by these 'off the shelf' biomaterials are significant and would represent a cornerstone for the future surgical management of patients with critical bone loss (231, 304).

For 'off the shelf' therapies to be utilised in clinical surgical practice for bone injury, they require the addition of MSCs that are readily available at the time of injury requiring surgical fixation. For open fractures, this is within 72 hours of injury (305). Therefore these MSCs will be allogenic to the recipient patient and either from a single donor source or a pooled bank of donor MSCs (306). Further rationale for the use of allogenic, pooled bank MSCs, is for regulatory and quality control reasons. Use of a stock bank MSCs allows for each batch to have full viral, bacterial and other contaminant testing as part of preclinical safety testing, in a way that individual donors for autologous MSCs don't. This ensures more detailed product characterisation and less individual variation in bioefficacy than would be the case for autologous cell donors. Finally, for the management of non-union, or for patients with high risk factors for poor bone healing, there may be clinical benefit and rationale to not use their autologous cells and instead use cells from a donor or donor pool known to have good healing propensity.

However, with the use of any allogenic cells, there is a theoretical risk of adaptive T cell immune responses and the possibility for acute or chronic rejection of the cellularised biomaterials due to the development of an alloresponse (307). Whilst MSCs have been described as immune ‘evasive’, advancing biomaterials cause differentiation into target cells which may provoke immune responses (308).

Human data are required for translation of promising in vivo animal model bioengineered technologies. To date there have been 13 clinical trials using MSCs biomaterials of which only 1 was using allogenic cells (309). This trial is the only one to publish preliminary results and at date of publication, for just 3 patients (310). All 3 patients had significant bone resorption at the biomaterial site between 6 – 12 months post implantation, shown on computerised tomography (CT) scan. As the surgery had reconstructed cranial defects, the authors were unable to obtain samples for histopathology so were unable to determine if this resorption was due to physical biomaterial failure to unite with the surrounding native bone, or due to resorption through alloresponses against the allogenic MSCs. The poor clinical translation of promising animal in *vivo* work is well established (311-313), for safer bench to bedside clinical translation, there is a need for in *vitro* human models capable of identifying possible poor translation before reaching patients (314). In a move to address this demand, the U.S. House of Representatives signed off on the ‘FDA Modernization Act 2.0’ in 2022 (315). This Act recognised the lack of specific human disease relevance and predictability in most animal modelling and removed the necessity to perform preclinical animal models. A much smaller animal trial is still required to demonstrate dose safety and efficacy, but the Act has significantly reduced the requirement for preclinical trial animal testing in the initial drug discovery and development of potential therapeutic

interventions for human disease (315). Unfortunately, no reflection of this has yet been enacted in the UK, at the MHRA level.

Models to assess the human immune response in *vitro* have been established, but predominantly focussed on the innate human immune responses of macrophages (316-318). Most immune interactions with biomaterials are focussed on macrophage polarisation and responses in *vivo* in mouse models (316, 319). The lack of adaptive immune response in *in vitro* modelling likely reflects the difficulty in establishing T cell responses that reflect the *in vivo* environment. T cells are usually exposed to antigen on APCs in the lymph node *in vivo* as a key initiating event and subsequent exposure to this antigen then triggers downstream rejection responses (320). This initiating event in lymph nodes cannot be replicated *in vitro* and therefore models of T cell responses become complicated to design.

3.2 Aims

- To establish an *in vitro* model capable of assessing human T cell activation responses to cellularised biomaterials

- To establish a method for priming of human T cells *in vitro* so that they can respond to antigen appropriately, without continuing to mount activation responses in the absence of further stimuli

3.3 Results

3.3.1 T cell priming using aCD3/aCD28 activator

For the *in vitro* T cells to be capable of mounting activation responses *in vitro*, in the absence of APCs, I needed to activate them. I chose to use a commercially available activator composed of beads coated in anti-CD3 and anti-CD28, as

these are reliable and easily available for consistency. Choice of T cell activator was determined based on a comparison of CD25+ expression in PBMCs activated for 3 days at each of the manufacturers recommended dosing [Figure 3.2]. Two different activators were compared; Miltenyi Biotech (Miltenyi) aCD3/aCD28 TransAct activator (*cat 130-128-758*) and Stemcell ImmunoCult™ aCD3/aCD28 activator (*SC, cat 10971*).

The Miltenyi activator led to higher T cell activation for both CD4+ and CD8+ cells [Figure 3.3]. Following activation with the Miltenyi activation, 76.8% of CD4 T cells expressed CD25 compared to 45.1% after Stemcell activation [Figure 3.3]. Furthermore, 83.7% of CD8 T cells activated by Miltenyi expressed CD25 versus 68.4% for Stemcell activation. Furthermore, Miltenyi activated T cells showed evidence of greater ‘blasting’ activity compared to Stemcell activated T cells. ‘Blasting’ is a term that refers to changes that an activated T cell typically undergoes including; doubling their size, their protein contents and increasing their total RNA contents 30-fold to prepare for proliferation (321). Miltenyi activated CD4+ T cells saw 75% ‘blasting’ (45.7% Stemcell activated) and Miltenyi CD8+ T cells had 79.6% ‘blasting’ (70.3% Stemcell activated).

The Miltenyi aCD3/aCD28 activator was concluded to be the superior activator based on CD25 expression and evidence of ‘blasting’ by flow cytometry. Miltenyi T cell TransAct aCD3/aCD28 activator, therefore, was used for the downstream modelling.

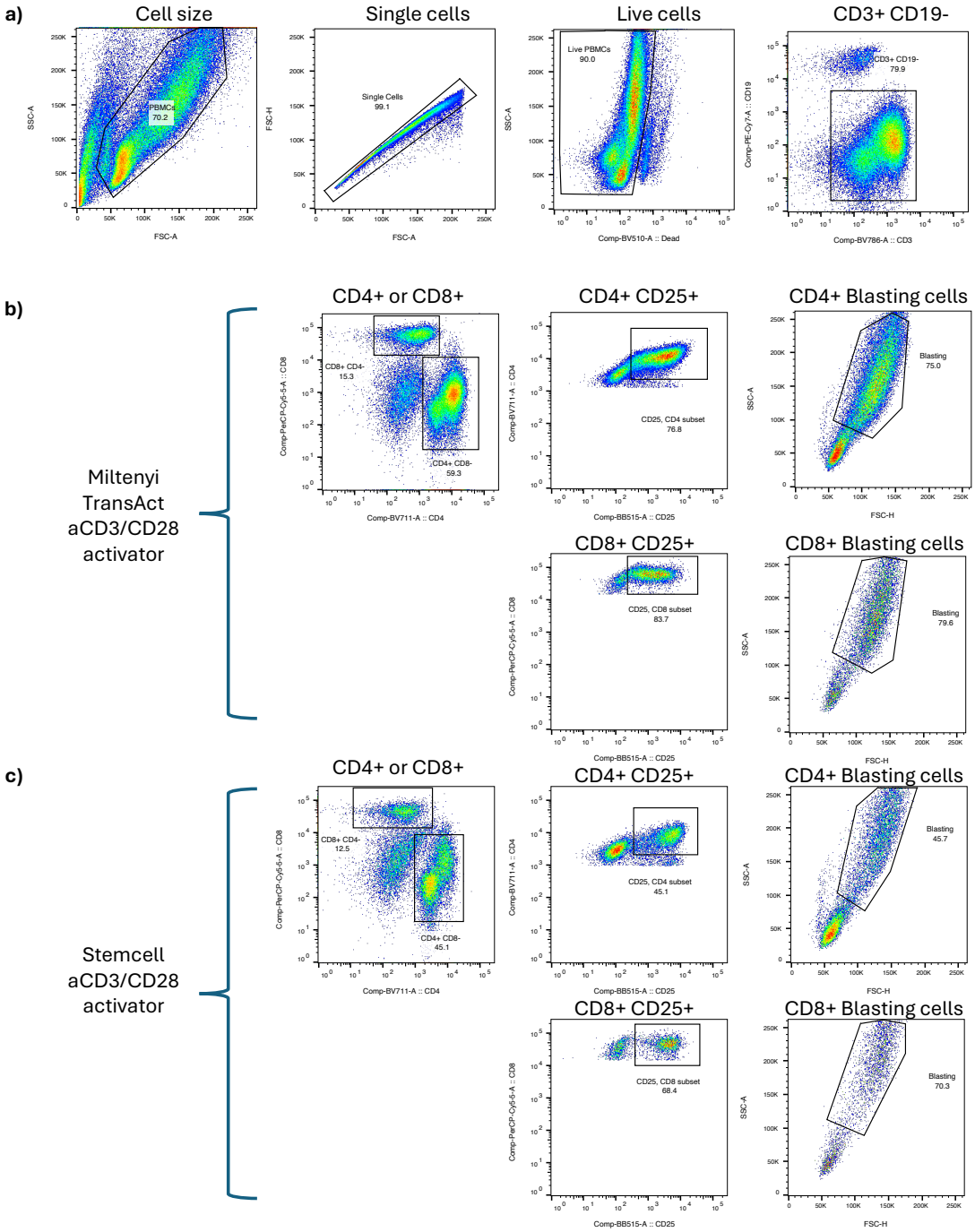

Figure 3-1: Representative gating of T cells isolated from a mixed PBMC population. Cells were stained as described in Materials and Methods and acquired of a BD Celesta. Labels indicate cell populations, and the numbers show the percentage of cells within each gate. (a) CD4+CD25+ and CD8+CD25+ T cells and blasting cells were identified for the two different activators Miltenyi (b) and Stemcell (c).

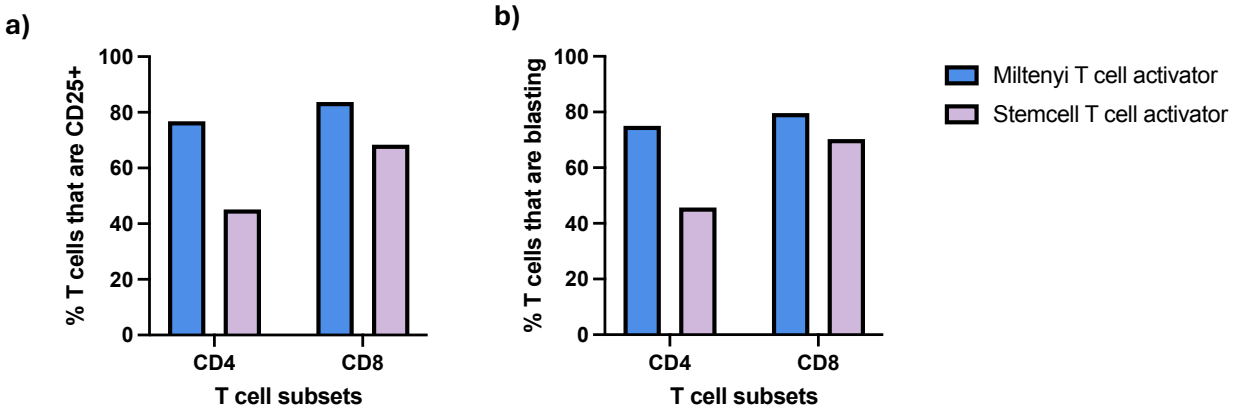

Figure 3-2: Comparison between commercially available T cell activators. (a) Percentage CD25+ expression by T cell subtype and (b) percentage blasting CD4 and CD8 T cells exposed to either Miltenyi Biotech aCD3/aCD28 T cell activator or Stemcell aCD3/aCD28 T cell activator. PBMCs exposed to T cell activator for 3 days at manufacturer recommended dosing. Data shown represents a biological n=1 in singlet.

3.3.2 Biomaterial formation

The glass or poly(ethyl acrylate) (PEA) coated, fibronectin (FN) and bone morphogenic protein 2 (BMP-2) biomaterials were prepared, and a mesenchymal stem cell (MSC) monolayer established over 3 days [methods 2.1.1 – 2.1.4]. I chose to work with the PEA, FN and BMP-2 MSC biomaterial as it has been characterised extensively by the Salmeron-Sanchez group over the last 10 years and therefore had a predictable profile against which to build the model of human T cell responses (182, 322).

Using immunofluorescence (IF) microscopy, I stained for DAPI, phalloidin and vinculin (VN) on both glass and PEA-coated/FN/BMP-2/MSC conditions. DAPI binds to double stranded DNA and therefore, stains cell nuclei. Phalloidin is highly selective for staining actin filaments (F-actin) and therefore shows the cell cytoskeleton. VN is a cytoskeletal protein associated with cell-cell and cell-matrix junctions and staining for VN highlights cell focal adhesion points. Figure 3-4 shows the glass conditions without the PEA material, there are fewer focal adhesion contact points and more linear MSC spread. In contrast, the increased focal adhesion points and greater cell spreading are clearly visualised in Figure 3-5, when MSCs were grown on the PEA biomaterial.

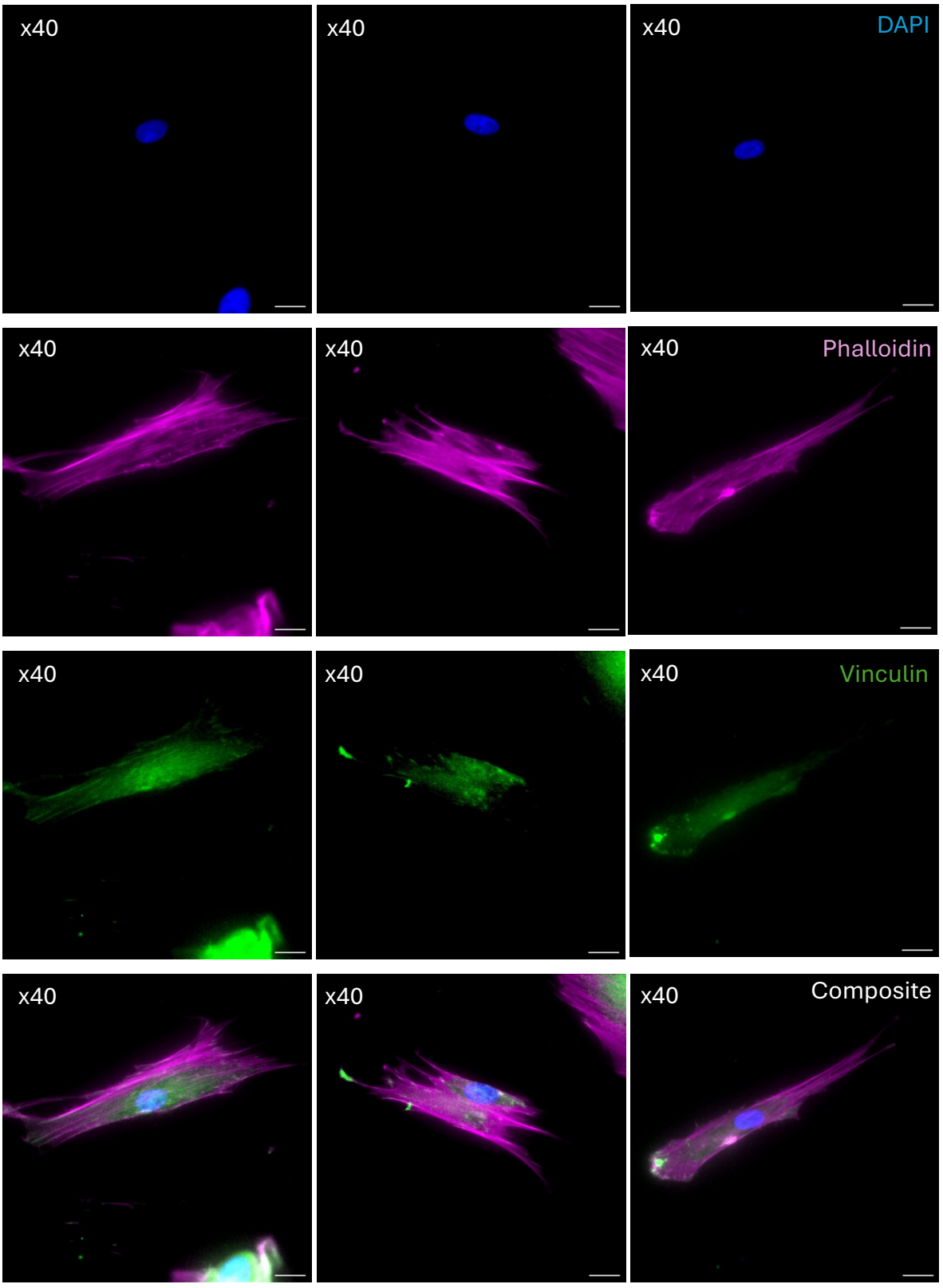

Figure 3-3: Immunofluorescence microscopy images of MSCs cultured for 3 days on glass cover slips with adsorbed FN and BMP-2. Staining shows Vinculin (VN) (green), phalloidin (magenta) and DAPI (blue). Scale bars are 100μm. Panels show three representative images showing focal adhesion points on the MSCs with a linear MSC morphology.

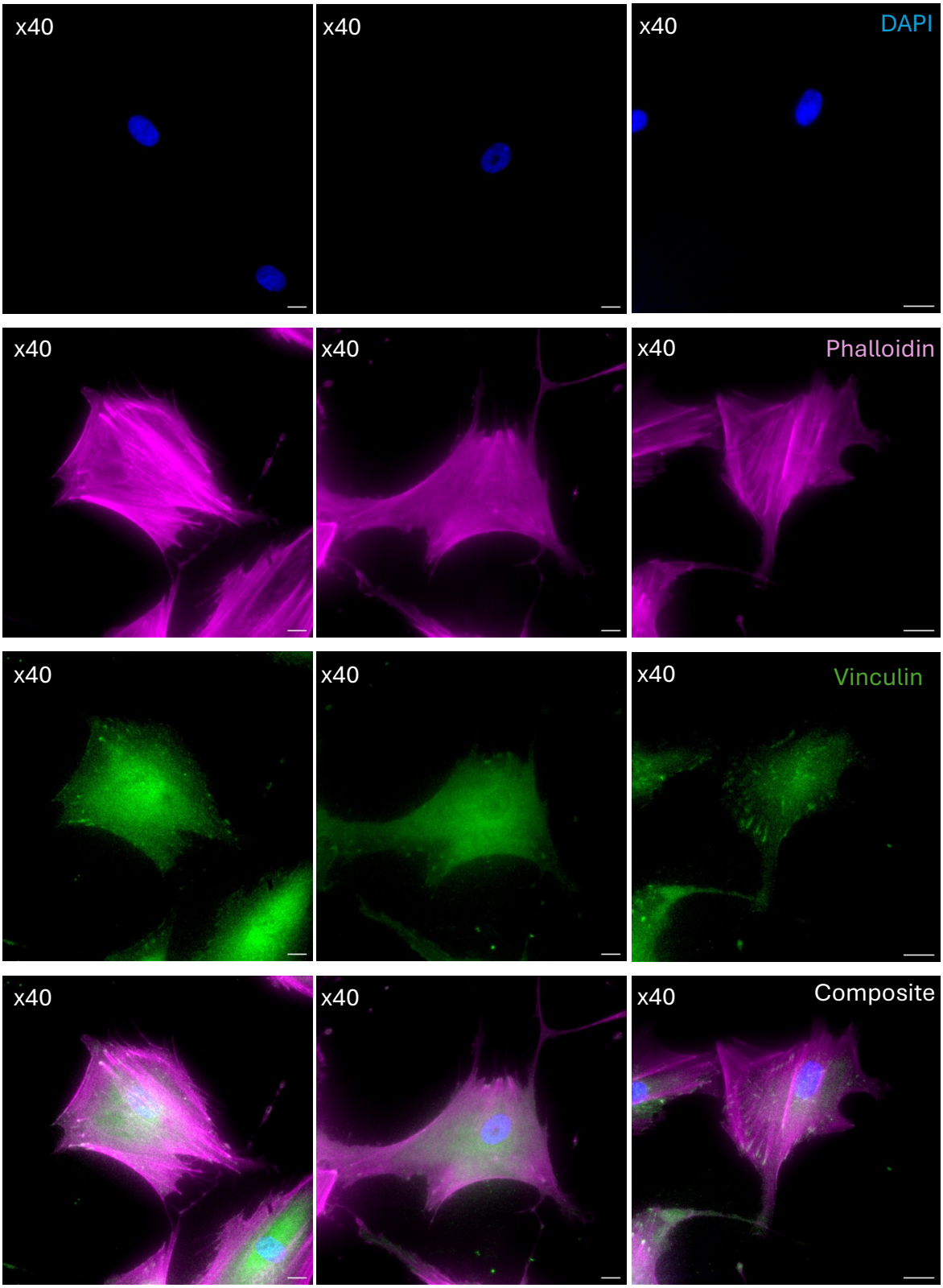

Figure 3-4: Immunofluorescence microscopy images of MSCs cultured for 3 days on PEA coated glass cover slips with adsorbed FN and BMP-2. Staining shows vinculin (VN) (green), phalloidin (magenta) and DAPI (blue). Scale bars are 100μm. Panels show three representative images showing increased focal adhesion points on MSCs with increased cell spread area when on PEA biomaterials.

3.3.3 T cell model response to biomaterial components

Having activated the T cells with the Miltenyi activator, I wanted to investigate if they were then capable of greater activation against any of the biomaterial component parts in combination with allogenic MSCs. T cells respond to foreign antigen but are thought to respond differently to immune 'privileged' MSCs and have been shown to be immune 'evasive' through suppression of T cell proliferation and promotion of Tregs and M2 macrophages (308, 323). Despite a known ability to express MHC class I molecules, MHC class II expression in MSCs is less well characterised. Biomaterial glycoproteins and coatings, in the absence of cells, are described as 'inert', as they lack antigen, and should not alter the T cell response (4). I hypothesised therefore that there may be differences between MSC and no MSC conditions but that there would be no differences in T cell activation, to any of the different combinations of the individual 'inert' biomaterial components.

The conditions within this experiment included: a PEA/MSCs only condition, a PEA/FN/MSCs condition, a PEA/FN/BMP-2/MSCs condition and finally, a PEA/FN/BMP-2/no MSCs condition. All conditions had matched glass controls without any PEA coatings to establish if the presence of PEA altered the response.

The flow panel included staining for viability, CD3, CD19, CD4, CD8 and CD25 surface markers [Figure 3.5]. Activation levels were globally high across all conditions irrespective of the presence or absence of allogenic MSCs [Figure 3.6]. It was evident that the aCD3/aCD28 activator was likely either having ongoing effects through a prolonged duration of action or it was still present in the cultures, as the cells were experiencing continued activation. Despite this persistent

activation across all conditions, CD4+CD25+ and CD8+CD25+ expression was higher than no cell controls in both PEA and glass biomaterials with FN/BMP-2.

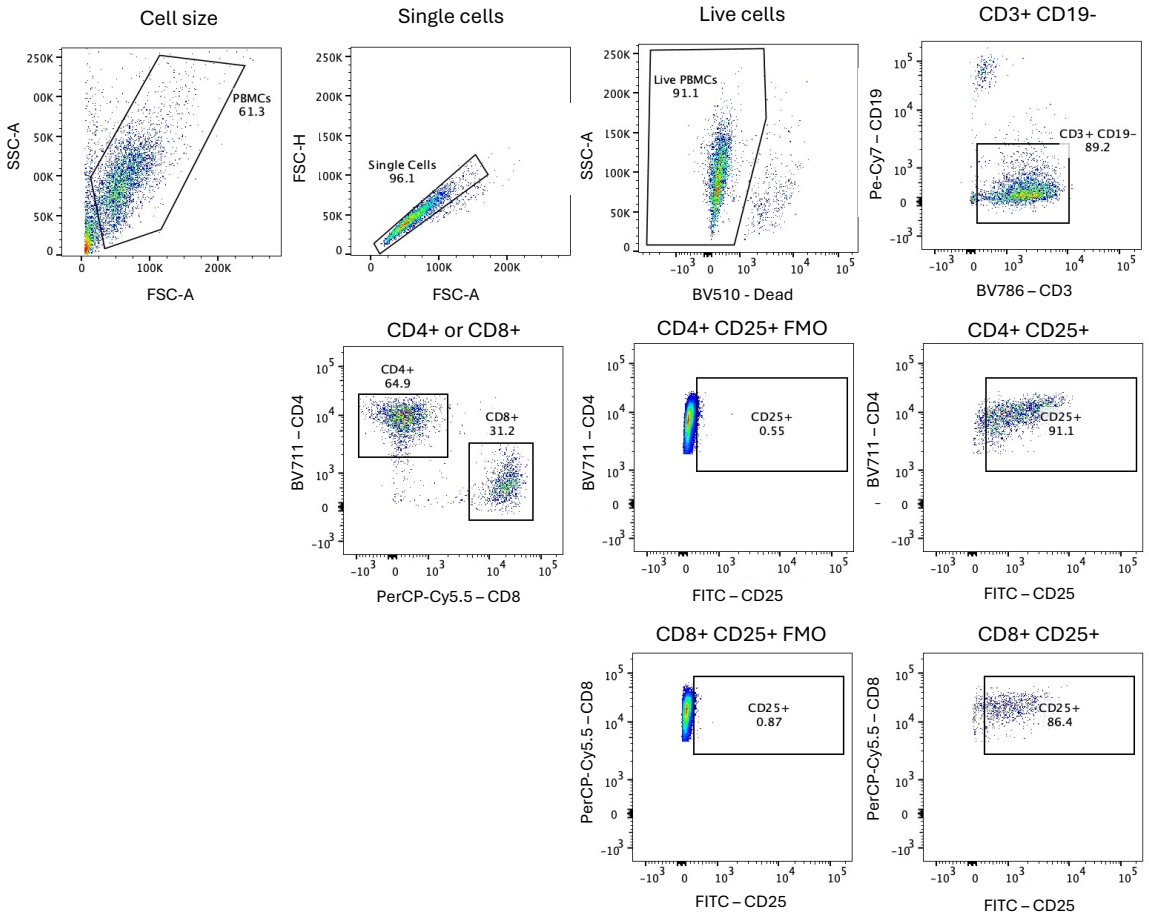

Figure 3-5: Representative gating of T cells isolated from a mixed PBMC population. Cells were stained as described in Materials and Methods and acquired of a BD Celesta. Labels indicate cell populations, and the numbers show the percentage of cells within each gate. CD25 FMOs shown for both CD4 and CD8 T cells.

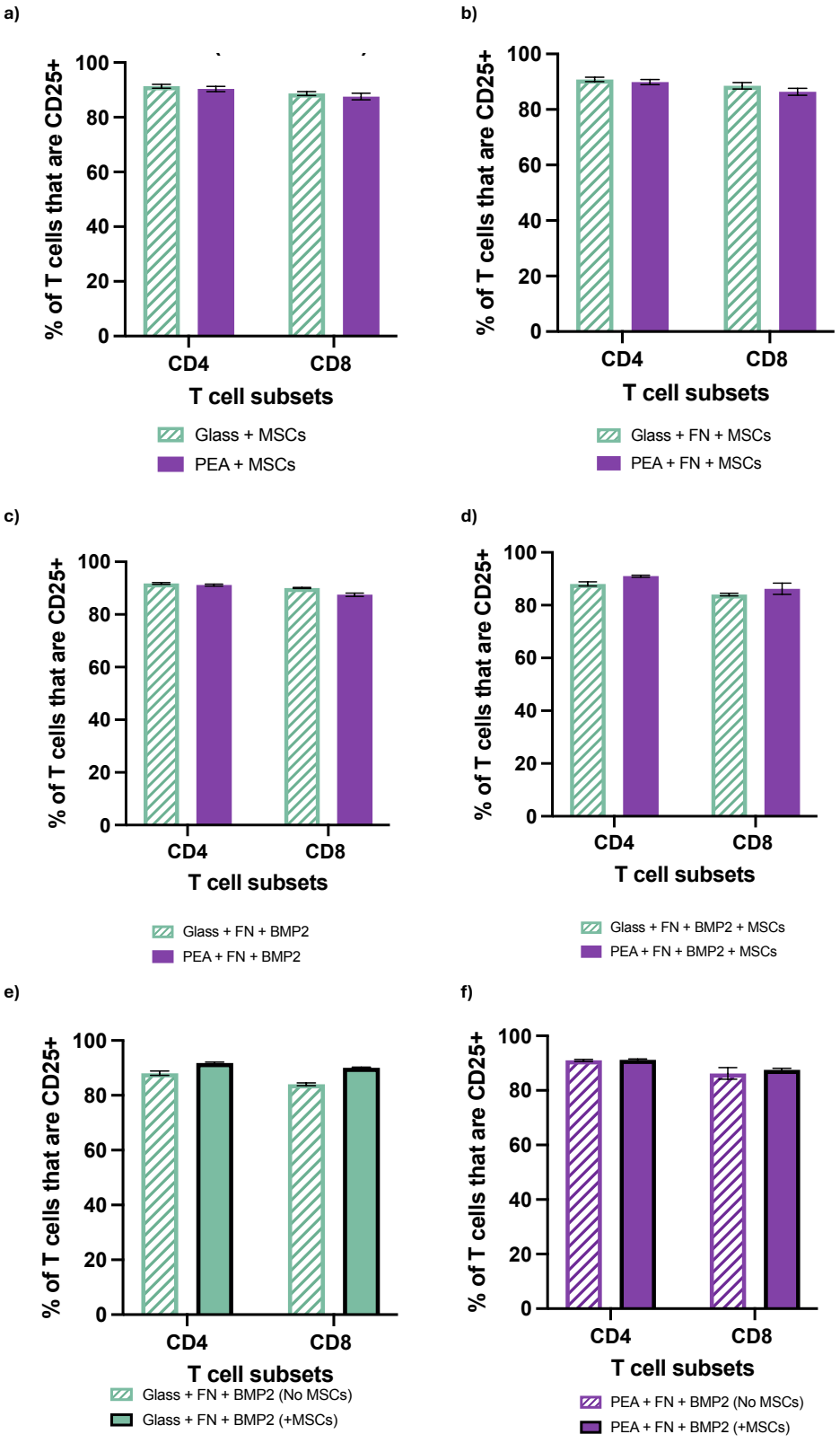

Figure 3-6: Levels of CD25+ expression in CD4+ and CD8+ T cells following T cell priming. Miltenyi T cell activator was used for 3 days at manufacturer recommended dosing and in 24hrs co-culture with different biomaterial compositions (a) Glass vs PEA cover slips with MSCs. (b) Glass vs PEA cover slips with FN and MSCs. (c) Glass vs PEA cover slips with FN and BMP-2 without cells (d) Glass vs PEA cover slips with FN, BMP-2 and MSCs. (e) Glass complete biomaterial with and without cells. (f) PEA complete biomaterial with and without cells. Data shown is a biological n=1. Graphed bars represent the mean of three technical replicates in one experiment. Error bars show the SEM.

3.3.4 T cell rest time course

With ongoing Miltenyi activator T cell activation during the last experiment, I first undertook a time course experiment to assess whether increasing periods of T cell rest, after activator removal, could stop ongoing activation responses in the absence of further stimuli. This would ultimately enable measurement of biomaterial-driven activation responses only.

T cells were primed and activated per previous methods and following Miltenyi activator removal, rested for 12, 24, 36 or 60 hours. The cells were collected and stained for flow cytometry analysis [methods 2.4.1 – 2.4.2]. Results highlighted that T cell viability reduced with increasing periods of cell rest in culture but remained above 80% overall [Figure 3-8]. Despite cell rest, CD25 expression remained higher than 80% across all timepoints for both CD4+ and CD8+ T cells, in the absence of any further stimulus or antigen. CD25 expression reduced marginally over the time course up until 60hrs, at which point that appeared to be a greater proportion of T cells expressing CD25. At the 60hr timepoint there was also greater cell death and therefore the increased CD25 expression could represent the CD25 expressing cells being more resistant to cell death [Figure 3-8].

From these results, it was evident that the periods of cell rest had not been successful, implying that the Miltenyi activator had not been fully removed from the cell culture or the cells, was perhaps used at too strong a dose for our intended purpose, or that the duration of action for initial T cell priming was too long.

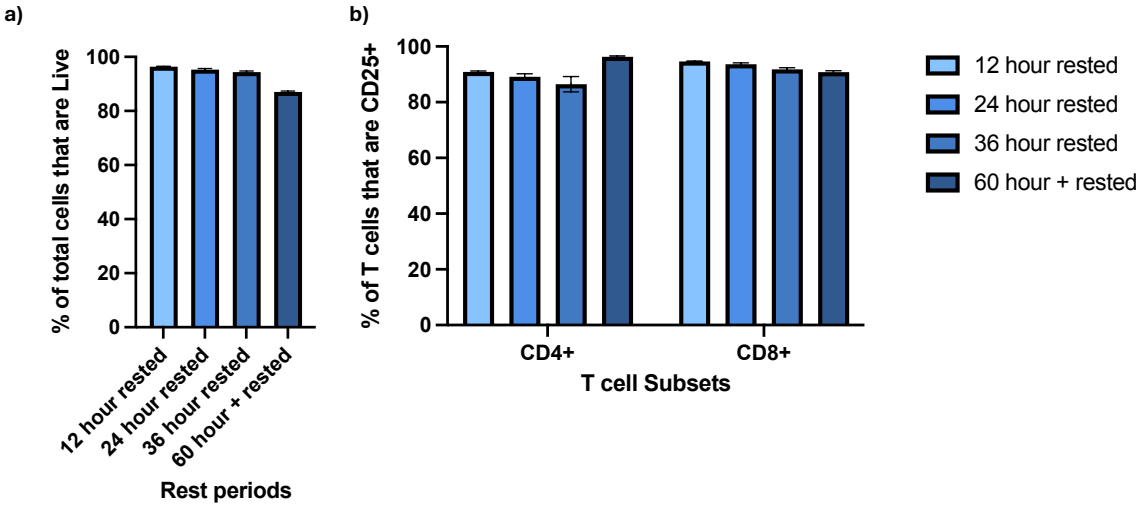

Figure 3-7: Cell rest following activation. T cell priming using Miltenyi T cell aCD3/aCD28 activator at manufacturer recommended dosing for 3 days, followed by removal of activator and increasing periods of cell rest: 12hrs, 24hrs, 36hrs or 60hrs. (a) T cell viability following rest periods (b) Percentage CD25 expression for CD4 and CD8 T cells after the different rest periods. Data shown represent a biological n=1. Graphed bars show the mean of two technical replicates in one experiment. Error bars show the SEM.

3.3.5 T cell activator lower dose and shorter incubation

The aim of this experiment was to establish if a lower dose of Miltenyi aCD3/aCD28 T cell activator, in combination with a shorter 24-hour (vs 3 day) activation period ('priming') would be sufficient to rest the T cells in the absence of further stimulus or antigen.

The cells were activated using 4 different dilutions of the Miltenyi aCD3/aCD28 T cell activator: 10μl of stock used at 1:100 with 990μl of T cell culture media (manufacturer recommended) and then a 1:500 dilution of stock, a 1:2500 dilution of stock or a 1:12500 dilution of stock [Appendix 1, 7.1]. The Miltenyi activator was left in culture with the cells for 24 hours before being removed and the cells then stained for flow cytometry analysis per [methods 2.4.1 – 2.4.2].

With a reduced activation or 'priming' time to 24 hours, CD25 expression was lower irrespective of Miltenyi activator dose, at less than 15% CD25 expression [Figure 3-9]. Even for the previously used manufacturer recommended dose of 10μl stock in 990μl culture media (dose 1), that had resulted in >80% activation in the previous experiment [Figure 3-8]. This implies that the reduced duration of action to 24 hours was successful in reducing overall activation levels in the priming of the T cells.

CD3 expression transiently reduces on activation of T cells (324). CD3 expression reduced on T cells activated with dose 1 and to a lesser extent in T cells activated with dose 2 of Miltenyi activator, before returning to baseline levels [Figure 3-9]. There was no CD3 downregulation seen for dose 3 or 4 implying they were too low to activate the T cells. The CD4+ CD25+ expression levels for dose 1 were 13.9% compared to 14.2% for dose 2 (a 1:500 dilution of stock Miltenyi activator). For

CD8+ T cells CD25+ expression for dose 1 was 7.88% compared to 6.53% for dose 2. Furthermore, dose 2 did cause some CD3 downregulation, so I decided to proceed for all future experimentation with a 1:5 dilution of stock Miltenyi activator for 24 hours to 'prime' the T cell component of the PBMCs.

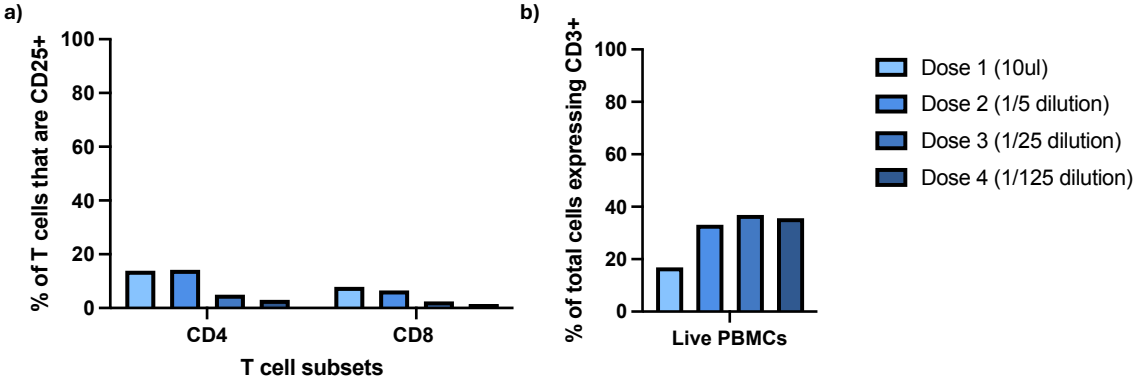

Figure 3-8: T cell activator reduced dosing. T cell priming using Miltenyi T cell aCD3/aCD28 activator at manufacturer recommended dose vs three dose dilutions: 1/5, 1/25, 1/125 dilution. T cell exposed to activator for 24 hours only. (a) Percentage CD25 expression for CD4 and CD8 T cells at the different doses of activator for 24hrs. (b) Percentage CD3 expression showing downregulation with dose 1 and to a lesser extent in dose 2. Graphed bars represent a biological n=1 with no replicates in one experiment.

3.3.6 T cell priming, rest and washes

I aimed to establish if the newly optimised method of T cell priming could be further improved to reduce activation levels to lower than 20% CD25 expression in the absence of further stimuli or antigen. In this experiment, I undertook extensive cell washing steps using different wash media, and trialled subsequent cell rest periods to reduce the activation levels of the cells.

The T cells were primed [methods 2.2.6] and then underwent cell washes in three different wash medias to establish the best method to remove the Miltenyi activator from the cells. The three different wash media were: normal T cell culture media, PBS with 2mM EDTA or PBS with 5mM EDTA [Appendix 1, 7.1]. The cells were washed in 50ml falcon tubes topped up with wash media to 50ml. They were then centrifuged at 300g for 10 minutes. The supernatant was then discarded, and the cells resuspended in a further 50ml of wash media to complete a total of 3 washes. Cells were then recounted using a haemocytometer [methods 2.2.9] and cultured for 0, 24 or 48 hours of cell rest in fresh T cell culture media in the 5% CO_2 37°C incubator [Appendix 1, 7.1].

The CD25 expression and CD3 MFI were similar at each timepoint for both CD4+ and CD8+ T cells, irrespective of the wash media used [Figure 3-10]. There were differences found between timepoints, with the most CD25 expression and biggest CD3 MFI downregulation found for cells undergoing 0 hours rest. A 24-hour rest period following the wash steps appeared to reduce the CD25 expression for both CD4+ and CD8+ T cells the most, even more so than a 48-hour rest period [Figure 3-10]. It was concluded that moving forward, T cells would be primed for 24 hours before washing 3 times with culture media and a subsequent 24-hour rest period before being used in the modelling.

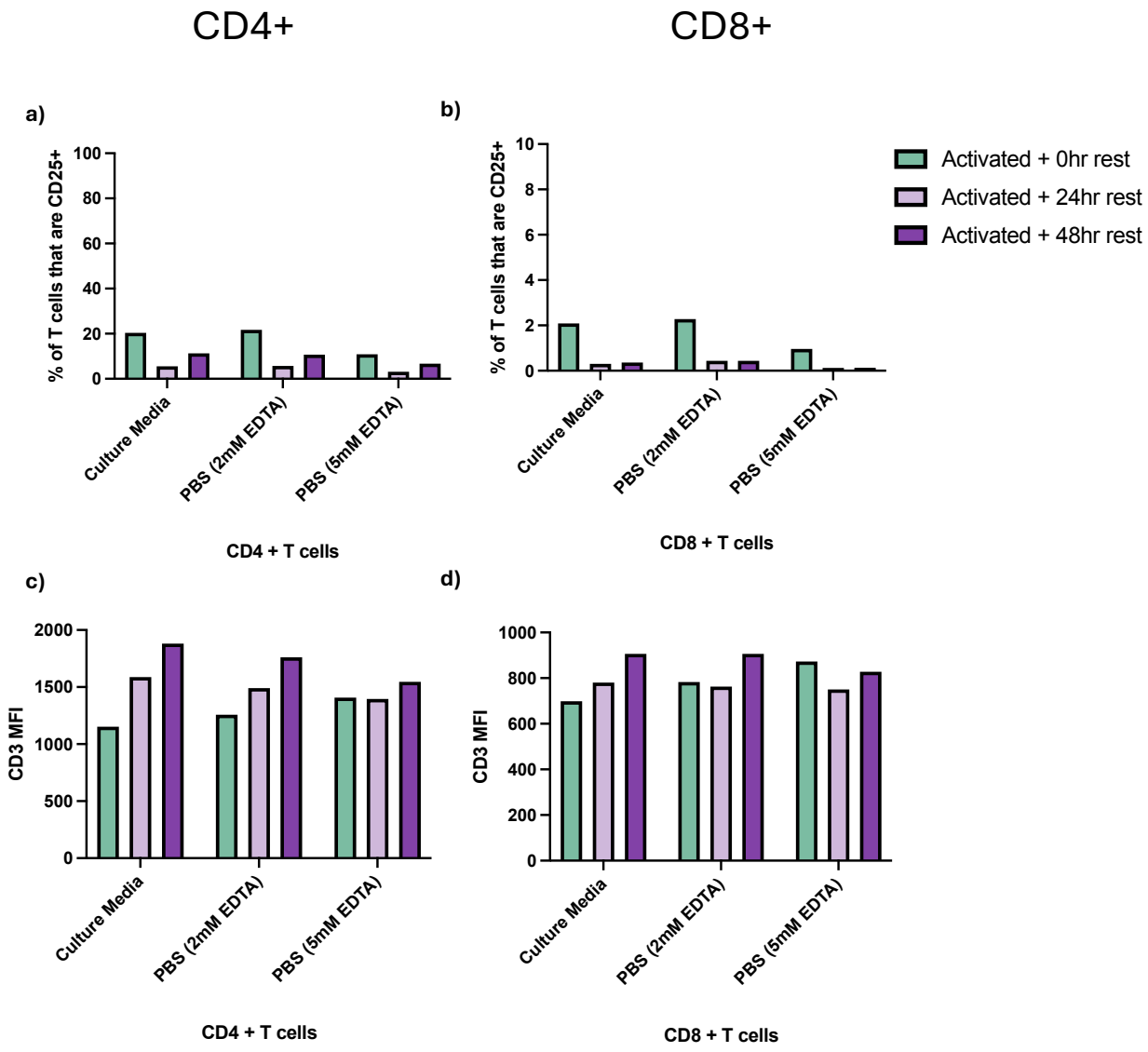

Figure 3-9: T cell activator removal with different wash medias. CD25 expression after 0hrs, 24hrs or 48hrs rest following T cell priming and subsequent washes with culture media, PBS (2mM EDTA) or PBS (5mM EDTA). Percentage CD25 expression for CD4 (a) and CD8 (b) T cells after different rest periods following wash steps with different media. MFI of CD3 expression for CD4 (c) and CD8 (d) T cells, after different rest periods following wash steps with different media. Graphed bars represent a biological n=1 with no replicates in one experiment.

3.3.7 T cell priming, rest and subsequent reactivation

With an optimised T cell priming protocol the aim of this experiment was to establish if the primed and subsequently rested T cells would be capable of responding to further activation.

Following priming, wash steps and rest, T cells were rested 24 hours as a negative control. Sample T cells were reactivated with a further 1:5 dilution of stock Miltenyi activator and returned to the 5% CO_2 37°C incubator for 24 hours.

The results demonstrate appropriately rested T cells with no increase in CD25 expression at 24 or 48 hours following activator removal [Figure 3-10]. Overall T cell CD25% expression at 24 hours rest in the negative control was 10.5% for CD4+ and 3.51% for CD8+ T cells. T cells that had been 24 hours rested and subsequently exposed to a further activator dose for 24 hours had increased CD25 expression for both CD4+ (51.0% vs 10.5%) and CD8+ (33.1% vs 3.51%) T cells. The T cells primed within the model are capable of mounting further activation responses in the presence of further stimuli and do not respond further in the absence of it, which is key to ensuring an appropriately controlled, reliable methodology for subsequent modelling.

Therefore, for all subsequent experiments the following protocol was used:

1. Activate at 1:500 dilution of stock Miltenyi aCD3/aCD28 activator for 24hrs
2. Harvest and wash the cells to remove the activator 3 times in culture media
3. Culture and rest the cells for 24 hours
4. Harvest and use in downstream experiments with the biomaterials

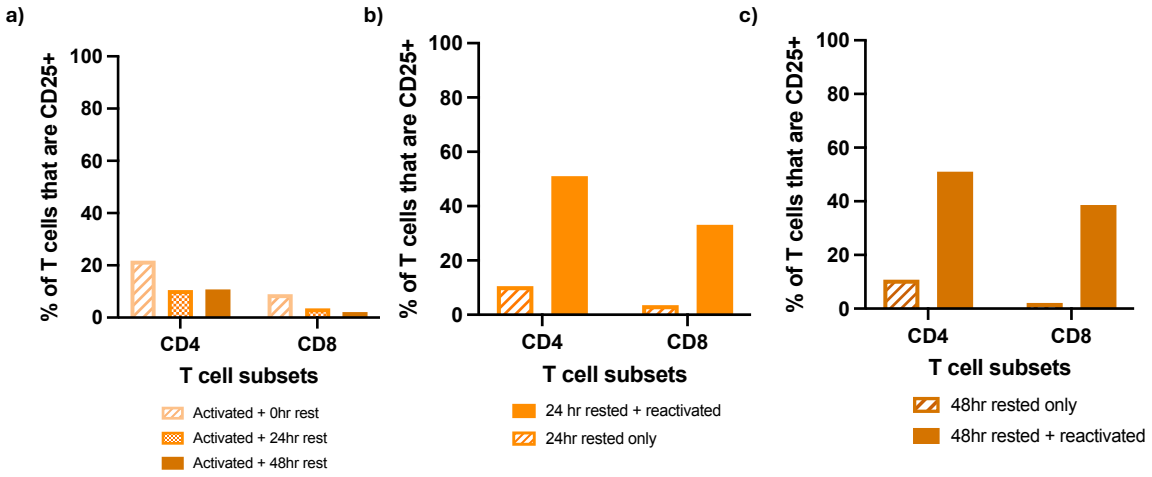

Figure 3-10: T cell reactivation following priming, wash steps and rest. (a) CD25 expression for CD4 and CD8 T cells after 0hrs, 24hrs or 48hrs rest following T cell priming. Low levels of CD25+ activation after 24hrs rest with no further reduction by 48hrs. (b) Percentage CD25 expression for CD4 and CD8 T cells after 24hrs rest followed by reactivation with further activator activation. (c) Percentage CD25 activation for CD4 and CD8 T cells after 48hrs rest and then 48rs reactivation. Both CD4 and CD8 T cells are capable of subsequent reactivation to the activator. Graphed bars show the mean of two technical replicates for a biological n=1.

3.3.8 Frozen vs fresh PBMC T cell viability

For long term experiment feasibility, I sought to establish if frozen, stored human PBMCs at -80°C, were as viable as freshly collected PBMCs. This would facilitate the isolation of PBMCs in advance of experiments and permit more biological donors being used per experiment.

A single donor's blood was freshly collected on the day of experimentation and the PBMCs isolated. The same donor's blood had been previously collected, the PBMCs isolated and then stored for 2 months and 6 months, at -80°C. The stored PBMCs were then thawed on the day of experimentation (methods 2.2.5). All three conditions (fresh, frozen 2 months, frozen 6 months) were then activated using the aCD3/aCD28 activator and rested per described methodology (methods 2.2.6 - 2.2.7). The samples were then stained with antibodies as per described methodology and ran on the flow cytometer (methods 2.4.1 - 2.4.2). The experiment was undertaken for biological n=1 and in technical triplicate.

The freshly taken blood sample had the highest viability at 95.3% viable. Viability subsequently reduced with increasing age of frozen PBMCs: mean 81.9% (2 months frozen) and 68.6% (6 months frozen) [Figure 3-11]. All three conditions saw higher viability in the cells that had been activated and rested when compared with unactivated matched controls. This implies that activated T cells survive better, irrespective of age and storage, in *in vitro* conditions.

In the freshly collected PBMC cell condition, 3.8% of T cells were CD4+CD25+ positive versus an increased 9.2% in the 6-month frozen condition. Similarly, only 0.34% were CD8+CD25+ in the freshly taken PBMCs versus an increased 6.0% in the 6-month stored [Figure 3-11]. Freshly collected PBMCs had higher viability and the lowest CD25+ expression levels after T cell priming and cell rest methodology

(2.2.6 - 2.2.7). However, whilst viability was reduced in the 2 months frozen PBMCs versus the fresh, activation levels remained the same.

I therefore concluded that freshly collected PBMCs should be used for downstream experimentation and modelling where possible, and if frozen PBMCs are required for use, use of maximum stored 2-month frozen PBMCs could be considered and predominantly for single stain cell controls for flow cytometry (methods 2.4.1).

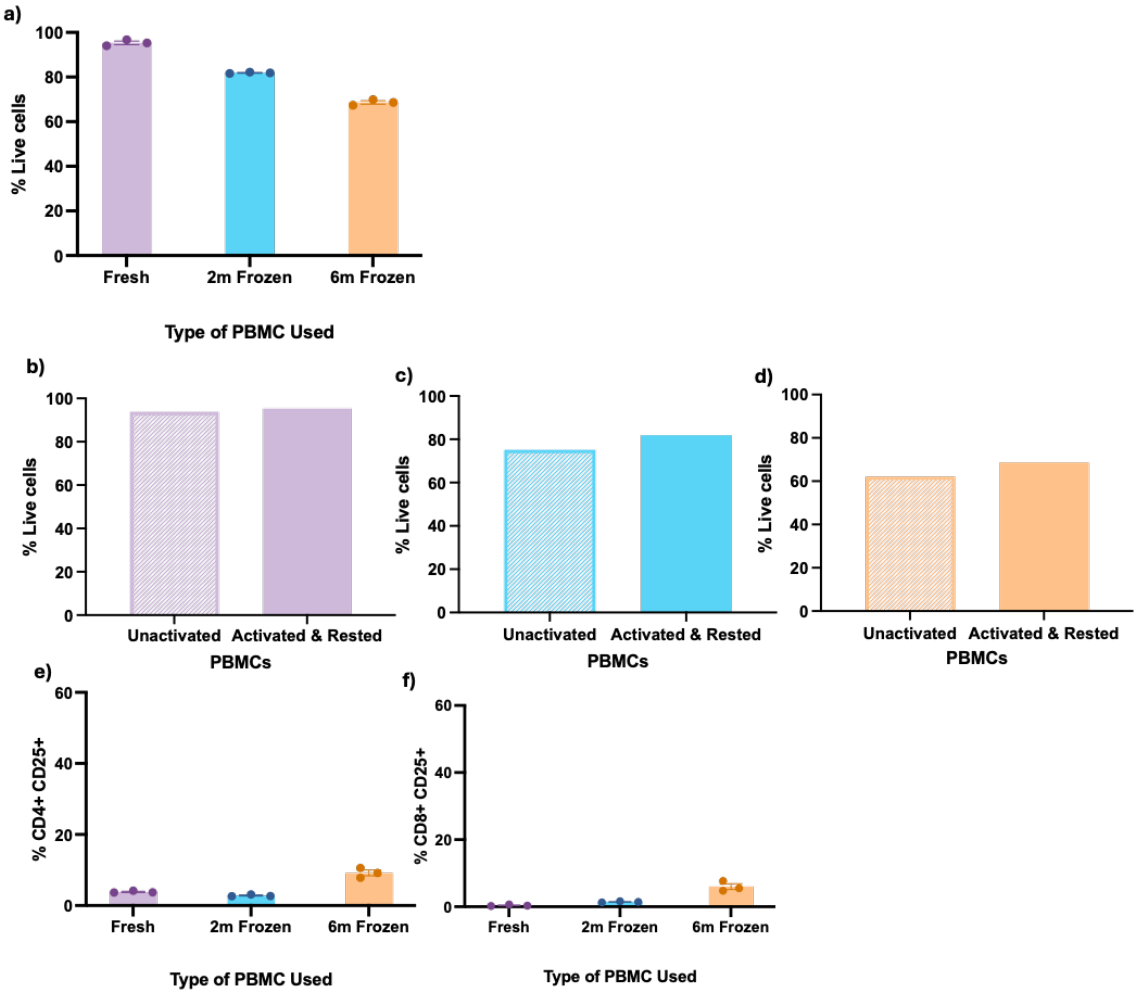

Figure 3-11: Frozen vs Fresh PBMC Viability. (a) Viability comparison between freshly harvested peripheral blood mononuclear cells (PBMCs), 2 months frozen PBMCs at -80℃ and 6 months frozen PBMCs at -80℃. Graphed bars show the mean of three technical replicates from one experiment. Error bars represent Standard Error of Mean (SEM). Biological n=1. (b) Viability of fresh PBMCs, frozen 2 months PBMCs (c), frozen 6 months PBMCs (d) in unactivated versus activated then rested conditions. (e) CD4 and (f) CD8 T cell activation by CD25+ expression post activation and subsequent activator removal and rest shown by type of PBMC used.

3.3.9 T cell response to biomaterial components for 24hrs

Following successful optimisation of the T cell priming methodology, the T cell modelling against the PEA vs glass biomaterials was repeated. All components of the biomaterial were tested in various combinations and both with and without allogenic MSCs with the primed T cells. Positive and negative controls saw appropriate responses with no global activation response as found previously [results 3.3.5].

Over a co-culture (T cells vs biomaterials) duration of 24 hours and with a biological n=1, there were no differences in T cell CD25+ expression between cellularised PEA or glass conditions in any conformation of biomaterial with or without functionalisation [Figure 3-12]. Overall, CD25 expression levels were higher than established previously [results 3.3.10] however, a different biological donor was used and again this optimisation experiment was carried out with an n=1 in technical replicate. There will be an element of inter donor variability for CD25 expression and importantly the expression at 24 hours was comparative to the negative control for both CD4+ and CD8+ T cells [Figure 3-12].

CD4+ T cell responses to glass/FN/BMP-2 with MSCs, saw a slightly higher CD4+ CD25+ expression than in no cell control [Figure 3-13]. However, for PEA/FN/BMP-2 biomaterials with MSCs, the CD25+ expression was marginally lower in both CD4+ and CD8+ T cells than in the no cell condition.

Overall, there was no clear difference in T cell response to PEA versus glass biomaterials in any configuration and no increased T cell activation seen at 24 hours co-culture.

I concluded that the different biomaterial components do appear to be relatively ‘inert’ and therefore moving forward for future experimentation, I will focus exclusively on two conditions:

1. A **‘cellularised’** biomaterial condition: PEA+FN+BMP-2**+MSCs**

2. An **‘acellular’** biomaterial control: PEA+FN+BMP-2 only

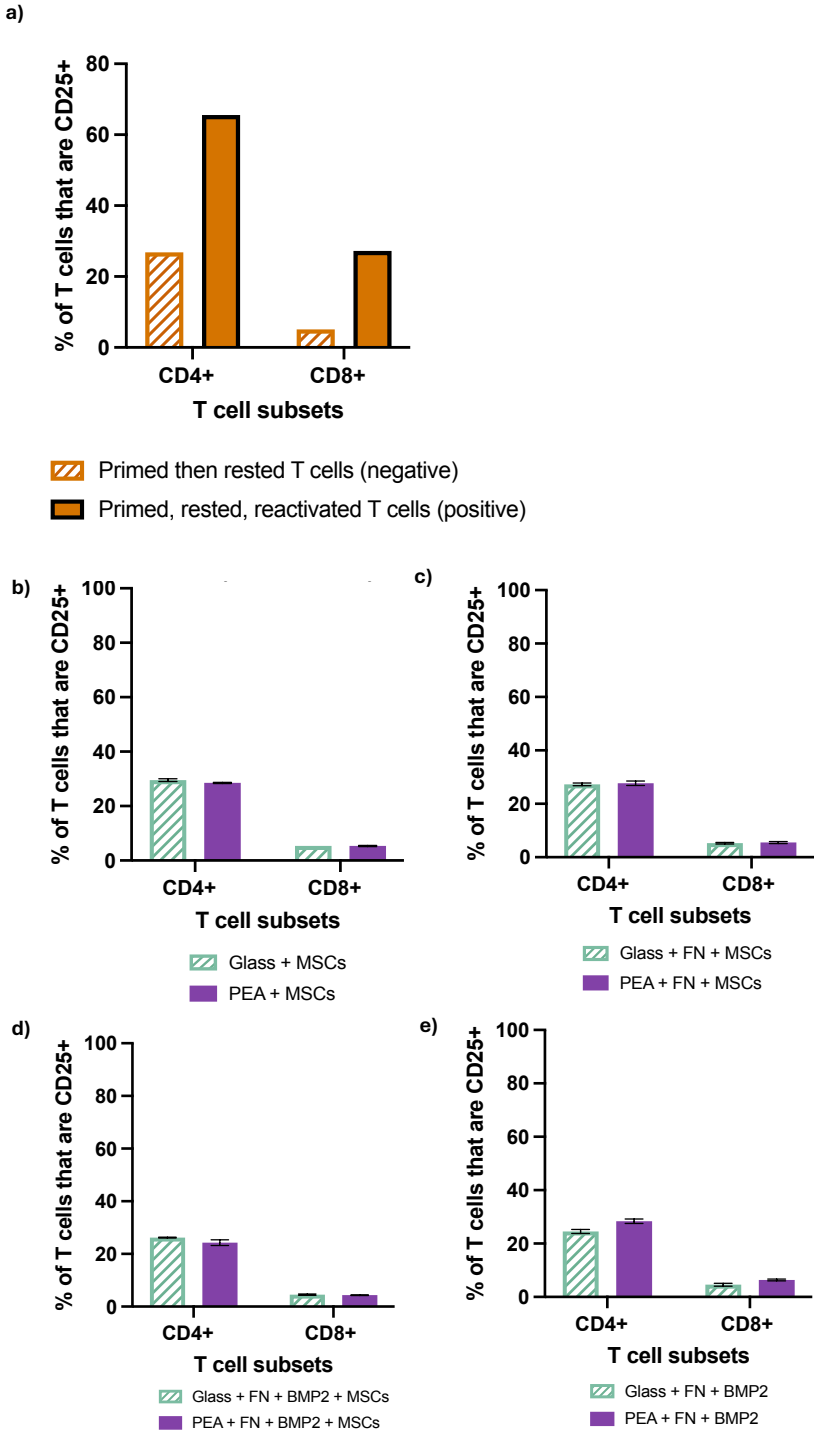

Figure 3-12: Optimised primed T cell response to biomaterial components. CD25 expression for CD4 and CD8 T cells after 24hrs rest following T cell priming. Co-cultured for 24hrs with glass or PEA biomaterial in various compositions. (a) CD25 expression for CD4 and CD8 T cells negative and positive controls. (b) Glass vs PEA biomaterial with MSCs. (c) Glass vs PEA with FN and MSCs. (d) Glass vs PEA with FN, BMP-2 and MSCs. (e) Glass vs PEA with FN and BMP2 without cells. No differences between glass or PEA materials and no increase in CD25 expression over negative control. Data shown is a biological n=1 and in technical triplicate, graphed bars show the mean with error bars for SEM.

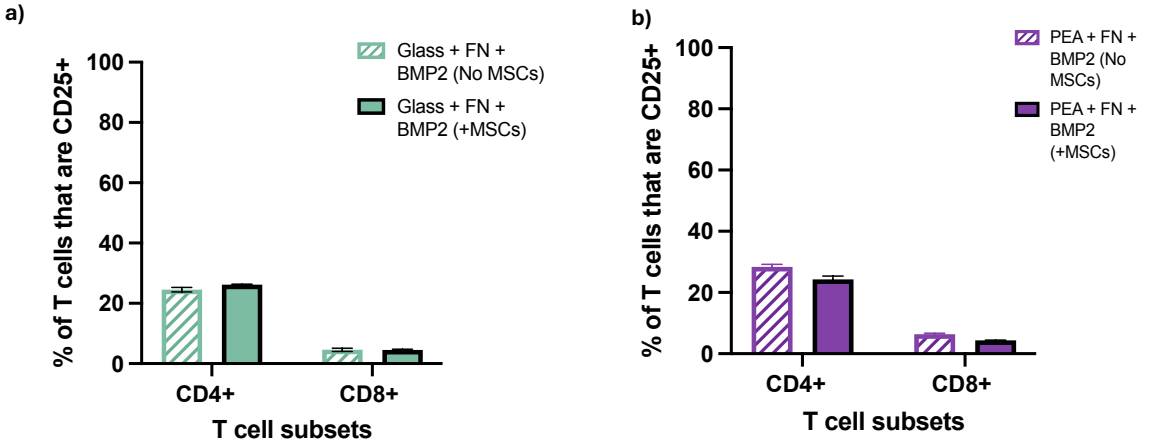

Figure 3-13: Optimised primed T cell response to biomaterial with and without MSCs over 24hrs. CD25 expression for CD4 and CD8 T cells after 24hrs rest following T cell priming with 1/5 dilution. Co-cultured for 24hrs with glass (a) or PEA (b) FN and BMP-2 biomaterial with and without MSCs. No differences shown between the cell and no cell conditions at 24 hours. Data shown is a biological n=1 and in technical triplicate.

3.3.10 T cells vs cellularised biomaterials for 48hrs

The previous experiment confirmed that the T cells did not mount increased CD25+ activation responses to the different biomaterial components, however the duration of co-culture for allowing response to allogenic MSCs to develop was only 24hrs. Alloresponses can be direct which occur within the first 6 months of the allograft, indirect predominating beyond 6 months, or semi-direct whose timeline for clinical rejection remains poorly understood (307). The extent of direct allorecognition relies on intact MHC recognition by T cells and can be rapid if enough MHC is present (307). This experiment aimed to co-culture the primed T cells with the PEA/FN/BMP-2 MSC biomaterials for up to 48hrs to see if any further response developed with increasing co-culture duration.

Negative controls showed that once primed and rested, the T cells maintained low levels of CD25 expression over time in the absence of further stimuli. In contrast to the prior experiment [results 3.3.11], the negative controls had returned to 10.6% CD25 expression after priming methodology, rising to 12.2% for CD4+ CD25+ expression even by 48 hours. This demonstrates donor variability in baseline CD25 expression across experiments. Positive controls demonstrated increasing CD25+ expression over increased incubation with the Miltenyi activator, with CD4+CD25+ expression back up to 90% by 48hrs exposure to activator [Figure 3-14].

At 24hrs there was again, no difference between cellularised allogenic MSC biomaterials and acellular controls for either CD4+ or CD8+ CD25+ expression. By 48hrs, the CD25+ expression had marginally increased for the CD4+ T cells but there were no differences between MSC biomaterials and no cell controls by 48 hours [Figure 3-14].

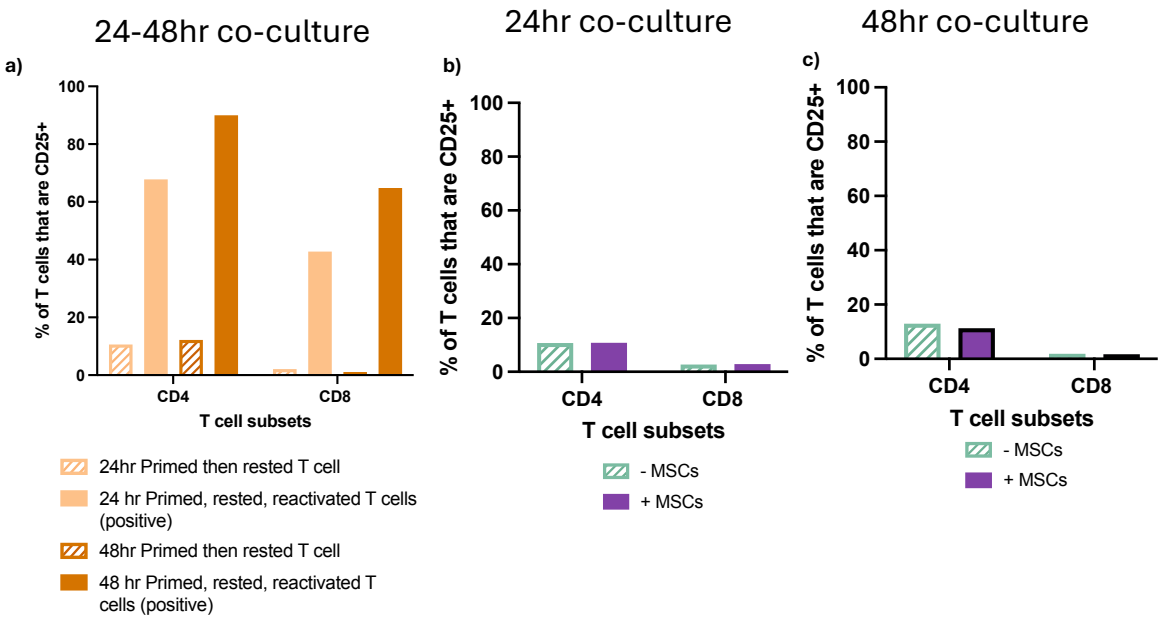

Figure 3-14: Optimised primed T cell response to biomaterial with and without MSCs over 48hrs. CD25 expression for CD4 and CD8 T cells after 24hrs rest following T cell priming. Co-cultured for 24hr and 48hrs with PEA, FN, BMP-2 biomaterials with and without MSCs. (a) Positive controls showing T cells reactivated with activator and negative controls showing T cells rested only (b) CD25 expression for CD4 and CD8 T cell subsets to cellularised biomaterial vs controls for 24hrs co-culture. (c) CD25 expression for CD4 and CD8 T cell subsets to cellularised biomaterial vs controls for 48hrs co-culture. No differences between cellularised biomaterial and control at either 24 or 48hrs co-culture. Data shown is a biological n=1 and in technical duplicate. Graphed bars represent the mean of two replicates in one experiment.

3.3.11 T cells vs MSC biomaterials in the presence of allogenic macrophages

The primed T cells are capable of further activation with a second exposure to 24hrs of the Miltenyi activator. Furthermore, CD25+ expression increases with longer re-exposure to the Miltenyi activator [results 3.3.12]. It remained unclear if, in the absence of Miltenyi activator, the primed T cells could further respond to antigen. To begin to investigate this, I first sought to test if co-culture in the presence of macrophages as APCs could increase the ability of T cells to respond to allogenic antigen. I isolated a donor's monocytes from PBMCs (donor A) and differentiated a proinflammatory M1 macrophage culture [methods 2.2.4]. I identified the macrophages using flow cytometry [Figure 3-15] and found that they were predominantly CD16+CD14+ pro-inflammatory M1 macrophages (98.9%) [Figure 3-16].

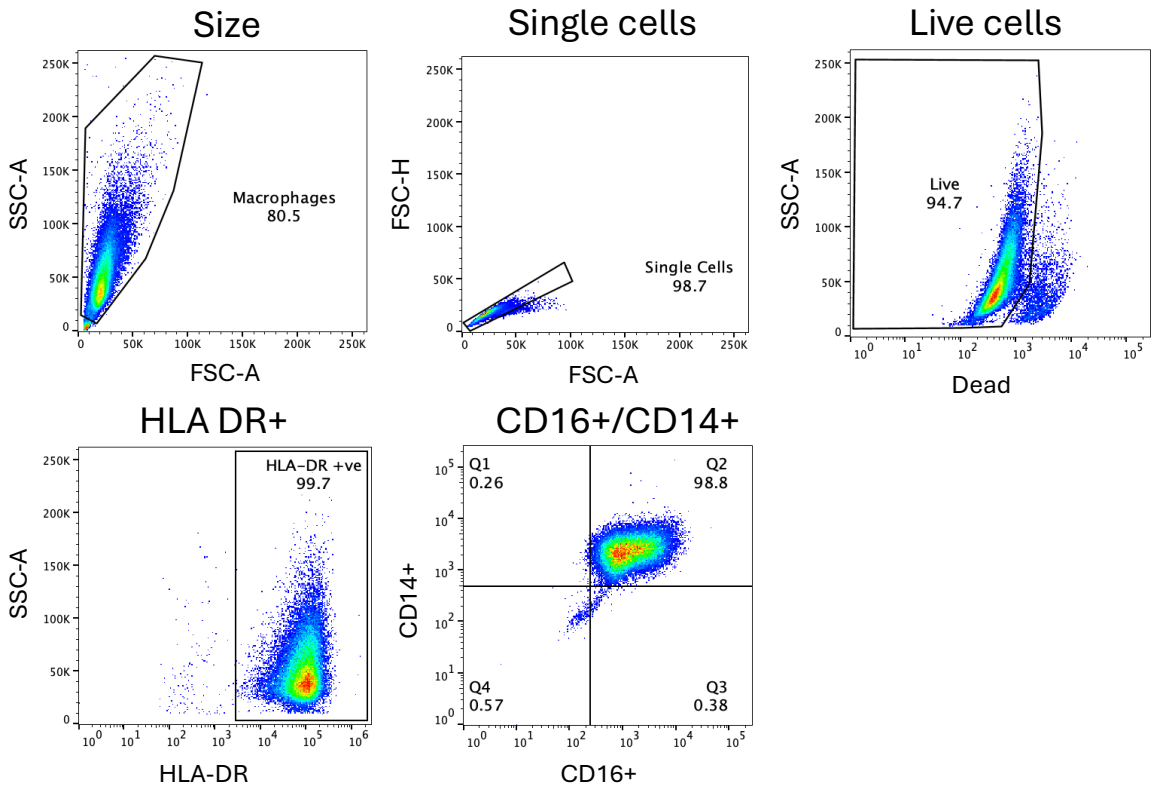

Figure 3-15: Representative gating of macrophage subsets isolated after 7 days culture. Cells were stained as described in Materials and Methods and acquired of a BD Celesta. Labels indicate cell populations, and the numbers show the percentage of cells within each gate. Cells were gated on size, single cells, viability, HLA DR expression (MHC II) and expression of CD16+ or CD14+.

I primed the T cells from a different donor (donor B), per previous methods, and began a co-culture of primed T cells from donor B, with allogenic macrophages from donor A; both were cultured along with either the cellularised MSC biomaterial or no cell control biomaterial for 48hrs [see methods: 2.4.3]. I strengthened the T cell activation panel to look at not just CD25+ expression, but also ICOS and PD1 expression [Figure 3-16]. When ICOS expression was globally high, I looked also at ICOS MFI to delineate any differences in amount of the molecule expressed by the cells.

At 48hrs co-culture in the presence of allogenic (donor A) macrophages only, or with the addition of MSC biomaterials or no cell controls, the primed (donor B) T cells did not mount any increased CD25, ICOS+, PD1+ expression, nor were there differences in ICOS MFI [Figure 3-17]. Whilst this was undertaken for a biological n=1 (donor A vs donor B), there was good reproducibility between the 4 technical repeats and no difference to controls. Furthermore, no increase in CD25 expression was seen in the negative control which was donor A macrophages with donor B primed T cells. Macrophages, unlike MSCs, are known to constitutively express MHC II and therefore T cells should begin to mount activation responses against allogenic macrophages reliably, but in this experiment at 48hrs no response was seen. I concluded that 48hrs co-culture duration was not long enough to allow any allogenic response to occur.

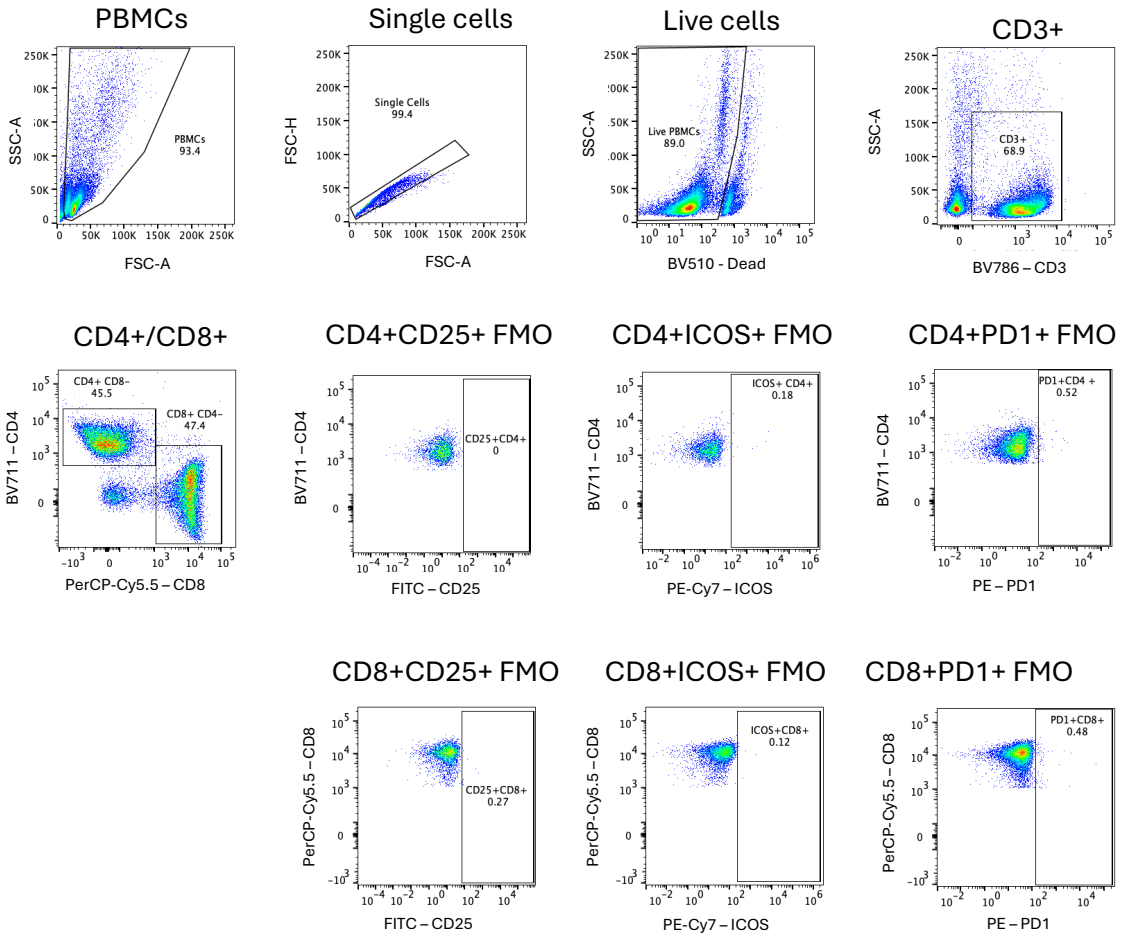

Figure 3-16: Representative gating of T cells isolated after 48hrs culture with MSC-biomaterials and allogenic macrophages. Cells were stained as described in Materials and Methods and acquired of a BD Celesta. Labels indicate cell populations, and the numbers show the percentage of cells within each gate. Frequency minus ones (FMOs) shown for newly added expanded T cell panel markers CD25+, ICOS+ and PD1+ expression.

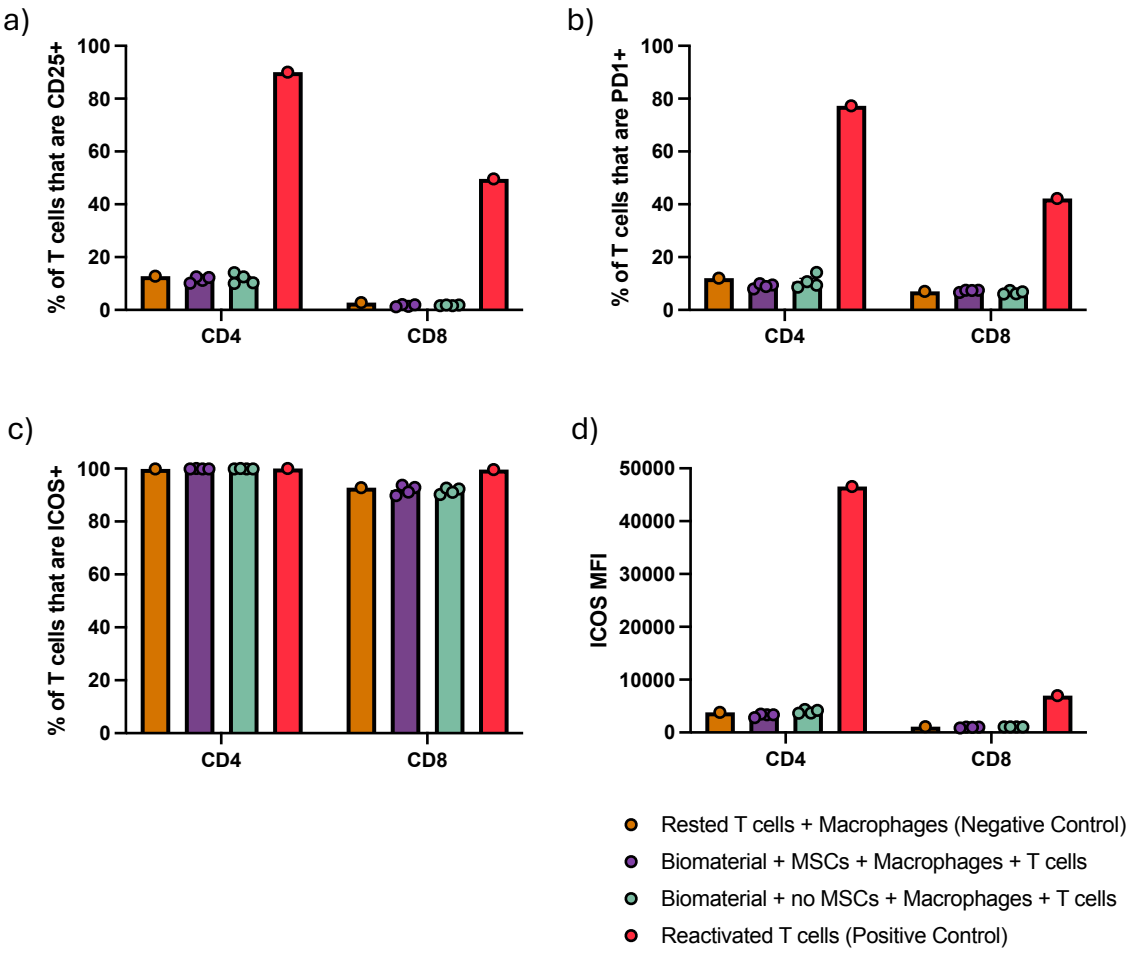

Figure 3-17: Primed T cell response to cellularised biomaterials in the presence of allogenic macrophages. Primed T cell activation shown through (a) CD25+, (b) PD1, (c) ICOS expression and (d) ICOS MFI for both CD4 and CD8 T cells. T cell responses to negative and positive controls and biomaterial with and without MSCs for 48hrs in the presence of allogenic macrophages shown. Graphed bars represent mean of 4 technical replicates within one experiment and a biological n=1. Error bars show SEM.

3.3.12 T cells vs allogenic macrophages up to 120hrs

To further test if the primed T cells could respond to foreign antigen, I sought to test them against a positive control cell known to express MHC class II. I had previously successfully isolated monocytes and differentiated them into M1 macrophages known to express MHC II [methods 2.2.4] and decided to use allogenic macrophages as the positive control cell. Given the results of the last experiment, in that 48 hours saw no increased response between donor A macrophages and donor B T cells at 48 hours [results 3.3.13], I sought to increase the co-culture duration to 3 to 5 days [methods 2.3.3]. For this experiment no biomaterials were used, and it was a two-cell co-culture between primed T cells and macrophages only.

The negative control (primed T cells without any co-culture) remained negative over the 5 days co-culture without increased CD25, ICOS MFI or PD1 expression [Figure 3-18]. Highest expression was seen in the positive control reactivated with the Miltenyi activator.

For CD4+ T cells, there was an increasing trend towards greater activation with significantly increased CD25 expression by 5 days co-culture (*, $p = 0.04$). In CD8+ T cells significant increases in CD25+ expression was found by 3 days co-culture (***, $p = 0.001$). No changes in the percentages of PD1 or ICOS MFI were found [Figure 3-18].

These data evidenced that the primed T cells used can respond to, both stimulus by further exposure to the Miltenyi activator, but also to allogenic antigen over 5 days of co-culture. For the remainder of the experiments, a minimum of 3 days and preferably, up to 5 days co-culture was used to ensure sufficient time to allow a detectable change in response (above controls). At 5 days co-culture, the primed

T cells have been *ex-vivo* for 7 days in culture without additional supplementary cytokines. Therefore, longer co-cultures beyond 5 days, in the absence of cytokine feeding were avoided, to limit the impact on cell death following extended *ex vivo* culture.

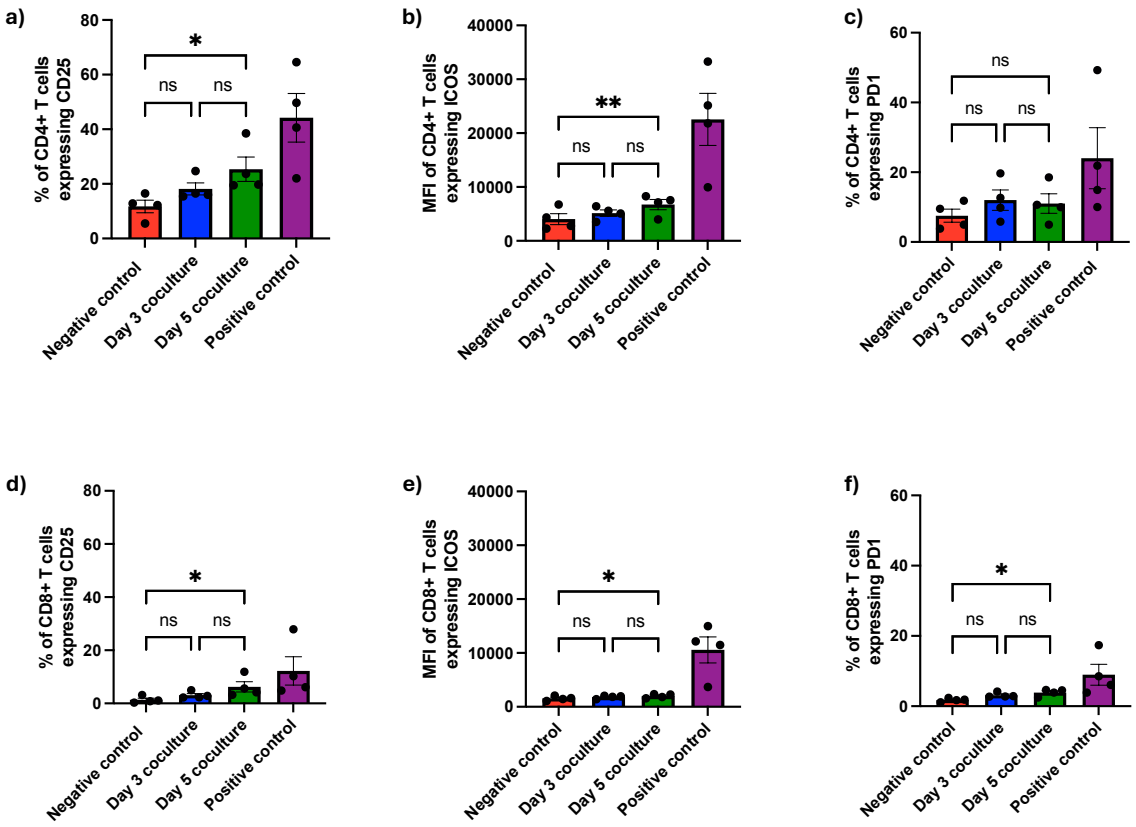

Figure 3-18: Primed T cell activation against allogenic macrophages in a mixed lymphocyte co-culture for up to 5 days. (a-c) CD4+ T cells and (d-f) CD8+ T cell responses to negative and positive controls and allogenic macrophages for 3 and 5 days co-culture. Bars represent the mean of. 4 biological replicates. Each data point is the mean of two technical replicates. Error bars represent the standard error of the mean. Data normally distributed and one-way anova statistical test performed with Bonferroni correction. P values = *p<0.05, **p<0.01, ***p<0.001, ****p<0.0001.

3.3.13 Optimised T cell Model

Following all the optimisation steps to build the T cell model the final schematic of the modelling methodology is shown [Figure 3-19].

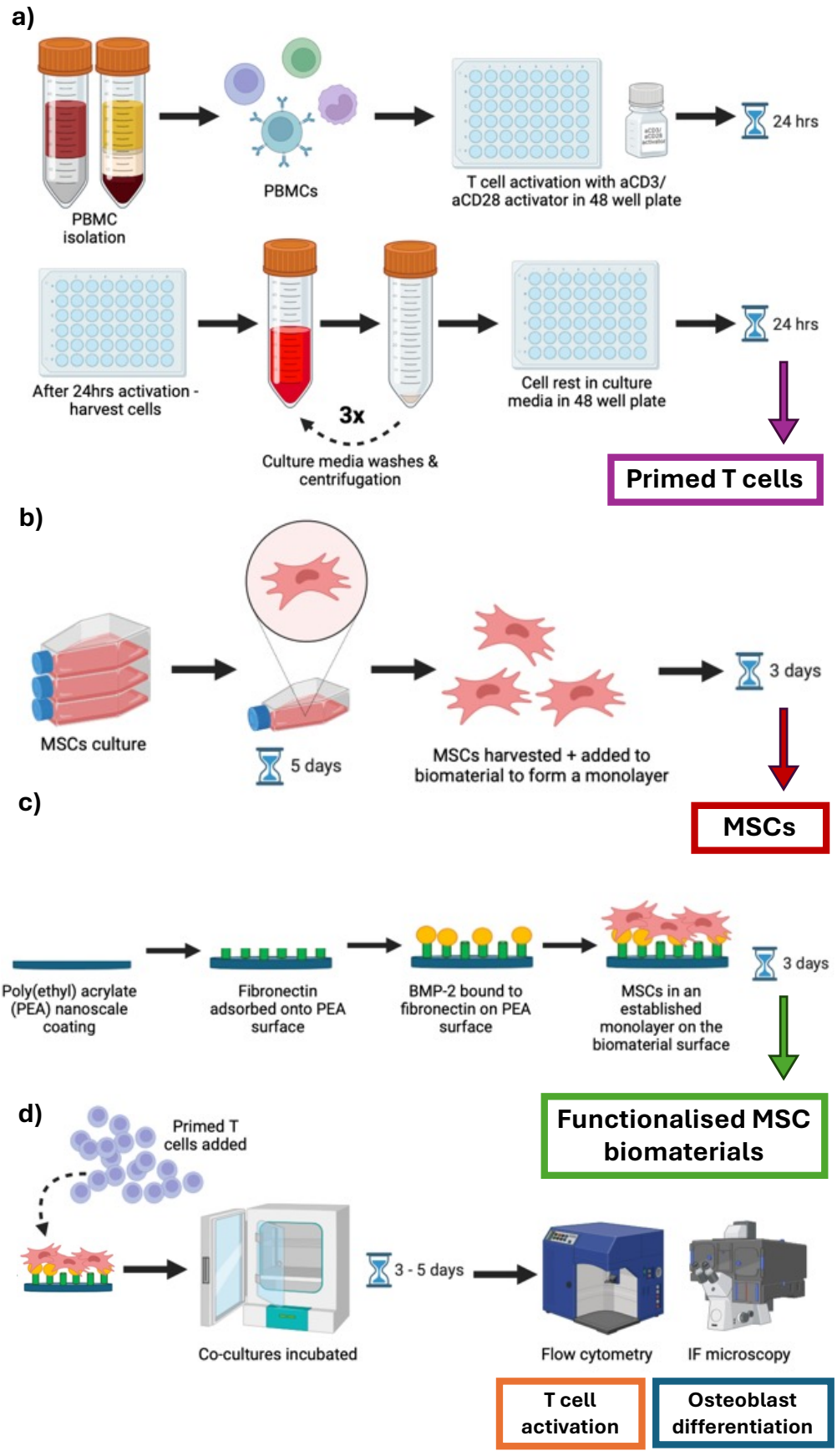

Figure 3-19: Diagram of the optimised T cell model. (a) Whole blood PBMC isolation, Miltenyi aCD3/aCD28 T cell activation, wash and rest steps to generate primed human T cells. (b) Human MSC culture to generate P3 or P4 MSCs for use in modelling. (c) Biomaterial formulation with PEA, FN, BMP-2 and establishment of a MSC monolayer. (d) Co-culture of primed T cells with MSC biomaterials for 3-5 days before flow cytometry or IF microscopy outputs. Created with BioRender.com

3.4 Discussion

The results of the T cell modelling establishment within this Chapter will be discussed in brief, but a more extensive discussion will follow [Chapter 6: Discussion].

3.4.1 A method for 'priming' human T cells in vitro

To model human T cell responses *in vitro*, firstly a method was required to activate T cells so that they were 'primed' and capable of future antigenic or stimuli responses and were no longer 'naïve'. Whilst activating T cells proved straightforward with market available aCD3/aCD28 activators (Miltenyi or Stemcell), the activation levels at manufacturer recommendation were >90%, defined by CD25+ expression. The primary challenge of the modelling was therefore establishing the optimum methodology to satisfactorily 'prime' the T cells, without over-activating them. This was achieved ultimately by reducing the dose of activator substantially and reducing the length of T cell activation. These data demonstrate that T cells can be activated with a 1:500 dilution of stock Miltenyi activator and a reduced activation time to 24 hours. After just one wash step, CD25+ expression reduced to 15% from >80% at manufacturer recommended protocol. This evidenced that 'priming' the T cells was possible with a change in activator dilution and duration of action.

3.4.2 An *in vitro* model of human T cell activation responses to cellularised biomaterials

To ensure the model was optimised for use in further experimentation, it was necessary to ensure the T cell 'priming' resulted in as low levels of CD25+ expression, post activator removal, as possible. The high levels of T cell activation

found in the early experiments, even after cell wash steps, demonstrated that the aCD3/aCD28 activator beads bound strongly to the T cells. A subsequent challenge was separating the cells from the activator to facilitate optimal cell rest. There were no differences found between wash media used, and therefore, culture media washes were performed three times resulting in a further reduction in CD25+ expression in CD4+ T cells to just 5.57% after 24 hours rest. Following low dose, short duration, increased washes and 24hr cell rest steps, CD25 expression remained low at 10.6% increasing only to 12.2% by 48hrs.

With an optimised ‘priming’ protocol, with satisfactory negative controls in the absence of further stimulation, next steps involved demonstrating that the model T cells could respond to both chemical and antigen stimulation as positive controls. The ‘primed’ CD4+ T cells were able to reach CD25 expression levels of 90% by 2 days in response to further aCD3/aCD25 activation and a mean 24.5% in the presence of allogenic macrophages over 5 days (n=4).

The T cells are primed over 2 days and then ran in co-culture with the biomaterial for 5 days (PBMCs are 7 days *ex-vivo*). This ensures that the T cells retain high viability and does not necessitate addition of any cytokines to the culture media which may skew downstream applications of the T cell modelling.

3.4.2.1 Model limitations

Having created an *in vitro* model of human T cell immune responses built upon a series of control experiments, there are limitations that should be acknowledged, and subsequent results interpreted within this context.

Firstly, an *in vitro* immune model of T cell responses focuses on T cell behaviour in isolation and does not recapitulate the *in vivo* complexities of the immune system and the cell-cell interactions that shape overall responses.

Secondly, the cell population used for the modelling is a mixed PBMCs population, meaning there are T cells, B cells, NK cells, monocytes and dendritic cells present within the modelling cultures. The proportions of these cells vary across individuals but typically 70-90% are lymphocytes, 10-20% are monocytes and 1-2% are dendritic cells. Within the lymphocyte component, anywhere from 70-85% are CD3+ T cells of which CD4:CD8 T cell ratio is approximately 2:1 (325). Arguably, modelling a mixed PBMC population is preferable, to better replicate the immune response *in vivo*, allowing for autologous macrophages and DCs to be present within the milieu, to facilitate antigen presentation to autologous T cells. Furthermore, the aCD3/aCD28 Miltenyi activator is a specific T cell only activator and therefore only the T cell component of the PBMC population will receive an activation signal during the 'priming' stage of the modelling, thereby controlling for effects on other cells. The activator used is also validated by Miltenyi R&D to be used on mixed PBMC populations for this purpose. Finally, all flow cytometry used to identify cells for model analysis, gated specifically on T cell specific markers, and therefore excluded all other cell types from the analyses. What cannot, within this modelling, be controlled for, is any interaction between other PBMC types and the T cells within the cultures, that may then subsequently affect the T cell response. A way to control for this would have been to undertake a T cell isolation stage after PBMC isolation, to negate all other cell types, to enable use of a pure T cell population. However, due to feasibility and cost reasons, this was felt to be unrequired and less replicative of *in vivo* conditions. Without an activation signal or supplementation in the culture media of any growth factors or cytokines, it is

unlikely many of the monocytes, dendritic, B or NK cells survived the co-culture durations used within the modelling.

Finally, in the reactivated T cells group (used as a positive control) the cells have been primed using the aCD3/aCD28 Miltenyi activator, rested and re-exposed to a further dose of the activator. It is possible that the ‘reactivated’ cells are just the cells that missed the activation signal on first exposure. This is unlikely as during first exposure on average 5-15% of CD4+ T cells showed evidence of activation with CD25 expression, and on re-exposure to the same concentration of activator, after ‘priming’ this increased to 80-90%. A way to control for this would be to sort the T cells into activated and unactivated populations post initial exposure to the aCD3/aCD28 activator, then rest them and reactivate with further exposure but separately and compare.

In summary, improvements to the modelling could be made with more time, money and manpower to make the experiment feasible. These improvements would include, using more donors to increase the power and enable gender and age matched comparisons, T cell isolation to use a pure population to control for any cell-cell interactions and cell sorting to ensure only truly reactivated cells were used as a positive control. Finally, as with all *in vitro* models, *in vivo* validity testing would confirm applicability of the model, however this is not feasible as would necessitate a human clinical trial.

Chapter 4 Immune modelling

4.1 Introduction

Establishing the immune response to functionalised MSC biomaterials is critical to the clinical translation of these promising technologies. With an optimised T cell protocol for modelling human immune responses *in vitro* established, I wanted to measure T cell surface marker activation responses to allogenic MSC biomaterials at various timepoints of their differentiation [Chapter 3].

The exact timescales for MSC differentiation into osteoblasts depends on the specific culture conditions and the tissue source of MSCs. However, it is generally accepted that between D7 and D14 metabolomic changes begin to commit the MSCs to their cell fate (326). At the MSC undifferentiated biomaterial day 3 (D3) timepoint, the MSCs have been in culture for less than a week and differentiation into osteoblasts is therefore yet to occur. Similarly, the literature reports osteoblast markers may be upregulated anytime from day 21 (D21) depending on individual culture conditions (327). I therefore chose to co-culture MSC/osteoblasts with the T cells at two timepoints at day 28 (D28) and a week later, at day 35 (D35) to ensure osteoblast differentiation had occurred and could be captured at one of these timepoints. The aim was to streamline this to just one representative late timepoint for future experimentation.

To determine if osteoblast differentiation had occurred, I planned to stain for late differentiation markers OCN and OPN (327). OCN is a non-collagenous protein hormone found in bone, it is the most abundant protein and is secreted exclusively by osteoblasts to regulate bone mineralisation (328). OPN is more versatile non-collagenous protein produced by osteoblasts, osteoclasts, T cells, macrophages

and neutrophils (329). OPN has multiple roles, including effects on both innate and adaptive immunity, as well as mineralisation and resorption of bone matrix (330).

4.2 Aims

- To use the established in *vitro* T cell model methodology to define human T cell responses to 3 days aged undifferentiated MSC biomaterials

- To differentiate MSC biomaterial into osteoblasts over 28 and 35 days and optimise the most reliable methodology to confirm differentiation

- To use the established in *vitro* T cell model to define human T cell responses to 28 days aged differentiated osteoblast biomaterials

- To use the established in *vitro* T cell model to define human T cell responses to 35 days aged differentiated osteoblast biomaterials

4.3 Results

4.3.1 Osteoblast differentiation from MSCs on biomaterials occurs by D28 in *vitro*

The adsorption of BMP-2 within the fibronectin biomaterial to enhance the differentiation of MSCs into osteoblasts is an established technique in the Salmeron-Sanchez lab (331). To confirm that in my hands, MSC differentiated into osteoblasts, I took three approaches to measure osteoblast defining molecules at day 28 and 35. Techniques used included both immunofluorescence microscopy and rt-qPCR for gene and protein expression of OCN and OPN, which are well-established markers of osteogenesis (332-338). Finally, assays were performed

for alkaline phosphatase as a hallmark of osteoblast differentiation and alizarin red staining for evidence of calcification.

Immunofluorescence (IF) microscopy was performed on D28 and D35 aged MSCs on the PEA, fibronectin and BMP-2 biomaterial, to confirm that in my hands the cells differentiated into osteoblasts. The imaging was done through the biomaterial coating leaving the cells in situ, having been fixed with formaldehyde [methods 2.6].

The MSCs, PEA, fibronectin and BMP-2 cultures were stained for DAPI, phalloidin and either OCN or OPN. As the cultures stained were never exposed to any other cell type other than the MSCs, the presence of OCN and OPN would be attributed to osteoblast differentiation specifically.

Results for the D28 cultures showed both OCN and OPN expression [Figure 4-1]. This was quantified for the available wells by taking an average of 6 images per well and reporting the mean [Figure 4-2]. Furthermore, on comparing BMP-2 versus no BMP-2 conditions, trends showed increased OCN and OPN expression when exposed to biomaterial containing growth factor BMP-2. The D35 culture images showed OCN and OPN expression, which was expected as differentiation confirmed on D28 images [Figure 4-3]. This further confirmed D28 alone would be sufficient for future experimentation, as the latest timepoint.

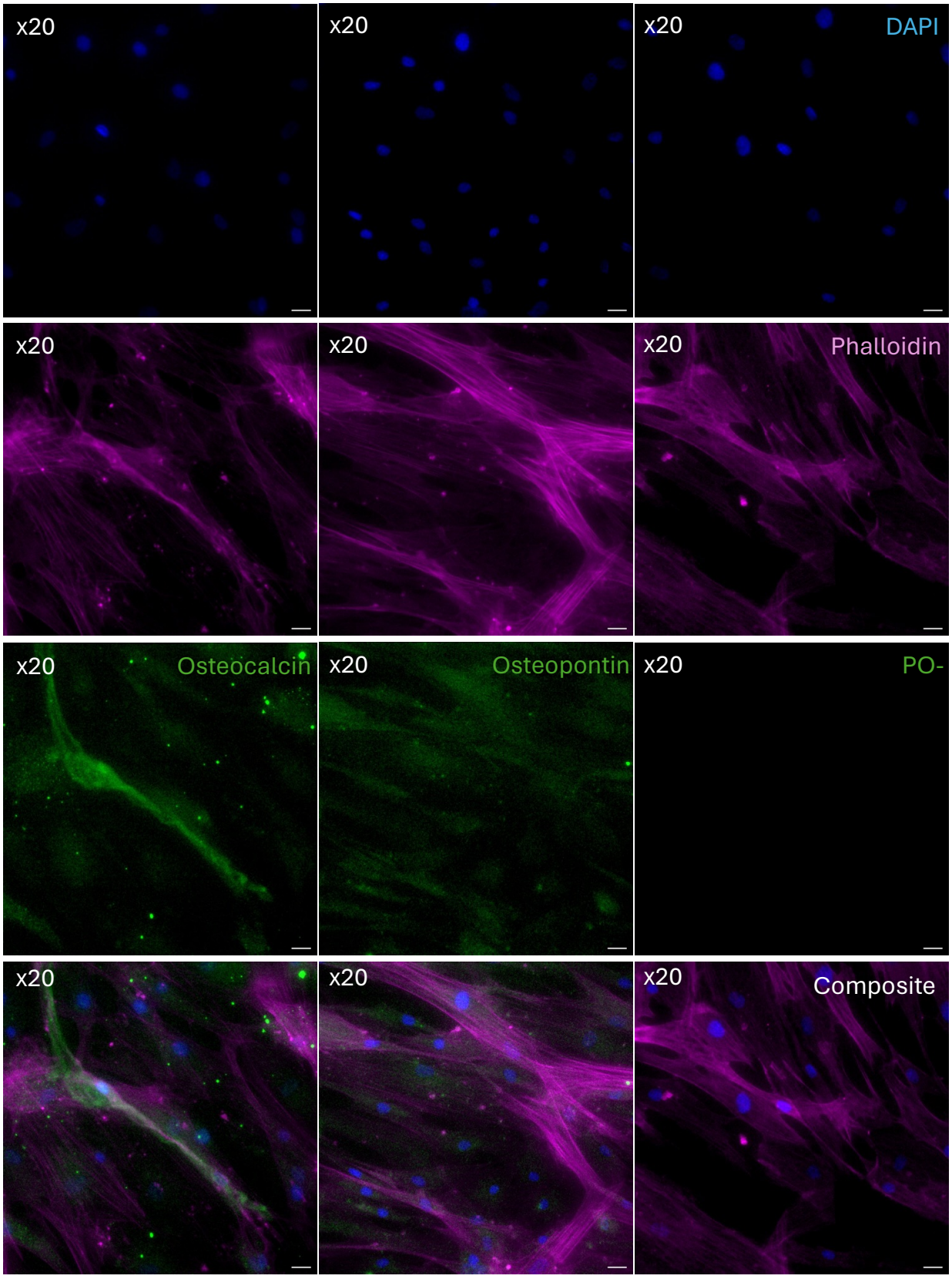

Figure 4-1: Immunofluorescence microscopy images of late time point D28 PEA, fibronectin, BMP-2 MSC biomaterials. Cells were stained for DAPI (blue), phalloidin (magenta) and osteoblast differentiation markers osteopontin or osteocalcin (green). Primary omission staining shown (PO-). Images are representative of one experiment, with 2 wells per condition and 6 images taken per well. Scale bars are 100uM.

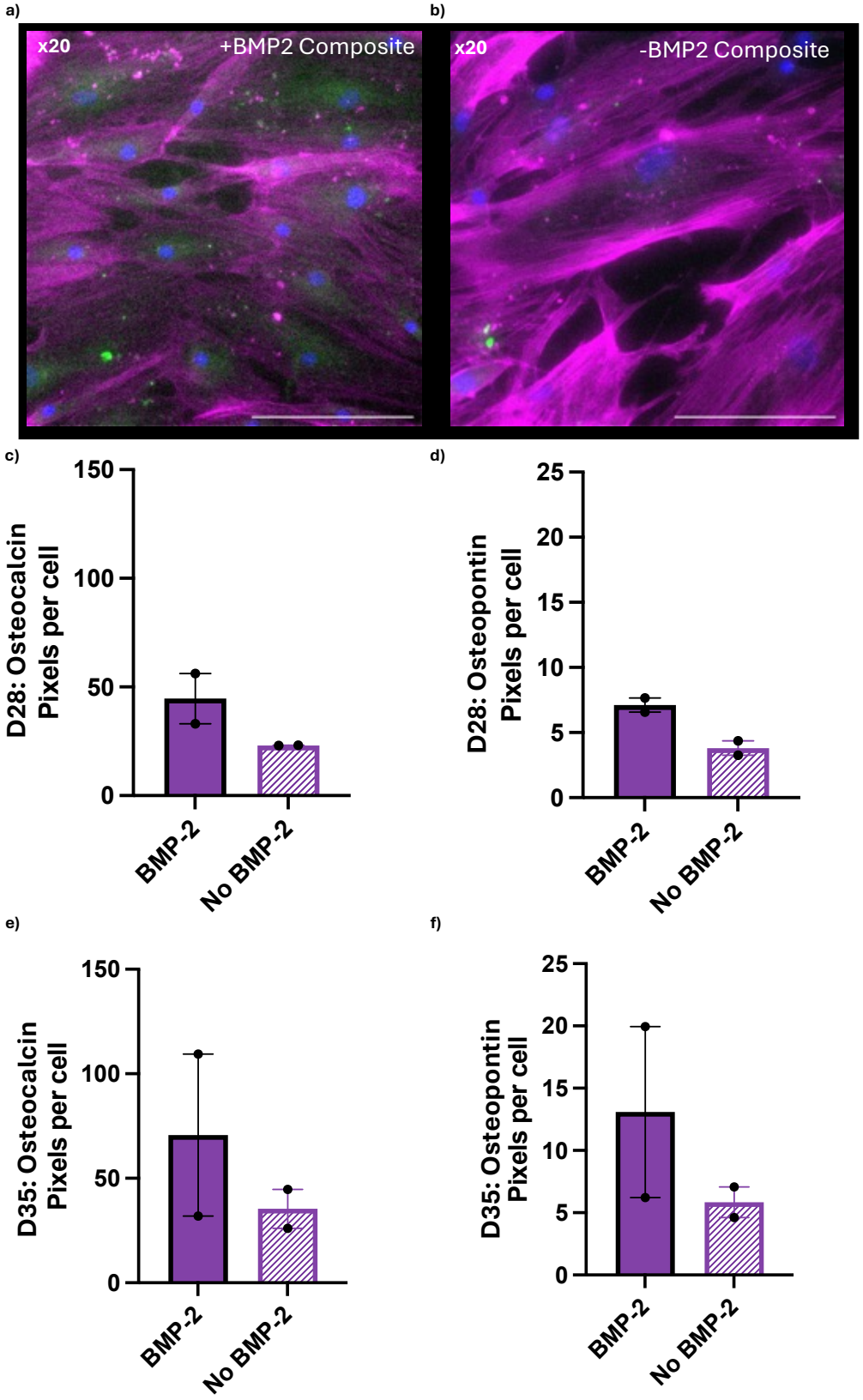

Figure 4-2: Quantification of immunofluorescence (IF) microscopy osteopontin and osteocalcin expression for biomaterials with MSCs. (a) IF image of D28 osteoblasts in the presence of BMP-2 – DAPI in blue, osteopontin in green, phalloidin in magenta, scale bars represent 100μm (b) IF image of D28 cells in the absence of BMP2. (c-d) Quantification of OCN and OPN expression in D28 and (e-f) D35 aged cells. Data points represent an average of immunofluorescence from 6 images per well normalized to cell number. Biological n=1 and 2 wells stained per time point. Bars represent the mean of the 2 wells and the error bars are the standard error of the mean.

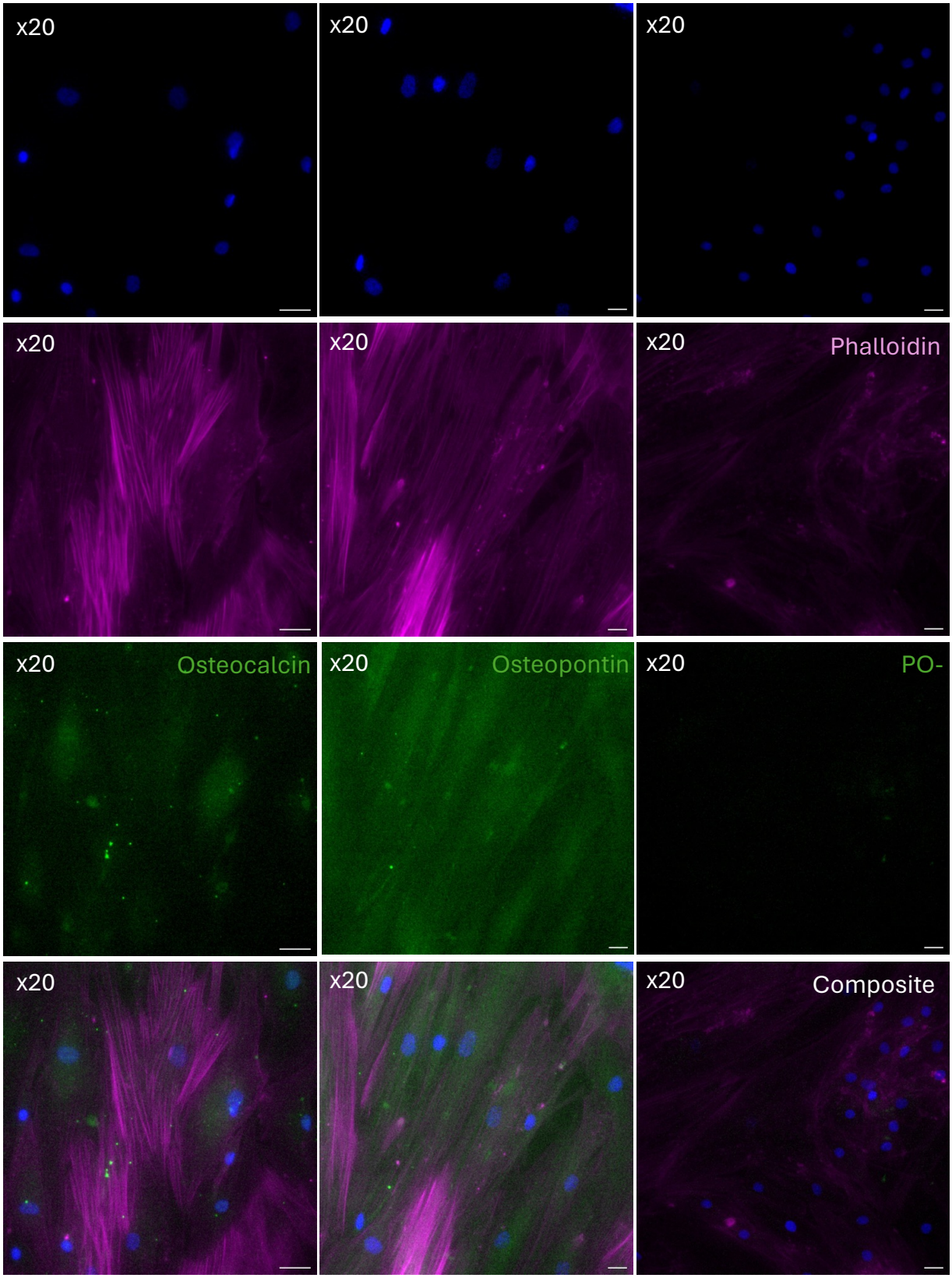

Figure 4-3: Immunofluorescence microscopy images of late time point D35 FN MSC biomaterials. Cells were stained for DAPI (blue), phalloidin (magenta) and osteoblast differentiation markers osteopontin or osteocalcin (green). Primary omission staining shown (PO-). Scale bars are 100uM. Images are representative of one experiment, with 2 wells per condition and 6 images taken per well.

4.3.2 D35 osteoblasts express ALP and show evidence of mineralisation

The 35 days aged osteoblast cultures on PEA with fibronectin and BMP-2 were stained for the presence of ALP and alizarin red [methods 2.6.4]. ALP is a phosphatase enzyme found across multiple organs including liver, bone kidneys and digestive system. It is a membrane-bound glycoprotein recognised as an early osteogenic marker secreted by osteoblasts; it functions to provide a high phosphate concentration at the osteoblast cell surface to aid bone mineralisation (339). Alizarin red staining is a technique to visualise any mineralisation that has occurred by cultured osteoblasts, by staining for calcium deposition.

The D35 MSC cultures showed both alizarin red and alkaline phosphatase staining suggestive of osteoblast differentiation with mineralisation and calcium deposition [Figure 4-4]. The areas towards the centre of each 24 well were the most mineralised in keeping with the cell cultures being most confluent in these regions.

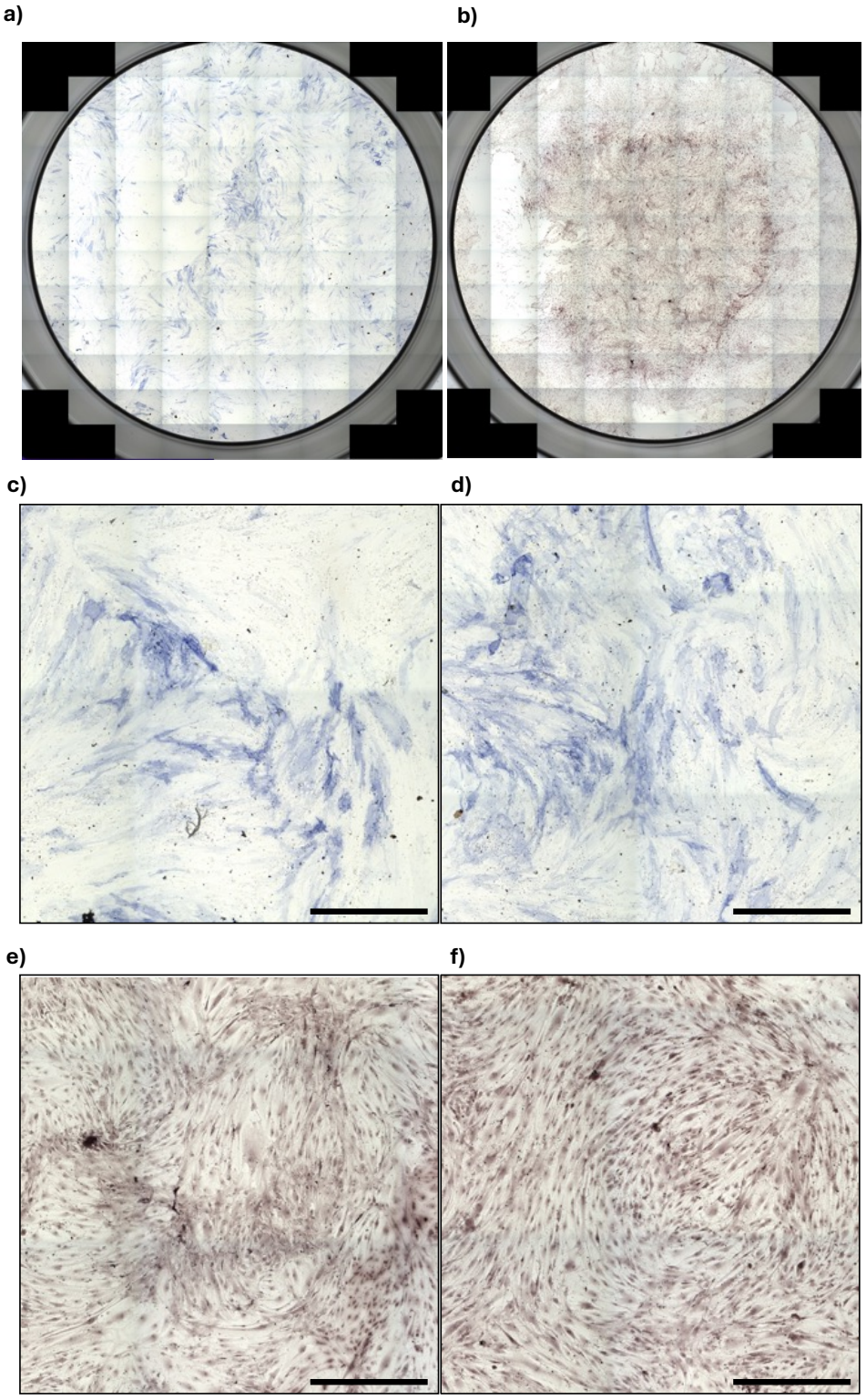

Figure 4-4: Multiple stitched microscopy images of D35 aged MSC biomaterials with 76 images combined to capture the whole 24-well (diameter 13mm). Results shown for both alkaline phosphatase staining (a) and alizarin red staining (b). Representative sections of interest shown for alkaline phosphatase (c-d) and alizarin red staining (e-f). Scale bars 50μm.

4.3.3 Rt qPCR reveals higher OCN expression in the presence of BMP-2 by D35

Reverse transcription qPCR was performed for the D28 and D35 MSC cultures to look for evidence of gene expression of osteoblast specific markers osteonectin (ON), OPN, OCN and ALP [Figure 4-5]. MSCs established on PEA and fibronectin only cultures were compared to MSCs established on PEA with fibronectin and the presence of growth factor BMP-2.

Mean gene expression at D28 trended higher in the BMP-2 conditions. However, the data showed large variance between technical replicates. At D35, OCN gene expression with BMP-2 present was higher than cells cultured in the absence of BMP-2 [Figure 4-5]. Trends for OPN and ON showed increases with BMP-2 exposure. Notably the expression of ALP reduced at the D35 timepoint. For future experimentation, it was therefore decided that immunofluorescence (IF) microscopy alone would be used to confirm osteoblast differentiation, by the expression of OCN and OPN, as markers on D28 aged MSC cultures.

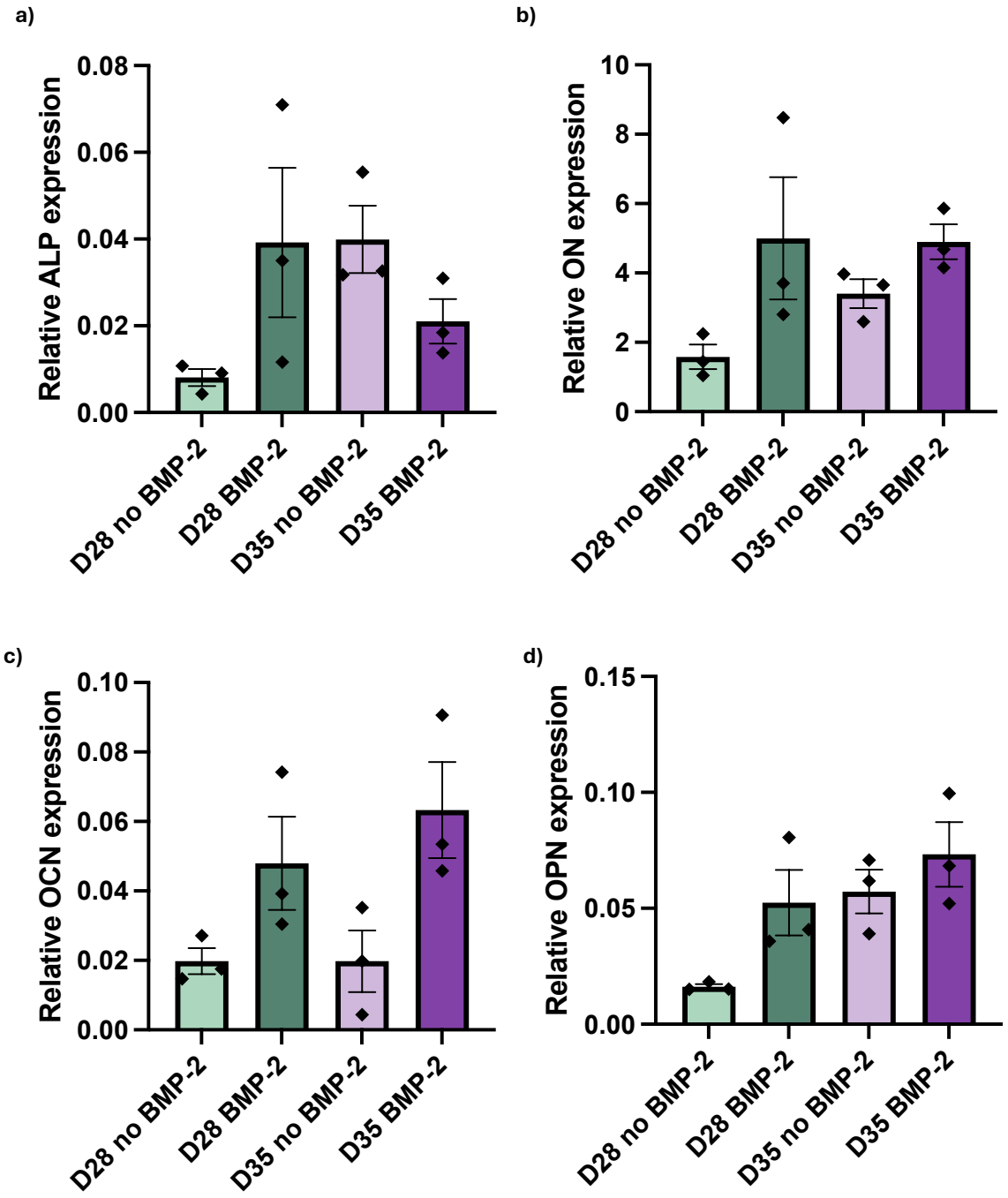

Figure 4-5: RT-qPCR results for D28 and D35 cultured MSC biomaterials. (a) alkaline phosphatase (ALP), (b) osteonectin (ON), (c) osteocalcin (OCN) and (d) osteopontin (OPN) gene expression levels normalized to the GAPDH housekeeping gene for both D28 and D35 MSC cultures. Bars represent the mean of 3 technical replicates from a biological n=1, error bars represent standard error of the mean.

4.3.4 Modelling Experimental Design

Having confirmed the presence of osteoblasts in my model, I then examined the T cell response at early and late stages of the culture. The MSC biomaterials were created as per prior methods and incubated with the T cell model for 3 to 5 days [methods 2.1]. The experiment modelling was run on 3 days aged MSCs on the PEA, fibronectin and BMP-2 biomaterials and then on 28 and 35 day MSCs differentiated into osteoblasts [Figure 4-6]. The output was flow cytometry using the established panel [Figure 4-7].

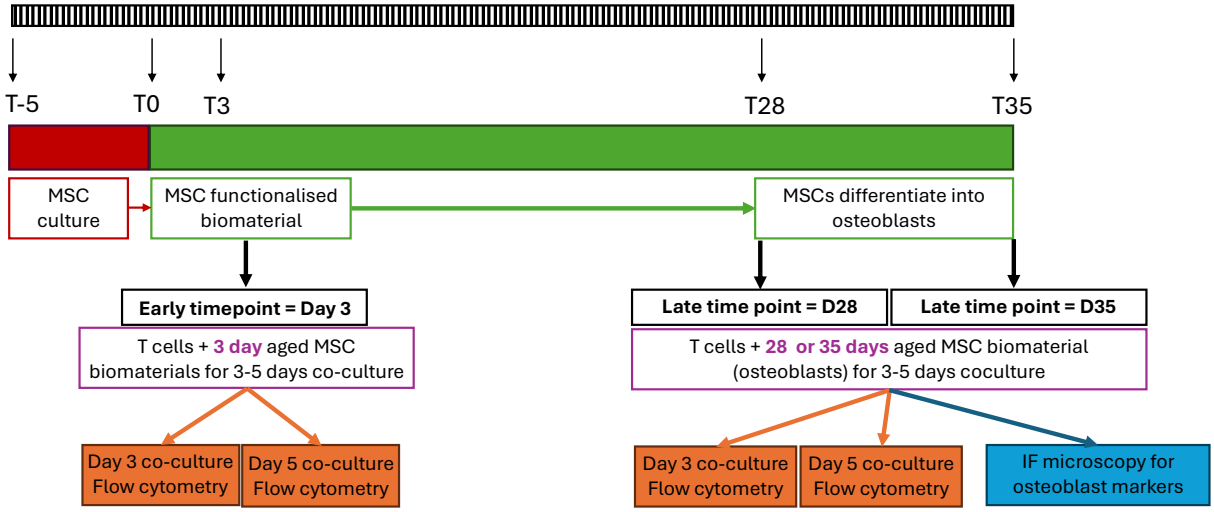

Figure 4-6: Diagram of experiment timeline for T cell modelling against early undifferentiated 3 day aged MSC biomaterials and mature 28 or 35 day differentiated osteoblasts. Modelling will be run for 3-5 days with flow cytometry at each time point. IF microscopy will be performed on 28 and 35 day aged biomaterials to look for osteoblast markers to confirm differentiation to target osteoblast cells.

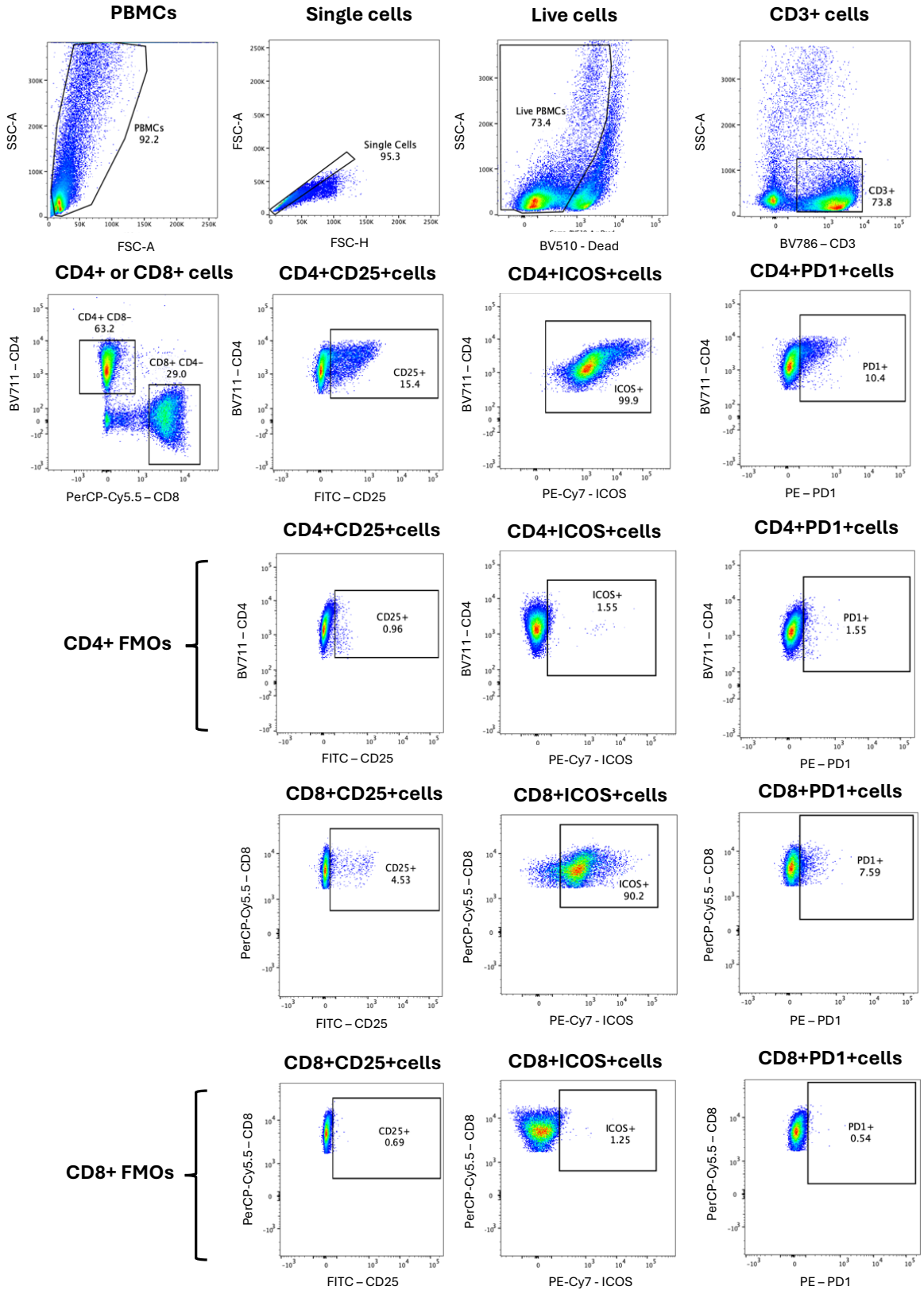

Figure 4-7: Representative gating of T cells 3 - 5 days after co-culture with early day 3 MSC biomaterials. Cells were stained as described in Materials and Methods and acquired of a BD Celesta. Labels indicate cell populations. The numbers show the percentage of cells within each gate. Gates shown for CD25+, ICOS+ and PD1+ as T cell activation markers. Gates were drawn using donor matched FMOs also shown.

4.3.5 MSC biomaterials provoke increased CD25 expression in T cells by D3 co-culture

At the earliest timepoint, day 3, the MSCs had been on the biomaterial for 3 days forming a monolayer, and the T cells were added for 3-5 days of co-culture. After only 3 days co-culture with human T cells, significant increases in CD25 expression were already seen for CD4+, but not CD8+, T cells [Figure 4-8].

After extended co-culture to 5 days, significant increases in CD25 expression were seen on both CD4+ and CD8+ T cells [Figure 4-9]. Expression of all markers trended higher in the MSC cellular conditions versus acellular controls, however these differences were not significant for ICOS MFI or PD1 expression at this early timepoint.

Data for the early timepoint, D3 co-culture, demonstrated that, despite literature suggesting MSCs are immune-privileged, by just 5 days co-culture within this modelling, significant increases in CD25 expression are seen for both CD4+ and CD8+ T cells.

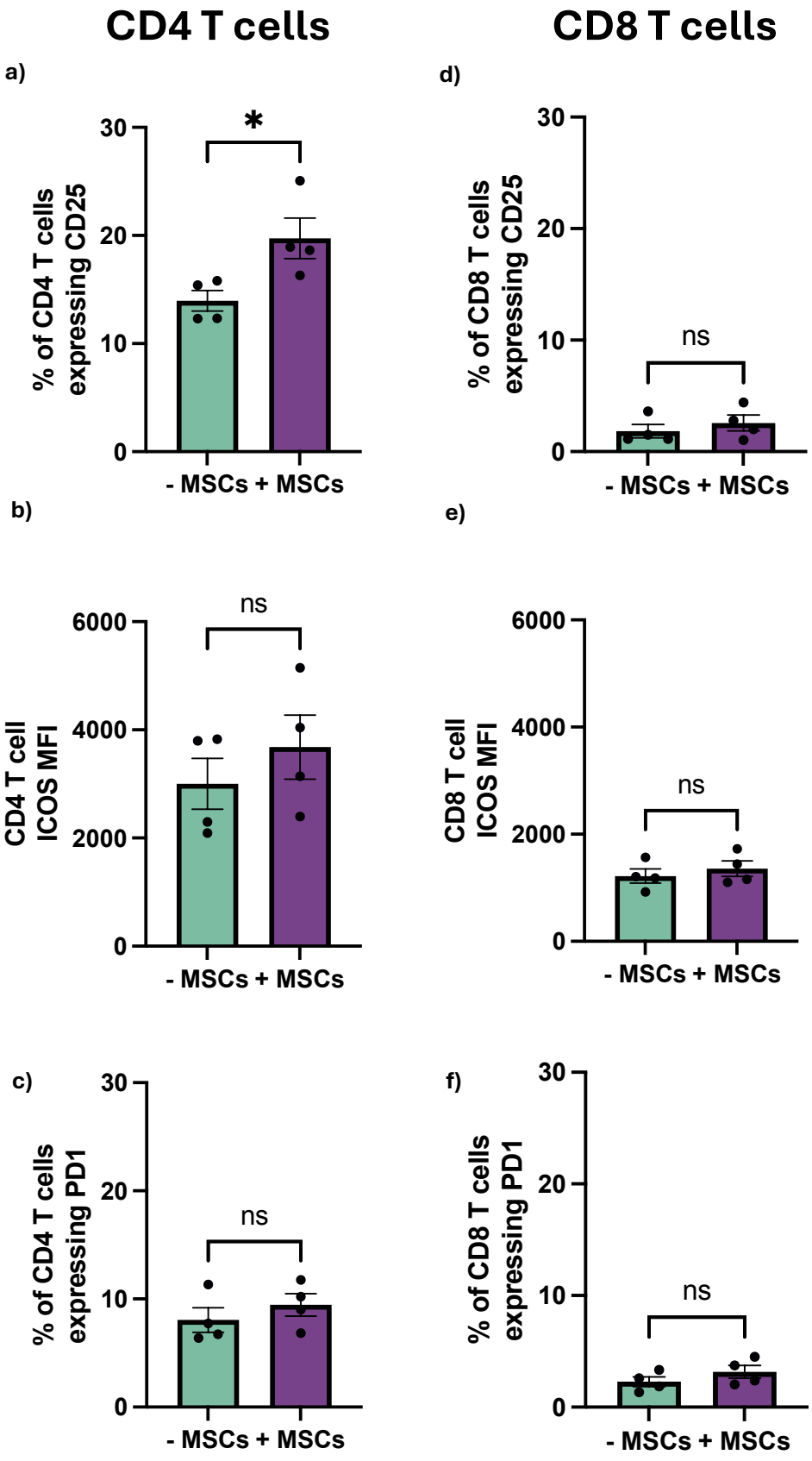

Figure 4-8: Flow cytometry results for early timepoint D3 co-culture with CD4 T cells (a-c) and CD8 T cells (d-f) with PEA, FN, BMP2 biomaterial with and without MSCs for 3 days. Graphs show flow cytometry levels of CD25, ICOS MFI and PD1 expression. Graphed bars show the mean of 4 biological donors, with each point being the mean of two technical replicates. Error bars show the standard error of the mean. Data was normally distributed and analysed using paired T tests. P values = *p<0.05, **p<0.01, ***p<0.001, ****p<0.0001.

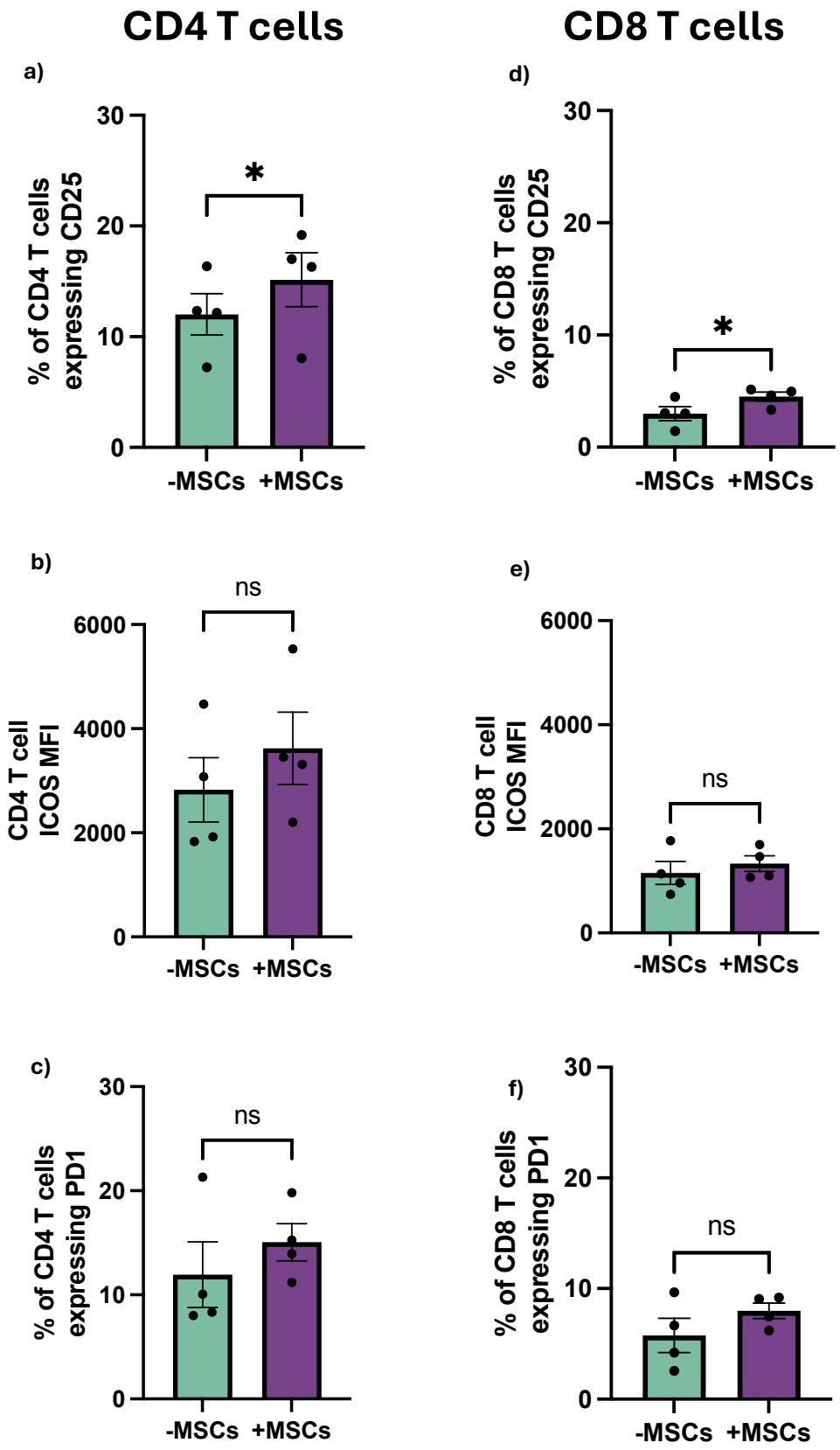

Figure 4-9: Flow cytometry results for early timepoint D3 co-culture with CD4 T cells (a-c) and CD8 T cells (d-f) with PEA, FN, BMP2 biomaterial with and without MSCs for 5 days. Graphs show flow cytometry levels of CD25, ICOS MFI and PD1 expression. Graphed bars show the mean of 4 donors, with each point being the mean of two technical replicates. Data was normally distributed and analysed using paired T tests. Error bars show the standard error of the mean. P values = *p<0.05, **p<0.01, ***p<0.001, ****p<0.0001.

4.3.6 D28 differentiated osteoblast biomaterials reveals broader T cell activation by D3

The cellularised biomaterials were cultured over 4 weeks with media changes and culture inspection via microscopy twice weekly, to ensure they remained viable. At day 28, the primed T cells were added to the osteoblast-differentiated culture and co-cultured for 3-5 days.

After 3 days co-culture with the maturing day 28 biomaterials, significant increases were seen in CD25, ICOS MFI and PD1 expression by CD4+ T cells [Figure 4-10]. Furthermore, significant increases in CD25 and PD1 expression were now seen for CD8+ T cells. CD8+ T cells ICOS MFI was not significantly different to controls.

After 5 days co-culture, expression of CD25 in both CD4+ and CD8+ T cells was higher than after 3 days culture, at 23.9% (vs 15.8%) and 8.04% (vs 4.35%) respectively. However, there was more biological variation seen in the data, with some outlying data points, so whilst trends remained the same, no significance was found between groups for CD25 or PD1 expression [Figure 4-11]. ICOS MFI was significantly higher in differentiated MSC biomaterial conditions versus controls for CD4+ T cells.

Together my data suggest that there is some limited activation of T cells by undifferentiated MSCs. However, as demonstrated by upregulation of later activation molecules ICOS and PD1, co-culture with osteoblasts led to more substantial T cell activation.

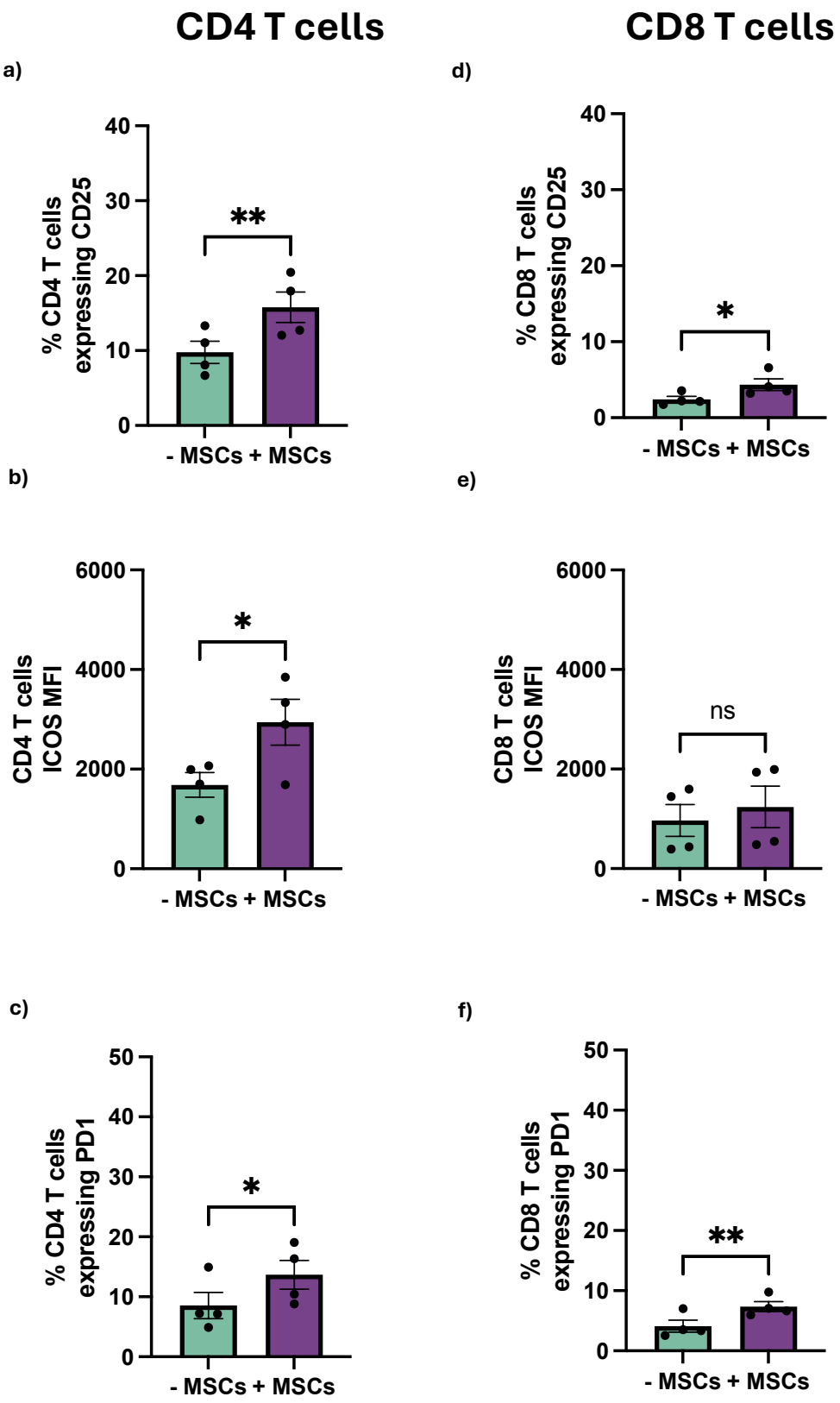

Figure 4-10: Flow cytometry results for late timepoint D28 co-culture with CD4 T cells (a-c) and CD8 T cells (d-f) with PEA, FN, BMP2 biomaterial with and without MSCs for 3 days. Graphs show flow cytometry levels of CD25, ICOS MFI and PD1 expression. Graphed bars show the mean the 4 biological replicates, with each point being the mean of two technical replicates. Error bars show the standard error of the mean. Biological donors were matched to the earlier D3 timepoint. Data was normally distributed and analysed using paired T tests. P values = *p<0.05, **p<0.01, ***p<0.001, ****p<0.0001.

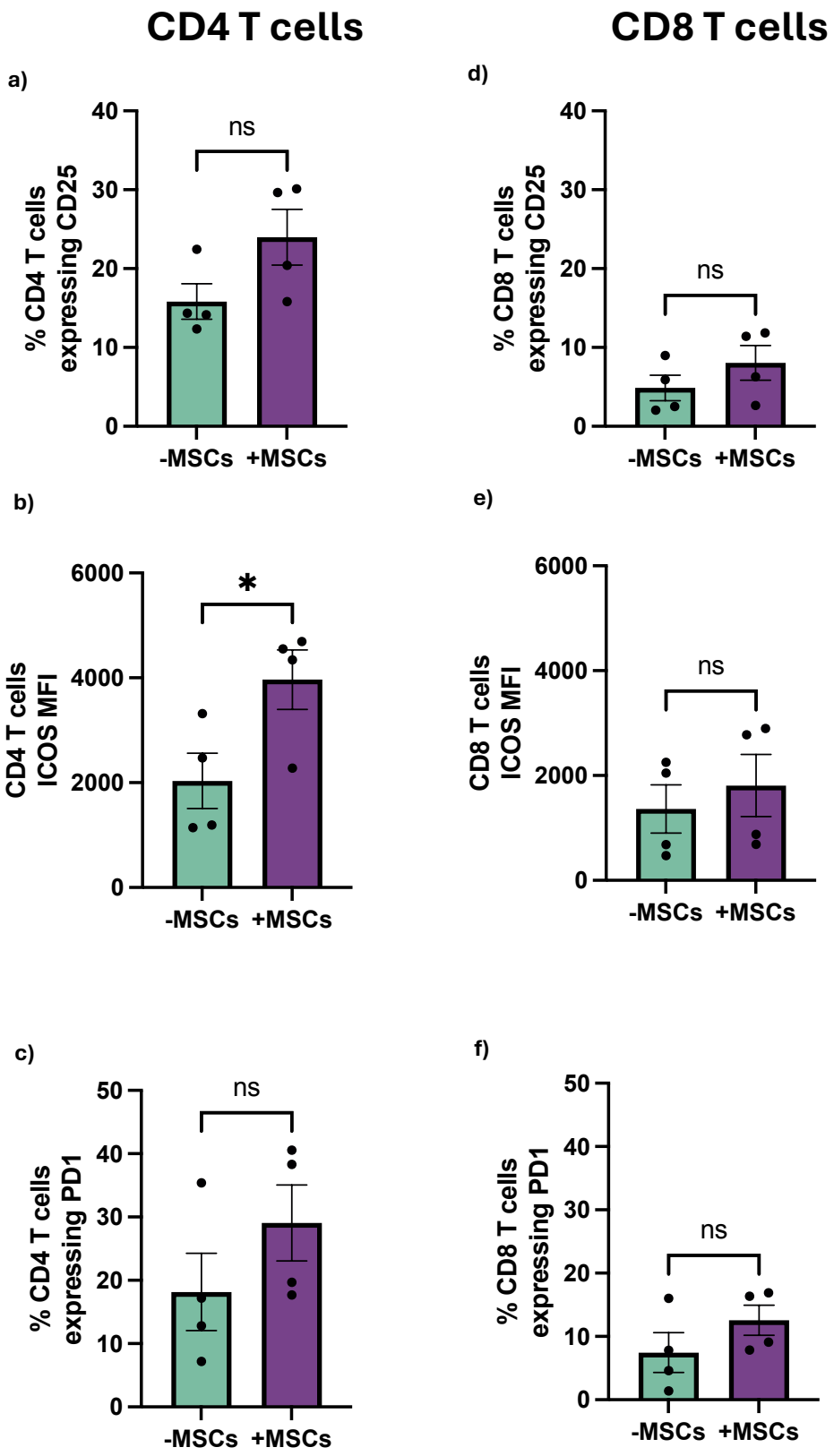

Figure 4-11: Flow cytometry results for late timepoint D28 co-culture with CD4 T cells (a-c) and CD8 T cells (d-f) with PEA, FN, BMP2 biomaterial with and without MSCs for 5 days. Graphs show flow cytometry levels of CD25, ICOS MFI and PD1 expression. Graphed bars show the mean the 4 biological replicates, with each point being the mean of two technical replicates. Error bars show the standard error of the mean. Biological donors were matched to the earlier D3 timepoint. Data was normally distributed and analysed using paired T tests. P values = *p<0.05, **p<0.01, ***p<0.001, ****p<0.0001.

4.3.7 D35 differentiated osteoblast biomaterials reveal ongoing T cell activation

The osteoblast biomaterials were cultured a further week (total 5) with media changes and culture inspection via microscopy twice weekly, to ensure the cells remained viable. At day 35, the primed T cells were added to the osteoblast-differentiated culture and co-cultured for 3-5 days.

After 3 days, there was a significant increase in CD4+ T cell ICOS MFI but no significant differences in CD25 or PD1 expression [Figure 4-12]. Similarly, no significant differences were detected in CD8+ T cells for CD25, ICOS MFI or PD1 expression. Akin to the day 28 results, there was a large spread of the data, and whilst trends were higher for expression of CD25, this did not achieve significance and appeared lower than at day 28 (mean 17.66%).

By 5 days co-culture with the 35 days matured cellularised biomaterials, CD25 expression by CD4+ T cells was significantly higher than no-cell controls, with 25.85% expression [Figure 4-13]. There were no significant differences for CD4+ ICOS MFI or PD1 expression. There were no significant differences for the CD8+ T cells.

At the D35 timepoint there was a significant increase in T cell CD25 expression by 5 days co-culture in cultures with as compared to without differentiated MSCs. At this timepoint, the cultures were older than had previously been tried by the group *in vitro*, and larger variances in data were seen with some outlying data points. As the pattern of the T cell response at D35 was akin to that at D28, it was decided that this would be the latest time point examined in future studies.

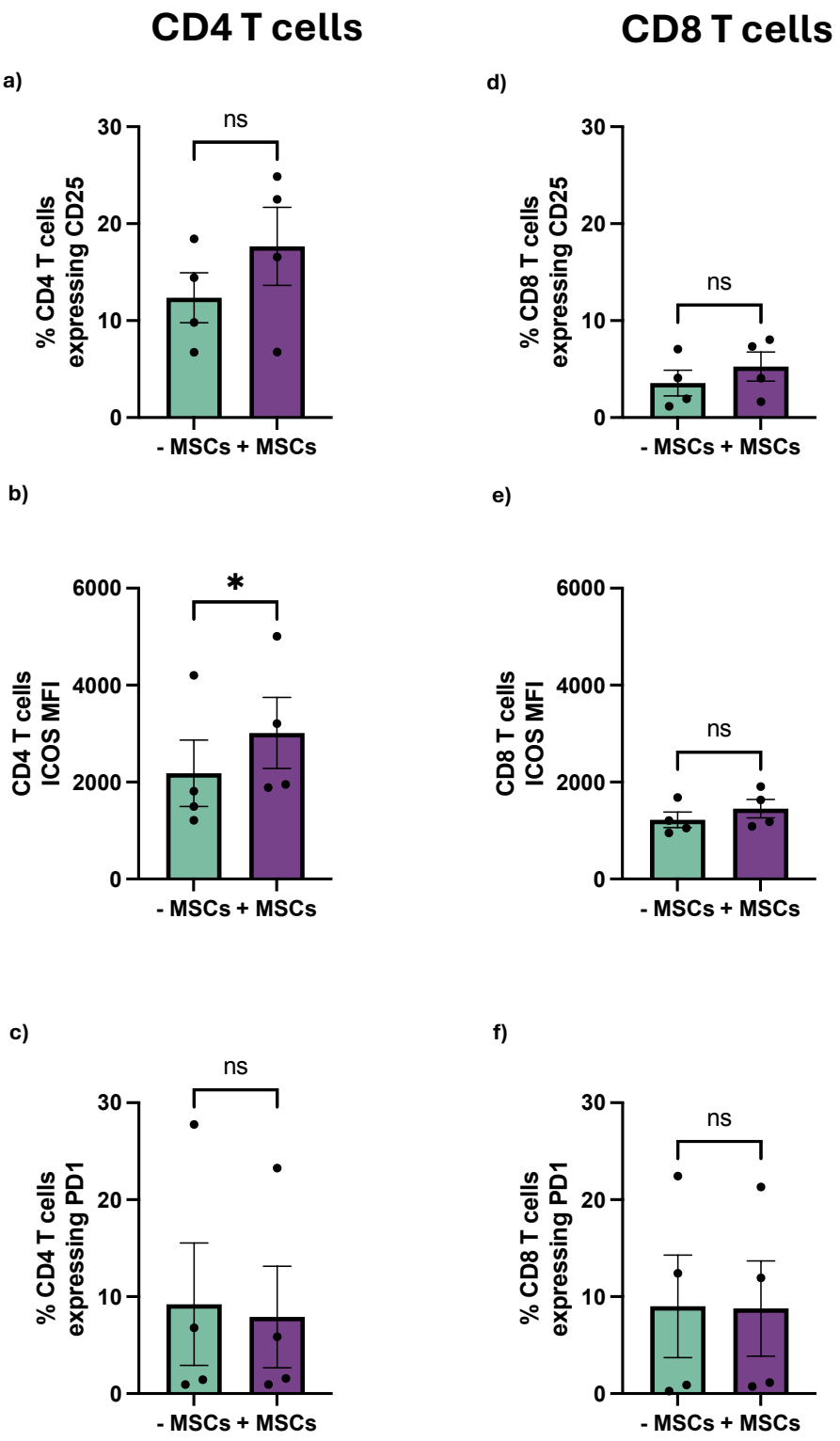

Figure 4-12: Flow cytometry results for late timepoint D35 co-culture with CD4 T cells (a-c) and CD8 T cells (d-f) with PEA, FN, BMP2 biomaterial with and without MSCs for 3 days. Graphs show flow cytometry levels of CD25, ICOS MFI and PD1 expression. Graphed bars show the mean of 4 donors, with each point being the mean of two technical replicates. Error bars show the standard error of the mean. Biological donors were matched to the earlier D3 and D28 timepoints. Data was normally distributed and analysed using paired T tests. P values = *p<0.05, **p<0.01, ***p<0.001, ****p<0.0001.

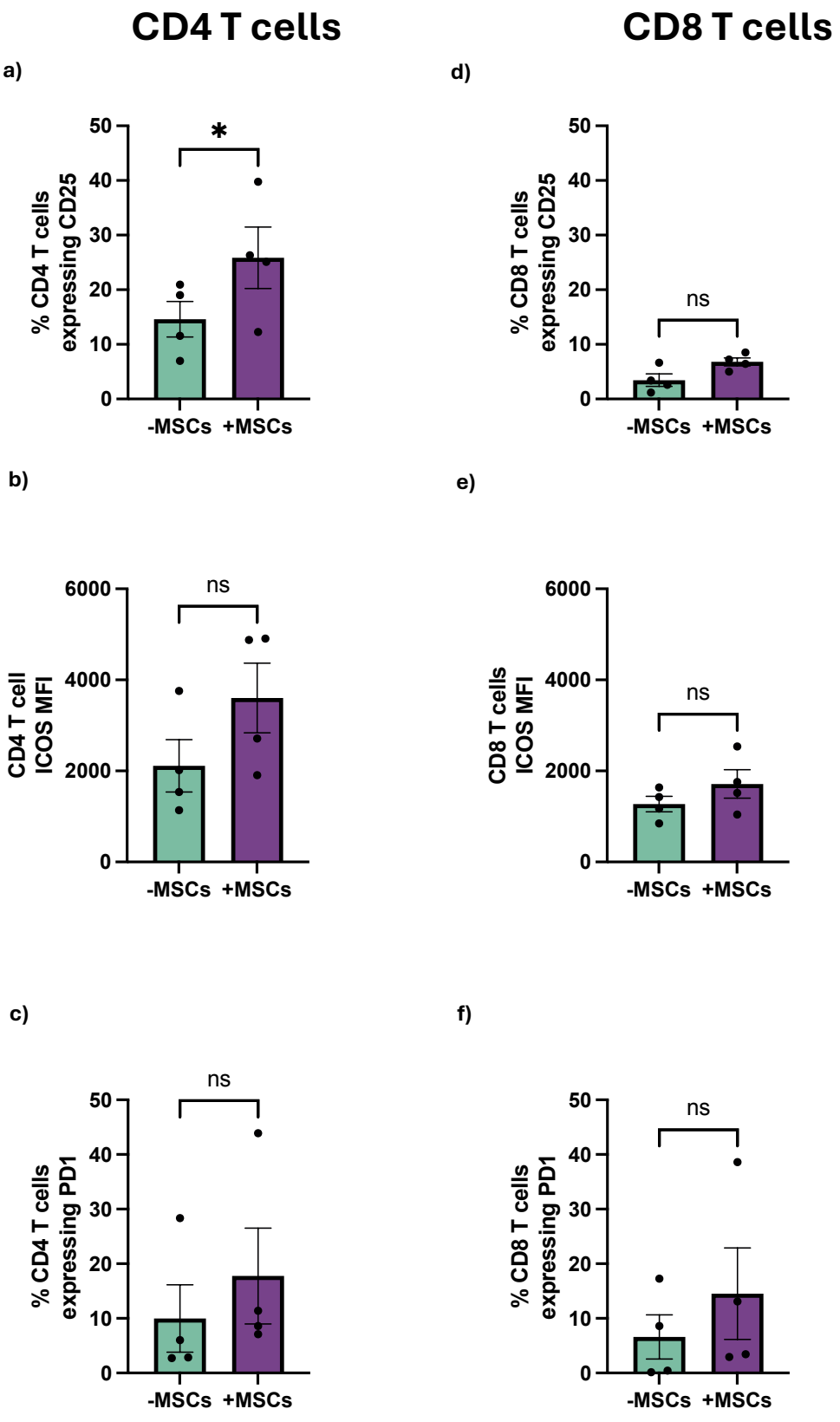

Figure 4-13: Flow cytometry results for late timepoint D35 co-culture with CD4 T cells (a-c) and CD8 T cells (d-f) with PEA, FN, BMP2 biomaterial with and without MSCs for 5 days. Graphs show flow cytometry levels of CD25, ICOS MFI and PD1 expression. Graphed bars show the mean of 4 donors, with each point being the mean of two technical replicates. Error bars show the standard error of the mean. Biological donors were matched to the earlier D3 and D28 timepoints. Data was normally distributed and analysed using paired T tests. P values = *p<0.05, **p<0.01, ***p<0.001, ****p<0.0001.

4.4 Discussion

The results of this Chapter, establishing the T cell response to both undifferentiated MSC and differentiated osteoblast biomaterials, will be discussed in brief, but a more extensive discussion will follow [see Final Discussion].

4.4.1 To optimise the most reliable methodology to confirm osteoblast differentiation

The data within this results chapter demonstrates evidence that the culture conditions used in this methodology, have resulted in osteoblastic differentiation of MSCs by D28. This is supported by increased OCN and OPN expression already by D28 observed by IF microscopy and seen in the trends of quantified IF normalised to cell number. This was further identified at D35 but was evident already by D28. RT-qPCR was undertaken on cell lysates from the cultures at D28 and D35, unfortunately there was not tight variance between technical replicates in the data and so no significant differences could be identified other than for increased OCN at D35 in the presence of BMP-2 growth factor.

ALP and alizarin red staining was only undertaken on D35 aged cultures and showed evidence of mineralisation and calcium deposition by this time point, but the assays were less reliable, and the nanoscale PEA coating began to peel away from the bottom of the 24-well in parts, making analysis difficult. Colleagues have anecdotally experienced difficulties with nanoscale coatings, in 2D cultures such as this, peeling when kept in culture greater than 4 weeks but this is not a phenomenon seen up to 4 weeks. This difficulty with integrity of the PEA coating, combined with the addition of little further information to confirm osteoblast differentiation, beyond the OCN/OPN IF microscopy, led to the decision to use IF microscopy to confirm osteoblast differentiation for future experiments.

4.4.2 To define T cell responses to 3, 28 and 35 days aged MSC biomaterials

The T cell modelling methodology established in results chapter 3, was used to measure changes in T cell surface marker expression to allogenic biomaterials [Figure 3-19]. This modelling was run at three timepoints: an early undifferentiated MSC (D3) timepoint and at later, osteoblast-differentiated (D28) and (D35) timepoints. The overarching aim was to define what the T cell response was at these time points, but also to identify the best late timepoint to proceed with for future experimentation.

Overall, at the early D3 MSC timepoint, significant increases in CD4+CD25 expression were seen as early as just 3 days co-culture but were higher and significant for CD8+CD25 expression by 5 days co-culture. This implies that the allogenic MSCs within the biomaterial are capable of triggering host immune responses from both CD4 and CD8 T cells. There were however no significant differences at the early timepoint for either ICOS MFI or PD1 expression.

Flow cytometry data at the late osteoblast timepoints appears to show overall higher CD25 expression than at the D3 timepoint. At D28, significant increases in CD25, ICOS MFI and PD1 expression were seen by 3 days co-culture. At D35, CD25 expression was significantly higher than controls at 5 days co-culture with the highest percentage expression of the 3 timepoints at 25.85%. Across the timepoints, the 4 donors showed biological variance in the extent of their T cell responses, but no difference was observed between male vs female (n= 2 for each). The data variance seemed to increase with the age of the culture, and the data had some potential outliers at the latest D35 timepoint.

The flow cytometry data indicated that there were T cell responses, predominantly in increased CD25 expression to D3, and both D28 and D35 cellularised biomaterials compared to non-cellularised biomaterial. The data was more consistent at D28 and therefore this supported moving forward with just the early D3 and late D28 timepoints for future experiments.

In summary, the primed T cell methodology was used to ascertain human T cell responses to D3, D28 and D35 allogenic biomaterials. Responses were found at all timepoints with evidence for a more mature activation response by D28. Osteoblast differentiation was confirmed primarily by IF microscopy expression of OCN and OPN by D28. Future experiments will focus on undifferentiated D3 MSC and osteoblast D28 timepoints.

Chapter 5 Immunomodulation of biomaterials

5.1 Introduction

Having established a working model of human T cell responses [Chapter 3] and defined the baseline T cell responses to D3 and D28 day aged MSC fibronectin biomaterials [Chapter 4], I sought to use the model to address immunomodulation approaches. I wanted to use the model to test if different alterations to the biomaterial composition or culture microenvironment, may affect either the T cells directly or the differentiation of the MSCs into osteoblasts, thereby indirectly affecting the T cells.

The first immunomodulation approach taken was to change the glycoprotein within the model from fibronectin to laminin. Laminins are a family of glycoproteins that provide integral structural scaffolding to basement membranes (340, 341). Each laminin is different, but they often function to regulate the migration of immune cells, and laminin overexpression has been associated with inflammatory diseases (340). Laminins are known to have multiple properties capable of interactions with human T cells, such as laminin 511 (LN511) promoting CD4+ T cell migration, monocyte adhesion, B cell adhesion and CD4+ T cell activation (340). I chose to use laminin 332 (LN332) as it's known immune function is to promote mature thymocytes, as opposed to direct effects on T cell activation (340). Furthermore, LN332 is a known negative regulator of osteoclastogenesis and promotes osteogenic differentiation (341). It has been found to be expressed by osteoblasts in bone tissues and has a key role in controlling bone remodelling through suppression of osteoclastogenesis (341). Laminins have been shown by our group previously to function well within hydrogels, as with fibronectin, capable of binding

BMP-2 and presenting this growth factor to facilitate MSC differentiation to osteoblasts, however, notably this was using Laminin 521 (342).

The second approach undertaken to immunomodulate the T cell responses to the fibronectin biomaterials was to make the microenvironment proinflammatory [see methods 2.4.4]. I wanted to see if an environment modelled on the M1 macrophage proinflammation at trauma and fracture haematoma sites would affect either the differentiation of the MSCs or the T cell responses to them (343, 344). Fracture healing is finely tuned and dependent on the balance of a host of pro and anti-inflammatory signals from a raft of immune cells and signals over a matter of weeks (345). The initial fracture haematoma environment following a fracture, is hallmarked by damage to blood vessels and an influx of MSCs, endothelial and immune cells that migrate into the site in a well-orchestrated process that has been shown to be one of the critical determinants of the healing outcome (345, 346). The initial inflammatory phase is tightly regulated and within 4 days of trauma, the fracture haematoma microenvironment develops osteogenic potential that enables ectopic bone formation and secondary bone healing to begin (347). OPN has been shown to be upregulated within fracture haematomas within 72hrs of the fracture occurring, although BMP2, 4 and 7 expression are relatively low during these initial healing responses (348). Over a few days, the fracture haematoma organises itself forming a fibrin network for the influx of osteogenic and chondrogenic progenitor cells (349). The primary immune cells at these fracture haematoma sites are initially macrophages, before recruitment of T cells thereafter (350-352). As such, the field of osteoimmunology has risen exponentially in recent years, owing to the potential for inflammatory cytokines being possible therapeutic targets to augment bone repair (345). By modelling a M1 macrophage proinflammatory microenvironment, I aimed to assess the effect

on MSC differentiation and subsequent T cell responses at both D3 and D28 of differentiation, using the established T cell model [see methods 2.4.4 & 2.4.5].

5.2 Aims

- To use the model to investigate if biomaterial modulation with laminin alters human T cell responses or osteoblast differentiation potential *in vitro*

- To investigate osteoblast MHCII expression at day 28 in the context of fibronectin, laminin and inflammation

- To use the model to investigate if proinflammation microenvironment modulation alters human T cell responses or osteoblast differentiation potential *in vitro*

- To interrogate the T cell responses further, as part of the modelling, through analysis of their transcription factors to identify subsets

- To investigate T cell functional responses, within the modelling, through analysis of cytokines and chemokines produced in co-cultures

5.3 Results

5.3.1 Immunomodulation with laminin biomaterials

The first approach to immunomodulation was to change the biomaterial composition to investigate if this altered the T cell response towards the biomaterial at an early (D3) or late (D28) timepoint. Any altered response could be due to a direct effect of the change in biomaterial on the T cells or due to the secondary effect caused by less differentiation, maintaining more of an MSC phenotype, thereby reducing the response of the T cells.

For this series of experiments, I used a PEA, LN322, BMP-2, MSCs biomaterial in comparison to the PEA, FN, BMP-2, MSCs biomaterial [methods 2.1.2 & 2.1.3]. Both were compared to their own acellular controls and the modelling used followed that described previously [results 3.3.13]. Immune modelling would occur at two timepoints, early undifferentiated MSC (D3) and late differentiated osteoblasts (D28) as optimised [Chapter 4]. Flow cytometry analysis of the T cells would occur at day 3 and 5 days of co-culture as previously [Figure 5-1].

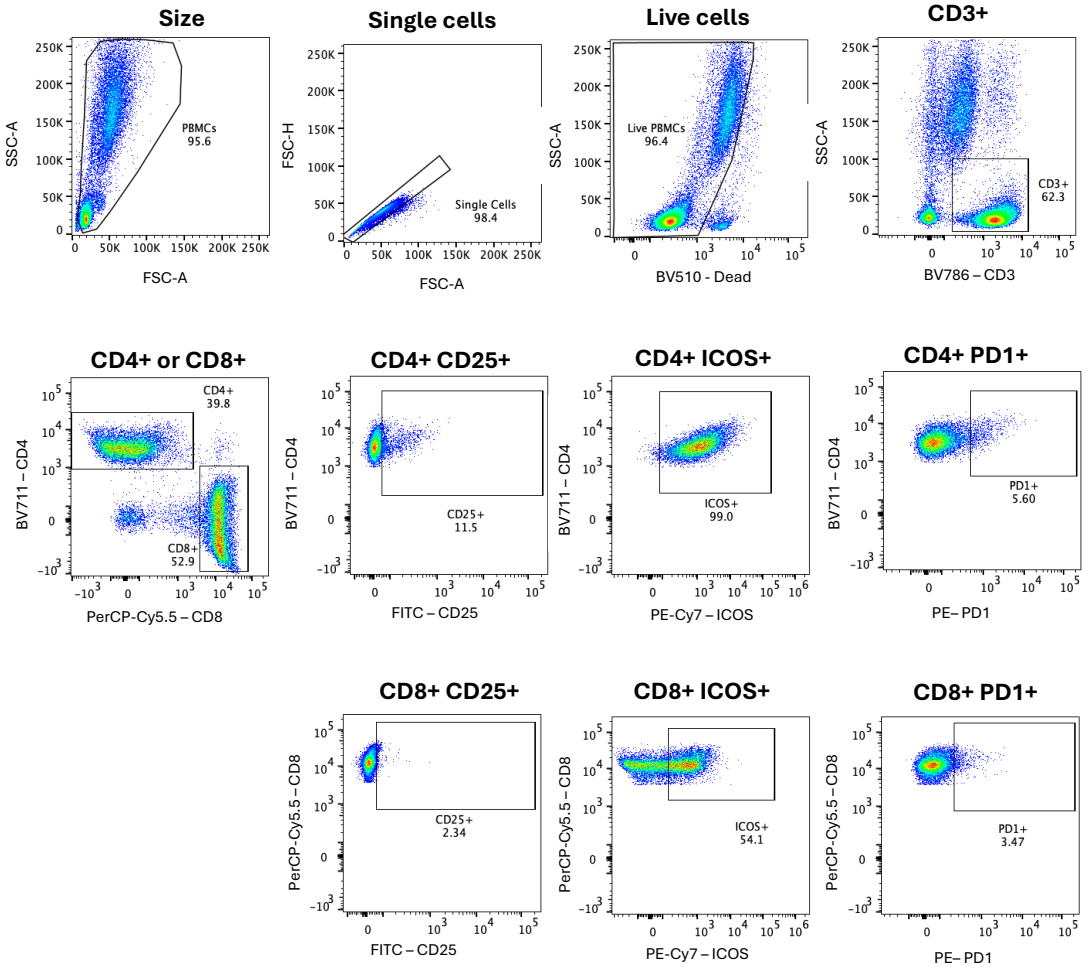

Figure 5-1: Flow gating strategy for T cell isolation and identification of T cell surface activation markers. Representative gating of T cells isolated 3 days after co-culture with early day 3 MSC biomaterial. Cells were stained as described in Materials and Methods and acquired of a BD Celesta. Labels indicate cell populations, and the numbers show the percentage of cells within each gate.

5.3.1.1 T cells co-cultured with either MSC fibronectin or MSC laminin biomaterials show evidence of activation

Supporting the data in chapter 4, there were significant increases in CD25 expression in CD4+ T cells by 3 days co-culture with the immature undifferentiated MSC fibronectin containing biomaterial [Figure 5-2]. ICOS, ICOS MFI and PD1 expression were not significantly altered and there were no significant differences found by 3 days co-culture for CD8+ T cells. In contrast, CD4+ T cells co-cultured with MSCs grown in the presence of laminin biomaterials for 3 days did not show evidence of activation by any of the markers. CD8+ T cells expression of CD25 increased in the presence of MSCs at this timepoint [Figure 5-2].

As for the experiments in Chapter 4, by 5 days of co-culture in samples with fibronectin biomaterial, both CD4 and CD8 T cells expressed more CD25 in the presence of MSCs compared to their absence. This difference achieved a greater level of statistical significance for CD4+ ($p=0.0003$) vs CD8+ T cells ($p=0.0142$) [Figure 5-3]. There were also significant increases in CD8+ ICOS MFI but ICOS and PD1 expression remained non-significantly changed at this early undifferentiated timepoint. For laminin biomaterials, significant increases in CD25 expression for both CD4+ ($p=0.0061$) and CD8+ ($p=0.0499$) T cells were found in the co-cultures containing MSCs [Figure 5-3]. Whilst this mirrored the fibronectin findings at this early undifferentiated timepoint, greater responses were seen across the more mature surface markers of T cell activation. There were significant increases in ICOS MFI and PD1 expression for CD4+ T cells as well as ICOS MFI, ICOS and PD1 expression for CD8+ T cells.

Overall, by 5 days co-culture the human T cells appeared to have more significant activation to the laminin MSC biomaterials versus matched acellular controls than

to fibronectin MSC biomaterials versus acellular matched controls. However, when individual T cell responses to cellularised laminin biomaterials are compared to responses to cellularised fibronectin biomaterials, no overall difference in responses were found [Figure 5-3].

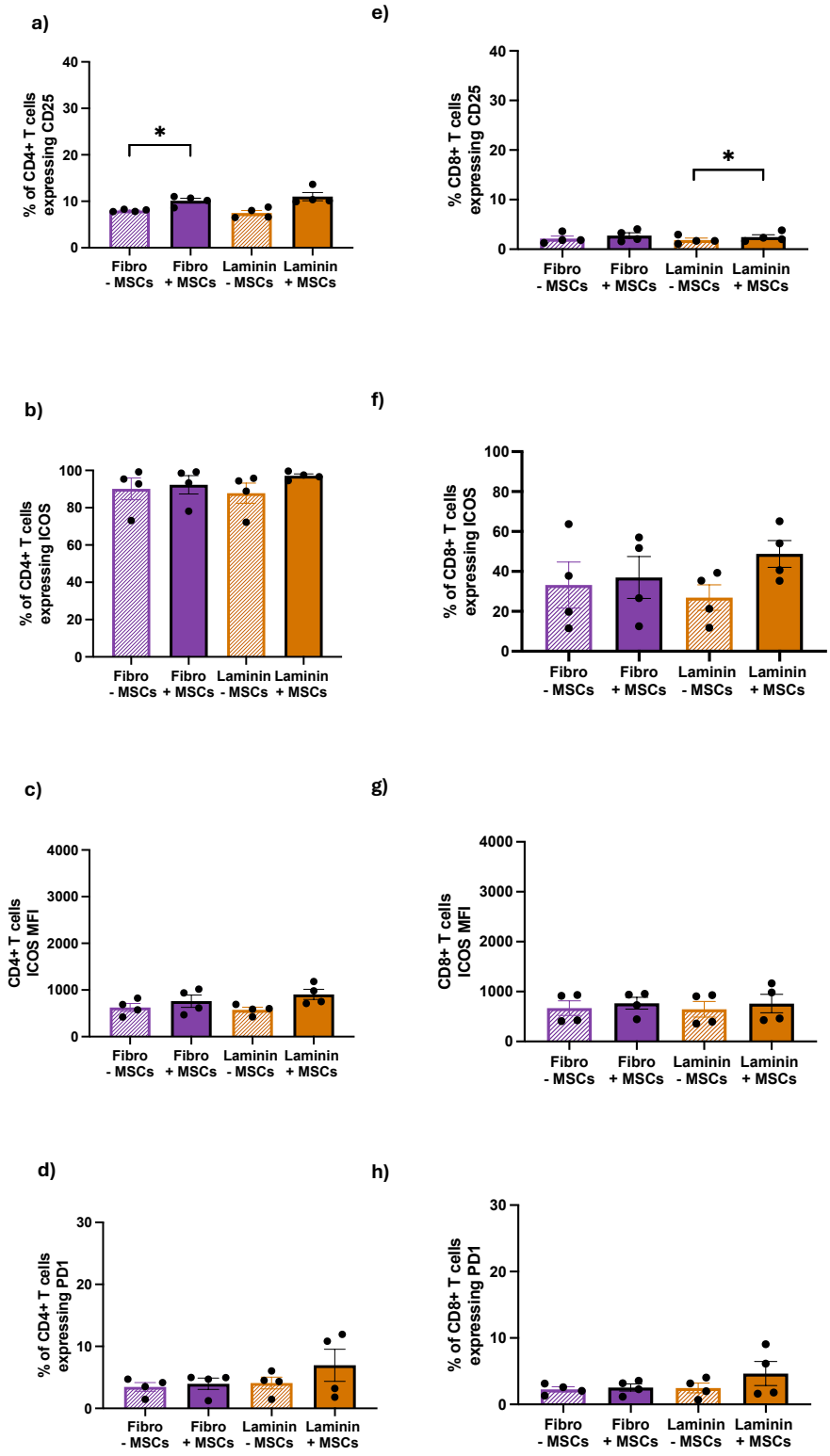

Figure 5-2: Flow cytometry data from the early D3 MSCs timepoint on fibronectin (fibro) (purple) and laminin (orange) biomaterials in co-culture with the T cell model for 3 days. Results shown for surface marker expression of CD25+, ICOS+, ICOS MFI and PD1 on CD4+ (a-d) and CD8+ (e-h) T cells. Bars represent the mean of 4 biological donors that were matched for both laminin and fibronectin modelling. Each data point is the mean of 2 technical replicates and the error bars represent the standard error of the mean. Data were normally distributed and analysed by paired T tests. P values = *p<0.05, **p<0.01, ***p<0.001, ****p<0.0001. Only significant results labelled in graphs.

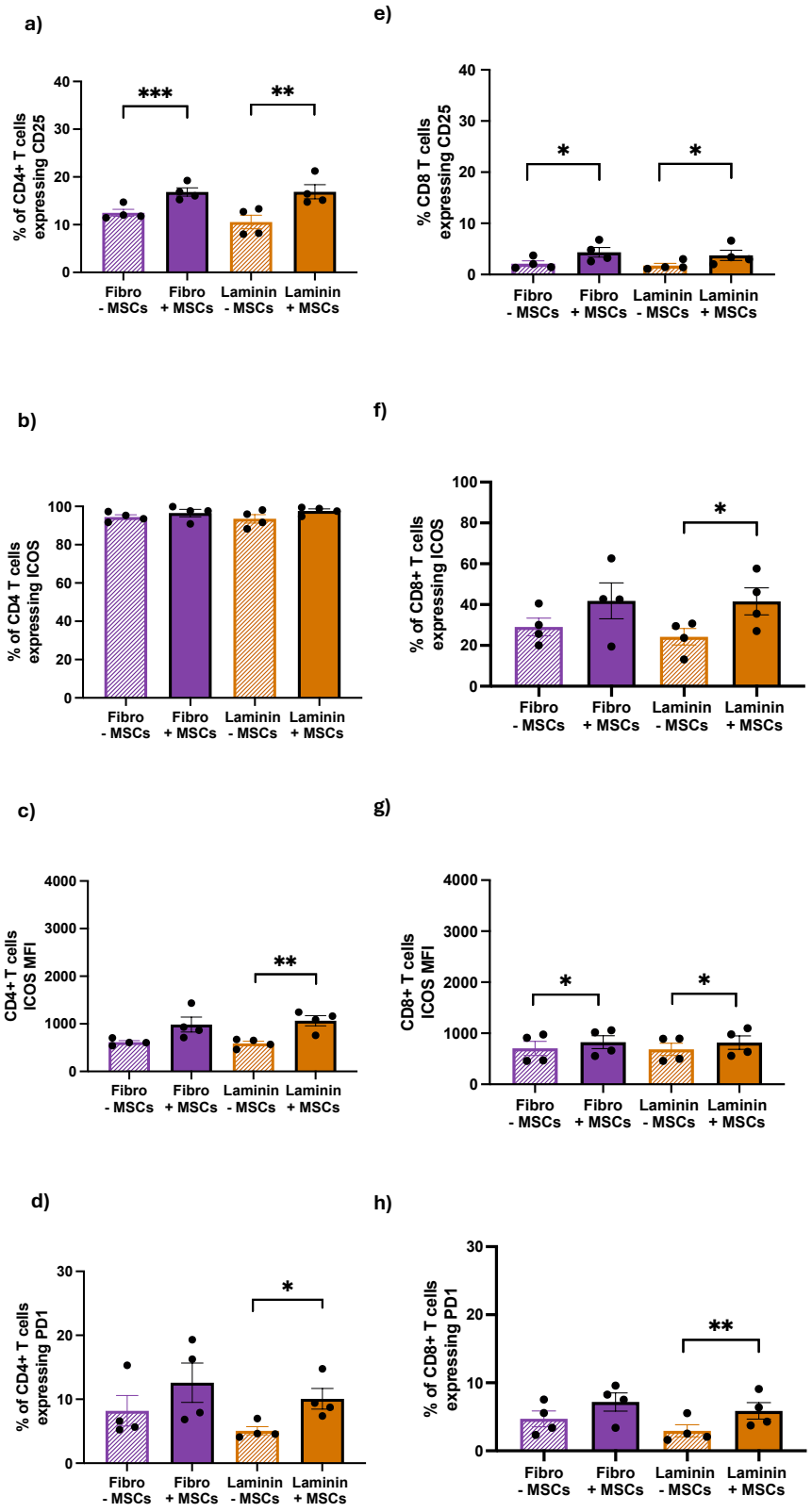

Figure 5-3: Flow cytometry data from the early D3 MSCs timepoint on fibronectin (fibro) (purple) and laminin (orange) biomaterials in co-culture with the T cell model for 5 days. Results shown for surface marker expression of CD25+, ICOS+, ICOS MFI and PD1 on CD4+ (a-d) and CD8+ (e-h) T cells. Bars represent the mean of 4 biological donors that were matched for both laminin and fibronectin modelling. Each data point is the mean of 2 technical replicates and the error bars represent the standard error of the mean. Data were normally distributed and analysed by paired T tests. P values = *p<0.05, **p<0.01, ***p<0.001, ****p<0.0001. Only significant results labelled in graphs.

5.3.1.2 Transcription Factor T cell Flow Cytometry Panel

To further interrogate the T cell responses following co-culture with the cellularised and acellular biomaterials, I used a second flow cytometry panel to identify the transcription factors produced by the T cells within the cultures. This panel identified T cells via my established viability, CD3+ and CD4+ or CD8+ and CD25+ surface markers. Additional intranuclear staining was carried out for forkhead box P3 (FOXP3) that is expressed by regulatory CD4 T cells and upregulated early after TCR stimulation (141). We also examined T-bet, which is found in activated CD8 T cells and T helper 1 CD4 T cells (353)[Figure 5-4]. Whilst GATA-binding protein 3 (GATA3) and RoRγt transcription factors were also initially stained for within the panel, these antibodies did not technically work at the concentrations used and therefore these data are excluded from the subsequent figures and analysis.

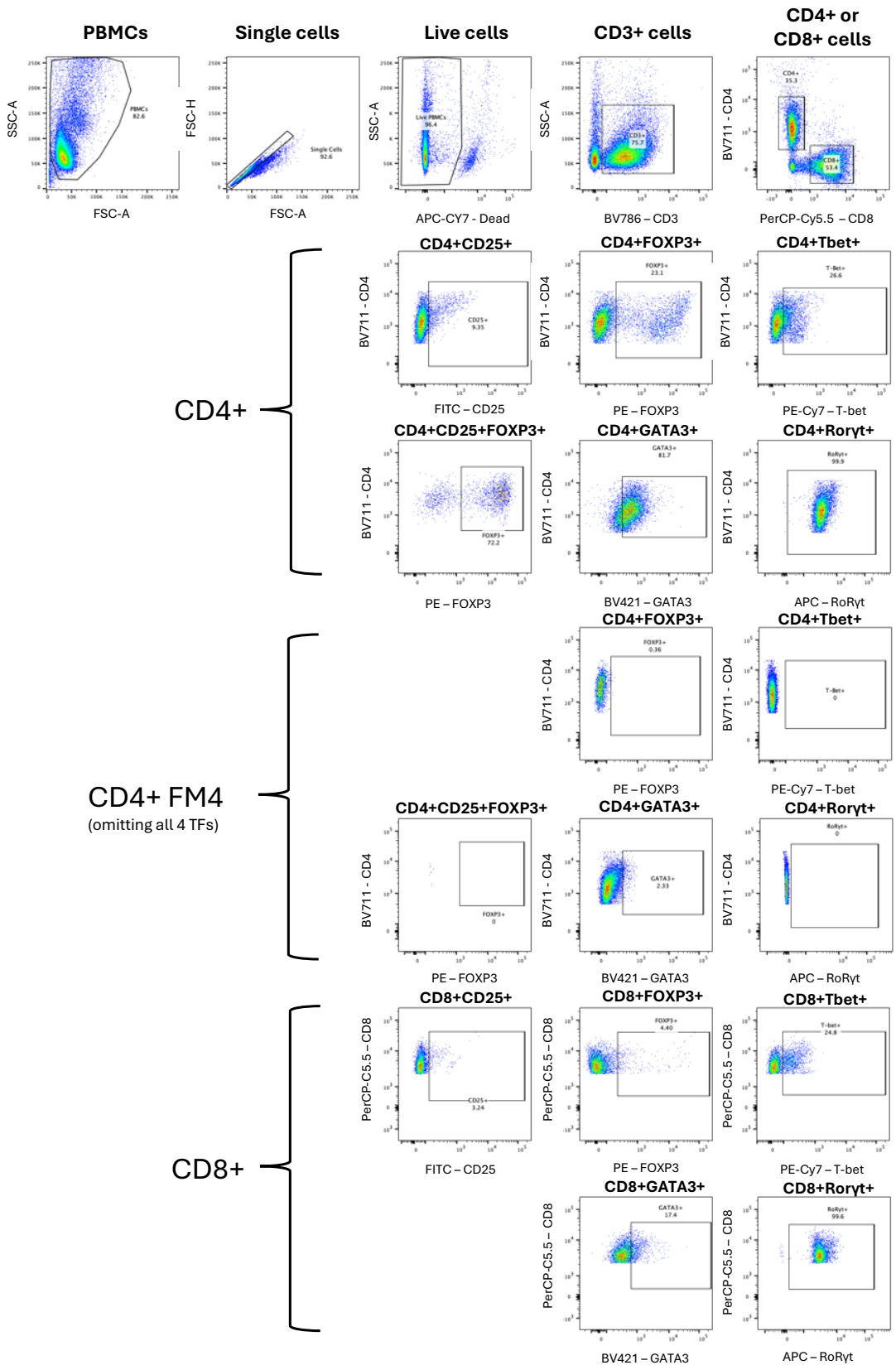

Figure 5-4 Flow gating strategy for T cell identification and identification of T cell surface activation markers in addition to intranuclear transcription factors. Representative staining of T cells from a co-culture with MSCs as descried in Materials and Methods and acquired on a BD Fortessa. Indicated populations are shown and numbers show the percentage of cells within the gates. FMOs shown for CD4+ T cells (CD8+ FMOs data not shown).

5.3.1.3 Intracellular staining for FOXP3 and T-bet reveals increased regulatory CD4+ T cells in cellularised biomaterial co-cultures

The transcription factor staining required intracellular (IC) staining following fixation with a specialised fix/perm reagent. IC-stained T cells were initially examined at day 3 of co-culture but unfortunately, there was a technical problem with the fixation at this timepoint and therefore results are only available for day 5 of co-culture, once the fixation issues had been resolved. On examining IC-stained T cells at day 5 of co-culture with MSC biomaterials, they had higher expression of CD25 than cells from acellular cultures [Figure 5-5]. This supports the data shown for the surface panel [Figure 5-3]. In co-culture with the MSC biomaterials, CD4+ T cells expressed significantly greater FOXP3+ than controls but there were no statistical differences for T-bet expression.

The majority of CD4+CD25+ T cells within this panel were also FOXP3+ implying they were Tregs [Figure 5-5]. However, Tregs that are CD4+CD25+FOXP3+ would be expected to also express PD1+ and/or ICOS+ (354). In the surface flow cytometry panel, T cells that were CD4+CD25+ were not always positive for PD1 and/or ICOS and approximately 35-40% of the CD4+ T cells expressed CD25+ but were negative for PD1 and ICOS, which is more indicative of an activation T cell response than a Treg response [Figure 5-6]. There was also evident inter-donor variability in CD4+CD25+FOXP3+ expression and some donors had increased percentages of these cells in the presence of MSCs and others in the absence [Figure 5-5, h]. Notably, within each donor's data there was consistency in response to MSCs versus no cell controls irrespective of fibronectin or laminin biomaterial. There were no significant differences for CD8+ CD25, FOXP3 or T-bet expression.

At the early D3 undifferentiated MSC timepoint, laminin MSC biomaterials co-cultured with T cells for 5 days led to significant increases in CD25 expression for CD4+ T cells only versus controls [Figure 5-5]. There were no significant differences in FOXP3 or T-bet expression for either CD4+ or CD8+ T cells.

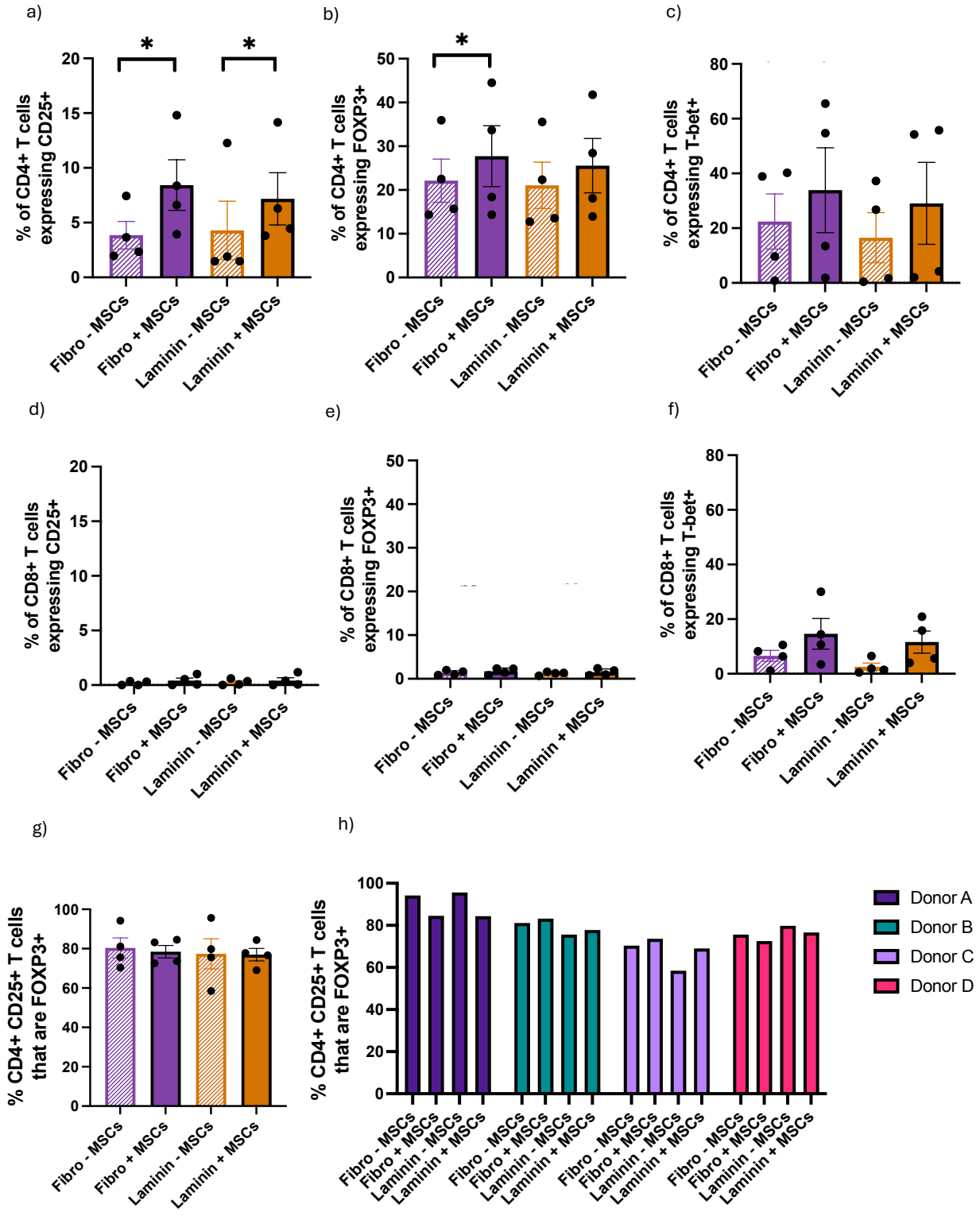

Figure 5-5: Transcription factor flow cytometry data for D3 early timepoint MSC biomaterials in co-culture with T cells for 5 days. CD4+ (a-c) and CD8+ T cells (d-f) percentage CD25+, FOXP3+ and T-bet+ expression. Proportion of CD4+CD25+FOXP3+ T regulatory cells (g) per donor (h). Bars in graphs a-g represent the mean of 4 biological donors with each data point being the mean of technical replicates. Error bars represent the standard error of the mean. Data were normally distributed and analysed by paired T tests. P values = *p<0.05, **p<0.01, ***p<0.001, ****p<0.0001. Only significant results labelled in graphs...

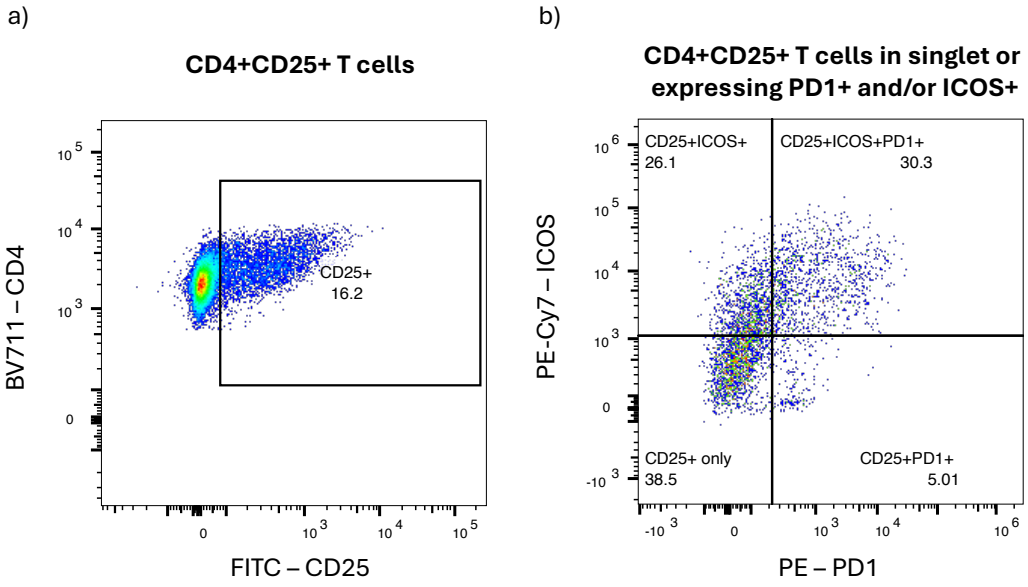

Figure 5-6: Example flow cytometry gating show proportions of CD4+CD25+ T cells also expressing ICOS+ and/or PD1+. Sample shown is from a single donor after T cell co-culture with the MSC biomaterial for 5 days. a) CD4+CD25+ T cells already gated through the gating strategy demonstrated earlier within this chapter. b) Proportion of CD4+CD25+ T cells that are singlets for CD25+ expression, doublets with either ICOS+ or PD1+ expression or triplets expressing all 3 markers of activation.

5.3.1.4 D28 MSC differentiated osteoblasts express major histocompatibility class II molecules in vitro

Immunofluorescence microscopy was undertaken on the fibronectin and laminin PEA, BMP-2, MSC biomaterials at day 28 to confirm osteoblast differentiation. This was done by staining for osteocalcin (OCN) and osteopontin (OPN) as previously described, in combination with phalloidin and DAPI [methods 2.6.1].

Images of the D28 fibronectin biomaterials clearly show bright phalloidin and DAPI staining and both OPN and OCN staining is evident across the samples [Figure 5-7]. The composite images show staining in green (OCN or OPN) in keeping with OPN and OCN cytoplasmic secretion during bone remodelling by osteoblasts [yellow arrows, Figure 5-7]. Whilst the primary omission shows some signal in the FITC (green) channel, this appears to be the phalloidin staining bleeding into that channel [red arrows, Figure 5-7]. The composite image does not show any additional FITC signal beyond that observed in the phalloidin stain. The sample composite images however all show additional intracellular staining in the FITC channel.

In comparison, the D28 cells on the laminin biomaterials appeared morphologically different to the cells seen on the D28 fibronectin biomaterials. On the laminin biomaterials the cells were more spindle and linear shaped and less rounded or osteoblast-like [Figure 5-8]. There was evidence of OPN and OCN staining in the laminin biomaterial conditions, however this subjectively appeared to be less than for fibronectin. The primary omission again showed some signal in the FITC (green) channel but again appeared to be the phalloidin staining bleeding through into the FITC channel. Composite images clearly show increase OCN and OPN in the samples versus primary omission.

Having established osteoblast differentiation, next steps required investigating the molecules that may drive the T cell response within the co-cultures. Therefore, the osteoblast D28 cultures were stained for expression of MHC class II (MHC II) molecules. A potential mechanism for T cell activation could be increased MHC-II upregulation by the osteoblasts, leading to greater CD4+ T cell TCR interactions. Subpopulations of *ex-vivo* osteoblasts are known to be able to express MHC II and act as antigen presenting cells (355, 356). However, the phenotype of the immature osteoblasts made *in vitro* within this modelling, differentiated by BMP-2 cues, within the different biomaterials remains unknown. To address this, immunofluorescence microscopy staining for DAPI, phalloidin and MHC II was performed at the D28 timepoint for both fibronectin and laminin biomaterials [methods 2.6.1].

In both fibronectin and laminin D28 biomaterial-differentiated, *in vitro* osteoblasts, there was evidence of MHC II staining [yellow arrows, Figure 5-9]. This staining was, subjectively, similar for both fibronectin and laminin biomaterials. The isotype control shows some signal in the FITC (green) channel, but the staining is not confined to the cells and is greater for the sample conditions [red arrows, Figure 5-9]. Albeit qualitative, the equivalent expression of MHC-II staining could support the hypothesis that MHC-II expression at D28 leads to greater TCR activation.

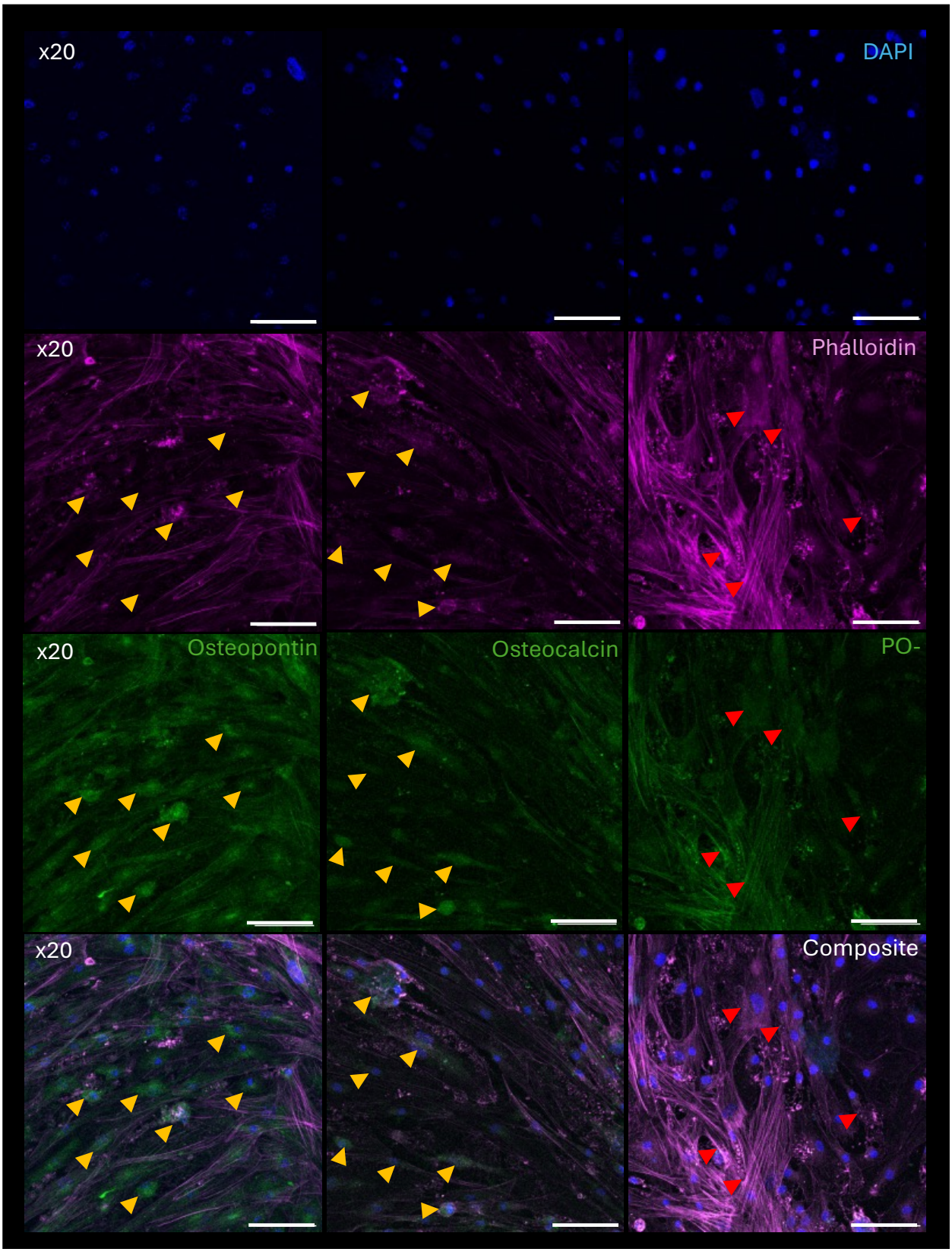

Figure 5-7: Immunofluorescence microscopy images of late time point D28 fibronectin osteoblast biomaterials. Cells were stained for DAPI (blue), phalloidin (magenta) and osteoblast differentiation markers osteopontin or osteocalcin (green). Primary omission staining shown (PO-). Representative images set to the same colour thresholds to facilitate comparison. Scale bar represents 100μM in all images. Yellow arrows highlight real staining, red arrows show bleed through from phalloidin channel.

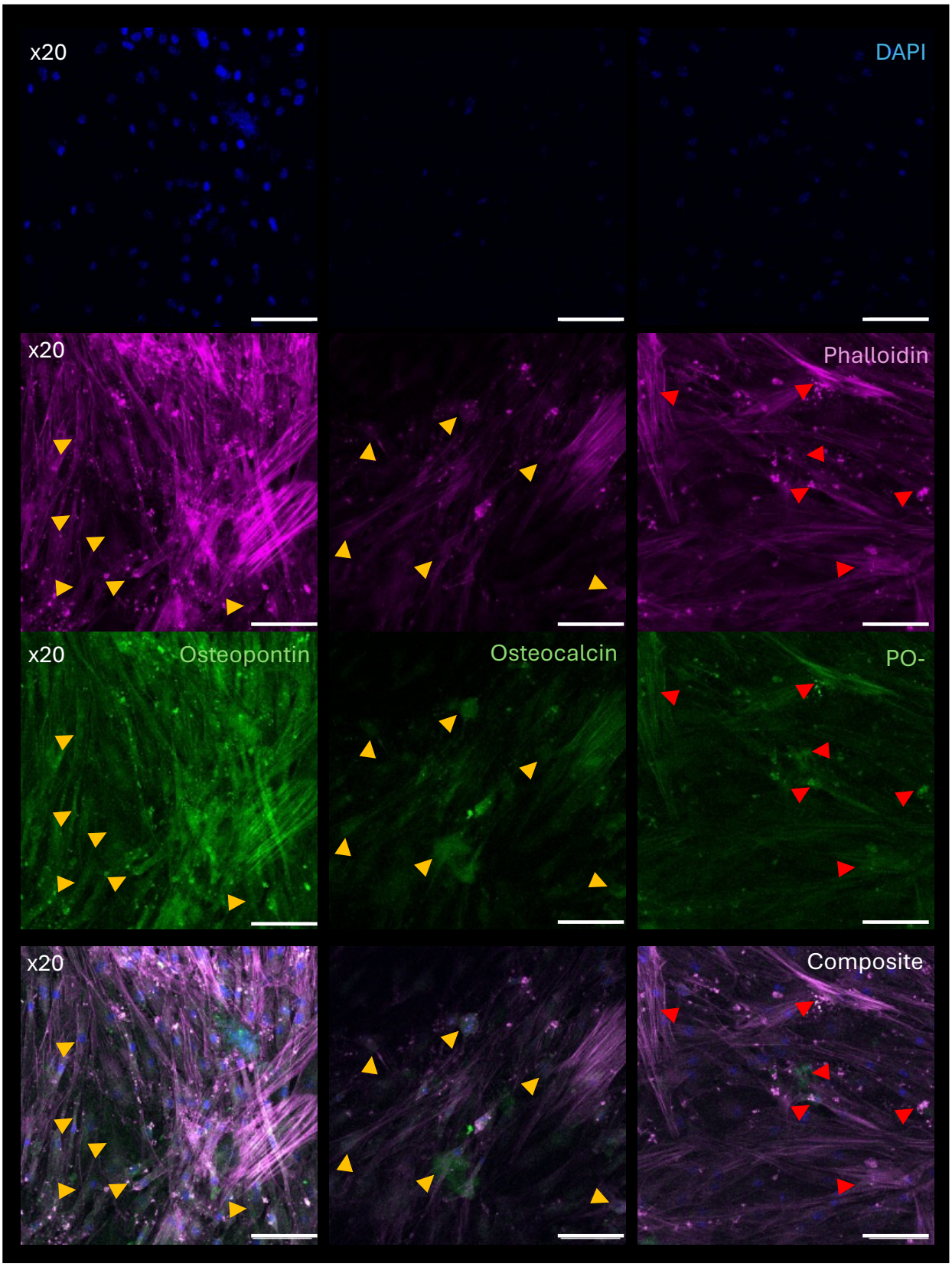

Figure 5-8: Immunofluorescence microscopy images of late time point D28 laminin MSC biomaterials. Cells were stained for DAPI (blue), phalloidin (magenta) and osteoblast differentiation markers osteopontin or osteocalcin (green). Primary omission staining shown (PO-). Representative images set to the same colour thresholds to facilitate comparison. Scale bar represents 100μM in all images. Yellow arrows highlight real staining, red arrows show bleed through from phalloidin channel

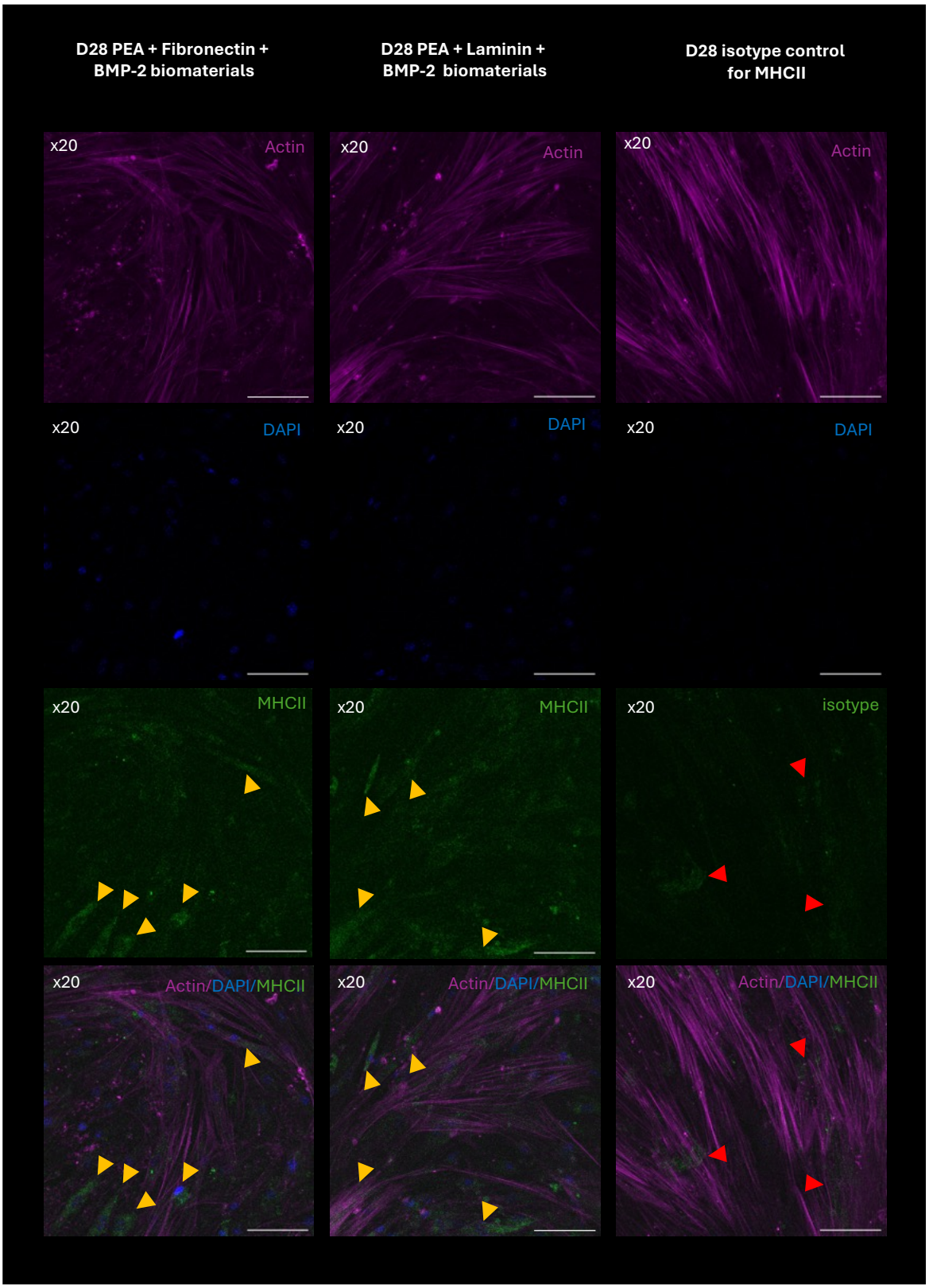

Figure 5-9: Immunofluorescence microscopy of D28 osteoblast fibronectin and laminin biomaterials stained for actin (magenta), DAPI (blue) and MHC-II (green). A representative panel of images is shown for fibronectin (left panel) and laminin (central panel) biomaterials as well as isotype control for MHC-II (right panel). Scale bar represents 100μM in all images and colour thresholds are the same to facilitate comparison.

5.3.1.5 T cells co-cultured with either osteoblast fibronectin or osteoblast laminin biomaterials show evidence of activation

As per the prior experiment optimisation, the late timepoint used for this series of experiments was 28 days following biomaterial culture with or without MSCs [Chapter 4]. Osteoblast differentiation would be confirmed via IF microscopy and as with the D3 timepoint, flow cytometry analysis at 3 and 5 days co-culture was undertaken using the same surface [Figure 5-1] and intranuclear staining panels [Figure 5-4].

After 28 days of MSC differentiation into osteoblasts on the fibronectin biomaterial, the T cells were added and the cells co-cultured for 3 days. Co-culture with differentiated osteoblasts led to a significant increase in CD25+ expression in CD4+ T cells over controls, in congruence with all preceding data [Figure 5-10]. There were no significant differences for CD4+ ICOS MFI, ICOS or PD1 expression. For CD8+ T cells, ICOS expression significantly increased in the cellular conditions [Figure 5-10].

The 3 day T cell co-culture with the mature D28 laminin biomaterials also led to a significantly increased in CD4+ CD25+ expression to the cellularised biomaterial compared to the control [Figure 5-10]. As with the fibronectin biomaterial, there were no significant differences for ICOS MFI, ICOS or PD1 expression for CD4+ T cells but significant increases in CD8+ ICOS expression in the presence of the differentiated osteoblasts [Figure 5-10].

After 5 days co-culture in the presence of osteoblast differentiated fibronectin biomaterials, CD4+ T cells expressed significantly more ICOS (by MFI), CD25 and PD1 compared to CD4+ T cell cultures with acellular fibronectin biomaterial [Figure

5-11]. Furthermore, CD8+ T cells cultured with osteoblasts had significant increases in CD25, ICOS and PD1 expression compared to control cultures at this timepoint. These data show that with increasing co-culture and exposure to the biomaterial allogenic cells, the T cells increase expression of surface markers of activation from 3 to 5 day co-culture, supporting previous findings [Chapter 3].

In contrast, at D28 CD4 and CD8 T cells co-cultured with cellularised laminin biomaterials for 5 days had significantly increased expression of CD25 only, with nonsignificant differences for ICOS MFI, ICOS and PD1 expression in comparison to T cells in control co-cultures [Figure 5-11]. There was no change in CD4+ response with increasing culture with T cells from 3 to 5 days at this timepoint for cellularised laminin biomaterials. However, by 5 days co-culture CD8+ T cells did show significant increases in CD25 expression and ICOS MFI to allogenic conditions which were not found after 3 days of co-culture [Figure 5-11].

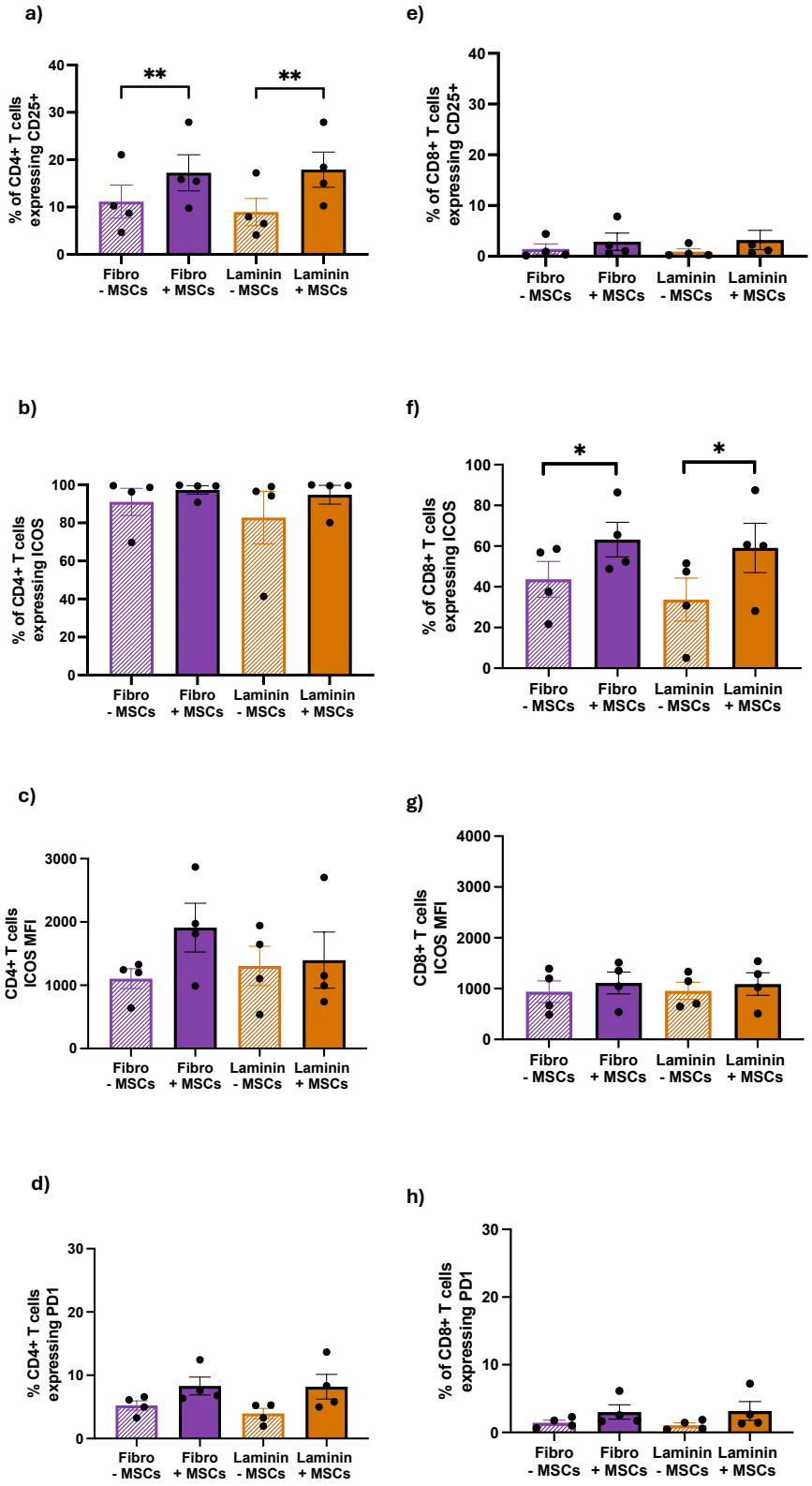

Figure 5-10: Flow cytometry data from the late D28 osteoblast timepoint on fibronectin (fibro) (purple) and laminin (orange) biomaterials in co-culture with the T cell model for 3 days. Results shown for surface marker expression of CD25+, ICOS+, ICOS MFI and PD1 on CD4+ (a-d) and CD8+ (e-h) T cells. Bars represent the mean of 4 biological donors that were matched for both laminin and fibronectin modelling. Each data point is the mean of 2 technical replicates and the error bars represent the standard error of the mean. Data were normally distributed and analysed using paired T tests. P values = *p<0.05, **p<0.01, ***p<0.001, ****p<0.0001. Only significant results shown on graph.

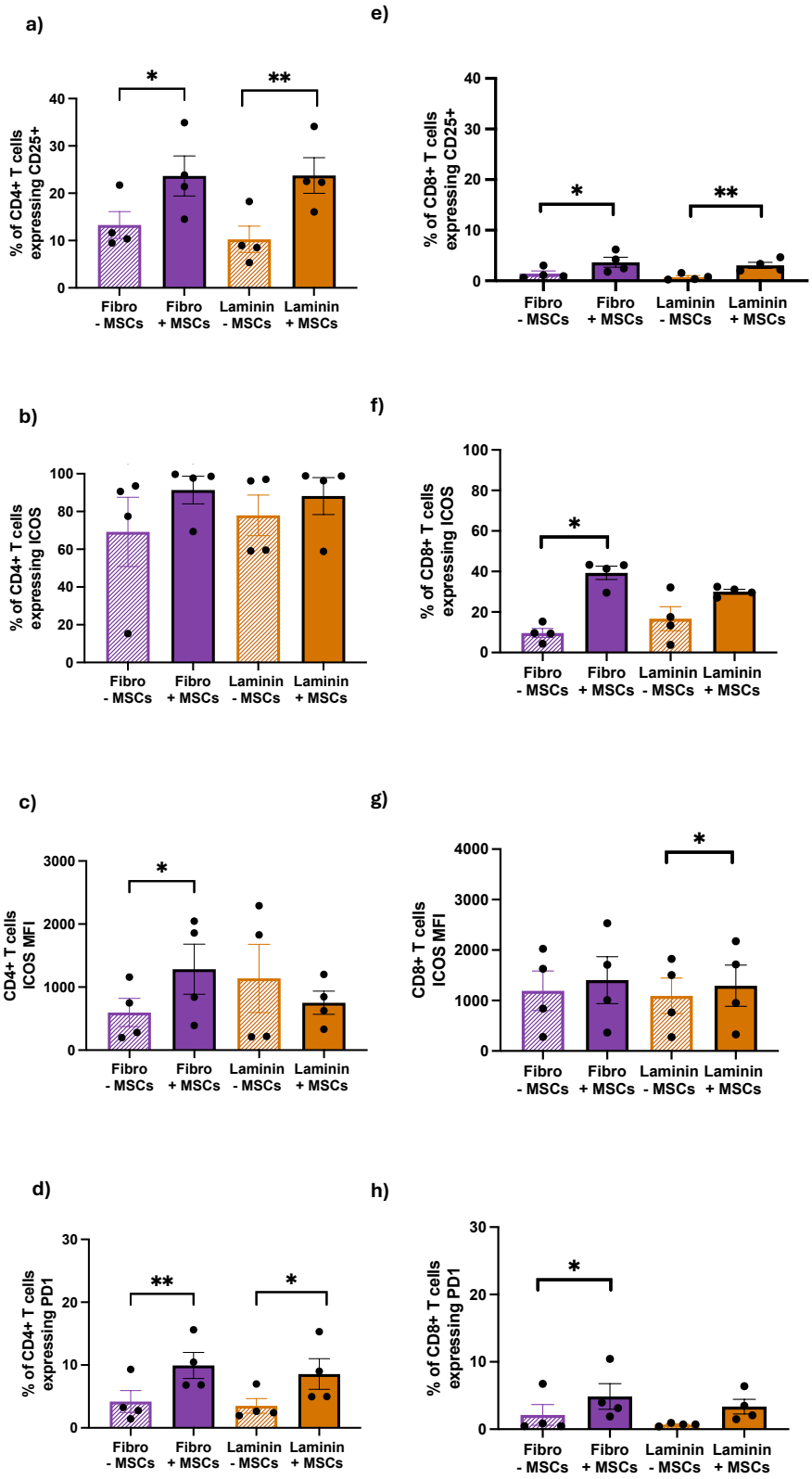

Figure 5-11: Flow cytometry data from the late D28 osteoblast timepoint on fibronectin (fibro) (purple) and laminin (orange) biomaterials in co-culture with the T cell model for 5 days. Results shown for surface marker expression of CD25+, ICOS+, ICOS MFI and PD1 on CD4+ (a-d) and CD8+ (e-h) T cells. Bars represent the mean of 4 biological donors that were matched for both laminin and fibronectin modelling. Each data point is the mean of 2 technical replicates and the error bars represent the standard error of the mean. Data were normally distributed and analysed using paired T tests. P values = *p<0.05, **p<0.01, ***p<0.001, ****p<0.0001. Only significant results shown on graph.

5.3.1.6 Intracellular staining for FOXP3 and T-bet suggest increased regulatory CD4+ and effector Th1 T cells in osteoblast biomaterial co-cultures

Having identified significant transcription factor changes at 5 days co-culture at the early undifferentiated D3 MSC timepoint, and having optimised the IC stain, I undertook flow cytometry staining for transcription factors at the D28 timepoint for both 3 and 5 days co-culture.

After 3 days co-culture with the fibronectin biomaterials, significant increases in CD25 expression were found on CD4 T cells co-cultured with osteoblasts compared to the acellular control in cells stained with the IC panel [Figure 5-12]. This matches the data from the surface only staining panel of these cells at this timepoint. There were modest but significant increases in the percentage of CD4+ T cells that were FOXP3+ in the osteoblast cultures compared to controls but no significant difference between the percentage of CD4+ cells that were expressing both CD25 and FOXP3 [Figure 5-12]. There were significant increases in T-bet expression for both CD4+ and CD8+ T cells when exposed to the allogenic osteoblast fibronectin conditions in contrast to the D3 timepoint [Figure 5-5]. There were no significant differences in CD8+ CD25 or FOXP3 expression [Figure 5-12].

The results for the transcription factors for laminin osteoblast conditions versus no cell controls were largely as for fibronectin, with significant increases in CD25+ and FOXP3+ expression for CD4+ T cells cultured with osteoblasts compared to controls [Figure 5-12]. No significant differences were seen in the percentage of CD4+ T cells that were both CD25+ and FOXP3+ positive in cells from the two types of co-culture. T-bet expression increased significantly in both CD4+ and CD8+ T cells in the osteoblast cultures, as with fibronectin. Similarly, there were

no significant changes in CD8 T cell expression of CD25 or FOXP3 expression between the cultures [Figure 5-12].

There are significant increases in FOXP3+ expression by both CD4+ and CD8+ T cells in T cells co-cultured with osteoblasts for 5 days in comparison to T cells in acellular control cultures [Figure 5-13]. At 5 days co-culture, as at 3 days co-culture, significant increases in T-bet expression were found for CD4+ and CD8+ T cells in the allogenic fibronectin conditions. However, no significant differences were found in the percentage of CD4+ T cells expressing FOXP3 and CD25. Furthermore, no significant differences in CD25+ expression were found for either CD4+ or CD8+ T cells in this panel at this time point.

For osteoblast laminin biomaterial conditions, at 5 days co-culture, no significant changes were found in CD25 or T-bet expression for either CD4+ or CD8+ T cells [Figure 5-13]. There were significant increases in the percentage of CD4+ T cells expressing FOXP3 but no increase in CD4+CD25+FOXP3+ cells as with fibronectin. Again, unlike at the early timepoint and in contrast to the surface panel staining, there was no significant difference in CD25 expression for either CD4+ or CD8+ T cells.

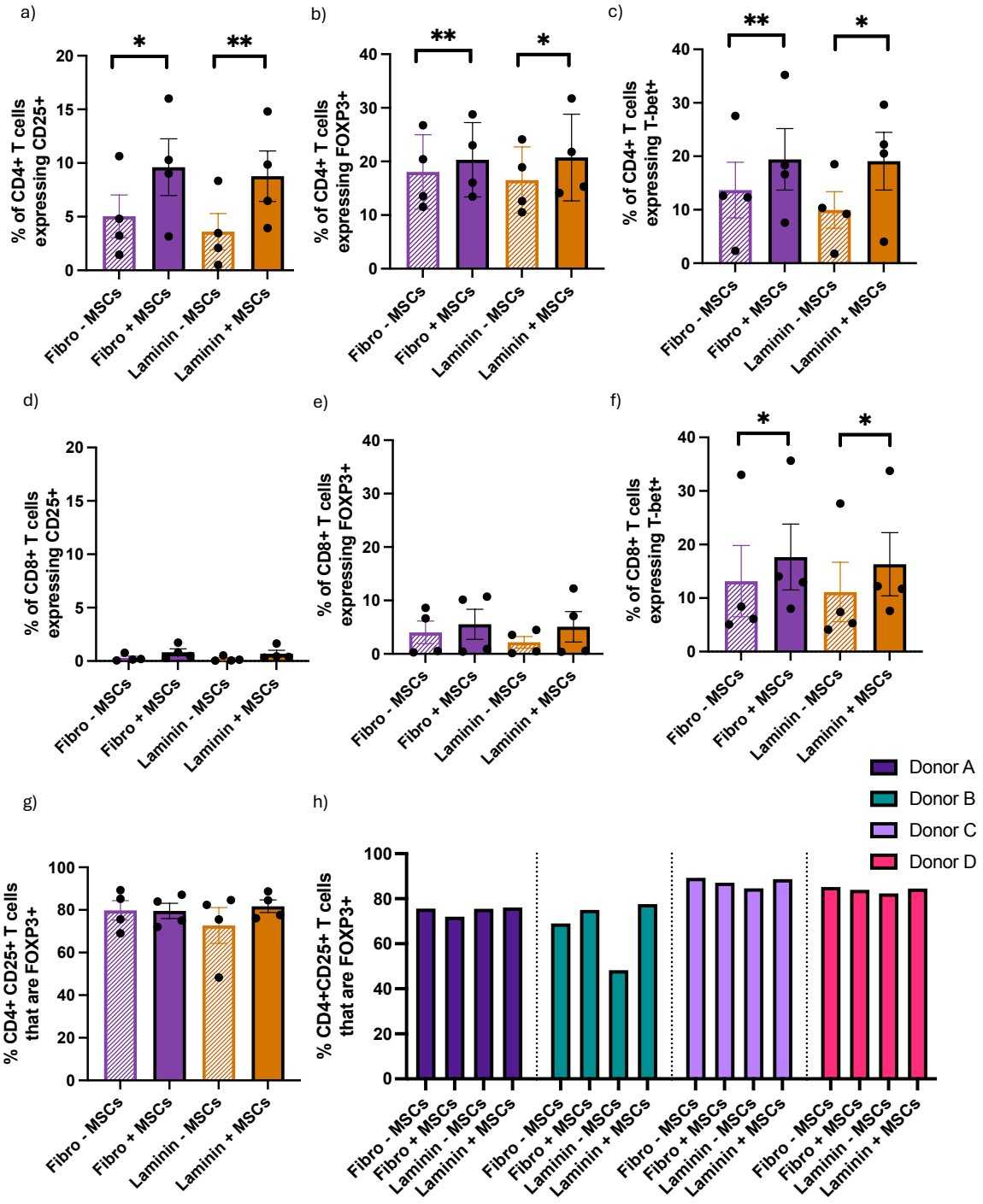

Figure 5-12: Transcription factor flow cytometry data for D28 late timepoint osteoblast biomaterials in co-culture with T cells for 3 days. CD4+ (a-c) and CD8+ T cells (d-f) percentage CD25+, FOXP3+ and T-bet+ expression. Proportion of CD4+CD25+FOXP3+ T regulatory cells per donor (g). Data represent n=4 and in technical replicate. Error bars represent the standard error of the mean. Data were normally distributed and analysed by paired T tests. P values = *p<0.05, **p<0.01, ***p<0.001, ****p<0.0001. Only significant results labelled in graphs

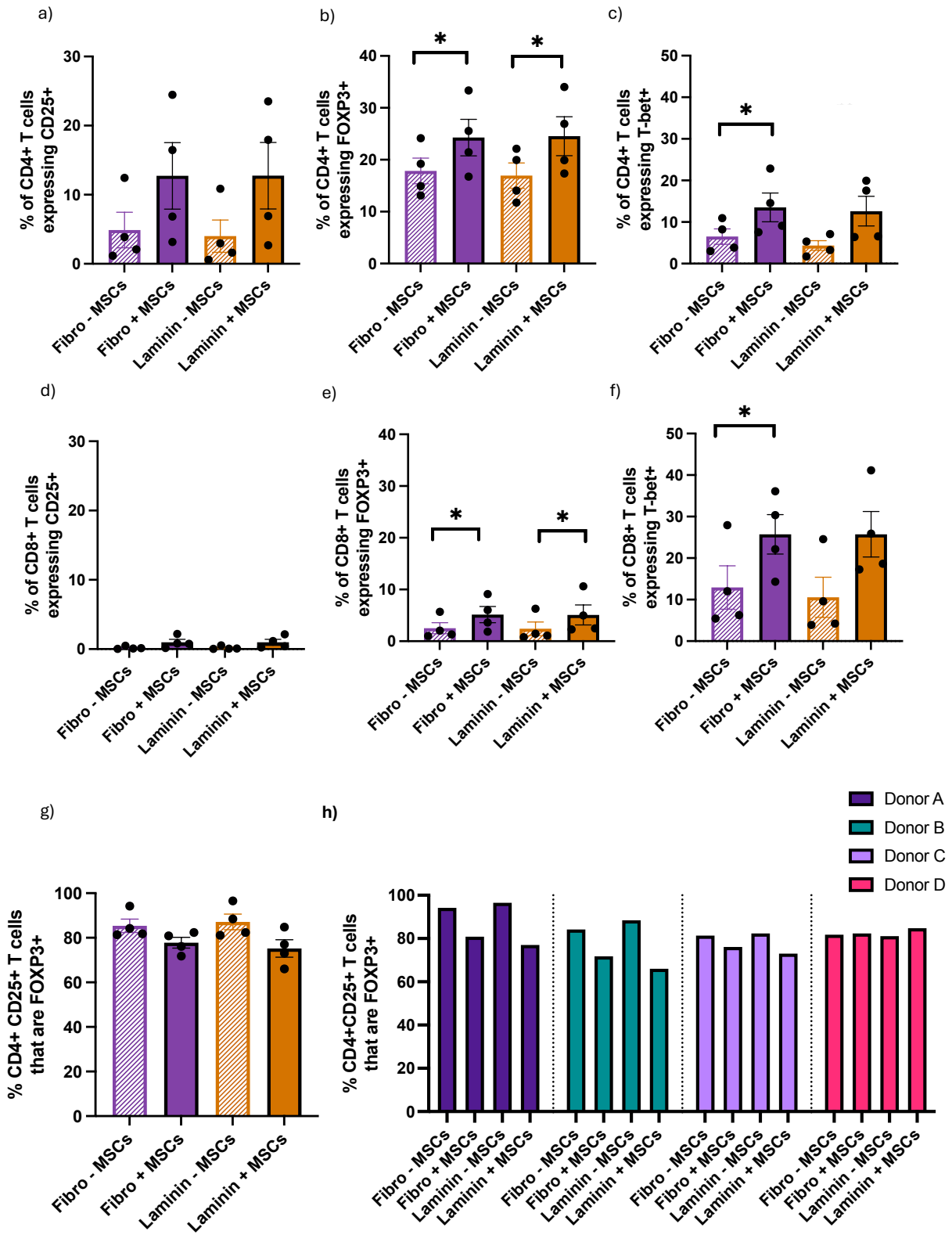

Figure 5-13: Transcription factor flow cytometry data for D28 late timepoint osteoblast biomaterials in co-culture with T cells for 5 days. CD4+ (a-c) and CD8+ T cells (d-f) percentage CD25+, FOXP3+ and T-bet+ expression. Proportion of CD4+CD25+FOXP3+ T regulatory cells (g) per donor (h). Graphed bars (a-g) represent the mean of 4 biological donors and each data point is the mean of two technical replicates. Error bars represent the standard error of the mean. Data were normally distributed and analysed by paired T tests. P values = *p<0.05, **p<0.01, ***p<0.001, ****p<0.0001. Only significant results labelled in graphs.

5.3.1.7 Luminex analysis soluble molecules in co-culture supernatants

The primed T cells were co-cultured at the early D3 MSC and late D28 osteoblast timepoints with fibronectin and laminin biomaterials with and without MSCs [results 4.3.4]. Supernatants from the acellular biomaterial (T cells but no MSCs) and cellularised biomaterial (T cells with MSCs) co-cultures were harvested and stored at -80°C until custom ordered Luminex assays could be performed [methods 2.8]. The Luminex sought to identify 74 analytes across the 74 supernatant samples (64 samples and 10 controls) taken after 3 days co-culture with the T cells [Appendix 2, 7.2].

The Luminex data was analysed on Prism software and two formal tests for identification of outliers (ROUT and Grubb methods) were performed on both the D3 and D28 timepoint data. This highlighted that donor D was an outlier at the D3 timepoint for fibronectin and Donor C for D3 laminin. No formal outliers were identified at the D28 timepoint for either biomaterial. Consequently, the early D3 timepoint analysis has an n=3 and the later D28 analysis has an n=4 accordingly. Data were tested for normality using a Shapiro-Wilk test and the majority of the Luminex analyte data were considered normally distributed. Data for a few different analytes in each data set were considered not normally distributed [Appendix 3, 7.3]. On examining the data, it was correlated to when minimum detectable levels of analytes had been detected in the acellular condition. Following advice from a colleague with statistical training, all data was treated as normally distributed allowing use of Paired t-tests to assess the differences between the +MSC and -MSCs samples. As there are only 3-4 samples in each condition, it is possible the data are normally distributed, but we have not sampled across the full range. Furthermore, as described by Krzywinski and Altman in a discussion piece in Nature Methods on statistical analysis in nonparametric

testing, small sample sizes can produce insensitivity to changes in the data when using a Wilcoxon test and lead to the reduced sensitivity of rank methods, sometimes making it impossible to achieve any *P* value lower than $\alpha = 0.05$ (357). This is related to the fact that the output of a rank-based test such as the Wilcoxon, relies on the probability that a value drawn from group A will be smaller or larger than one drawn from group B, with no regard for their absolute differences (357). Within my data, IL-6 and IL-10 for example, demonstrate clearly that the cytokine was present in the +MSC samples and absent in the control sample, describing these data as not different, due to the nonparametric testing on small sample number, countered a common-sense approach to assessment of the results.

The results of the Luminex revealed undetectable expression of IL-7, IL-23 and IL-35 in the immune panels and undetectable expression of adrenocorticotropic hormone (ACTH), parathyroid hormone (PTH) and fibroblast growth factor-23 (FGF23) in the bone panels, across all experimental timepoints and conditions.

5.3.1.8 Fibronectin MSC biomaterials in co-culture with T cells for 3 days reveal a mixed T helper response

The fibronectin allogenic MSC biomaterial in co-culture with the primed human T cells produced a globally higher amount of inflammatory cytokines and chemokines than no MSC controls [Figure 5-15]. To understand whether this micro-environment was driving a regulatory tolerance response driven by the MSCs, or an activation/rejection response driven by the T cells, the cytokines/chemokines were categorised into six groups: growth factors, Th1, Th2, Th17, regulatory or activation/cytotoxic responses. To enable easier interpretation of the large volume of data obtained from the Luminex analysis, the significant

results for all timepoints are summarised by cytokine group, biomaterial type and timepoint in Venn diagrams [Figure 5-14].

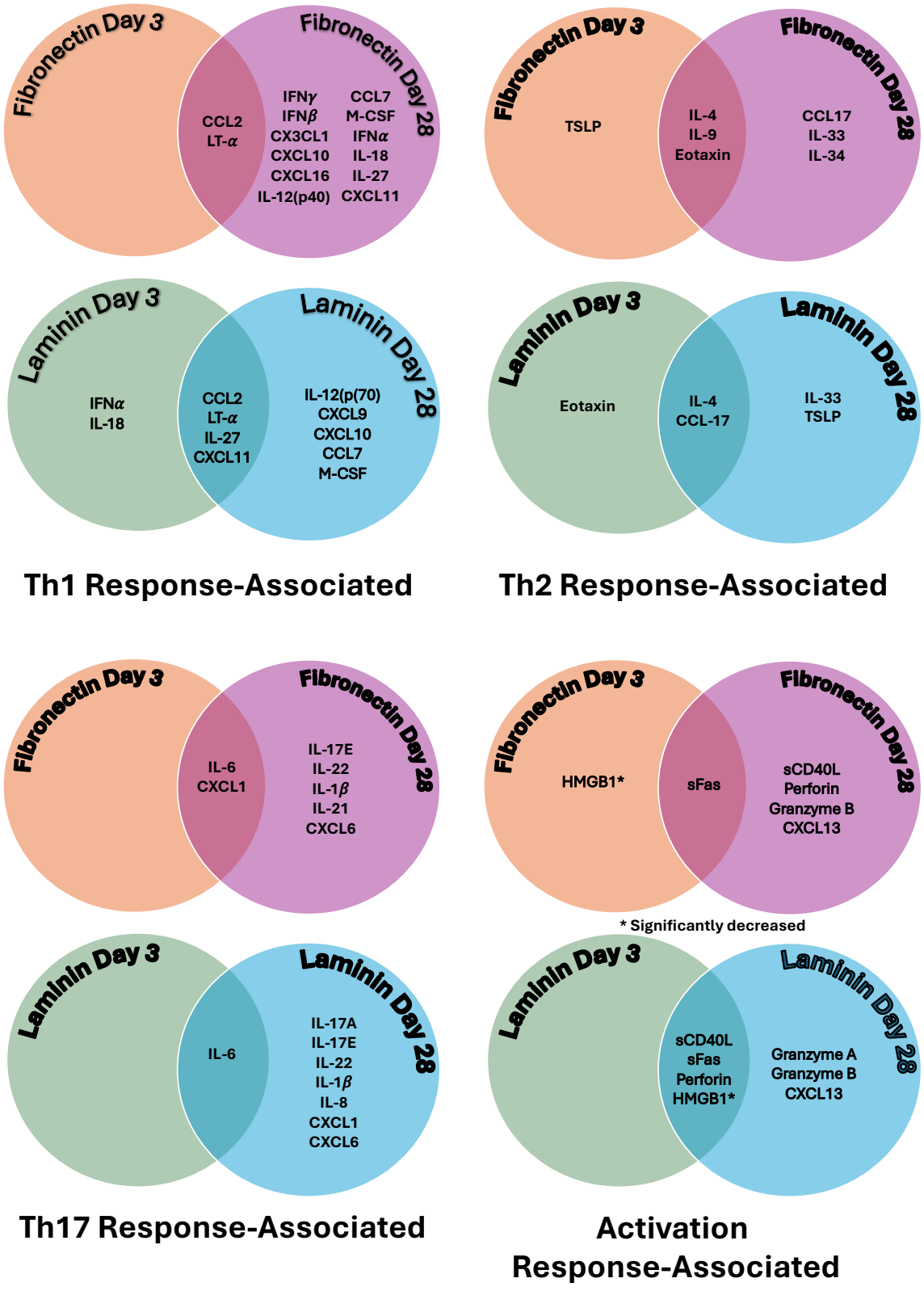

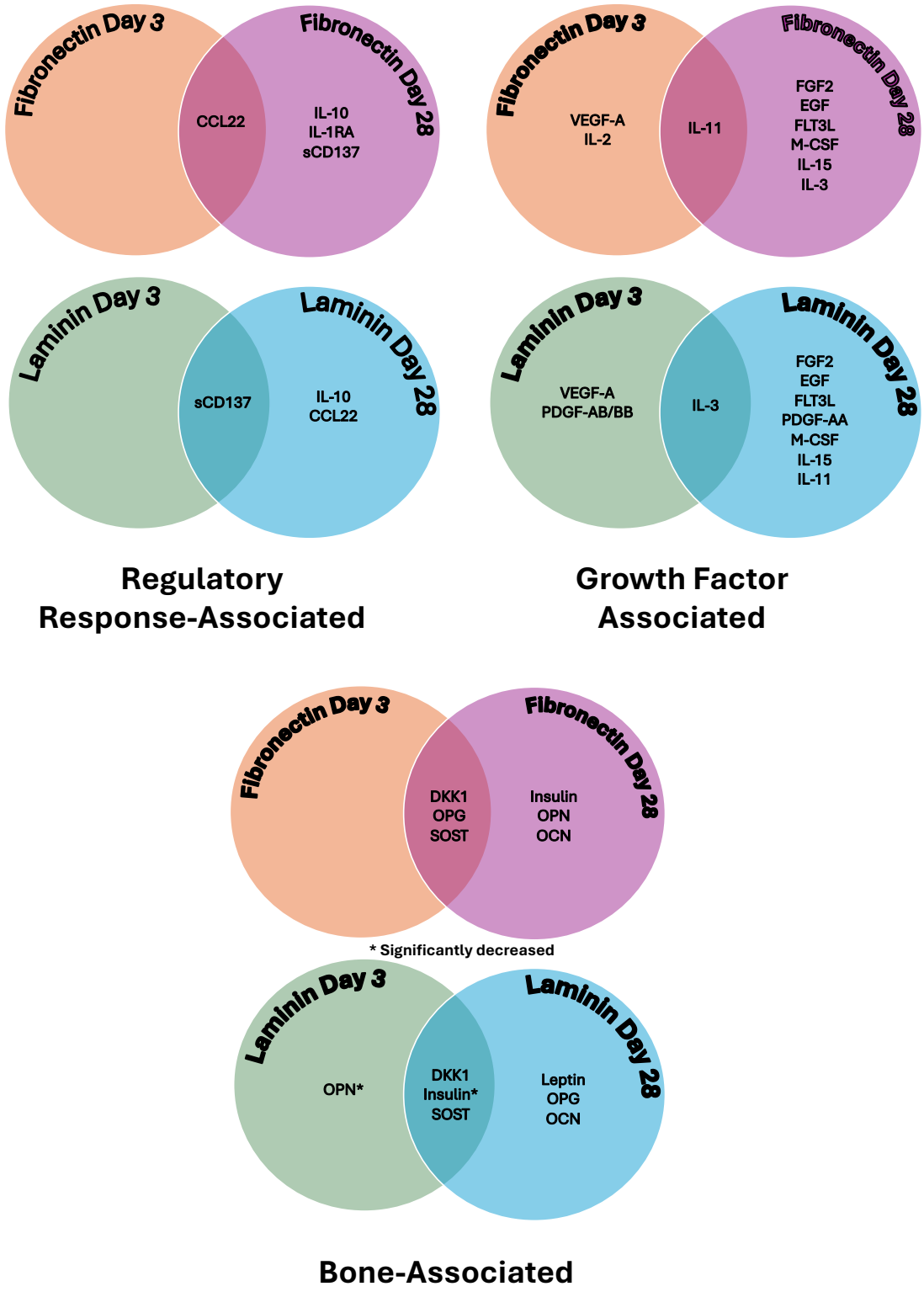

Figure 5-14: Summary Venn diagrams of cytokine groups showing increased numbers of significant increases at day 28 co-culture with osteoblast biomaterials and T cells on laminin or fibronectin biomaterials. Groups were classified as Th1, Th2, Th17, activation/cytotoxic, regulatory, growth factor or bone associated.

In all heatmap figures, analytes are grouped based on the Luminex kit and referred to based on their names used in these kits. In contrast, in the bar charts comparing the amounts of the analytes between co-cultures of T cells and MSCs/osteoblasts with T cells and acellular biomaterials, systematic names are used. In the text, both names are given when the analyte is first described and the systematic name used subsequently.

A Th1 response is responsible for cell-mediated immunity and is associated with eradication of pathogens and tumours, as well as perpetuating autoimmune responses (358). Through the production of IFN-γ, macrophages are stimulated to phagocytose and undertake intracellular killing of microbes (359). Other actions induced by cytokines from Th1 cells are upregulation of the expression of MHCI and MHCII molecules and ICAM-1 on other cells such as fibroblasts and to induce proinflammatory cytokine secretion (359). Conversely, a Th2 response is associated production of increased IL-4, IL-5 and IL-13 (358).

There were few differences in expression of Th1 cytokines in supernatants taken from day 3 co-cultures containing MSCs grown in the presence of fibronectin with or without MSCs [Figure 5-15]. The exceptions were, Chemokine ligand 2 (CCL2, formerly MCP-1), and lymphotoxin-α (LT-α, formerly TNFβ) were significantly higher in the presence of allogenic MSCs [Figure 5-15]. Several Th2 associated cytokines were also significantly increased in the allogenic MSC condition compared to the acellular control, IL-4, IL-9, eotaxin and thymic stromal lymphopoietin (TSLP) were all increased [Figure 5-16].

A Th17 response is defined by the production of IL-17 and results in a highly inflammatory effect on stromal cells, causing greater productions of inflammatory cytokines and recruitment of leucocytes (360). Additionally, the literature supports

a key role for Th17 CD4+ T cells in transplant rejection and cytokines IL-17, IL-6, IL-1, IL-21 and IL-22 have been implicated (360, 361). At the early timepoint, there were no significant differences in expression of IL-17A, IL-17E, IL-17F in fibronectin co-cultures with or without MSCs. However, significant increases in IL-6 and chemokine ligand 1 (CXCL1, formerly GROα) were found in allogenic compared to acellular conditions [Figure 5-17].

There is a distinct subpopulation of CD4+ T cells called Tregs that have immunosuppressive functions and are critical to immunological tolerance (362). However, identification of human Treg cells is complicated by the expression of more diverse surface markers than in mice and the co-expression of these hallmark surface markers on both Tregs and T effector cells (363). As the FOXP3 staining in the flow cytometry panel was difficult to interpret, the presence of several molecules associated with regulatory cells was assessed, including Tregs. Cytokines were categorised based on being regulatory in function, rather than specific to just Treg function, and of those only CCL22, formerly macrophage-derived chemokine) was significantly increased at the early D3 fibronectin MSC biomaterial co-culture compared to the acellular control culture [Figure 5-18]. Notably there was no significant increase in IL-10 expression at this timepoint, albeit a trend for higher levels in the presence of MSCs was found.

In the group of cytokines/chemokines categorised as associated with activation or cytotoxic immune responses, a significant increase was found for soluble Fas (sFas) in the MSC containing compared to acellular biomaterial samples. In the MSC biomaterial condition, high mobility group box 1 (HMGB-1) significantly decreased compared to acellular biomaterial controls [Figure 5-19].

Grouped under growth factors, IL-2, IL-11 and vascular endothelial growth factor A (VEGF-A) expression was significantly higher in the fibronectin MSC biomaterial condition compared to the acellular control [Figure 5-20]. No other significant differences were found between allogenic and acellular controls at the early timepoint for the fibronectin biomaterial.

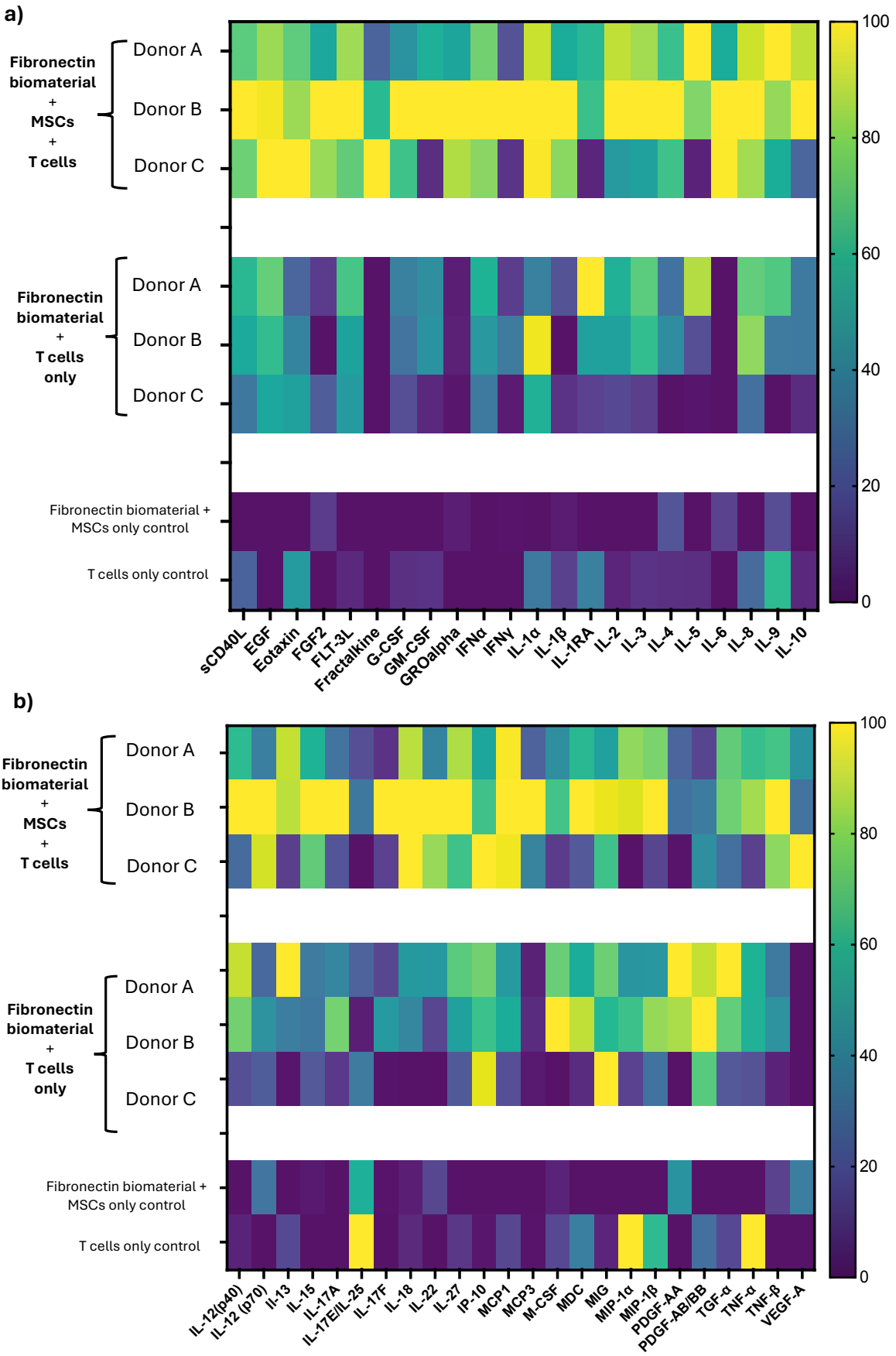
a)
Fibronectin biomaterial + MSCs + T cells
Donor A
Donor B
Donor C
Fibronectin biomaterial + T cells only
Donor A
Donor B
Donor C
Fibronectin biomaterial + MSCs only control
T cells only control
sCD40L
EGF
Eotaxin
FGF2
FLT-3L
Fractalkine
G-CSF
GM-CSF
GROalpha
IFNα
IFNγ
IL-1α
IL-1β
IL-1RA
IL-2
IL-3
IL-4
IL-5
IL-6
IL-8
IL-9
IL-10
100
80
60
40
20
0
b)
Fibronectin biomaterial + MSCs + T cells
Donor A
Donor B
Donor C
Fibronectin biomaterial + T cells only
Donor A
Donor B
Donor C
Fibronectin biomaterial + MSCs only control
T cells only control
IL-12(p40)
IL-12 (p70)
Il-13
IL-15
IL-17A
IL-17E/IL-25
IL-17F
IL-18
IL-22
IL-27
IP-10
MCP1
MCP3
M-CSF
MDC
MIG
MIP-1α
MIP-1β
PDGF-AA
PDGF-AB/BB
TGF-α
TNF-α
TNF-β
VEGF-A
100
80
60
40
20
0

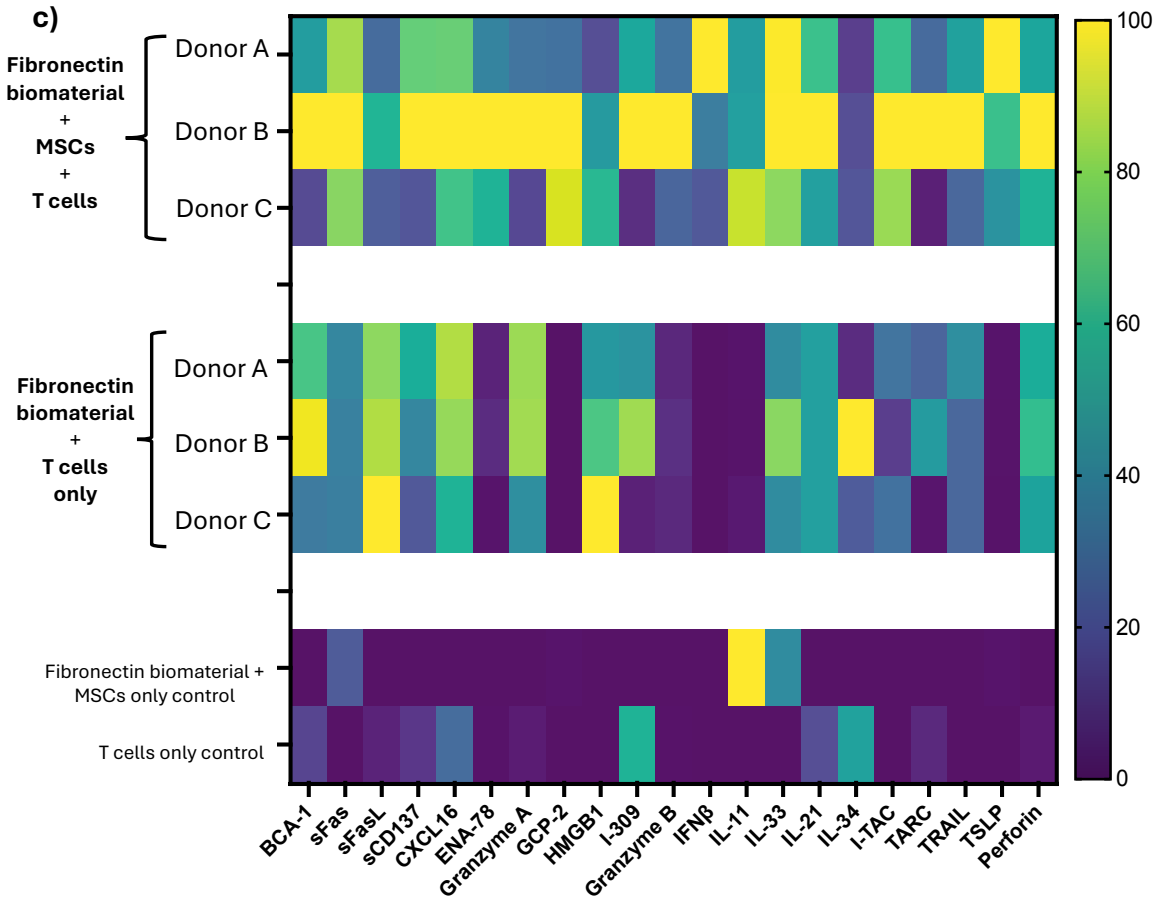

Figure 5-15: Heatmaps comparing the cytokine profile of the culture supernatants following 3 days of co-culture of activated T cells and 3 day undifferentiated MSC fibronectin biomaterials with T cells cultured for 3 days in the presence of acellular fibronectin biomaterials. Control supernatants are from MSC biomaterial only and T cell only conditions. The heatmap analytes are grouped based on the individual Luminex assays. (a) 23 analytes shown (b) 24 analytes shown (c) 21 analytes shown. Yellow represents the highest percentage expression and dark blue the lowest. Crosses represent missing data values. All data shown have been normalised with 0% representing the lowest value in the data set and 100% representing the highest value. When values were below the lowest detectable range of the standard curve, the value used was the minimal detected concentration per manufacturer's published guidance.

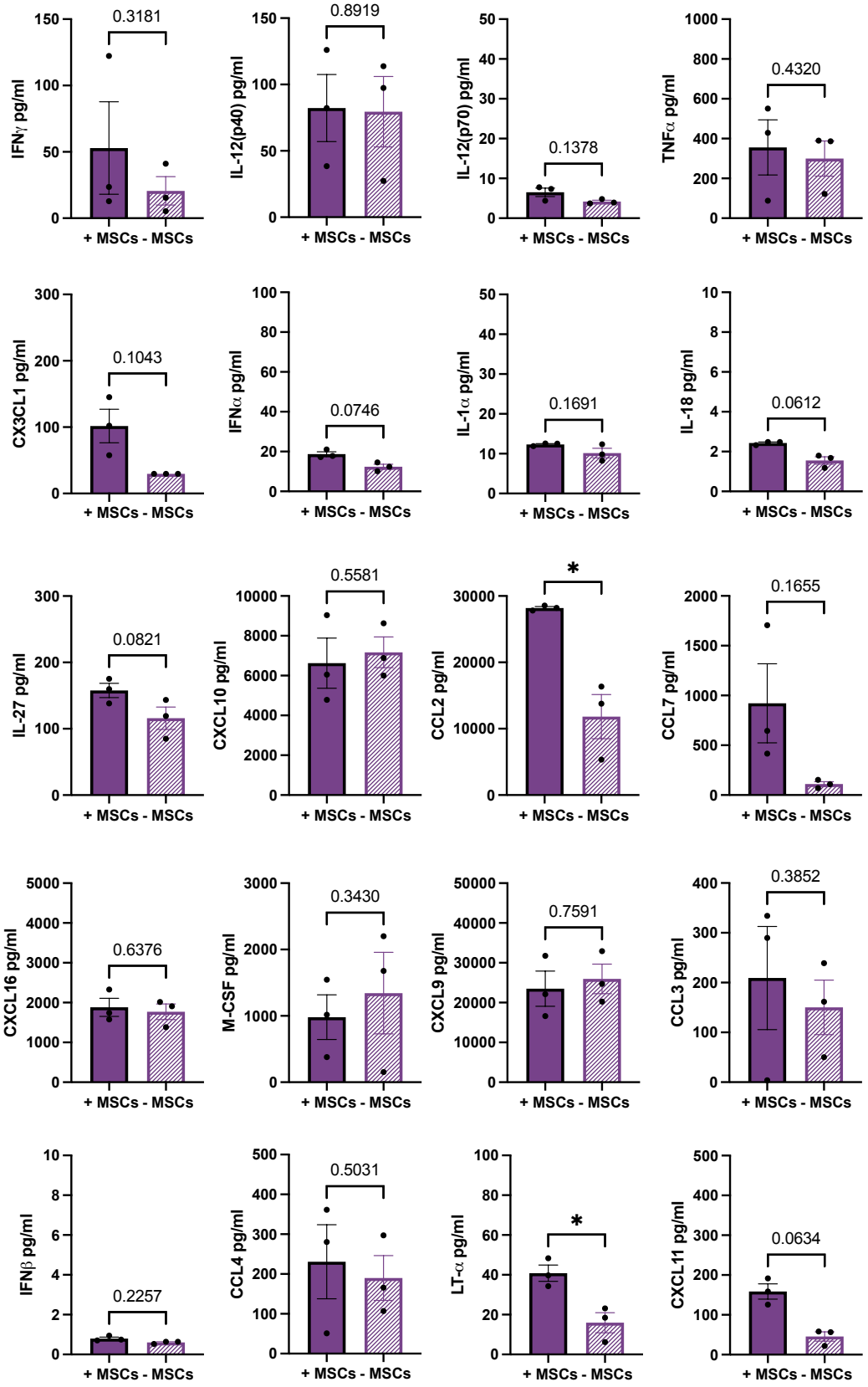

Figure 5-16 Few analytes that are associated with Th1 responses were increased after T cell co-culture in the presence of MSC biomaterials. Graphs represent individual paired T tests between MSC fibronectin biomaterials and no cell controls at the early D3-MSC timepoint. Bars represent the average of 3 biological donors and each data point is the mean of two technical replicates. Error bars represent the standard error of the mean. Data were analysed using paired T tests. P values = *p<0.05, **p<0.01, ***p<0.001, ****p<0.0001.

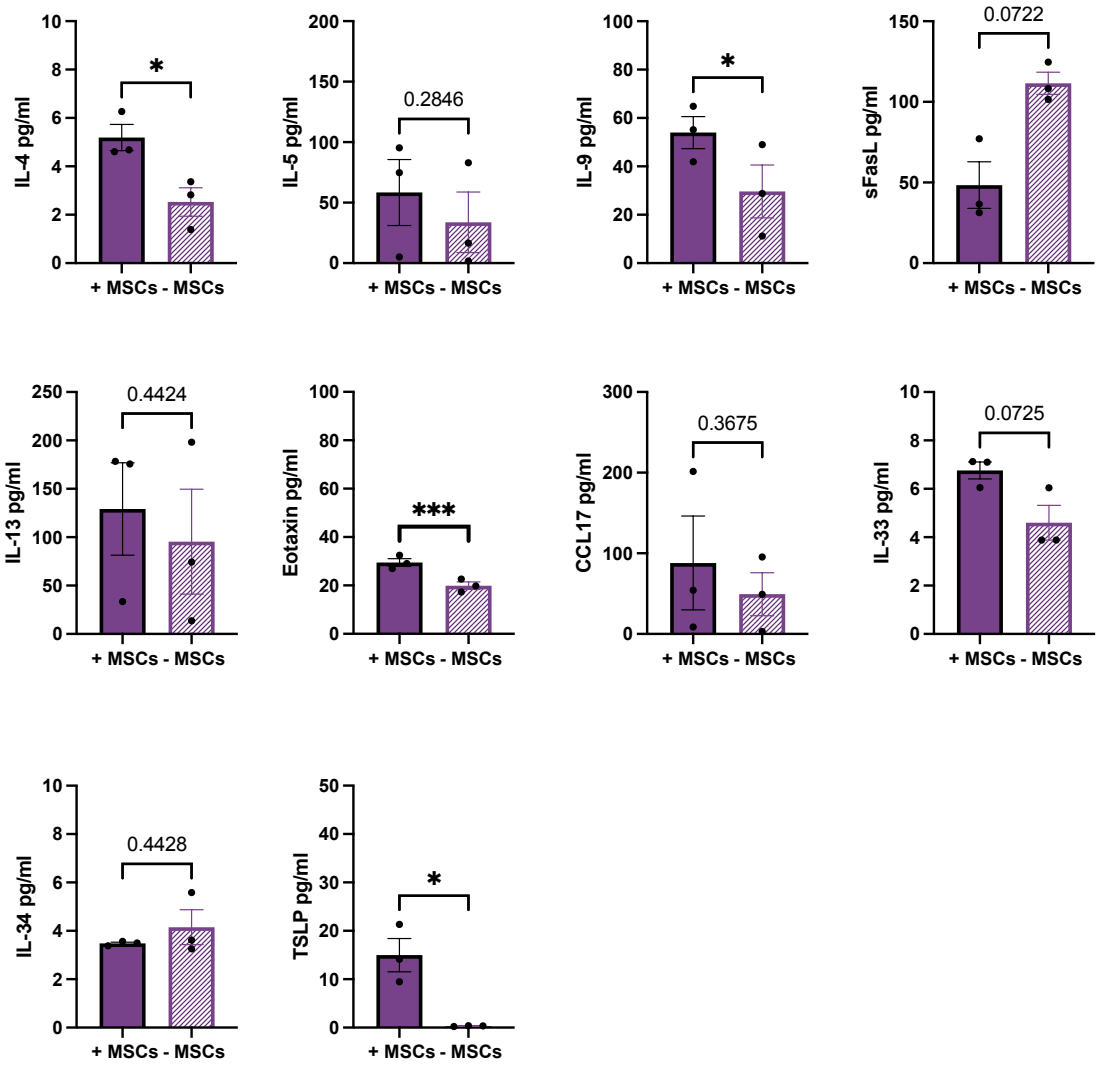

Figure 5-17: A number of analytes that are associated with Th2 responses were increased after T cell co-culture in the presence of MSC biomaterials. Graphs represent individual paired T tests between MSC fibronectin biomaterials and no cell controls at the early D3 timepoint. Bars represent the average of 3 biological donors and each data point is the mean of two technical replicates. Error bars represent the standard error of the mean. Data were analysed using paired T tests. P values = *p<0.05, **p<0.01, ***p<0.001, ****p<0.0001.

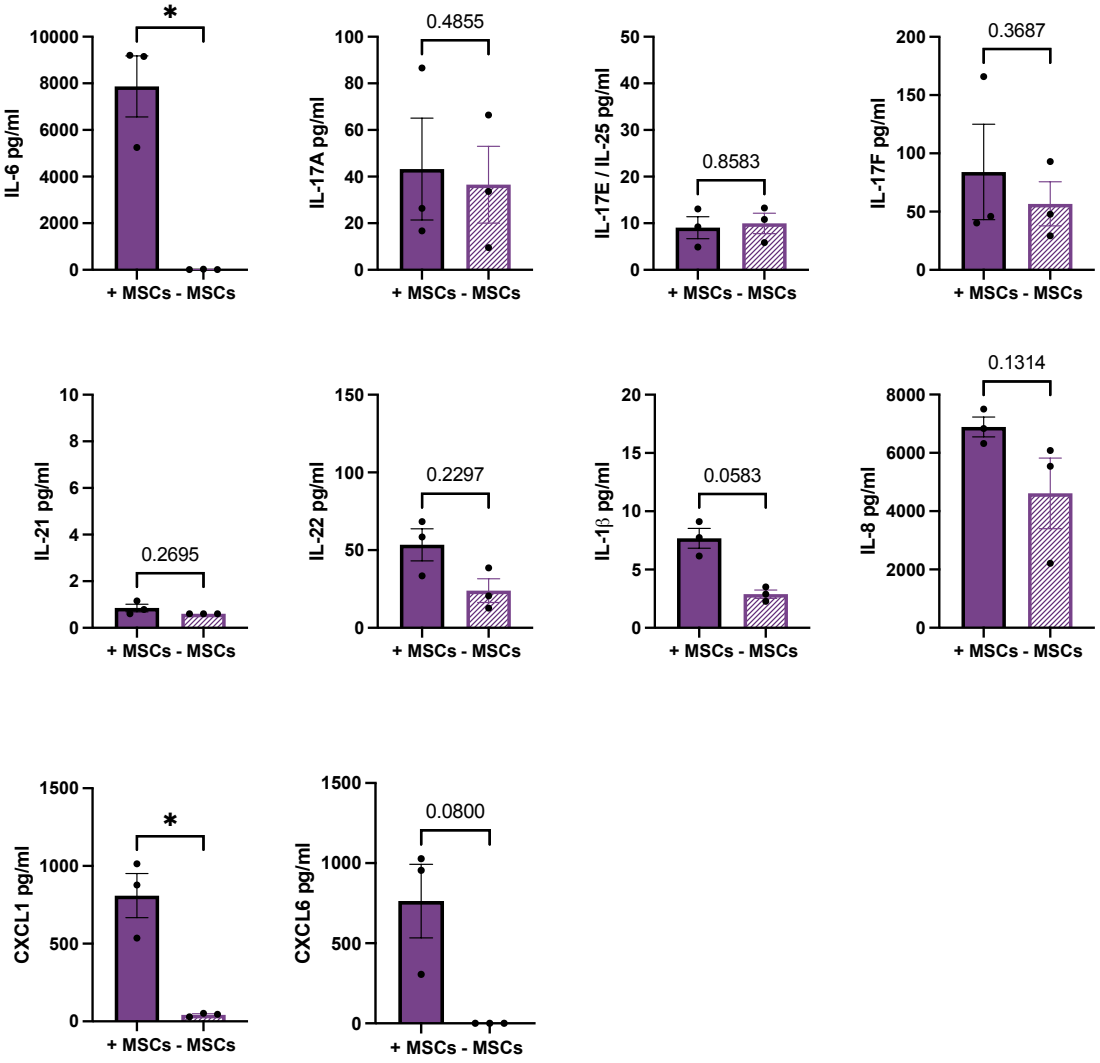

Figure 5-18: Few analytes that are associated with Th17 responses were increased after T cell co-culture in the presence of MSC biomaterials. Graphs represent individual paired T tests between MSC fibronectin biomaterials and no cell controls at the early D3 timepoint. Bars represent the average of 3 biological donors and each data point is the mean of two technical replicates. Error bars represent the standard error of the mean. Data were analysed using paired T tests. P values = *p<0.05, **p<0.01, ***p<0.001, ****p<0.0001.

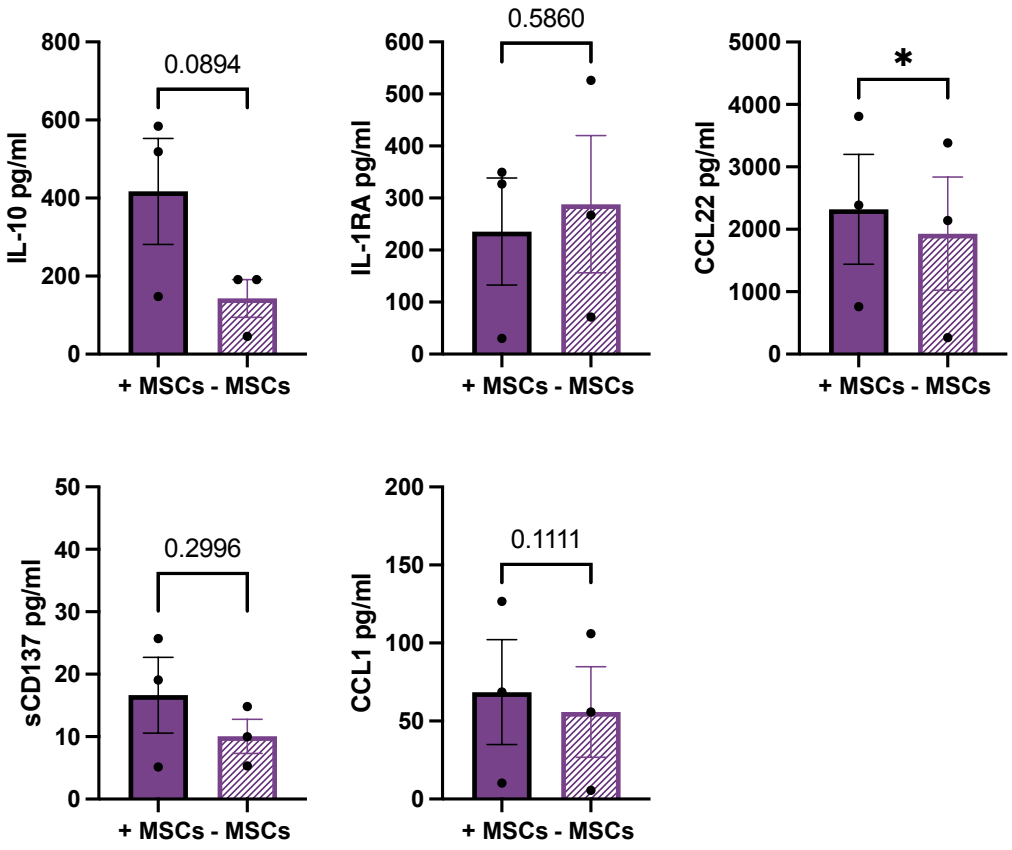

Figure 5-19: Few analytes that are associated with regulatory responses were increased after T cell co-culture in the presence of MSC biomaterials. Graphs represent individual paired T tests between MSC fibronectin biomaterials and no cell controls at the early D3 timepoint. Bars represent the average of 3 biological donors and each data point is the mean of two technical replicates. Error bars represent the standard error of the mean. Data were analysed using paired T tests. P values = *p<0.05, **p<0.01, ***p<0.001, ****p<0.0001.

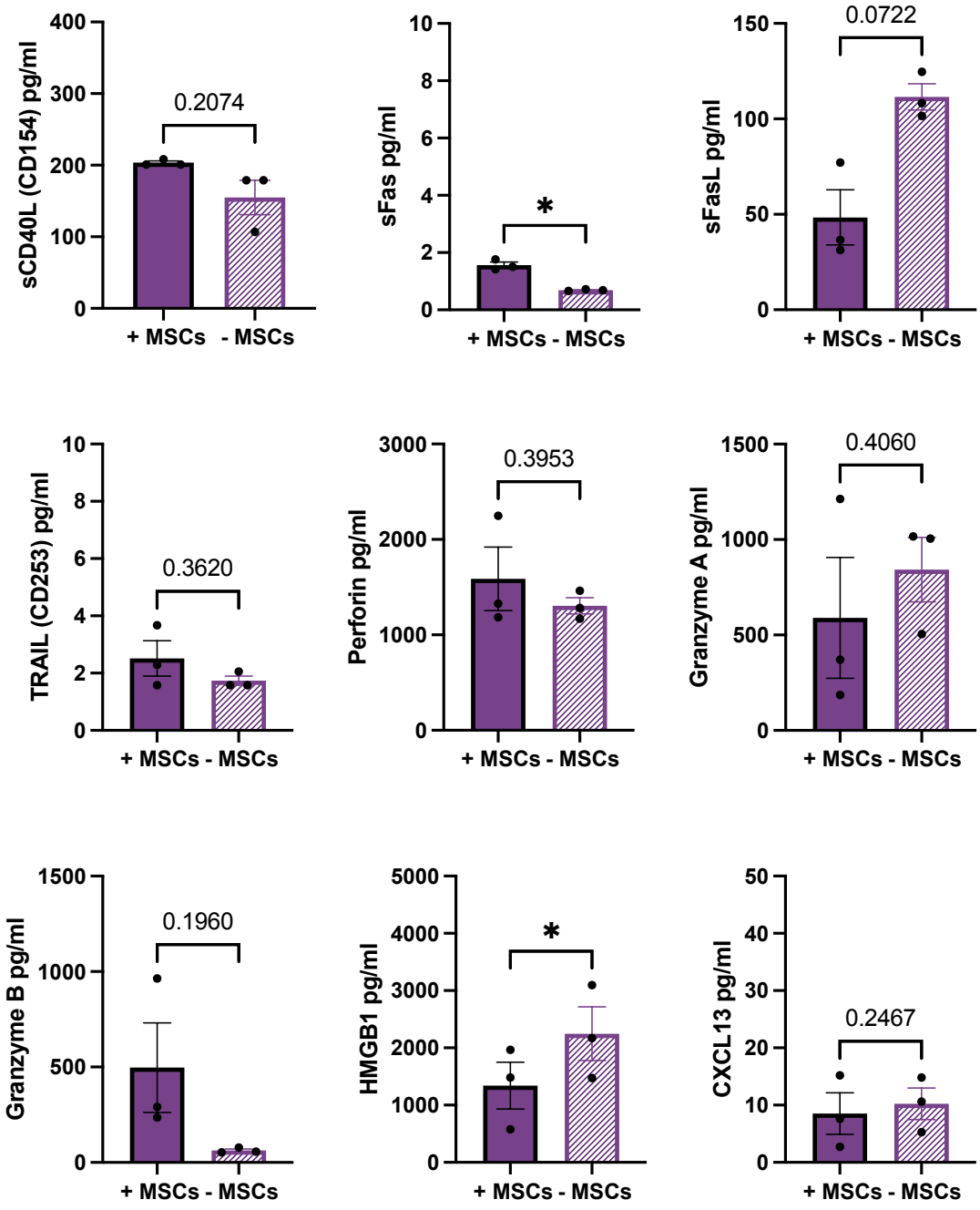

Figure 5-20: Few analytes that are associated with activation responses were increased after T cell co-culture in the presence of MSC biomaterials. Graphs represent individual paired T tests between MSC fibronectin biomaterials and no cell controls at the early D3 timepoint. Bars represent the average of 3 biological donors and each data point is the mean of two technical replicates. Error bars represent the standard error of the mean. Data were analysed using paired T tests. P values = *p<0.05, **p<0.01, ***p<0.001, ****p<0.0001.

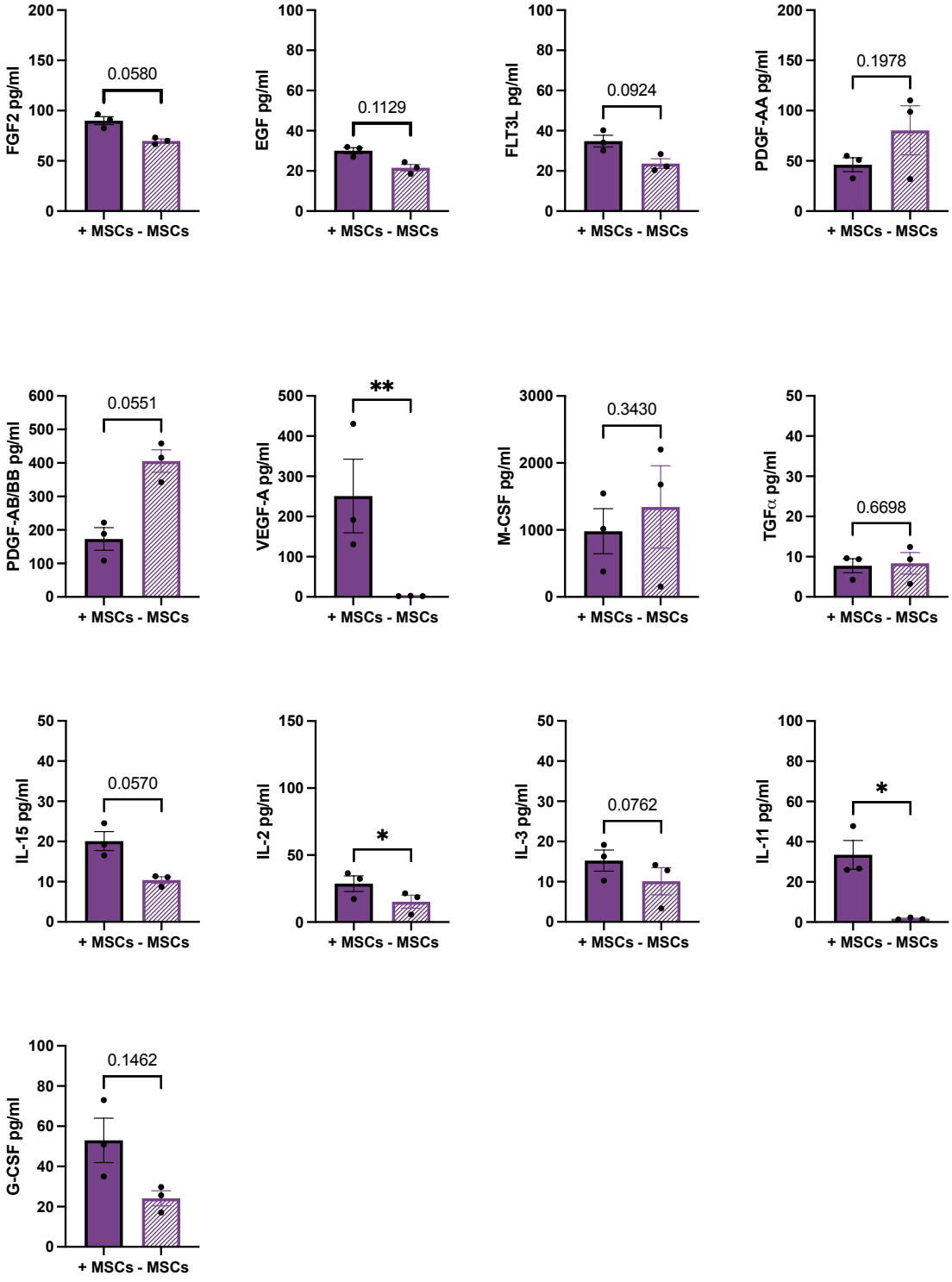

Figure 5-21: Few growth factors significantly increased expression after T cell co-culture in the presence of MSC biomaterials. Graphs represent individual paired T tests between MSC fibronectin biomaterials and no cell controls at the early D3 timepoint. Bars represent the average of 3 biological donors and each data point is the mean of two technical replicates. Error bars represent the standard error of the mean. Data were analysed using paired T tests. P values = *p<0.05, **p<0.01, ***p<0.001, ****p<0.0001.

5.3.1.9 D3 Laminin MSC biomaterials led to an increase in the number of Th1 and activation-categorised cytokines in co-culture with T cells for 3 days compared to fibronectin containing cultures

Overall, the fibronectin D3 data indicate a mixed response by the T cells in response to the cellularised biomaterial, with higher numbers of significant increases in Th2-associated cytokines than Th1, Th17 or activation-associated. I next examined whether the response to laminin containing biomaterials led to a similar mixed T helper response.

The laminin MSC biomaterial in co-culture with the primed human T cells produced a globally higher amount of inflammatory cytokines and chemokines than the no MSC biomaterial with T cells matched control [Figure 5-21]. As with the fibronectin biomaterial, to understand whether the MSC were driving a regulatory tolerance response, or an activation/rejection response driven by the T cells, I grouped the cytokines/chemokines into growth factors and Th1, Th2, Th17, regulatory or activation/cytotoxic responses [Figure 5-14].

Th1 associated cytokines and chemokines, CCL2 and LTα, were significantly higher in the laminin MSC D3 biomaterial and T cell co-cultures compared to the acellular control, as had been for the fibronectin [Figure 5-22]. Further significant increases were seen in the laminin MSC+ conditions for IL-18, IL-27 and C-X-C motif chemokine 11 (CXCL11, formerly interferon-inducible T cell alpha chemoattractant or I-TAC) compared to the acellular biomaterial control. IFNγ also increased in the two cell co-culture between the MSCs and the T cells compared to the supernatant from the control culture. The remaining cytokines showed no significant changes at the early timepoint.

As with the D3 fibronectin MSC condition, the laminin MSC biomaterial had increased IL-4, eotaxin and CCL17 (formerly thymus and activation regulated chemokine or TARC) at the early timepoint [Figure 5-23]. IL-5 appeared to have a nonsignificant increase in the MSC condition in co-culture with the T cells. No other significant differences were found between the T cell cultures with and without MSC.

For Th17 response-associated analytes, a significant increase was found for IL-6 [Figure 5-24]. CXCL1 and CXCL 6 (formerly known as granulocyte chemotactic protein 2, GCP-2) appeared to be increased in MSC conditions but this was nonsignificant. This mirrors the response seen within the fibronectin biomaterial allogenic co-cultures. Categorised as associated with regulatory responses, significant increases were found in soluble CD137 (sCD137) only and this differs to the fibronectin timepoint where no significance was found [Figure 5-25]. Similar to fibronectin, IL-10, was raised but nonsignificant in the presence of MSC biomaterials versus controls.

Activation or cytotoxic response-associated analytes that increased significantly with exposure to allogenic cells included, sFas as with fibronectin, but additionally significant increases in soluble CD40L (sCD40L, also known as CD154) and perforin were found [Figure 5-26]. Furthermore, high mobility group box 1 (HMGB1) protein significantly decreased in the presence of laminin MSC biomaterials as it had done in co-cultures between T cells and D3 fibronectin biomaterials. No other significant differences between the T cells groups culture with and without MSCs were found in the activation/cytotoxic analytes at this timepoint.

Finally, several growth factors increased significantly in supernatants from cultures containing T cells with MSCs compared to T cells alone, even at this early D3 timepoint on laminin biomaterials. As with the fibronectin biomaterial data, VEGF-A was significantly increased in the MSC biomaterial conditions as was IL-3, IL-15 and PDGF-AB/BB [Figure 5-27]. IL-2 and IL-11 reflected the same increased trends as with fibronectin but for laminin were nonsignificant.

Overall, at the D3 MSC timepoint, significant increases were found for more Th1 and activation-associated cytokines in the presence of laminin biomaterials [Figure 5-14]. However, Th2, Th17, regulatory-associated and growth factor associated analytes significantly increased in the presence of both biomaterial types. This implies a mixed Thelper response to the biomaterials at the early undifferentiated MSC stage.

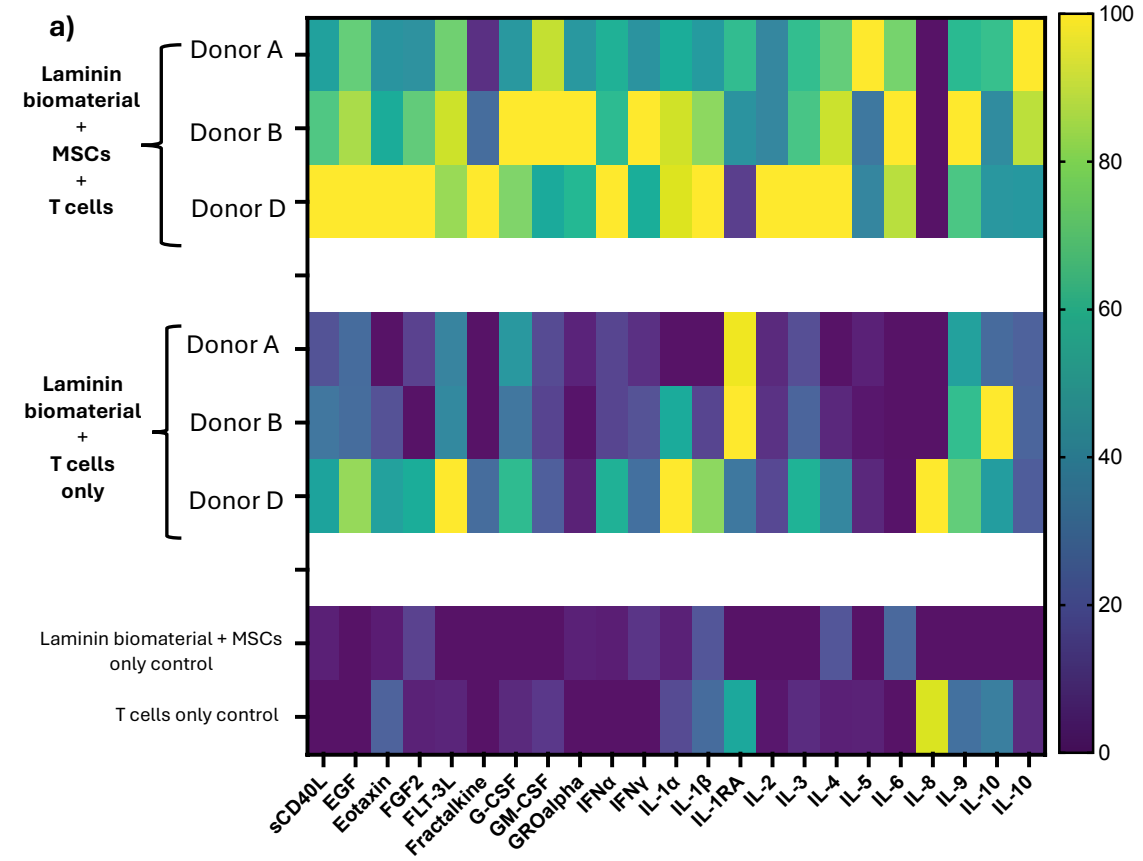
a)
Laminin biomaterial + MSCs + T cells
Donor A
Donor B
Donor D
Laminin biomaterial + T cells only
Donor A
Donor B
Donor D
Laminin biomaterial + MSCs only control
T cells only control
sCD40L
EGF
Eotaxin
FGF2
FLT-3L
Fractalkine
G-CSF
GM-CSF
GROalpha
IFNα
IFNγ
IL-1α
IL-1β
IL-1RA
IL-2
IL-3
IL-4
IL-5
IL-6
IL-8
IL-9
IL-10
IL-10
100
80
60
40
20
0

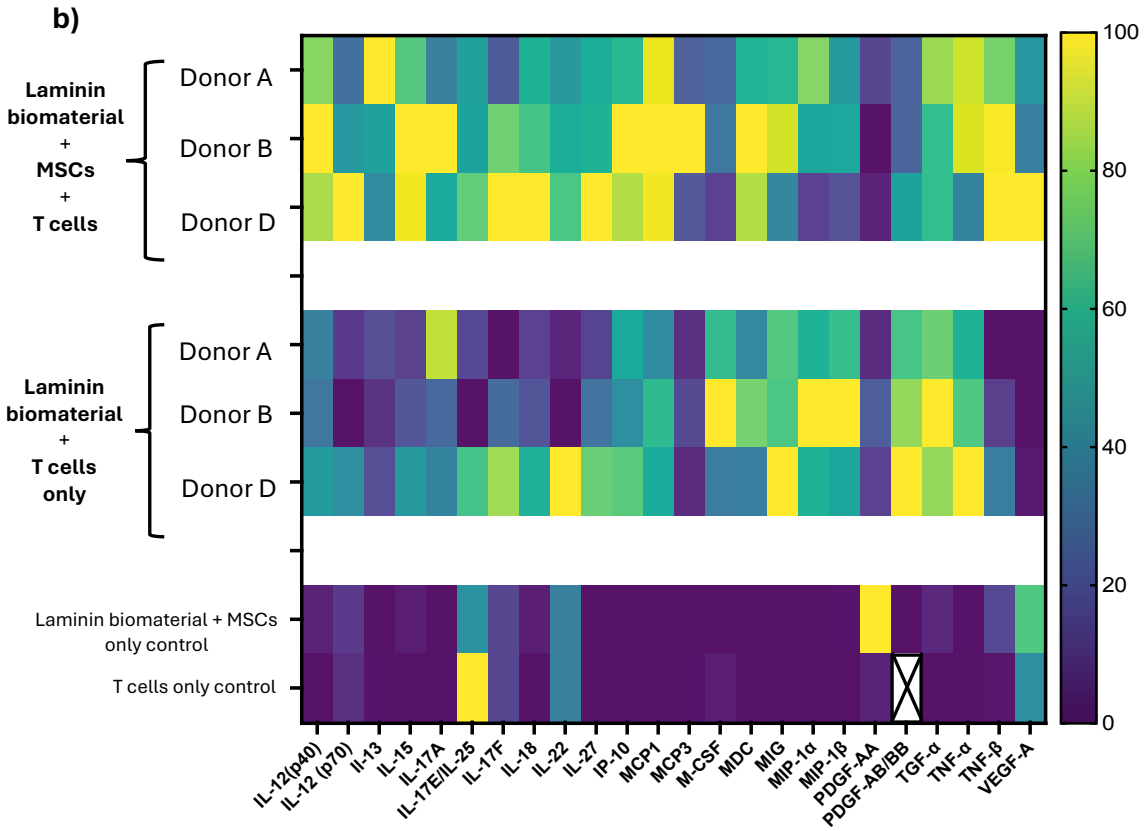
b)
Laminin biomaterial + MSCs + T cells
Donor A
Donor B
Donor D
Laminin biomaterial + T cells only
Donor A
Donor B
Donor D
Laminin biomaterial + MSCs only control
T cells only control
IL-12(p40)
IL-12 (p70)
Il-13
IL-15
IL-17A
IL-17E/IL-25
IL-17F
IL-18
IL-22
IL-27
IP-10
MCP1
MCP3
M-CSF
MDC
MIG
MIP-1α
MIP-1β
PDGF-AA
PDGF-AB/BB
TGF-α
TNF-α
TNF-β
VEGF-A
100
80
60
40
20
0

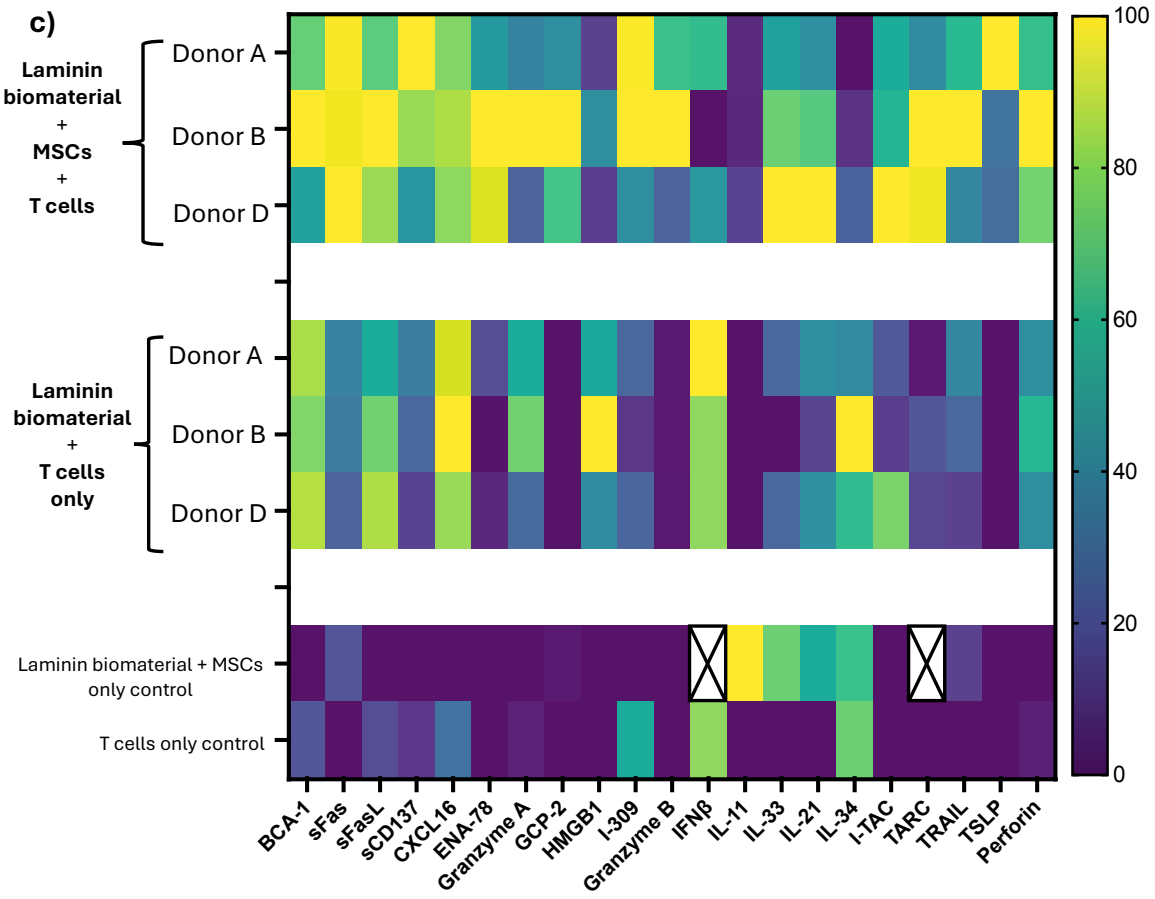

Figure 5-22: Heatmaps comparing the cytokine profile of the culture supernatants following 3 days of co-culture of activated T cells and 3 day undifferentiated MSC laminin biomaterials with T cells cultured for 3 days in the presence of acellular laminin biomaterials. Control supernatants are from MSC biomaterial only and T cell only conditions. The heatmap analytes are grouped based on the individual Luminex assays. (a) 23 analytes shown (b) 24 analytes shown (c) 21 analytes shown. Yellow represents the highest percentage expression and dark blue the lowest. Crosses represent missing data values. All data shown have been normalised with 0% representing the lowest value in the data set and 100% representing the highest value. When values were below the lowest detectable range of the standard curve, the value used was the minimal detected concentration per manufacturer's published guidance

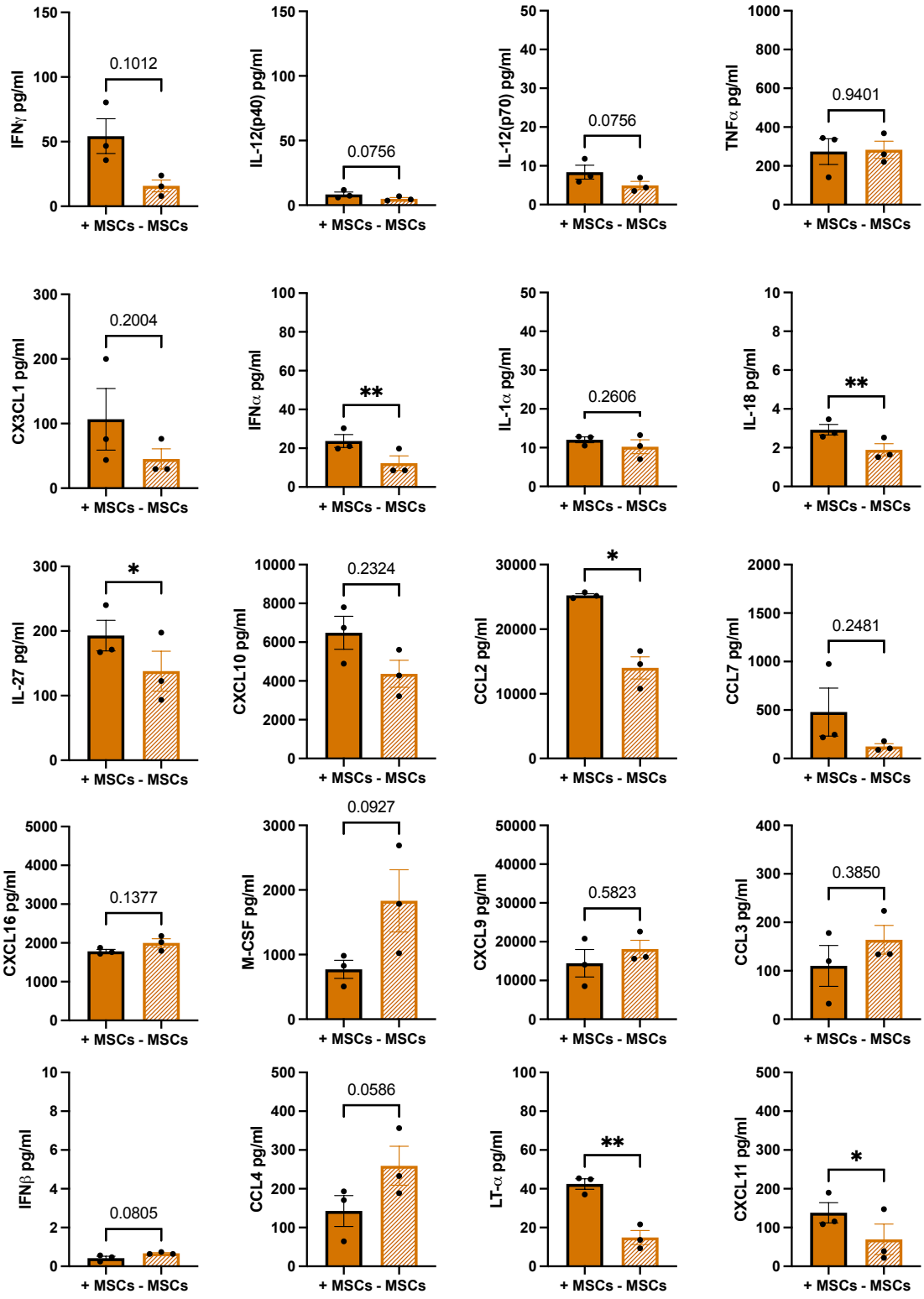

Figure 5-23: Increases found in analytes that are associated with Th1 responses after T cell co-culture in the presence of MSC biomaterials. Graphs represent individual paired T tests between MSC laminin biomaterials and no cell controls at the early D3 timepoint. Bars represent the average of 3 biological donors and each data point is the mean of two technical replicates. Error bars represent the standard error of the mean. Data were analysed using paired T tests. P values = *p<0.05, **p<0.01, ***p<0.001, ****p<0.0001.

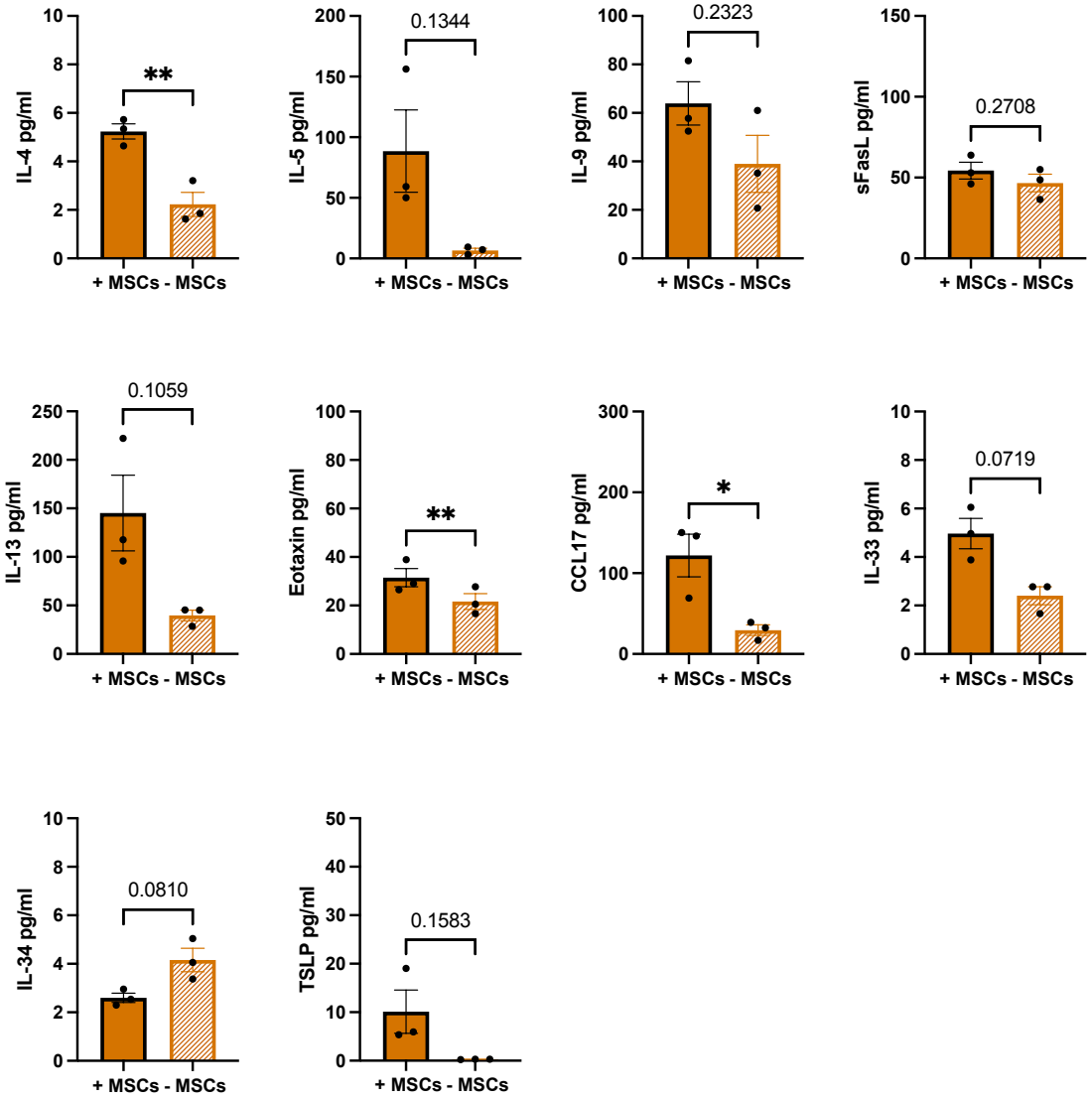

Figure 5-24: Few analytes that are associated with Th2 responses were increased after T cell co-culture in the presence of MSC biomaterials. Graphs represent individual paired T tests between MSC laminin biomaterials and no cell controls at the early D3 timepoint. Bars represent the average of 3 biological donors and each data point is the mean of two technical replicates. Error bars represent the standard error of the mean. Data were analysed using paired T tests. P values = *p<0.05, **p<0.01, ***p<0.001, ****p<0.0001.

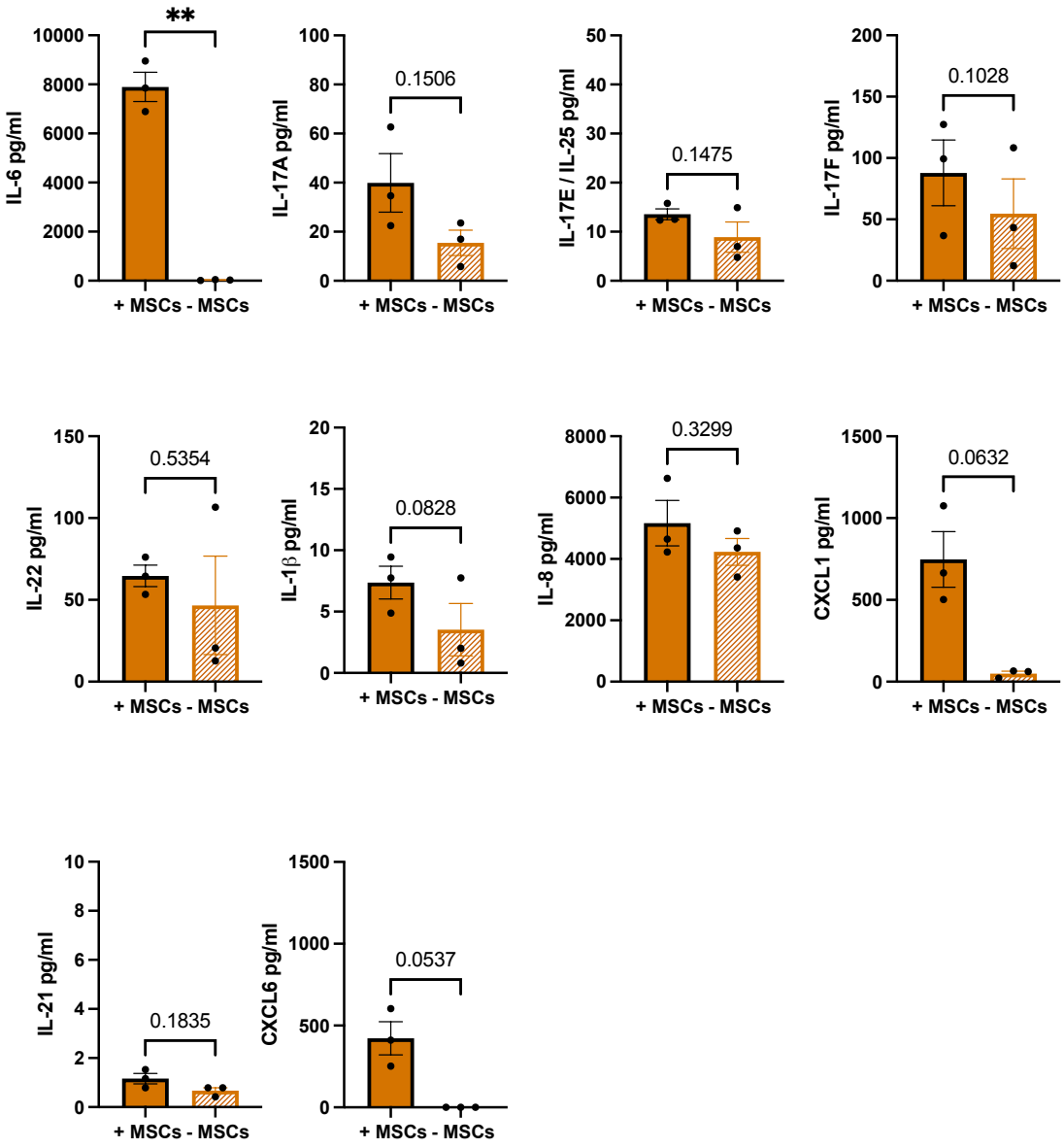

Figure 5-25: Few analytes that are associated with Th17 responses were increased after T cell co-culture in the presence of MSC biomaterials. Graphs represent individual paired T tests between MSC laminin biomaterials and no cell controls at the early D3 timepoint. Bars represent the average of 3 biological donors and each data point is the mean of two technical replicates. Error bars represent the standard error of the mean. Data were analysed using paired T tests. P values = *p<0.05, **p<0.01, ***p<0.001, ****p<0.0001.

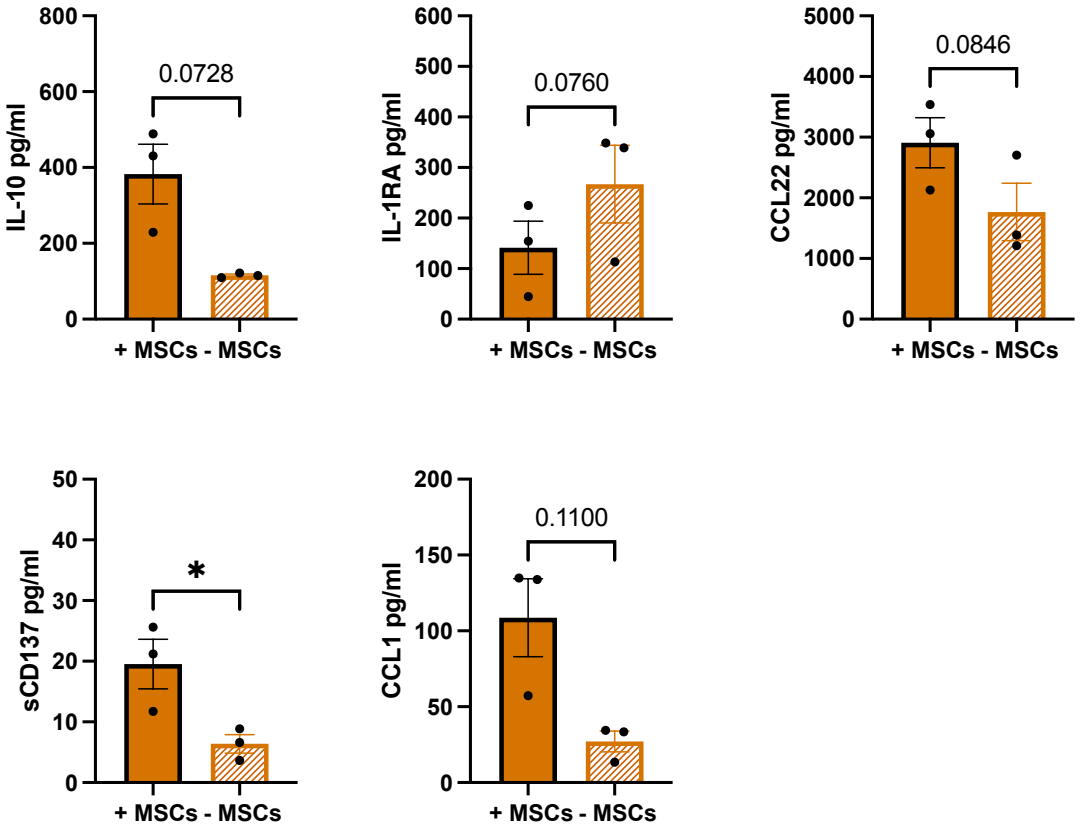

Figure 5-26: Few analytes that are associated with regulatory responses were increased after T cell co-culture in the presence of MSC biomaterials. Graphs represent individual paired T tests between MSC laminin biomaterials and no cell controls at the early D3 timepoint. Bars represent the average of 3 biological donors and each data point is the mean of two technical replicates. Error bars represent the standard error of the mean. Data was analysed using paired T tests. P values = *p<0.05, **p<0.01, ***p<0.001, ****p<0.0001.

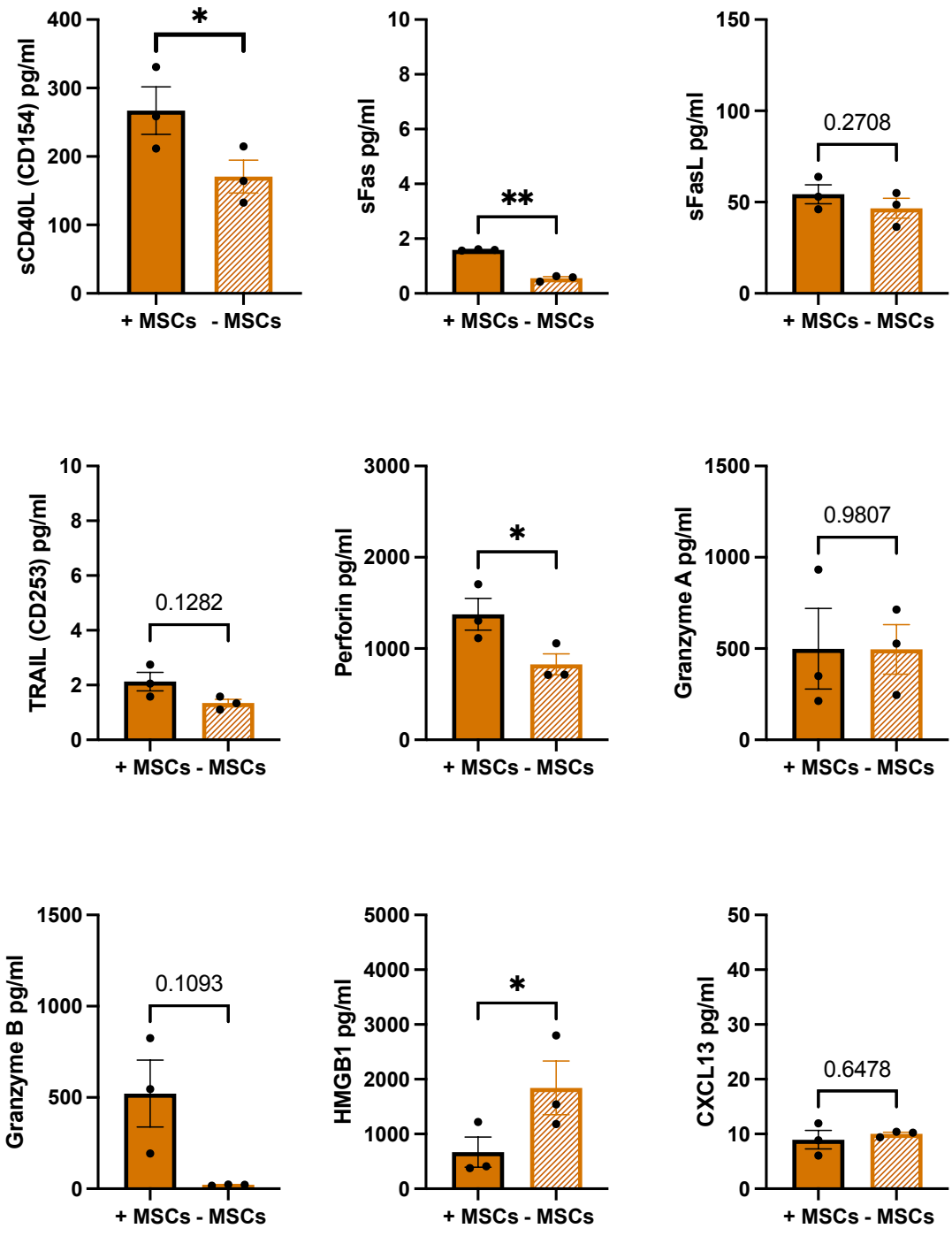

Figure 5-27: A number of analytes that are associated with activation responses were increased after T cell co-culture in the presence of MSC biomaterials. Graphs represent individual paired T tests between MSC laminin biomaterials and no cell controls at the early D3 timepoint. Bars represent the average of 3 biological donors and each data point is the mean of two technical replicates. Error bars represent the standard error of the mean. Data were analysed using paired T tests. P values = *p<0.05, **p<0.01, ***p<0.001, ****p<0.0001.

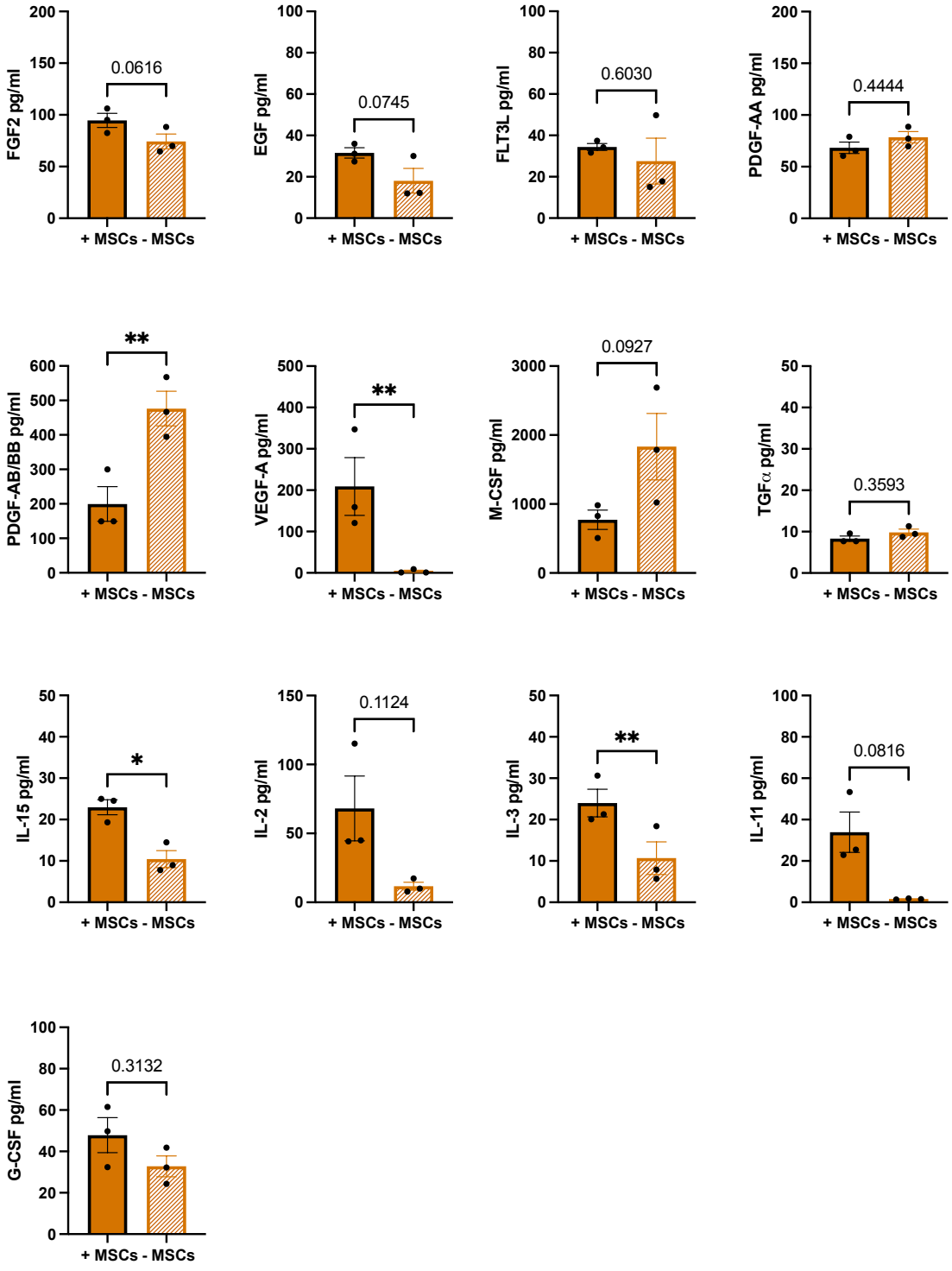

Figure 5-28: Many growth factors were increased after T cell co-culture in the presence of MSC biomaterials. Graphs represent individual paired T tests between MSC laminin biomaterials and no cell controls at the early D3 timepoint. Bars represent the average of 3 biological donors and each data point is the mean of two technical replicates. Error bars represent the standard error of the mean. Data were analysed using paired T tests. P values = *p<0.05, **p<0.01, ***p<0.001, ****p<0.0001.

5.3.1.10 D3 MSC biomaterials in co-culture with T cells for 3 days generate mixed cytokine responses for osteogenesis

The Luminex panel for bone related chemokines and cytokines consisted of Dickkopf-related protein 1 (DKK1), insulin, leptin, Osteoprotegerin (OPG), OCN, OPN and sclerostin (SOST) [Appendix 2, 7.2]. As highlighted previously, ACTH, PTH and FGF-23 were undetectable within any of the co-culture results and therefore have been excluded from the analysis. Again, summary Venn diagrams are provided for ease of reference [Figure 5-14].

The heatmap for fibronectin biomaterials highlights a global increase in bone-associated analytes in both the T cell co-culture with allogenic fibronectin MSC condition and the MSCs only control [Figure 5-28].

Significant increases in expression of DKK1 and OPG were found in the supernatants from T cell D3 MSC co-cultures in the presence of fibronectin biomaterials versus no MSC controls [Figure 5-28]. There were no significant differences for OCN or OPN implying the allogenic MSCs, as expected at just 3 days, had not differentiated into osteoblasts. Whilst SOST levels in supernatants from the co-cultures were significantly higher than no MSC controls, the raw amount of cytokine in pg/ml was at the bottom of the standard curve and likely not biologically significant.

The heatmap highlights a mixed response in upregulated markers for the laminin co-cultures [Figure 5-29]. DKK1, leptin, OPG, OC and SOST appear to see proportionally higher expression in the MSC and T cell laminin co-culture than T cell laminin biomaterial controls amongst the normalised data. Whereas conversely, insulin and OPN were higher in the no MSC laminin biomaterial with T

cell only co-culture. The laminin MSC biomaterial only condition had some expression of DKK1, OPG, OC and SOST on the heat map, however this appeared to increase when T cells were added into the co-culture and overall normalised expression on the heat map is higher.

In the laminin MSC biomaterial and T cell co-culture, significant increases were found for DKK1, OPG and SOST compared to co-cultures without MSCs. This mirrors the findings in the fibronectin containing cultures [Figure 5-30]. Significant decreases were seen in OPN and insulin in the presence of MSC laminin biomaterials and T cells co-cultures.

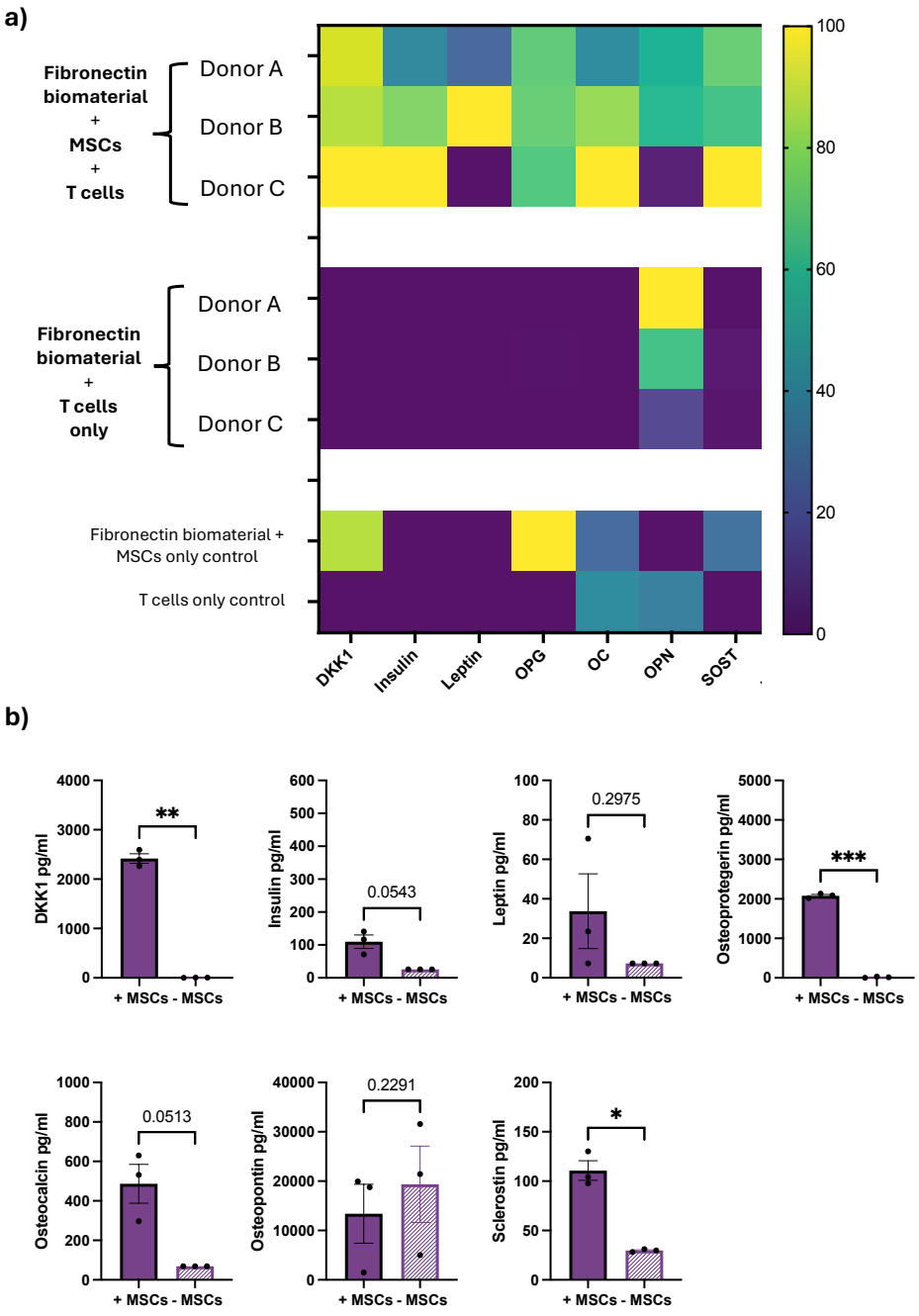

Figure 5-29: a) Heatmaps comparing the cytokine profile of the culture supernatants following 3 days of co-culture of activated T cells and 3 day undifferentiated MSCs cultured in the presence of fibronectin biomaterials with T cells cultured for 3 days in the presence of fibronectin acellular biomaterials. Control supernatants are from MSC biomaterial only and T cell only supernatant shown. 7 bone analytes shown. Yellow represents the highest percentage expression and dark blue the lowest. Crosses represent missing data values. All data shown has been normalised with 0% representing the lowest value in the data set and 100% representing the highest value. When values were below the lowest detectable range of the standard curve, the value used was the minimal detected concentration per manufacturer's published guidance. b) Individual analyte comparisons. Graphs represent individual paired T tests between MSC fibronectin biomaterials and no cell controls at the early D3 timepoint. Bars represent the average of 3 biological donors and each data point is the mean of two technical replicates. Error bars represent the standard error of the mean. Data were analysed using paired T tests. P values = *p<0.05, **p<0.01, ***p<0.001, ****p<0.0001.

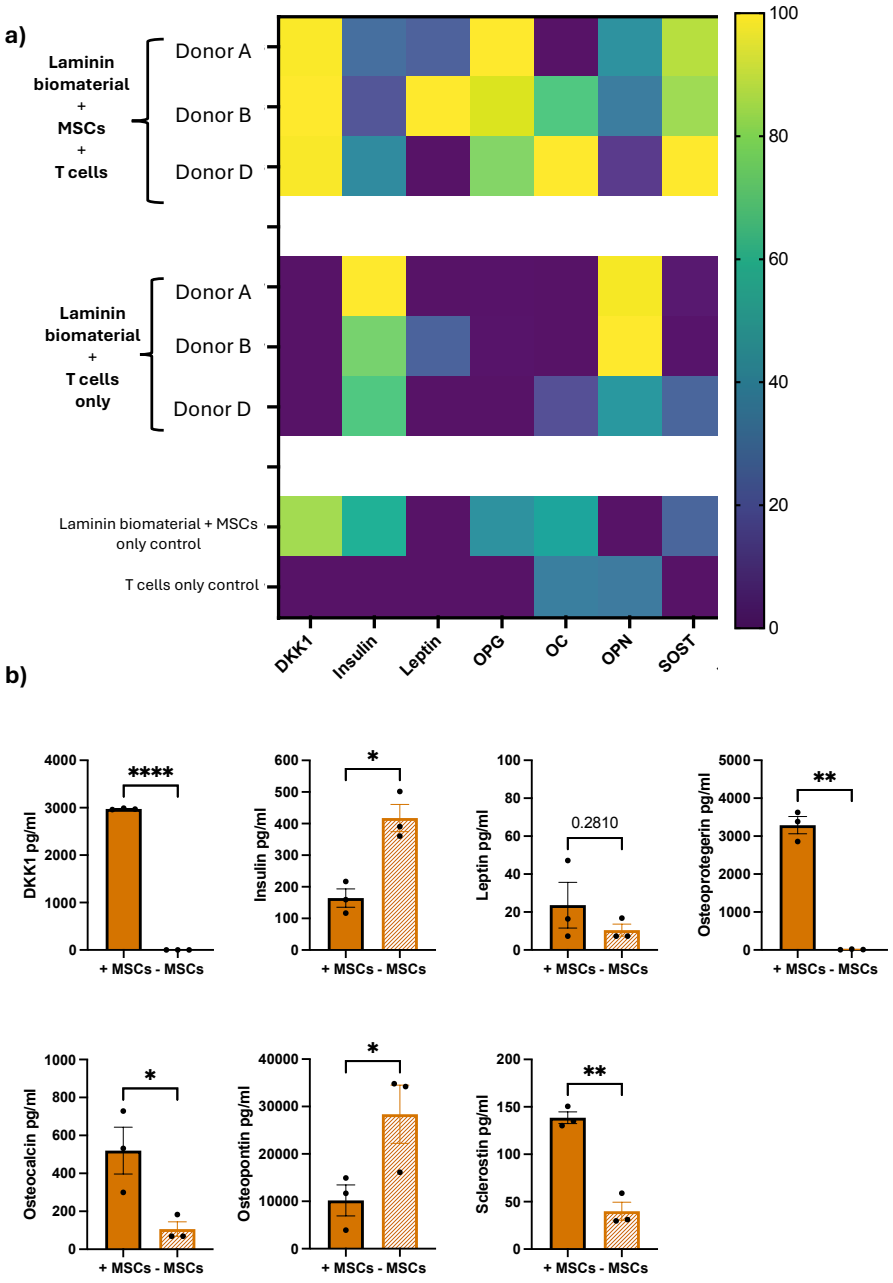

Figure 5-30: a) Heatmap comparing the cytokine profile of the culture supernatants following 3 days of co-culture of activated T cells and 3 day undifferentiated MSCs cultured in the presence of laminin biomaterials with T cells cultured for 3 days in the presence of laminin acellular biomaterials. Control supernatants are from MSC biomaterial only and T cell only supernatant shown. 7 bone analytes shown. Yellow represents the highest percentage expression and dark blue the lowest. Crosses represent missing data values. All data shown has been normalised with 0% representing the lowest value in the data set and 100% representing the highest value. When values were below the lowest detectable range of the standard curve, the value used was the minimal detected concentration per manufacturer's published guidance. b) Individual analyte comparisons. Graphs represent individual paired T tests between MSC laminin biomaterials and no cell controls at the early D3 timepoint. Bars represent the average of 3 biological donors and each data point is the mean of two technical replicates. Error bars represent the standard error of the mean. Data were analysed using paired T tests. P values = *p<0.05, **p<0.01, ***p<0.001, ****p<0.0001.

5.3.1.11 D28 Fibronectin osteoblast biomaterials generate significant Th1, Th17 and activation responses

At the D28 timepoint, the heat maps for immune analytes in the fibronectin osteoblast and T cell co-culture condition appear globally higher than in the matched no osteoblast, T cell biomaterial control [Figure 5-30]. This is notably marked when viewed in contrast to the D3 timepoint [Figure 5-15].

Overall, significant increases were found in more analytes following a comparison of the supernatants from osteoblast (+Obs) T cell co-culture and the no osteoblast (-Obs) T cell only culture at this time point compared to the D3 MSC time point [Figure 5-31]. Within Th1-associated cytokines, significant increases were found in LT-α, IFNα, IFNβ, IFNγ, IL-12(p40), IL-18, IL-27, CXCL10, CXCL11, CXCL16, CCL2, CCL7, CX3CL1 and macrophage colony-stimulating factor (M-CSF) [Figure 5-32]. For Th2 associated cytokines, significant increases were found in IL-4, IL-9 and eotaxin as with the D3 timepoint results for fibronectin in the co-cultures compared to cultures without osteoblasts [Figure 5-33]. Additionally, there were significant increases in IL-34, IL-33 and CCL17 in the osteoblast and T cell co-cultures compared to cultures in the absence of the osteoblasts.

As with the Th1 response, there was more evidence of a Th17 response at the later D28 osteoblast timepoint compared to the D3 timepoint. There were significant increases in IL-6 and CXCL1, as at D3, as well as IL-17E, IL-21, IL-22 and CXCL6 in comparison to the no osteoblast control [Figure 5-34]. Furthermore, activation or cytotoxic response associated analytes increased at D28 too, with significantly more sCD40L, sFas, CXCL13, granzyme B and perforin in the co-cultures compared to the T cell-acellular control [Figure 5-36].

Regulatory-associated cytokine IL-10, which had not been significantly raised at D3, was significantly increased in the T cells cultures with osteoblasts compared to cultures without osteoblasts at D28 [Figure 5-35]. Further significant increases between these two groups were found for sCD137, IL-1RA and CCL22.

Growth factors globally increased in the osteoblast and T cell co-culture on the fibronectin biomaterial compared to cultures without osteoblasts. At the early D3 timepoint only IL-2, IL-11 and VEGF-A were significantly increased but by D28, significant increases between T cell cultures with and without osteoblasts were found for M-CSF, IL-3, IL-11, IL-15, epidermal growth factor (EGF), FMS-like tyrosine kinase 3 ligand (FLT3L) and vascular endothelial growth factor A (VEGF-A) [Figure 5-37]. IL-2 was raised but not significantly ($p=0.0605$) in the presence of osteoblasts.

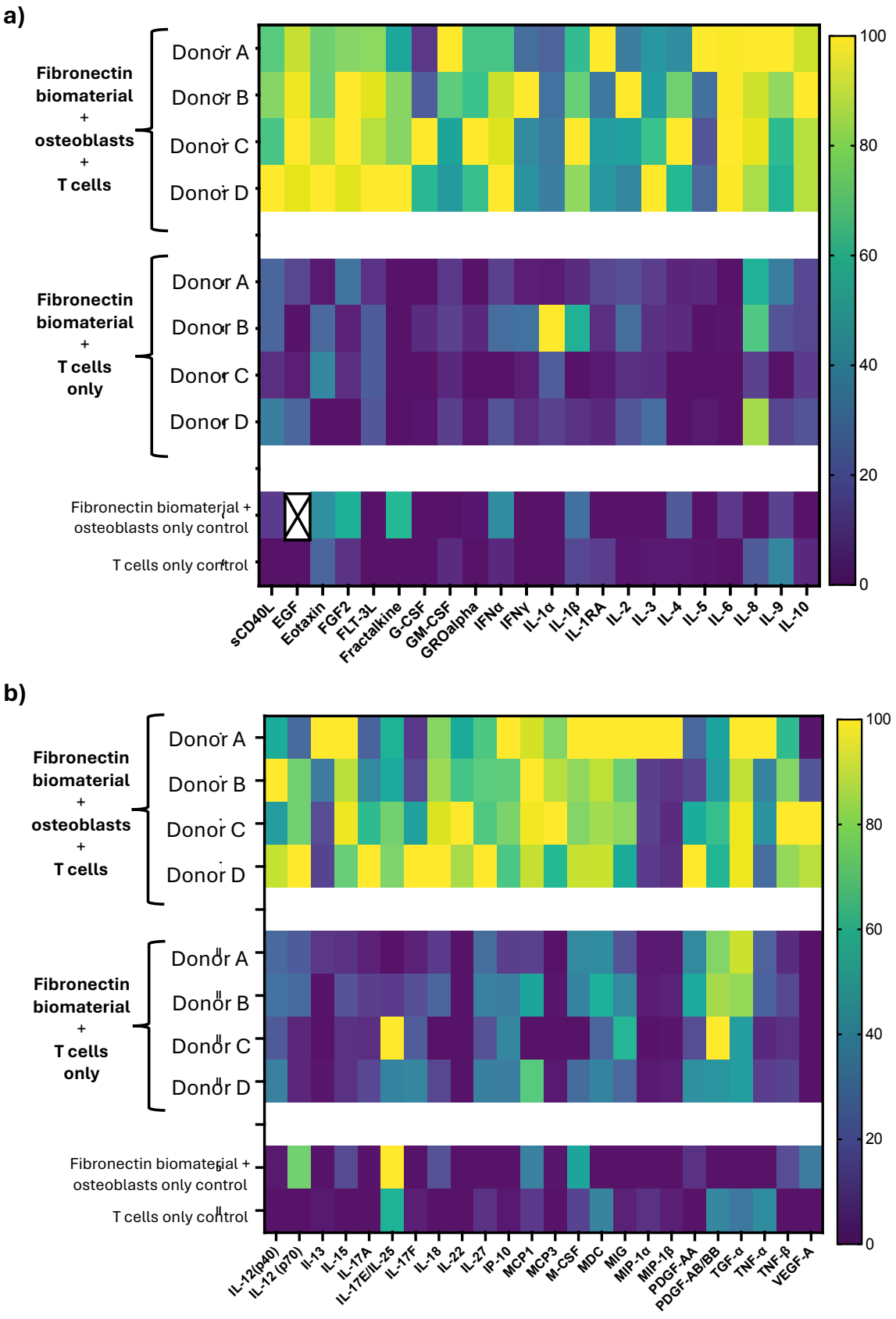
a)
Fibronectin biomaterial + osteoblasts + T cells
Donor A
Donor B
Donor C
Donor D
Fibronectin biomaterial + T cells only
Donor A
Donor B
Donor C
Donor D
Fibronectin biomaterial + osteoblasts only control
T cells only control
sCD40L
EGF
Eotaxin
FGF2
FLT-3L
Fractalkine
G-CSF
GM-CSF
GROalpha
IFNα
IFNγ
IL-1α
IL-1β
IL-1RA
IL-2
IL-3
IL-4
IL-5
IL-6
IL-8
IL-9
IL-10
100
80
60
40
20
0
b)
Fibronectin biomaterial + osteoblasts + T cells
Donor A
Donor B
Donor C
Donor D
Fibronectin biomaterial + T cells only
Donor A
Donor B
Donor C
Donor D
Fibronectin biomaterial + osteoblasts only control
T cells only control
IL-12(p40)
IL-12 (p70)
Il-13
IL-15
IL-17A
IL-17E/IL-25
IL-17F
IL-18
IL-22
IL-27
IP-10
MCP1
MCP3
M-CSF
MDC
MIG
MIP-1α
MIP-1β
PDGF-AA
PDGF-AB/BB
TGF-α
TNF-α
TNF-β
VEGF-A
100
80
60
40
20
0

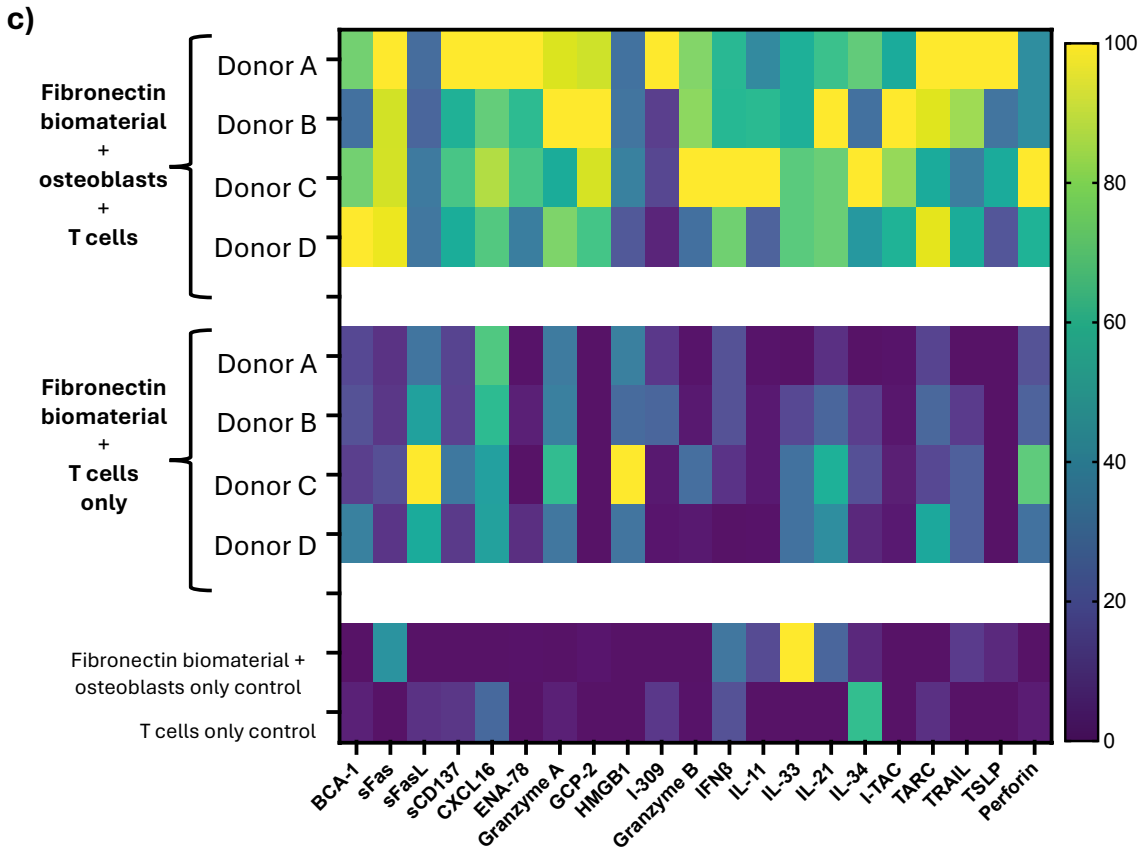

Figure 5-31: Heatmaps comparing the cytokine profile of the culture supernatants following 3 days of co-culture of activated T cells and 28 day differentiated osteoblasts cultured in the presence of fibronectin biomaterials with T cells cultured for 3 days in the presence of fibronectin acellular biomaterials. Control supernatants are from osteoblast biomaterials only and T cell only supernatant shown. The heatmap analytes are grouped based on the individual Luminex assays (a) 23 analytes shown (b) 24 analytes shown (c) 21 analytes shown. Yellow represents the highest percentage expression and dark blue the lowest. Crosses represent missing data values. All data shown has been normalised with 0% representing the lowest value in the data set and 100% representing the highest value. When values were below the lowest detectable range of the standard curve, the value used was the minimal detected concentration per manufacturer's published guidance.

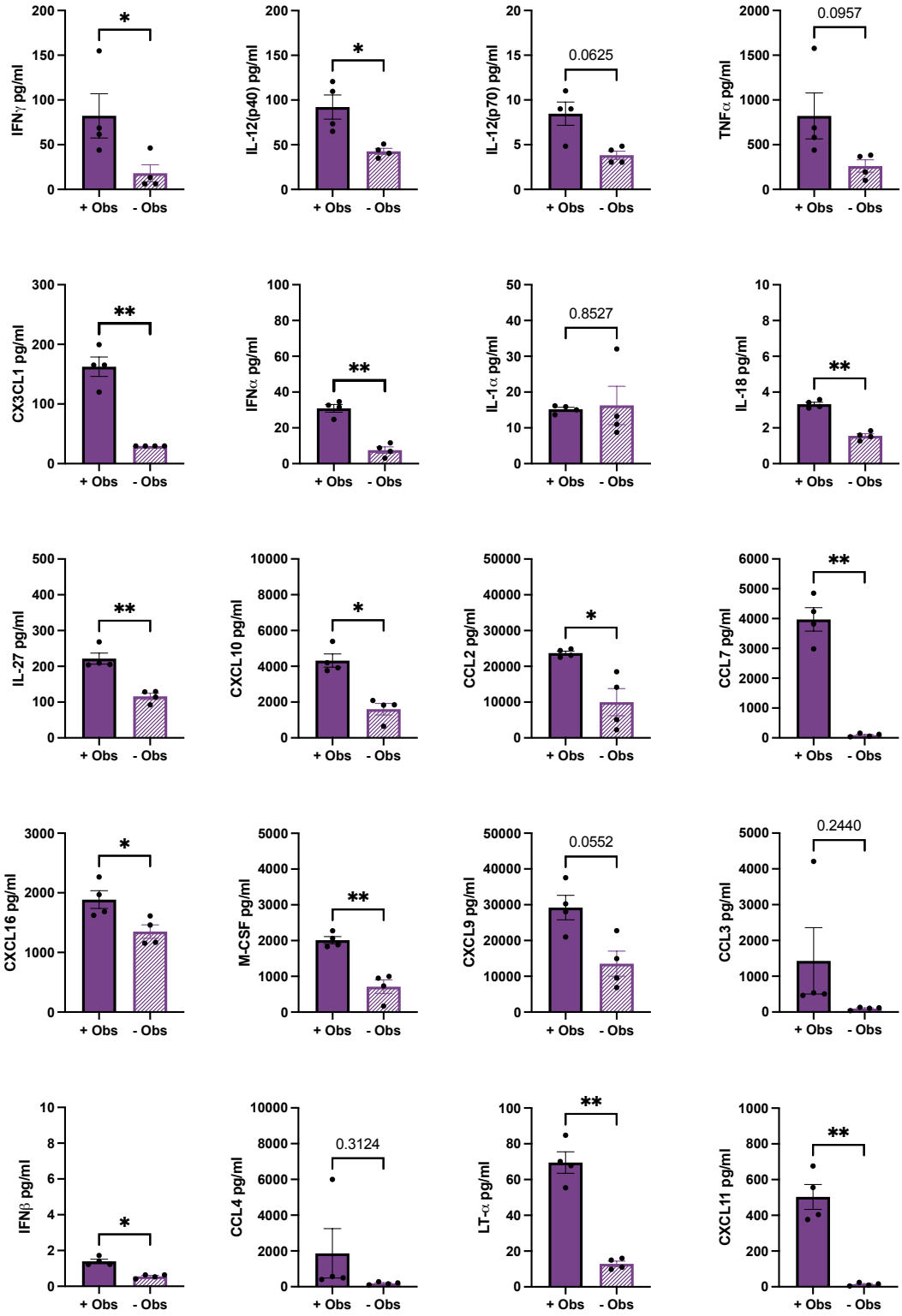

Figure 5-32: Many cytokines classified as Th1 response-associated increased in 3 days co-culture with D28 osteoblast fibronectin biomaterials. Graphs represent individual paired T tests between Osteoblast (+Obs) fibronectin biomaterials and no cell (-Obs) controls at the late D28 osteoblast timepoint. Bars represent the average of 4 biological donors and each data point is the mean of two technical replicates. Error bars represent the standard error of the mean. Data were analysed using paired T tests. P values = *p<0.05, **p<0.01, ***p<0.001, ****p<0.0001.

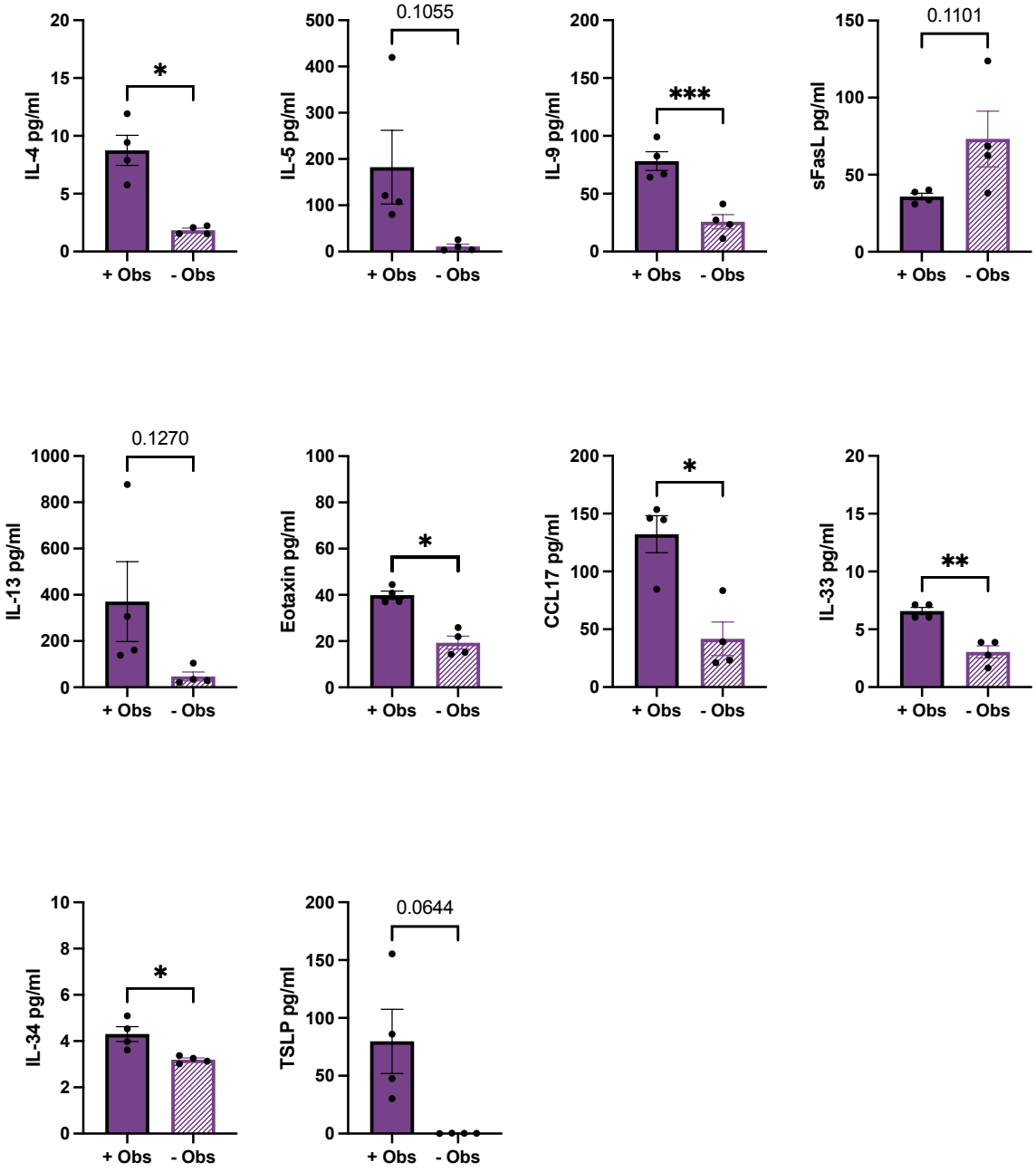

Figure 5-33: Few cytokines classified as Th2 response-associated increased in 3 days co-culture with D28 osteoblast fibronectin biomaterials. Graphs represent individual paired T tests between Osteoblast (+Obs) fibronectin biomaterials and no cell (-Obs) controls at the late D28 osteoblast timepoint. Bars represent the average of 4 biological donors and each data point is the mean of two technical replicates. Error bars represent the standard error of the mean. Data were analysed using paired T tests. P values = *p<0.05, **p<0.01, ***p<0.001, ****p<0.0001.

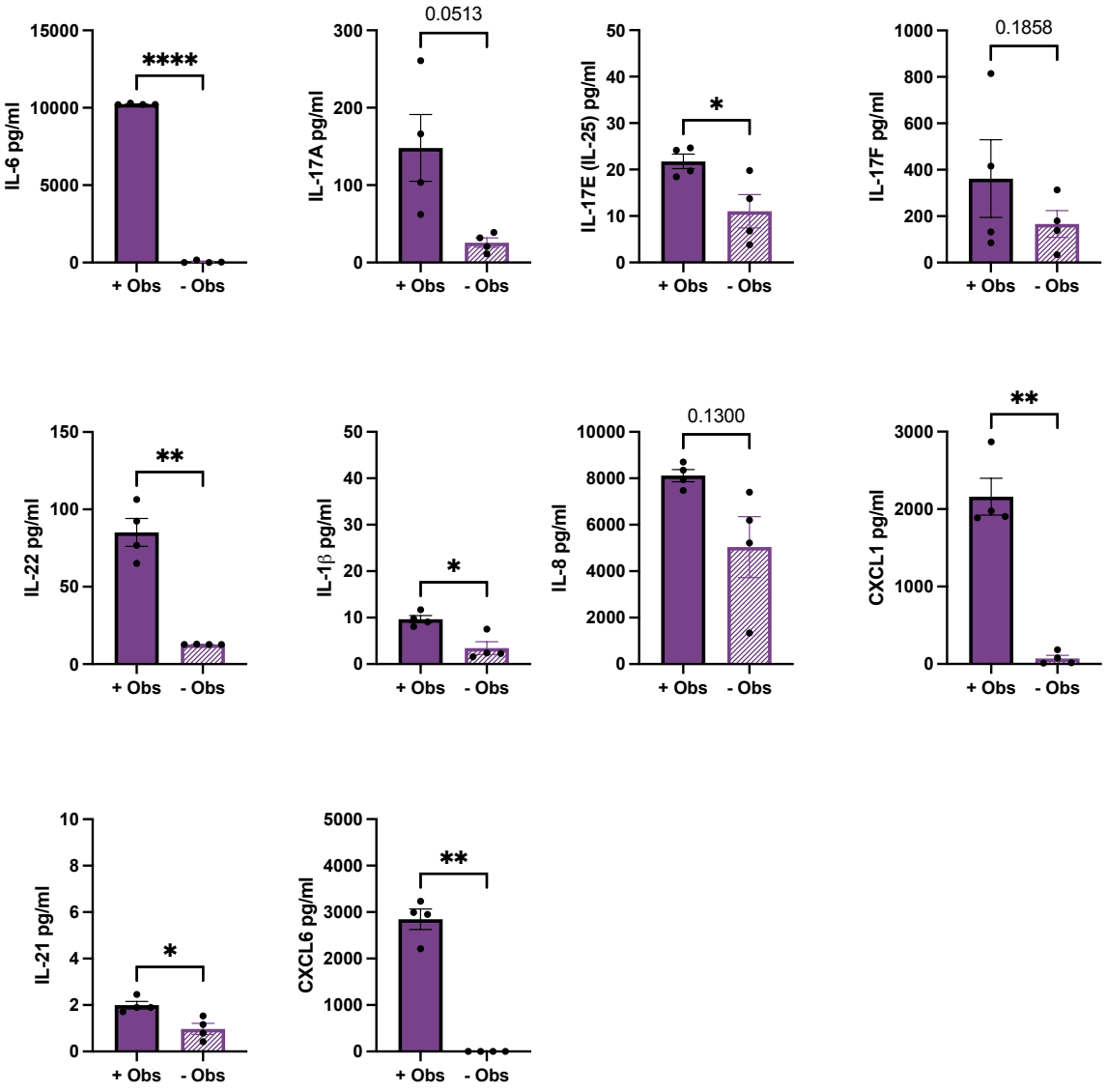

Figure 5-34: Many cytokines classified as Th17 response-associated increased in 3 days co-culture with D28 osteoblast fibronectin biomaterials. Graphs represent individual paired T tests between Osteoblast (+Obs) fibronectin biomaterials and no cell (-Obs) controls at the late D28 osteoblast timepoint. Bars represent the average of 4 biological donors and each data point is the mean of two technical replicates. Error bars represent the standard error of the mean. Data were analysed using paired T tests. P values = *p<0.05, **p<0.01, ***p<0.001, ****p<0.0001.

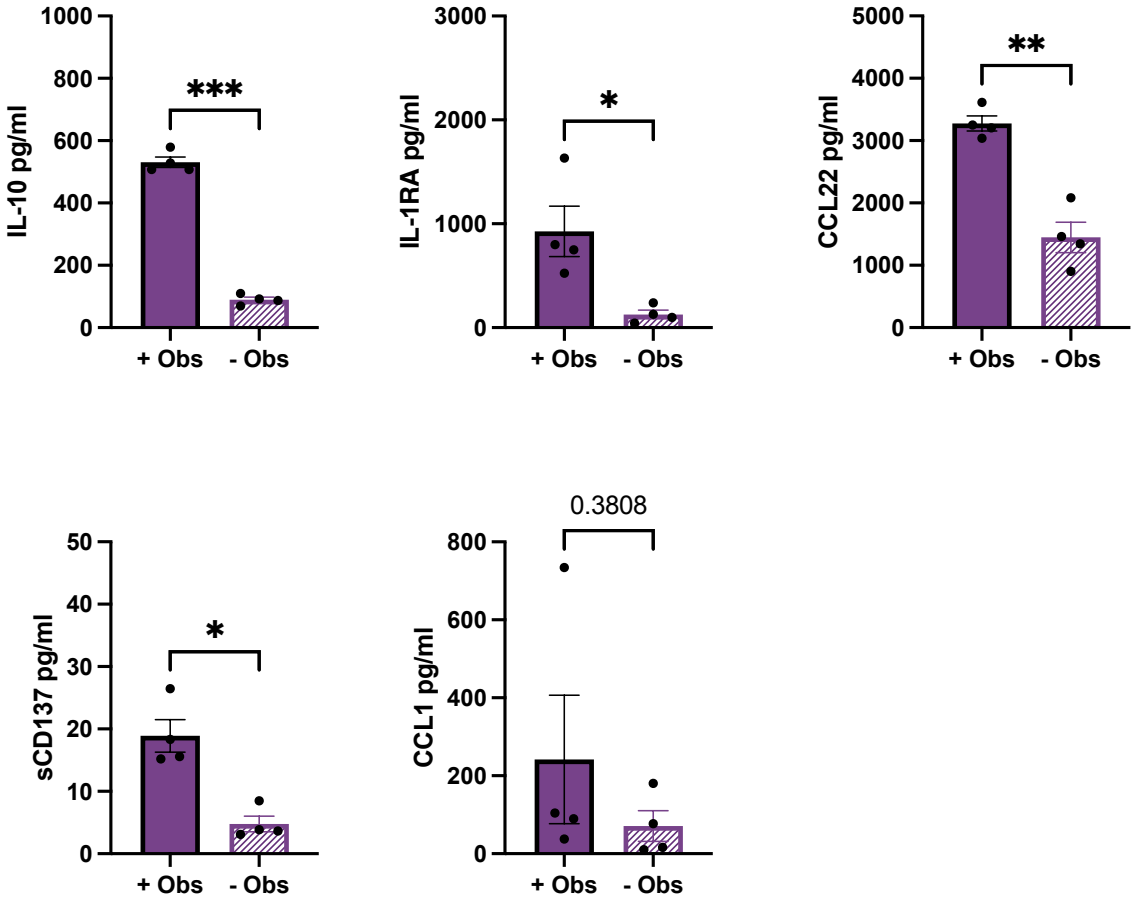

Figure 5-35: Many cytokines classified as regulatory increased in 3 days co-culture with D28 osteoblast fibronectin biomaterials. Graphs represent individual paired T tests between Osteoblast (+Obs) fibronectin biomaterials and no cell (-Obs) controls at the late D28 osteoblast timepoint. Bars represent the average of 4 biological donors and each data point is the mean of two technical replicates. Error bars represent the standard error of the mean. Data were analysed using paired T tests. P values = *p<0.05, **p<0.01, ***p<0.001, ****p<0.0001.

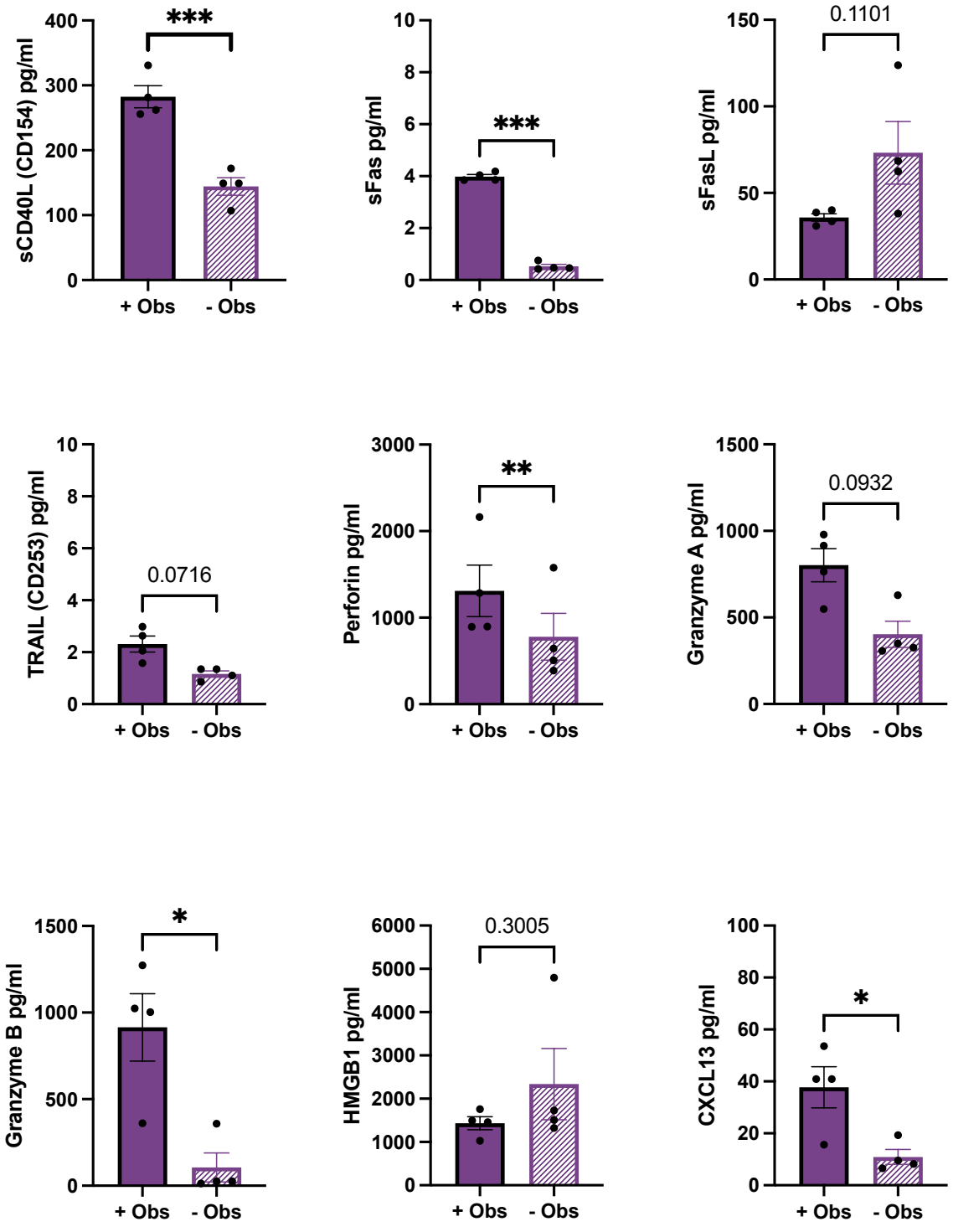

Figure 5-36: Many cytokines classified as cytotoxic or activation-associated increased in 3 days co-culture with D28 osteoblast fibronectin biomaterials. Graphs represent individual paired T tests between Osteoblast (+Obs) fibronectin biomaterials and no cell (-Obs) controls at the late D28 osteoblast timepoint. Bars represent the average of 4 biological donors and each data point is the mean of two technical replicates. Error bars represent the standard error of the mean. Data were analysed using paired T tests. P values = *p<0.05, **p<0.01, ***p<0.001, ****p<0.0001.

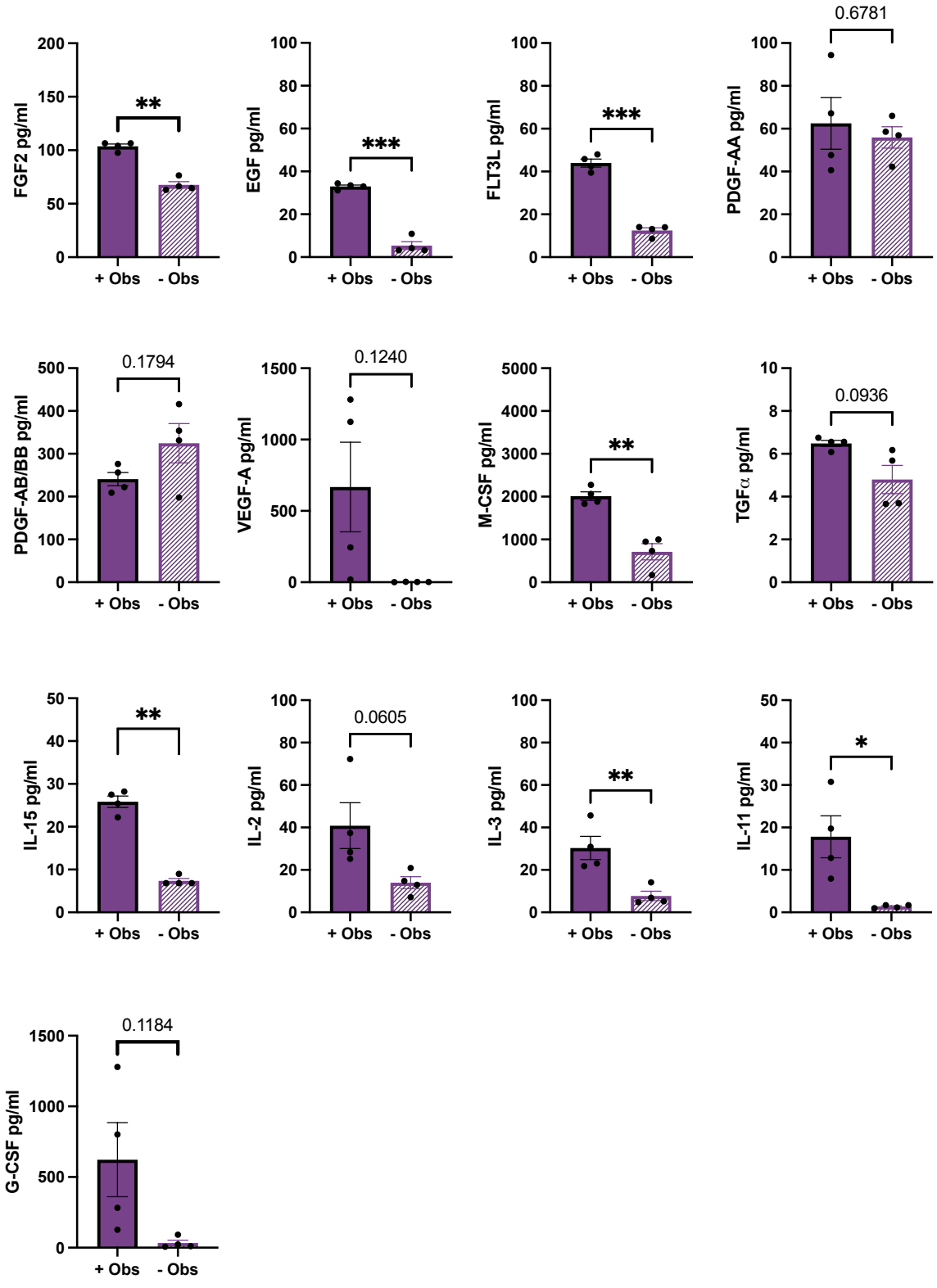

Figure 5-37: Many growth factors increased in 3 days co-culture with D28 osteoblast fibronectin biomaterials. Graphs represent individual paired T tests between Osteoblast (+Obs) fibronectin biomaterials and no cell (-Obs) controls at the late D28 osteoblast timepoint. Bars represent the average of 4 biological donors and each data point is the mean of two technical replicates. Error bars represent the standard error of the mean. Data were analysed using paired T tests. P values = *p<0.05, **p<0.01, ***p<0.001, ****p<0.0001.

5.3.1.12 D28 Laminin osteoblast biomaterials provoked a predominantly Th17 and activation response in 3 days co-culture with T cells

As found in the cultures with fibronectin biomaterials, there appeared to be more inflammatory cytokines found in the T cell with osteoblasts co-cultures compared to T cell only no osteoblast controls [Figure 5-38].

Th1-response associated cytokines that increased significantly in the osteoblast co-culture compared to the T cell cultures with acellular biomaterials on both biomaterial types were LT-α, CCL2, CCL7, CXCL10, CXCL11, M-CSF and IL-27 [Figure 5-39]. IFNγ was significantly increased for fibronectin osteoblasts in co-culture with T cells at D28 whereas it was not significantly increased for laminin osteoblast co-cultures, through trended up. Further significant increases were found for IL-12(p70) and CXCL9 (formerly monokine induced gamma, MIG).

As with fibronectin at this timepoint, Th2-response associated cytokines IL-4, IL-33 and CCL17 increased significantly in the osteoblast T cell co-culture condition compared to the T cells cultured with acellular biomaterial [Figure 5-40]. TSLP expression was also significantly raised in the laminin osteoblast and T cell co-culture compared to acellular controls, this is similar to fibronectin condition though the increase was nonsignificant ($p=0.0644$).

Significant increases were found for several Th17-associated analytes in the co-cultures compared to the T cell-acellular biomaterial controls. These differences largely mirrored those found in the fibronectin D28 co-culture results [Figure 5-41]. More IL-6 and CXCL6 were found in the presence of osteoblasts at both D3 and D28 compared to acellular controls. At D28, increased levels of IL-17A, IL-17E,

IL8, IL-22, IL-1β and CXCL1 were also found in the co-cultures with osteoblasts versus acellular controls.

Of the analytes classed as regulatory, more IL-10 and sCD137 were found in the T cell: osteoblast co-cultures compared to supernatants from T cells cultured with acellular biomaterial both at D3 and D28 [Figure 5-42]. Additionally, CCL22 was increased in the osteoblast co-culture supernatants at D28.

Similar to the fibronectin data, there were many more analytes associated with cytotoxicity and activation responses by D28 in laminin osteoblast co-cultures with T cells compared to D3 [Figure 5-43]. Significant increases were found for sFas, HMGB1, sCD40L and Granzyme B, in the T cell: osteoblast co-cultures compared to T cells cultured with acellular biomaterial at both D3 and D28. At D28, Granzyme A, perforin and CXCL13 were also increased. HMGB1 is an activation signal associated with classical proinflammatory responses and acts as a signalling mediator of ongoing damage (364). It was significantly increased in the no MSC condition for both biomaterial types and in the D28 no osteoblast laminin condition, implying greater T cell damage in these conditions.

More growth factors were increased in the D28 T cell: osteoblast co-culture conditions compared to acellular controls. Increases were found in FGF2, EGF, FLT3L, M-CSF, IL-3, IL-11, and IL-15 in co-cultures of T cells and osteoblasts in comparison to T cells cultured with acellular biomaterial. This mirrors the data with fibronectin biomaterials [Figure 5-44]. In contrast, platelet-derived growth factor AA (PDGF-AA) was only significantly increased in the presence of osteoblasts versus acellular controls in the laminin and not in the fibronectin biomaterials.

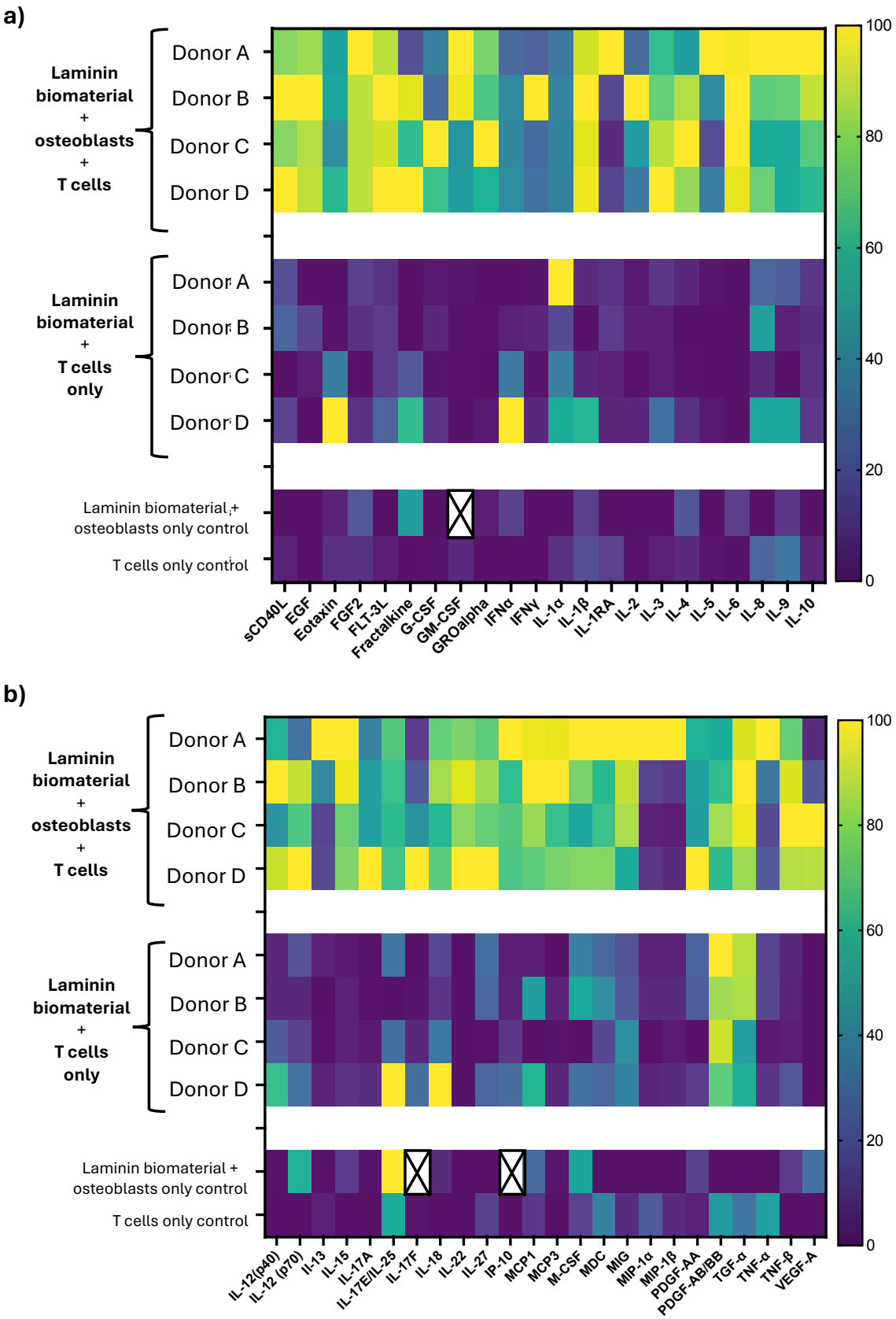
a)
Laminin biomaterial + osteoblasts + T cells
Donor A
Donor B
Donor C
Donor D
Laminin biomaterial + T cells only
Donor A
Donor B
Donor C
Donor D
Laminin biomaterial + osteoblasts only control
T cells only control
sCD40L
EGF
Eotaxin
FGF2
FLT-3L
Fractalkine
G-CSF
GM-CSF
GROalpha
IFNα
IFNγ
IL-1α
IL-1β
IL-1RA
IL-2
IL-3
IL-4
IL-5
IL-6
IL-8
IL-9
IL-10
100
80
60
40
20
0
b)
Laminin biomaterial + osteoblasts + T cells
Donor A
Donor B
Donor C
Donor D
Laminin biomaterial + T cells only
Donor A
Donor B
Donor C
Donor D
Laminin biomaterial + osteoblasts only control
T cells only control
IL-12(p40)
IL-12 (p70)
IL-13
IL-15
IL-17A
IL-17E/IL-25
IL-17F
IL-18
IL-22
IL-27
IP-10
MCP1
MCP3
M-CSF
MDC
MIG
MIP-1α
MIP-1β
PDGF-AA
PDGF-AB/BB
TGF-α
TNF-α
TNF-β
VEGF-A
100
80
60
40
20
0

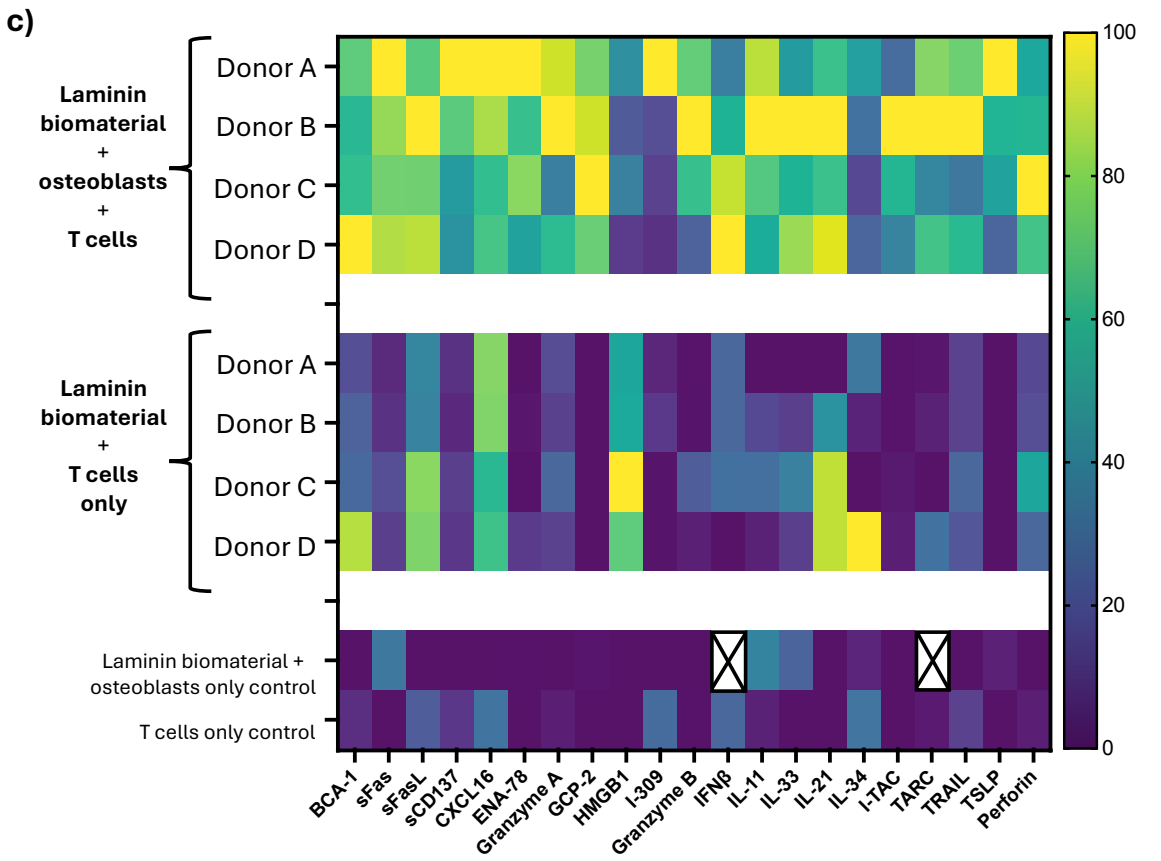

Figure 5-38: Heatmaps comparing the cytokine profile of the culture supernatants following 3 days of co-culture of activated T cells and 28 day differentiated osteoblasts cultured in the presence of laminin biomaterials with T cells cultured for 3 days in the presence of laminin acellular biomaterials. Control supernatants are from osteoblast biomaterials only and T cell only supernatant shown. The heatmap analytes are grouped based on the individual Luminex assays (a) 23 analytes shown (b) 24 analytes shown (c) 21 analytes shown. Yellow represents the highest percentage expression and dark blue the lowest. Crosses represent missing data values. All data shown has been normalised with 0% representing the lowest value in the data set and 100% representing the highest value. When values were below the lowest detectable range of the standard curve, the value used was the minimal detected concentration per manufacturer's published guidance.

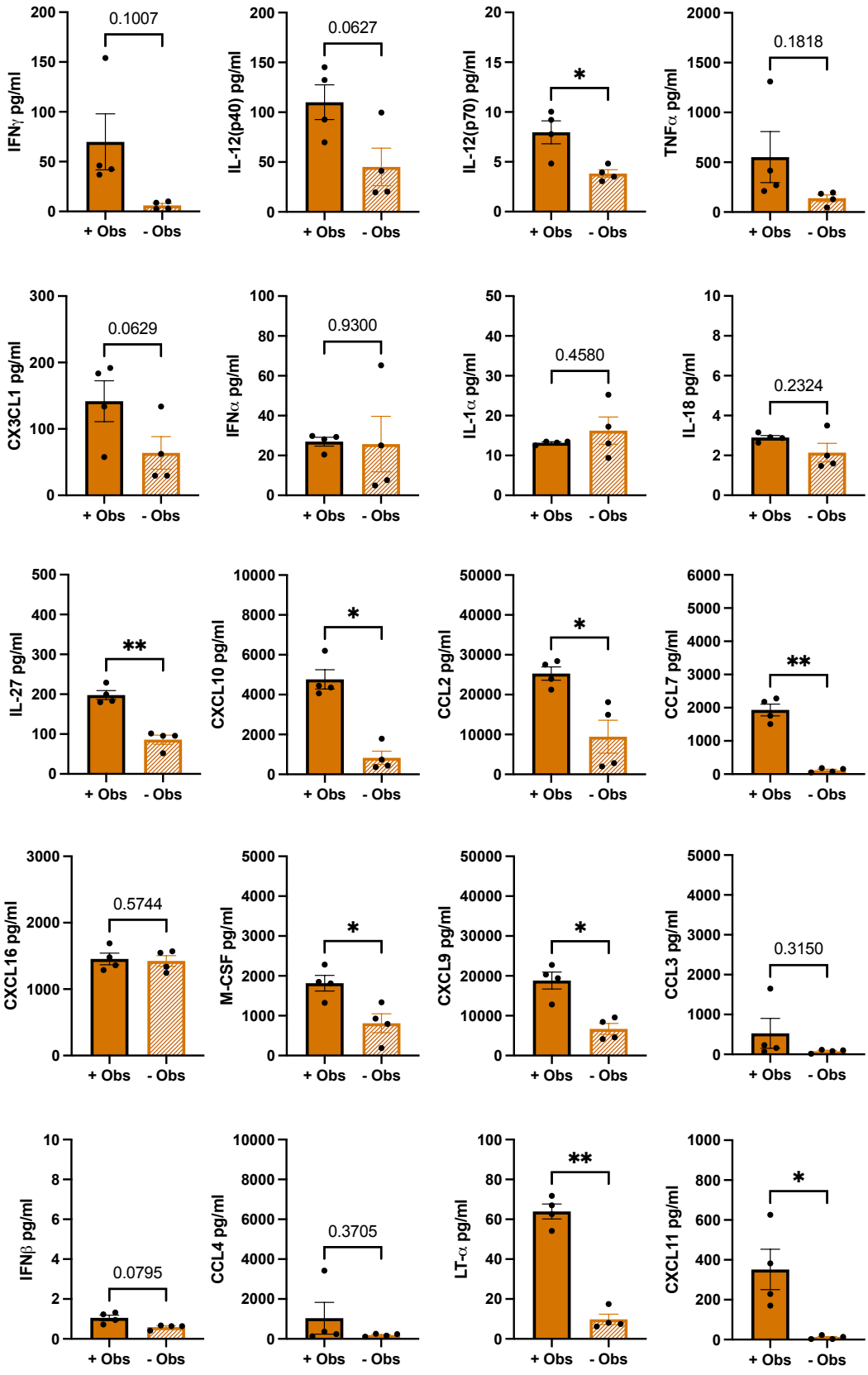

Figure 5-39: Many cytokines classified as Th1 response-associated increased in 3 days co-culture with D28 osteoblast laminin biomaterials. Graphs represent individual paired T tests between Osteoblast (+Obs) laminin biomaterials and no cell (-Obs) controls at the late D28 osteoblast timepoint. Bars represent the average of 4 biological donors and each data point is the mean of two technical replicates. Error bars represent the standard error of the mean. Data were analysed using paired T tests. P values = *p<0.05, **p<0.01, ***p<0.001, ****p<0.0001.

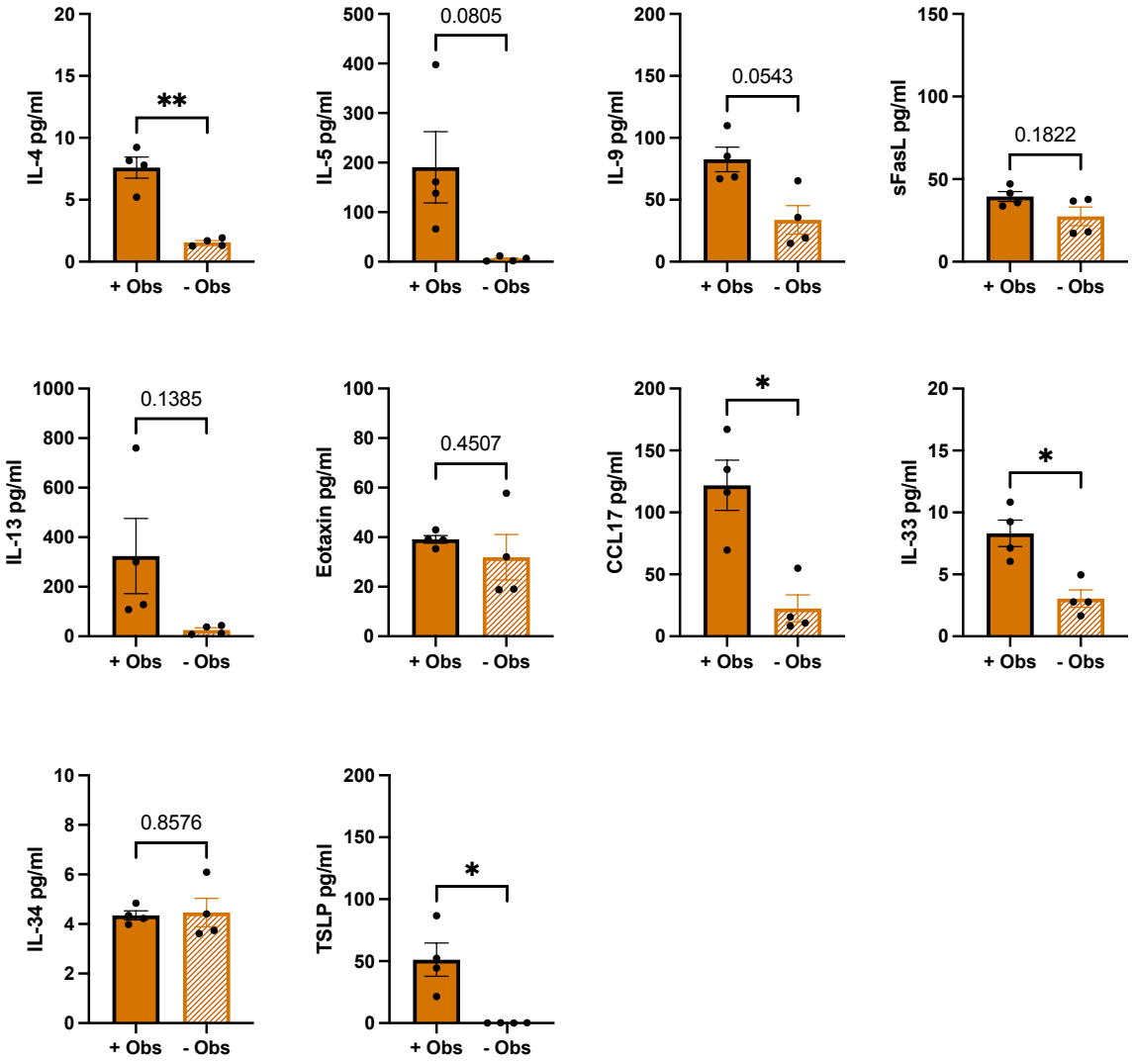

Figure 5-40: Few cytokines classified as Th2 response-associated increased in 3 days co-culture with D28 osteoblast laminin biomaterials. Graphs represent individual paired T tests between Osteoblast (+Obs) laminin biomaterials and no cell (-Obs) controls at the late D28 osteoblast timepoint. Bars represent the average of 4 biological donors and each data point is the mean of two technical replicates. Error bars represent the standard error of the mean. Data were analysed using paired T tests. P values = *p<0.05, **p<0.01, ***p<0.001, ****p<0.0001.

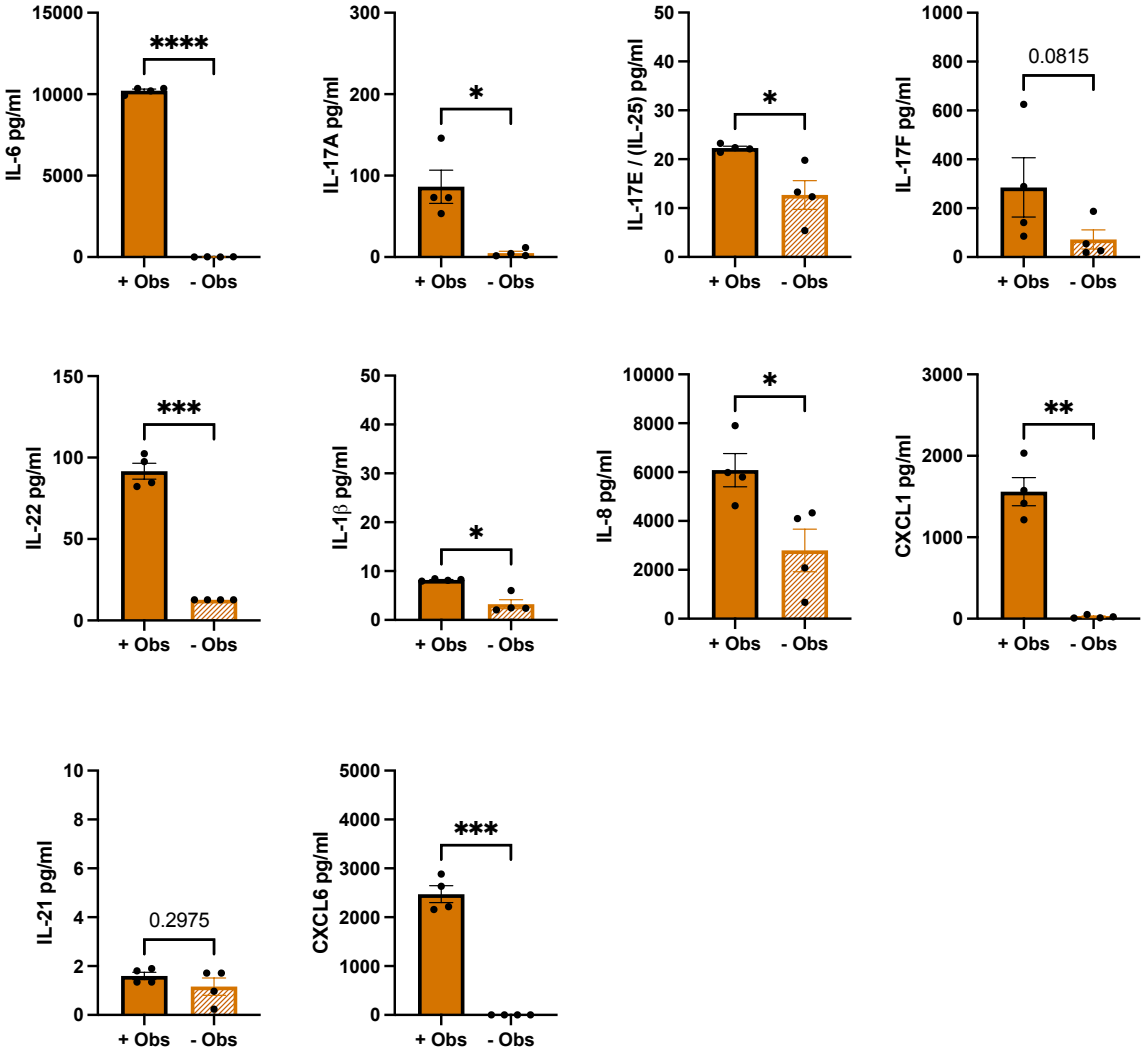

Figure 5-41: The majority of cytokines classified as Th17 response-associated increased in 3 days co-culture with D28 osteoblast laminin biomaterials. Graphs represent individual paired T tests between Osteoblast (+Obs) laminin biomaterials and no cell (-Obs) controls at the late D28 osteoblast timepoint. Bars represent the average of 4 biological donors and each data point is the mean of two technical replicates. Error bars represent the standard error of the mean. Data were analysed using paired T tests. P values = *p<0.05, **p<0.01, ***p<0.001, ****p<0.0001.

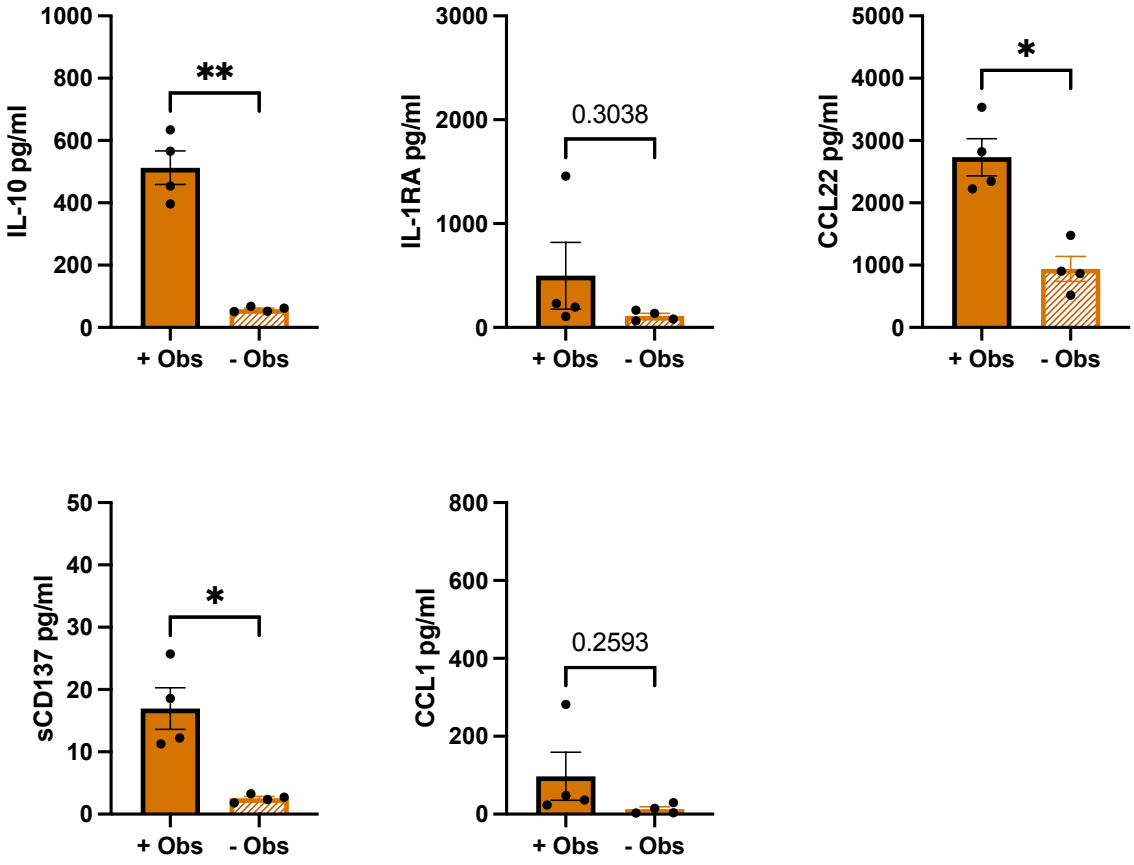

Figure 5-42: Few cytokines classified as regulatory response-associated increased in 3 days co-culture with D28 osteoblast laminin biomaterials. Graphs represent individual paired T tests between Osteoblast (+Obs) laminin biomaterials and no cell (-Obs) controls at the late D28 osteoblast timepoint. Bars represent the average of 4 biological donors and each data point is the mean of two technical replicates. Error bars represent the standard error of the mean. Data were analysed using paired T tests. P values = *p<0.05, **p<0.01, ***p<0.001, ****p<0.0001.

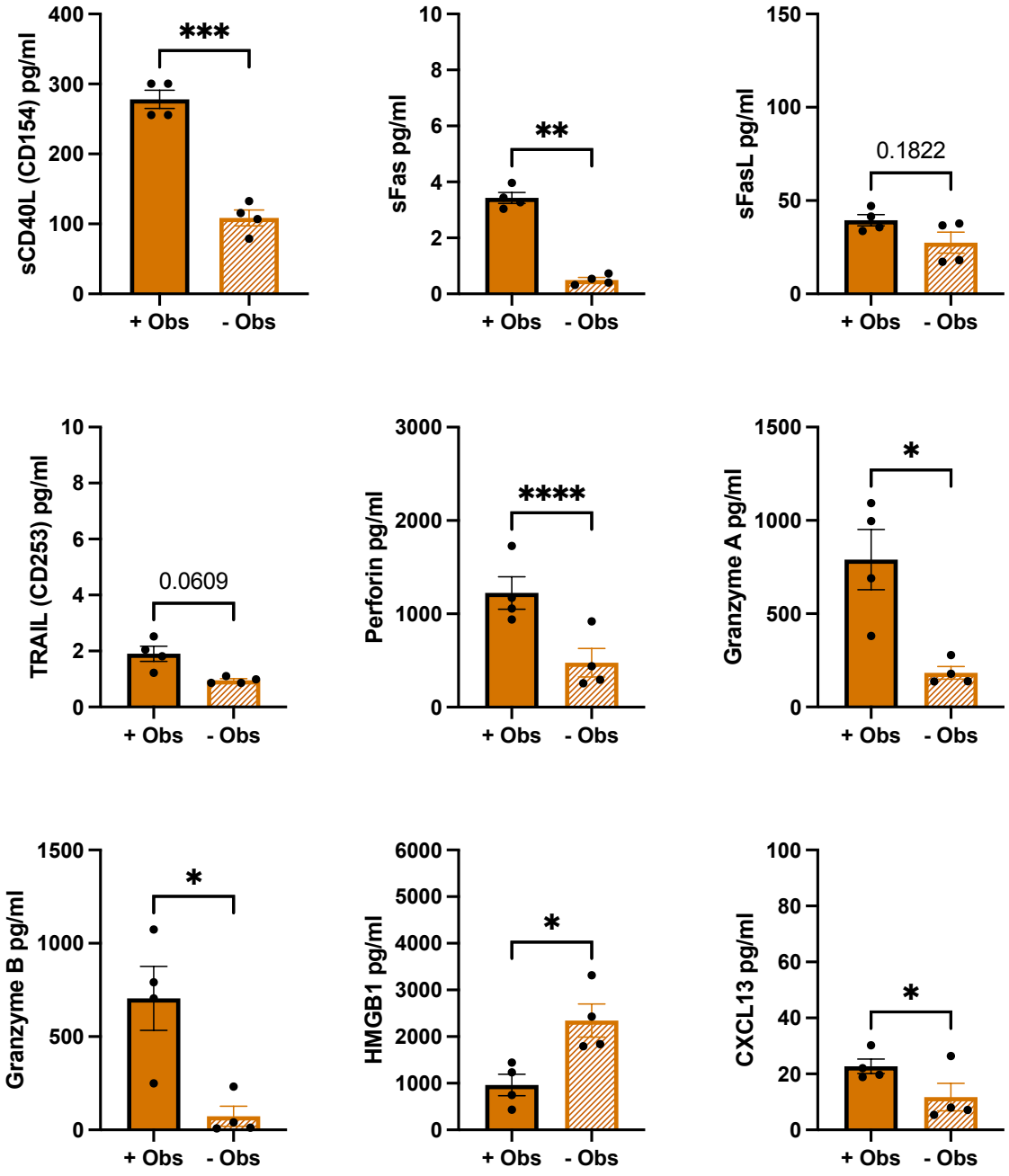

Figure 5-43: Many cytokines classified as cytotoxic or activation-associated increased in 3 days co-culture with D28 osteoblast laminin biomaterials. Graphs represent individual paired T tests between Osteoblast laminin biomaterials and no cell controls at the late D28 osteoblast timepoint. Bars represent the average of 4 biological donors and each data point is the mean of two technical replicates. Error bars represent the standard error of the mean. Data were analysed using paired T tests. P values = *p<0.05, **p<0.01, ***p<0.001, ****p<0.0001.

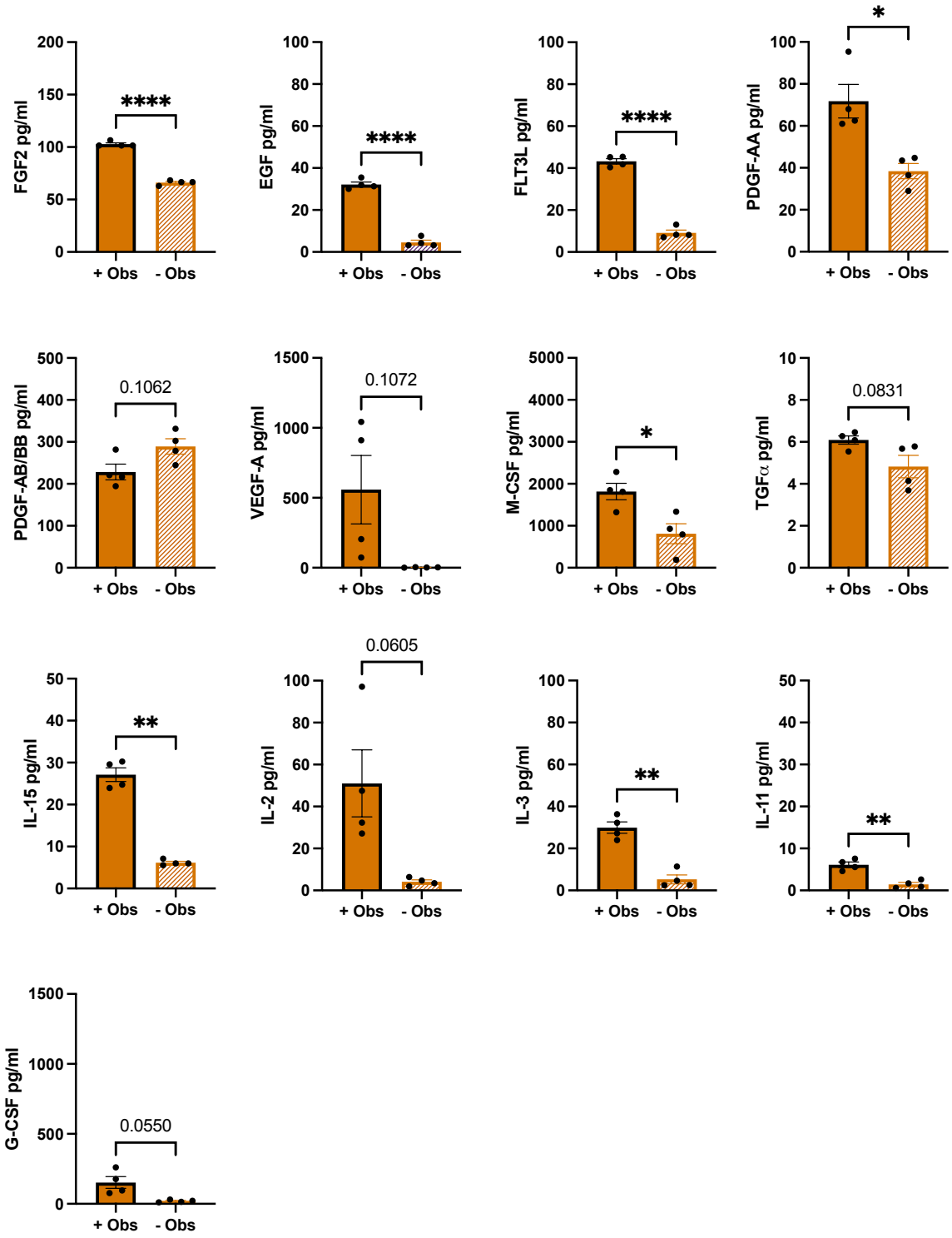

Figure 5-44: A number of growth factors increased in 3 days co-culture with D28 laminin osteoblast biomaterials. Graphs represent individual paired T tests between Osteoblast (+Obs) laminin biomaterials and no cell (-Obs) controls at the late D28 osteoblast timepoint. Bars represent the average of 4 biological donors and each data point is the mean of two technical replicates. Error bars represent the standard error of the mean. Data were analysed using paired T tests. P values = *p<0.05, **p<0.01, ***p<0.001, ****p<0.0001.

5.3.1.13 D28 osteoblast biomaterials produce several osteogenic analytes to aid osteogenesis

The analyte data from the Luminex bone analysis showed increasing evidence for osteogenic differentiation within the co-cultures [Figure 5-45]. As at D3, significant increases were seen in DKK1, OPG and SOST in cultures with T cells and osteoblasts in comparison to T cell-acellular fibronectin biomaterial cultures. The pg/ml levels of these were consistent with those found at D3 [Figure 5-29]. At D28 however, significant increases were also found in OCN and OPN in the osteoblast+ cultures, which supports the immunofluorescence data at this same timepoint, that osteogenesis had occurred. Finally, insulin was significantly higher in the osteoblast and T cell co-culture compared with the T cells cultures with the acellular biomaterial.

Data are shown in a heatmap for D28 laminin biomaterials [Figure 5-46]. A comparison of analytes in supernatants from co-cultures of T cells and osteoblasts with T cells cultured with acellular laminin biomaterials, were similar to the results from the D3 timepoint. DKK1, OPG, leptin and SOST were increased in the T cells cultures in the presence of osteoblasts. Notably, based on the pg/ml amounts of these analytes, these molecules were not increasing from D3 to D28. In the supernatant from cultures of T cells and acellular laminin biomaterials insulin was increased in the no osteoblast controls. In contrast to the data for the fibronectin biomaterial at D28, no significance was found for OPN in the D28 laminin biomaterials, but OCN was increased significantly, implying less of an osteoblast phenotype in the presence of laminin compared to fibronectin biomaterials.

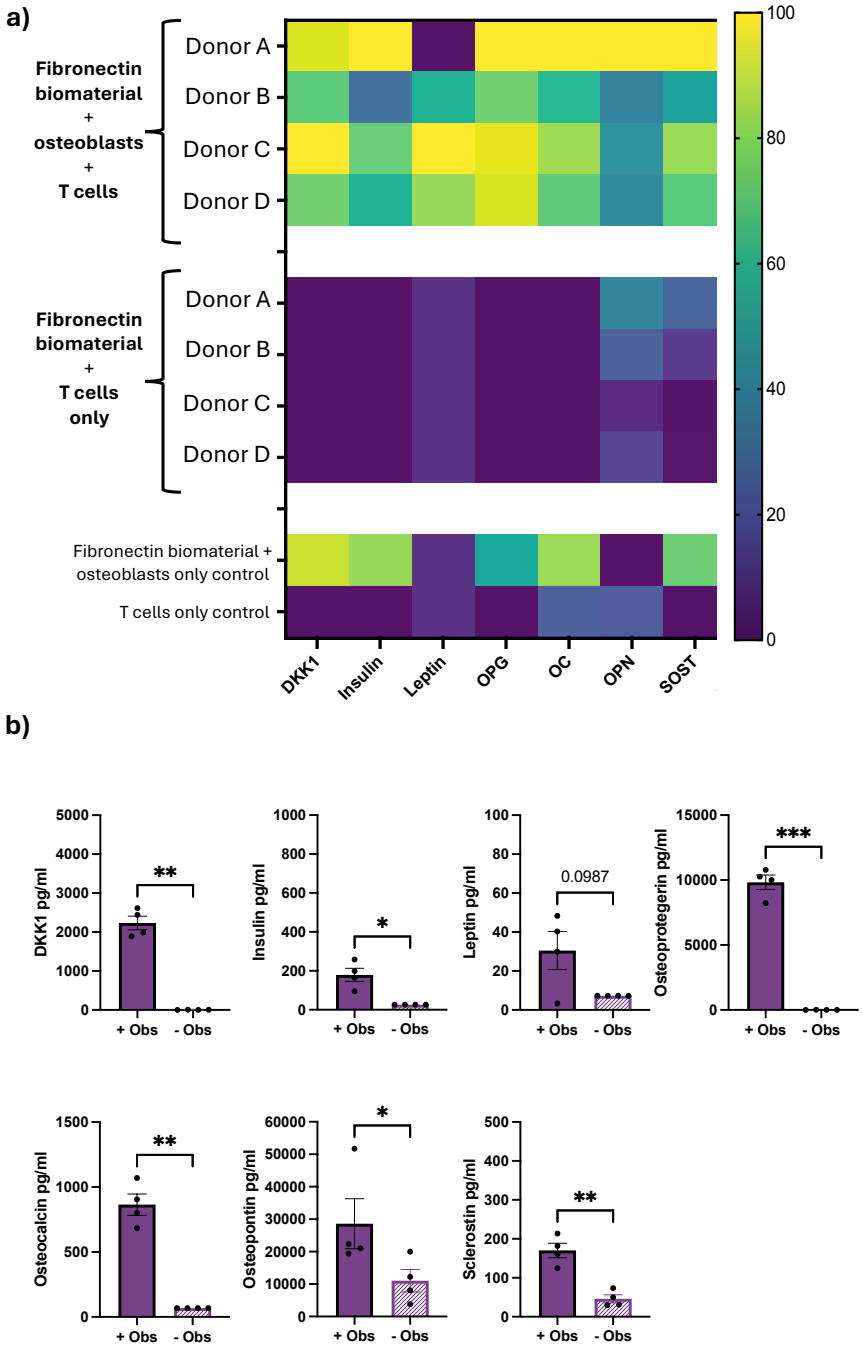

Figure 5-45: a) Heatmaps comparing the cytokine profile of the culture supernatants following 3 days of co-culture of activated T cells and 28 day differentiated osteoblasts cultured in the presence of fibronectin biomaterials with T cells cultured for 3 days in the presence of fibronectin acellular biomaterials. Control supernatants are from osteoblast biomaterial only and T cell only supernatant shown. 7 bone analytes shown. Yellow represents the highest percentage expression and dark blue the lowest. Crosses represent missing data values. All data shown has been normalised with 0% representing the lowest value in the data set and 100% representing the highest value. When values were below the lowest detectable range of the standard curve, the value used was the minimal detected concentration per manufacturer's published guidance. b) Individual analyte comparisons. Graphs represent individual paired T tests between Osteoblast (+Obs) fibronectin biomaterials and no cell (-Obs) controls at the late D28 timepoint. Bars represent the average of 4 biological donors and each data point is the mean of two technical replicates. Data were analysed using paired T tests. P values = *p<0.05, **p<0.01, ***p<0.001, ****p<0.0001.

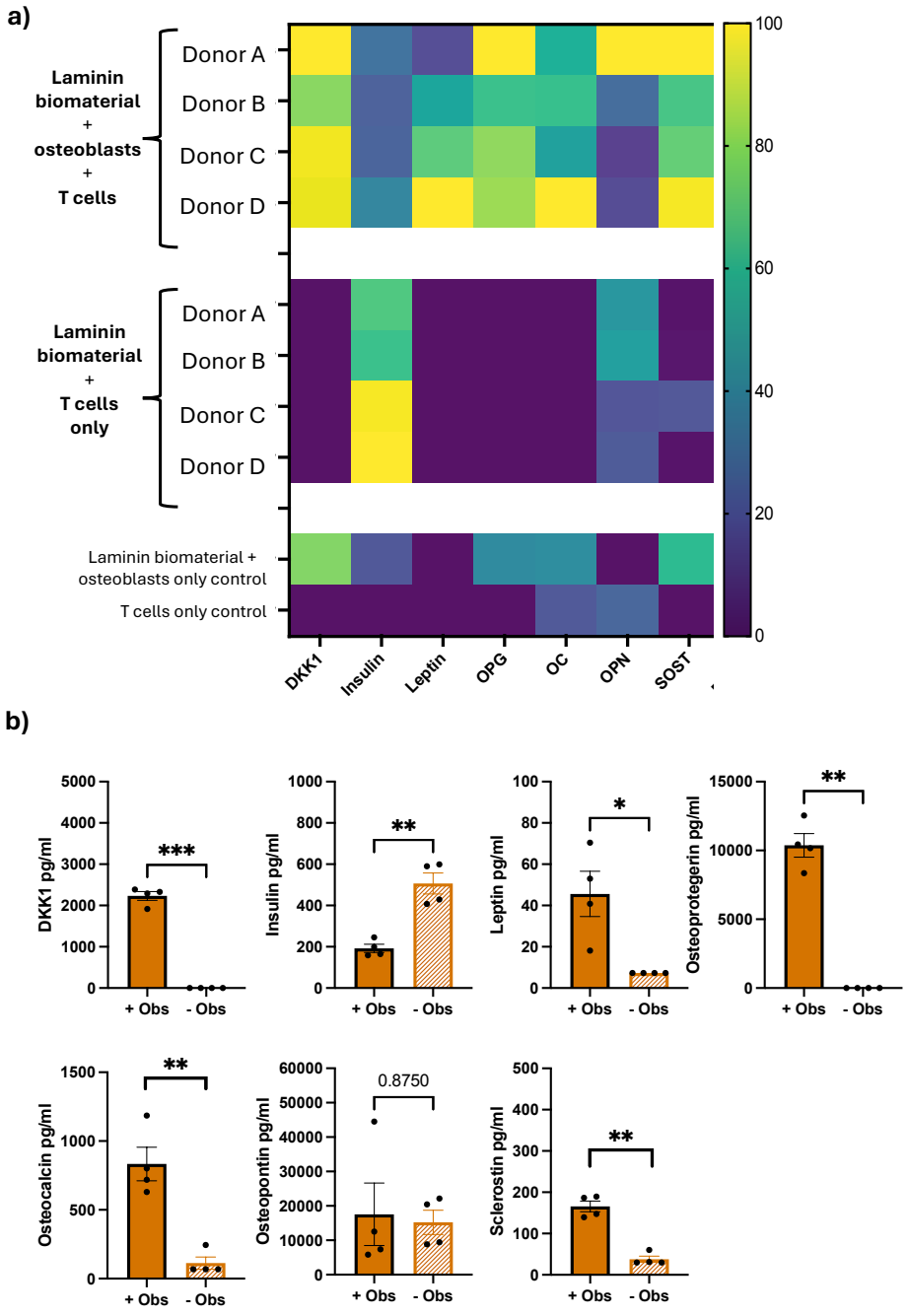

Figure 5-46: a) Heatmaps comparing the cytokine profile of the culture supernatants following 3 days of co-culture of activated T cells and 28 day differentiated osteoblasts cultured in the presence of laminin biomaterials with T cells cultured for 3 days in the presence of laminin acellular biomaterials. Control supernatants are from osteoblast biomaterials only and T cell only supernatant shown. 7 bone analytes shown. Yellow represents the highest percentage expression and dark blue the lowest. Crosses represent missing data values. All data shown has been normalised with 0% representing the lowest value in the data set and 100% representing the highest value. When values were below the lowest detectable range of the standard curve, the value used was the minimal detected concentration per manufacturer's published guidance. b) Individual analyte comparisons. Graphs represent individual paired T tests between Osteoblast (+Obs) laminin biomaterials and no cell (-Obs) controls at the late D28 timepoint. Bars represent the average of 4 biological donors and each data point is the mean of two technical replicates. Data were analysed using paired T tests. P values = *p<0.05, **p<0.01, ***p<0.001, ****p<0.0001.

5.3.1.14 Small differences in cytokine profile are evident by D28 for fibronectin versus D28 laminin cellularised biomaterials

Formal statistical outlier exclusion was done for the D3 samples, with donor D excluded for the fibronectin biomaterials and Donor C for the laminin biomaterials. As such, I am unable to directly compare D3 cellularised fibronectin (n=3, donors A, B, C) with D3 cellularised laminin (n=3, donors A, B, D). However, for the D28 samples, no formal outliers were identified for either biomaterial and therefore the two cellularised biomaterials can be directly compared at this timepoint.

Overall, a small number of the total analysed cytokines showed significant differences between the two biomaterials (cellularised fibronectin vs cellularised laminin) [Figure 5-47]. I have summarised the significant results only, by previously described cytokines groups; Th1, Th2, Th17, regulatory, activation/cytotoxic, growth factor or bone association [Figure 5-47]. Th1-associated cytokines that were significantly higher in the cellularised fibronectin condition were CCL7, CXCL9, CXCL11, TNFα, IFNβ, IL-27, IFNα and IL-1α. Th1-associated cytokines had the highest number of significant differences out of the cytokine groups. Th17-associated cytokines that were again significantly higher for the fibronectin biomaterial were CXCL1, IL-8 and IL-21. IL-1RA was the only activation/cytotoxic associated analyte significantly raised for the D28 fibronectin versus the laminin osteoblast biomaterial. The only regulatory-associated cytokine significantly increased for fibronectin was sFas with very subtle differences in overall amount of cytokine [Figure 5-47]. Osteopontin was significantly higher in the cellularised fibronectin biomaterial when compared to the cellularised laminin biomaterial, no significant differences were found between the two biomaterials for Th2-associated or growth factor associated cytokines [Figure 5-47].

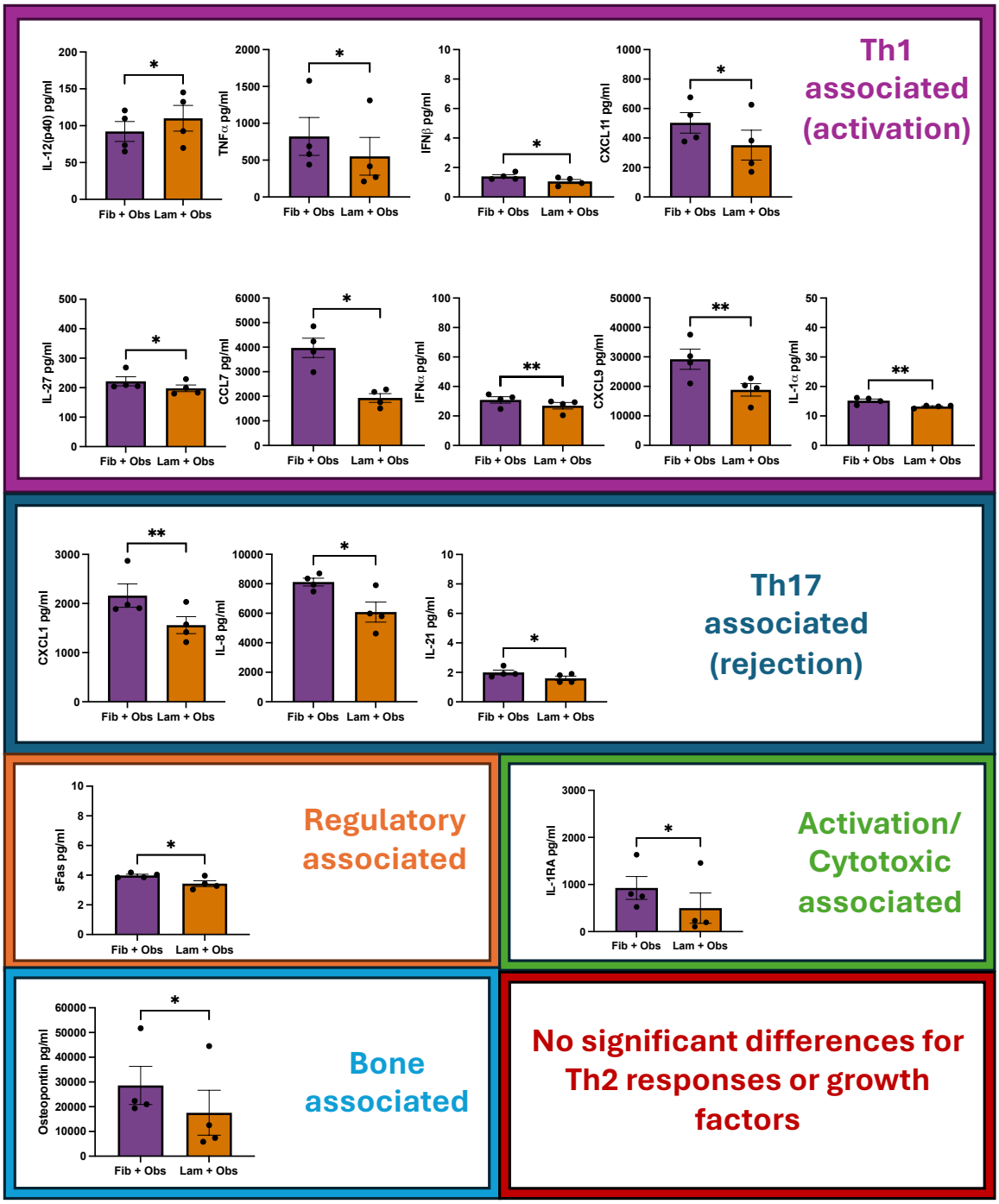

Figure 5-47: Summary of grouped cytokines highlighting significant differences between D28 cellularised fibronectin biomaterial and D28 cellularised laminin biomaterial. Graphs represent individual paired T tests between D28 Osteoblast (+Obs) fibronectin biomaterials and D28 Osteoblast laminin biomaterials. Bars represent the average of 4 biological donors and each data point is the mean of two technical replicates. Error bars represent the standard error of the mean. Data were analysed using paired T tests. P values = *p<0.05, **p<0.01, ***p<0.001, ****p<0.0001.

5.3.2 Immunomodulation by exposure to a proinflammatory microenvironment

In the first set of experiments in this chapter, I modulated the biomaterial itself by changing the glycoprotein. To modulate the model in a different way, in the following experiments, I wanted to investigate if an altered microenvironment would affect MSC differentiation and/or the subsequent T cell responses. Laminin biomaterials had shown some evidence in the Luminex data, of reduced osteoblast differentiation. I therefore chose to move forwards with just fibronectin biomaterials.

Human monocytes were obtained from PBMCs isolated from an NHS leucocyte cone that contains a large number of cells. They were cultured and differentiated into M1 classically proinflammatory macrophages over 8 days [methods 2.4.4]. I collected supernatant from these cultures to produce a large volume of conditioned 'proinflammatory' media to be used to supplement the normal media used in the established MSC to osteoblast differentiation experiment [methods 2.4.5]. Characterisation of the components of this conditioned media can be found in the appendix [Appendix 4, 7.4].

There were 4 different conditions across the 28 day cultures;

1. **No inflammation**: MSCs cultured in normal MSC media.

2. **3 Day Inflammation**: MSC media supplemented with the inflammatory supernatant for 3 days and then returned to normal MSC media for a further 25 days for D28 experiments or used for the D3 T cell co-cultures.

3. **14 Day Inflammation**: MSC media supplemented with the inflammatory supernatant for 14 days and then returned to normal MSC media for a further 14 days.

4. **28 Day Inflammation**: MSC media supplemented with the inflammatory supernatant for the full 28 days of MSC culture.

Activated T cells were added to the MSCs cultures after 3 or 28 days of MSC differentiation [Figure 5-48]. At the D28 timepoint all 4 conditions were co-cultured with the same donor's T cells to assess responses to the cells after different proinflammatory exposures over their differentiation. All co-cultures were undertaken with normal media so that the T cells were never exposed directly to proinflammatory signals that could bias their response. All co-cultures were analysed after 5 days. Flow cytometry was undertaken at both D3 and D28 timepoints and IF microscopy to identify osteoblast markers at D28.

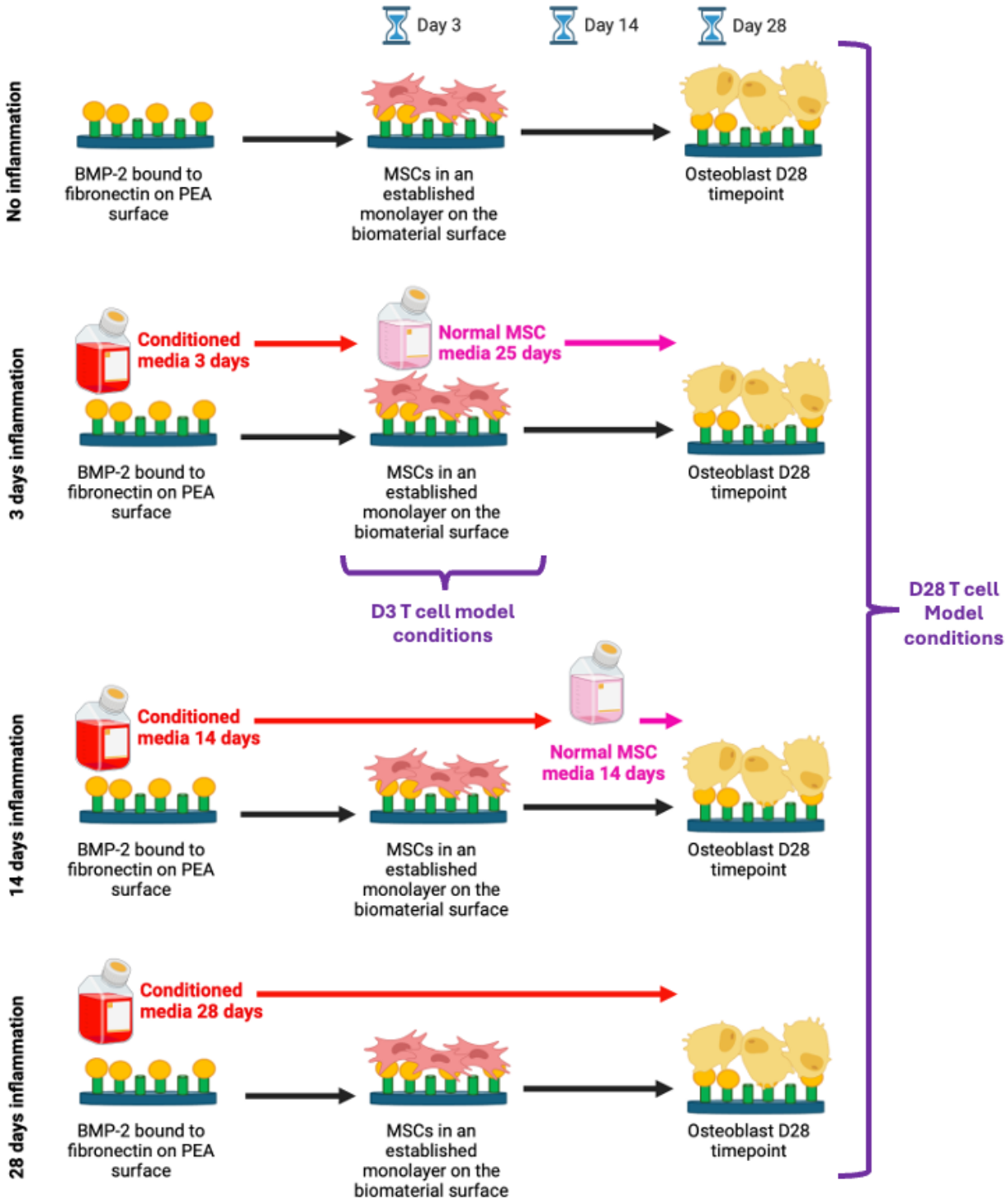

Figure 5-48: Experimental schematic for MSC differentiation over 28 days in presence of 4 different states of inflammation. At day 3 (D3) T cells were co-cultured with either MSC fibronectin biomaterials grown for 3 days in normal media or conditioned proinflammatory media. At day 28 (D28) T cells were co-cultured with osteoblast biomaterials grown for 28 days in normal media, 3 days conditioned proinflammatory:25 days normal media, 14 days conditioned proinflammatory: 14 days normal media or 28 days conditioned proinflammatory media. At time of T cell co-culture all media was changed to normal media. Co-cultures with T cells were for 5 days. Created with BioRender.com

5.3.2.1 Exposure to inflammation over 3 days led to small increases in CD8, but not CD4, T cell response to MSC biomaterials

I compared the expression of the T cell activation markers, CD25, ICOS and PD1 and transcriptions factors, FOXP3, GATA-3, RoRγt and T-bet, in co-cultures between activated T cells and D3 MSCs in the absence versus the presence of the inflammatory supernatant. For these experiments, I modified the protocol used for the transcription factor panel, reducing the fixation and staining periods. This led to an improved CD25 signal compared to the longer fixation/staining periods used in the experiments described above. I also found more consistent GATA-3 and RoRγt staining and have included these data [Figure 5-49].

For CD4 T cells, the inflammatory supernatant led to a non-significant increase in expression of the three surface markers [Figure 5-50]. In contrast, the inflammatory supernatant led to significant but modest increases in both ICOS MFI and PD1 expression on CD8+ T cells. The inflammatory supernatant did not alter the expression of the Transcription factors in CD4 nor CD8 T cells [Figure 5-51] and no changes in the proportion of CD4+ Tregs were observed [Figure 5-52].

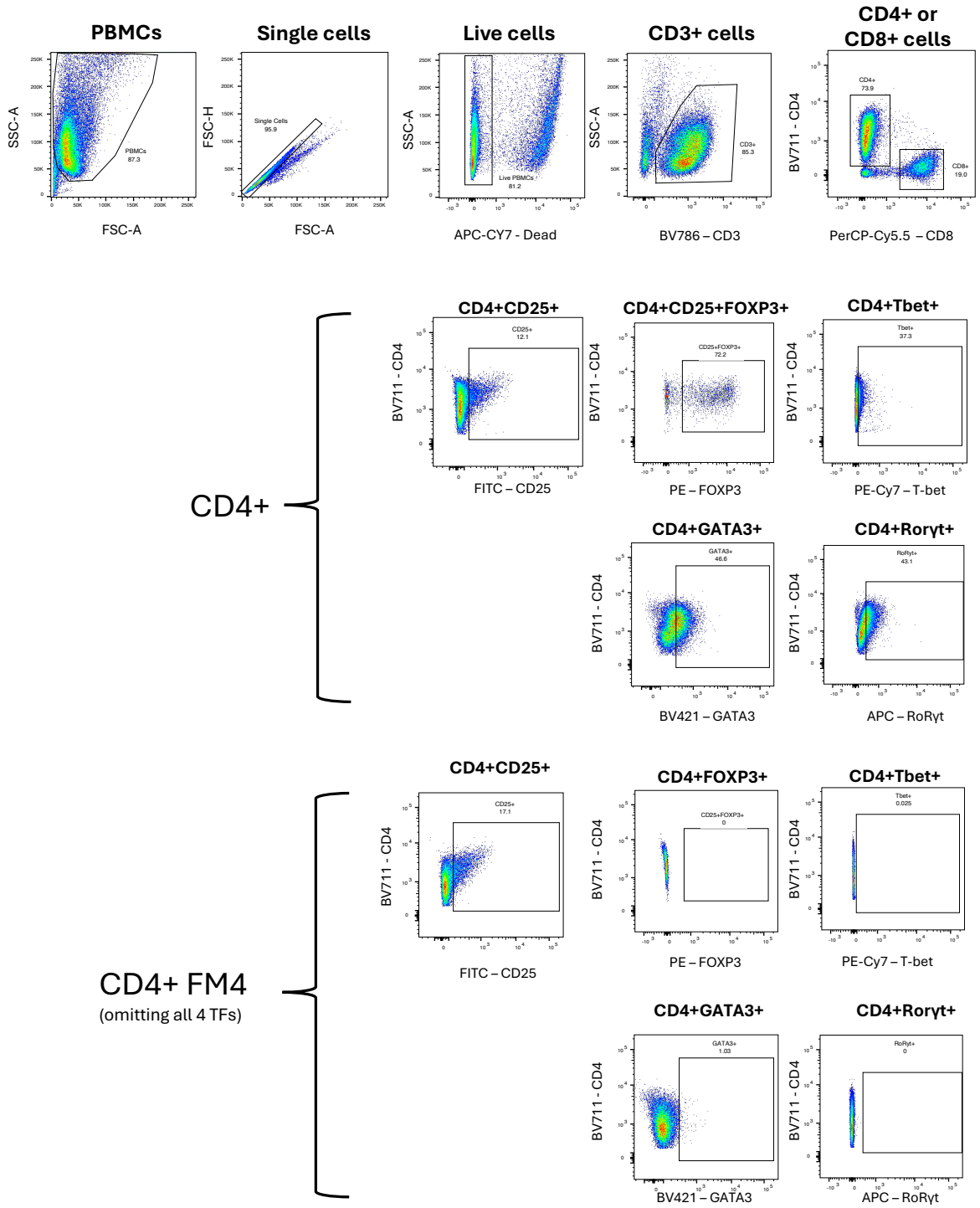

Figure 5-49: Flow gating strategy for T cell identification and identification of T cell surface activation markers in addition to intranuclear transcription factors. Representative staining of T cells from a co-culture with MSCs as descried in Materials and Methods and acquired on a BD Fortessa. Indicated populations are shown and numbers show the percentage of cells within the gates. Representative staining evidencing successful RoRγt and GATA3 staining. CD4 data only shown with FMOs (CD8+ data and FMOs not shown).

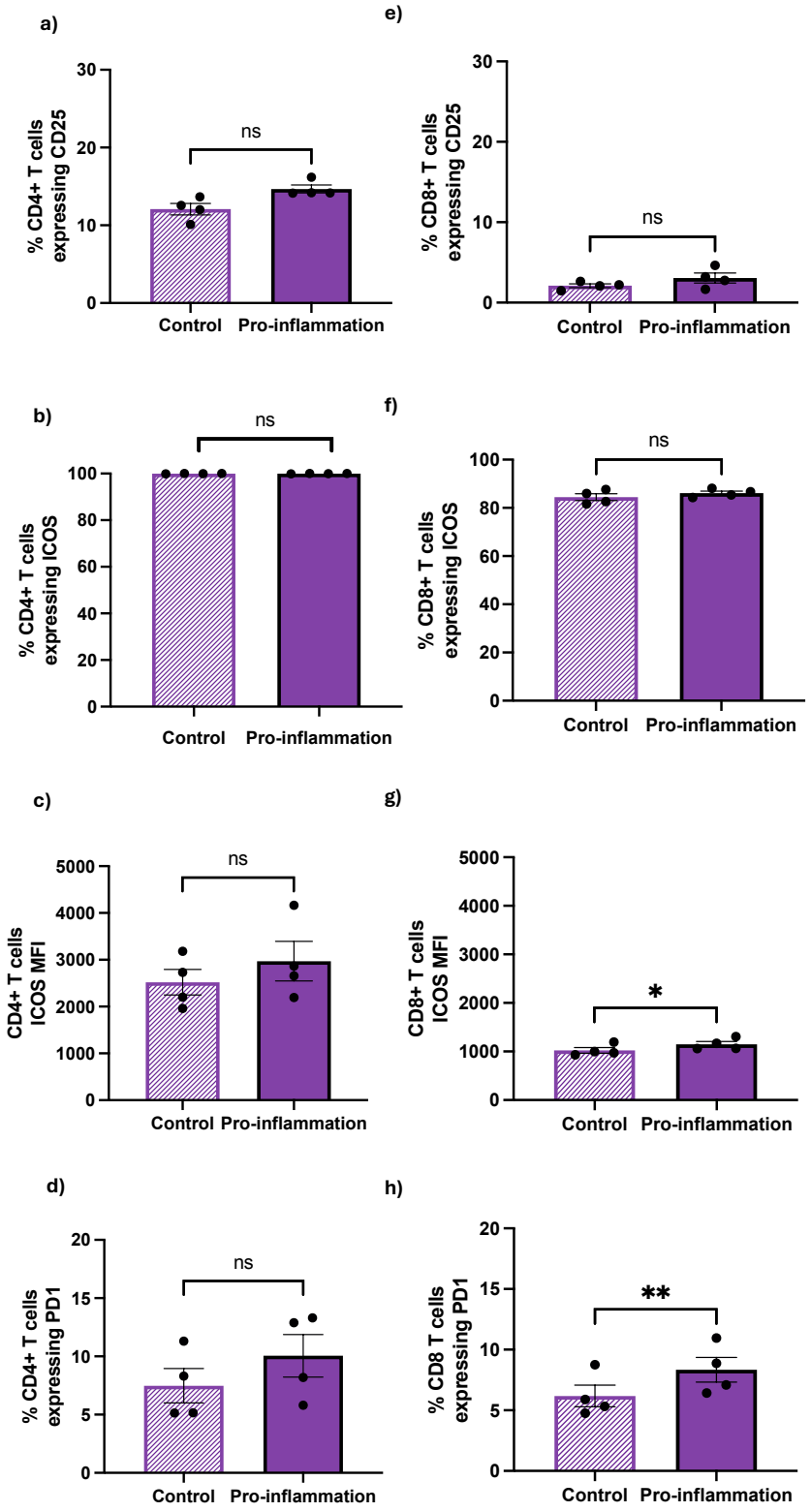

Figure 5-50: Limited differences in T cell response to MSC biomaterials grown for 3 days with and without inflammation. Early D3 MSC timepoint on FN biomaterials in co-culture with the T cell model for 5 days either with control media or conditioned proinflammatory media. Results shown for flow cytometry for surface marker expression on CD4+ (a-d) and CD8+ (e-h) T cells. Results shown for CD25+, ICOS+, ICOS MFI and PD1. Bars represent the mean of 4 biological donors and each point represent the average of two technical replicates. Error bars are the standards error of the mean. Data were normally distributed and analysed by paired T tests. P values = *p<0.05, **p<0.01, ***p<0.001, ****p<0.0001.

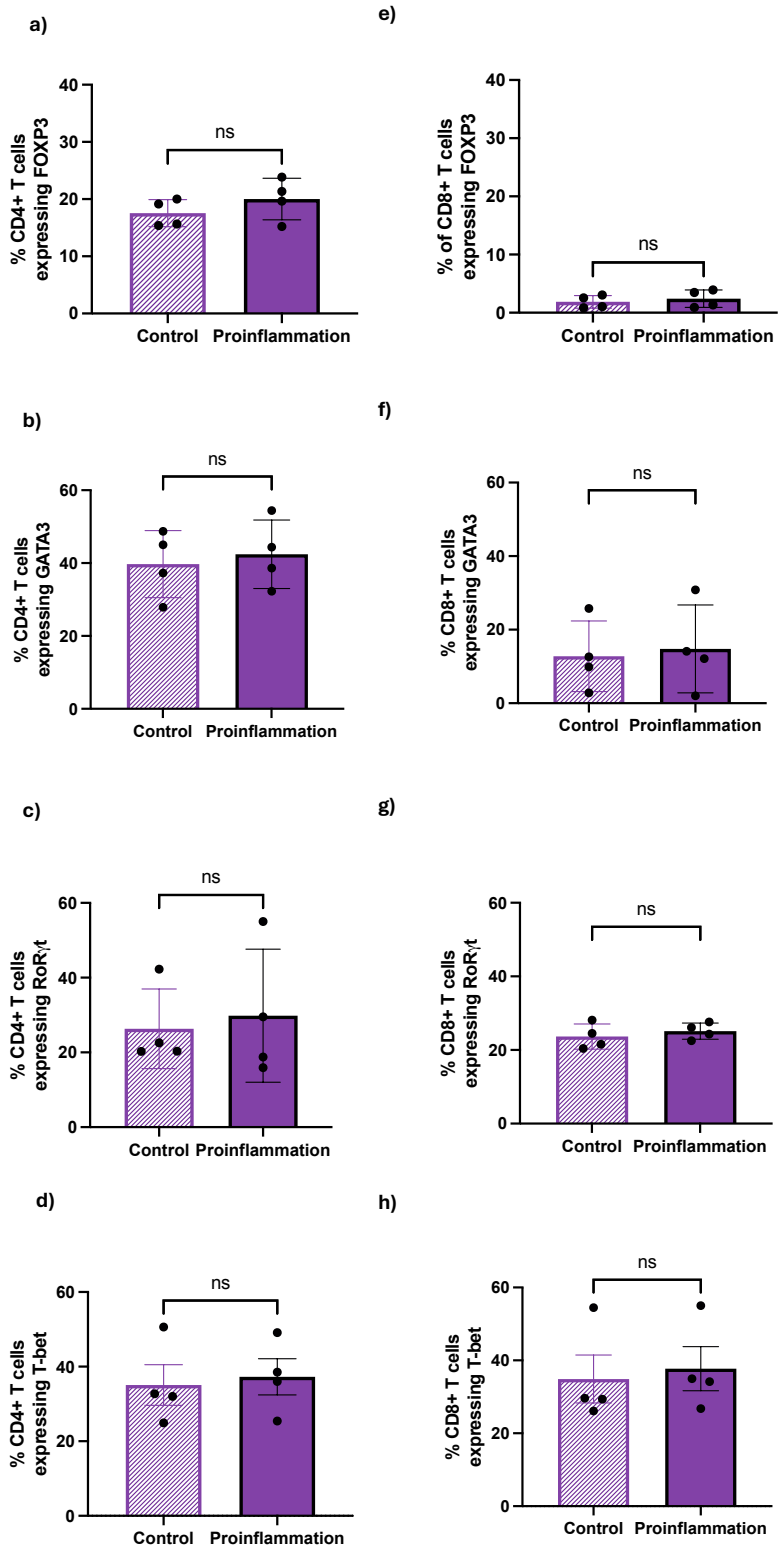

Figure 5-51: No differences in T cell transcription factor expression to MSC biomaterials grown with and without inflammation. Early D3 MSC timepoint on FN biomaterials in co-culture with the T cell model for 5 days either with control media or conditioned proinflammatory media. Results shown for flow cytometry for transcription factor intranuclear marker expression on CD4+ (a-d) and CD8+ (e-h) T cells. Results shown for FOXP3+, GATA3+, RoRyt+ and T-bet+ cells. Bars represent the mean of 4 biological donors and each point represent the average of two technical replicates. Error bars are the standards error of the mean. Data were normally distributed and analysed by paired T tests. P values = *p<0.05, **p<0.01, ***p<0.001, ****p<0.0001.

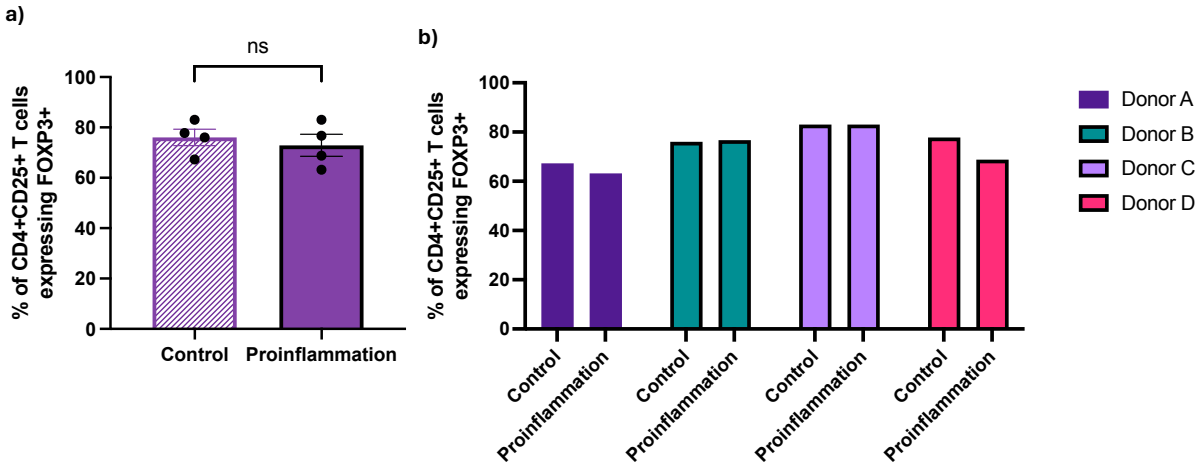

Figure 5-52: No differences in expression of Tregs to 3 day cultured MSC biomaterials either with or without inflammation. Transcription factor flow cytometry data for D3 early timepoint MSC biomaterials in co-culture with the T cell model for 5 days either with control media or conditioned proinflammatory media for 3 days before switching to normal unconditioned media. a) Expression of FOXP3 by CD4+CD25+ T cells and b) proportions per donor of CD4+CD25+FOXP3+ T cells. Bars represent the mean of 4 biological donors and each point represent the average of two technical replicates. Error bars are the standards error of the mean. Data were normally distributed and analysed by a paired T test. P values = *p<0.05, **p<0.01, ***p<0.001, ****p<0.0001.

5.3.2.2 D28 timepoint: cell differentiation assessments

As the MSCs in this experiment were cultured in vastly different conditions to those grown previous experiments, it was hypothesised that their differentiation into osteoblasts may be compromised. I undertook immunofluorescence (IF) microscopy as previous, to look for later osteoblast markers OCN and OPN. I also examined MHCII expression by IF microscopy.

5.3.2.3 Sustained exposure to proinflammatory media inhibits growth and survival of MSCs

From examining the MSCs via a light microscope throughout the 28 days culture, I observed that by D28 most of the cells grown in 14-28 days of conditioned proinflammatory media were altered. This was not apparent during the first week of the cultures. For example, in the 14 days and 28 days inflammation exposed groups, there were very few cells left in the cultures by D28, markedly less than all prior experiments performed in normal media, and this was not observed in the cultures of cells grown in normal media for 25-28 days. As such, no formal parameter for MSC quantification had been planned into this experiment as, prior there had always been full tissue culture well cell confluence throughout the experiment. Additionally, the cells were less likely to form a monolayer as they were fewer in number. In order to document this, prior to beginning the 5 day T cell co-culture at experiment D28, I obtained images of the cell cultures that had been grown under 0, 3, 14 or 28 days of inflammation [Figure 5-53]. The images in the control (no inflammatory media), show healthy, confluent cultures and this was largely similar in the cultures that had received 3 days of proinflammatory media, before completing their growth in normal MSC media. The third condition, that grew for 14 days in inflammatory conditioned media before reverting to normal

MSC culture media for a further 14 days, appeared to have the largest reduction in cell number in all the cultures. This was future quantified on DAPI staining and there was a significant reduction in cells over the duration of their exposure to conditioned inflammatory media [Figure 5-54]. Furthermore, the cell morphology in both the 14 and 28 day inflammation groups appeared more spindle and stellate shaped, with larger areas of non-confluence in each well [Figure 5-53].

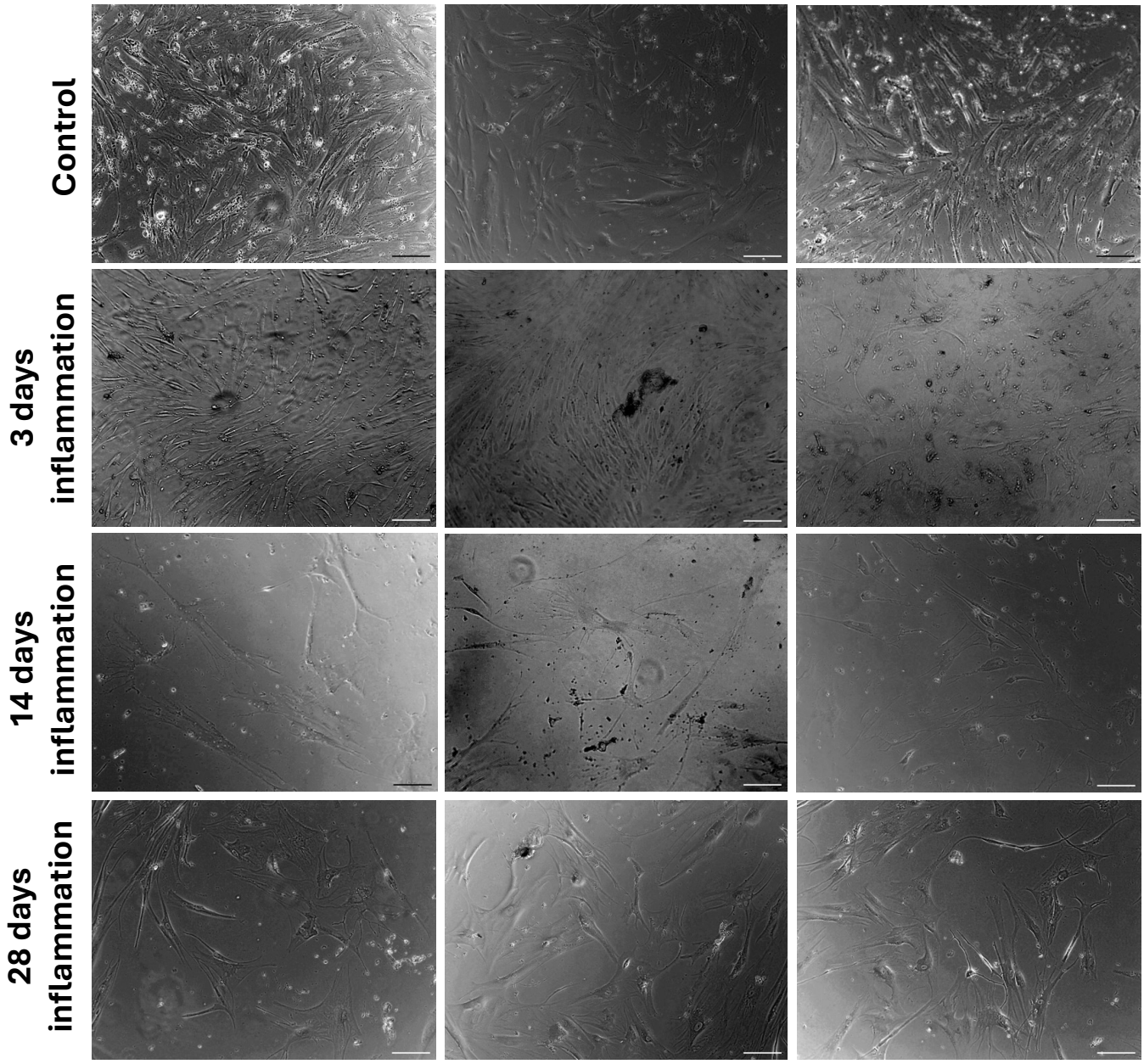

Figure 5-53: Cell morphology becomes more spindle-like, sparse and less confluent after 14 and 28 days exposure to conditioned inflammatory media. At D28 MSC culture, prior to any T cell addition, wells were imaged on an EVOS microscope. Panels show three representative images per condition taken from different wells: normal control media only, cells exposed to 3, 14 or 28 days of conditioned inflammatory media. Scale bars represent 100μm.

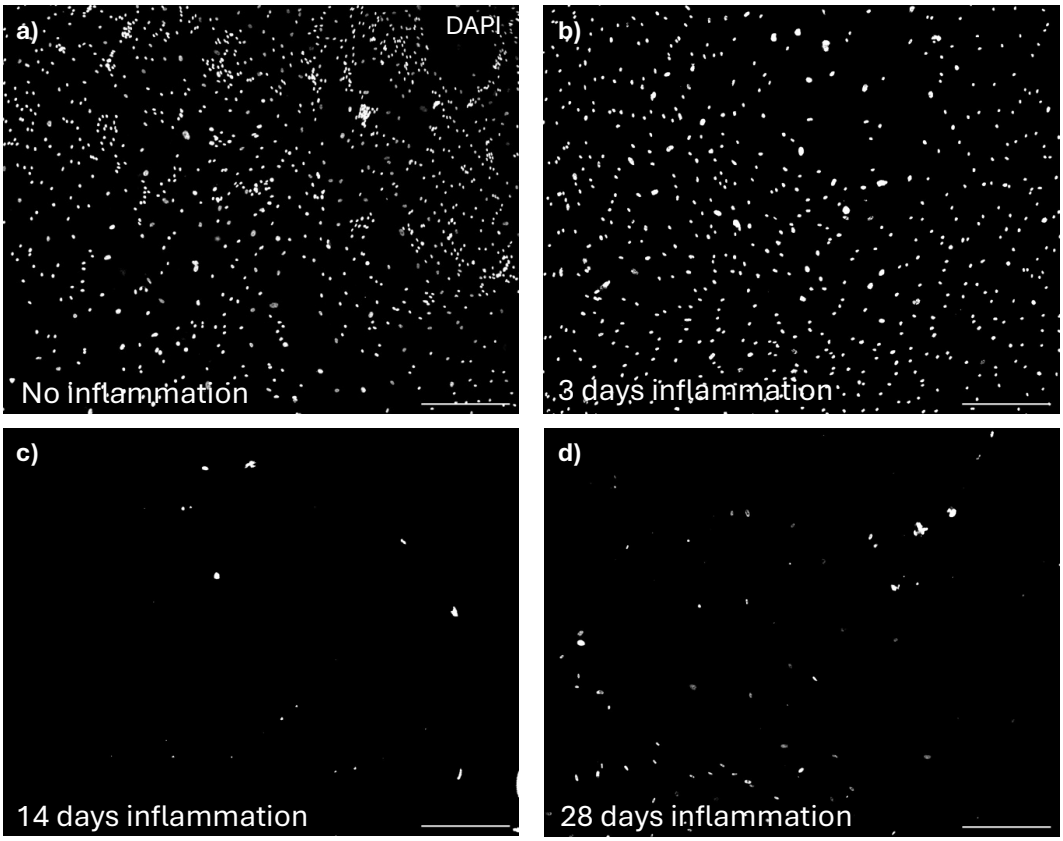

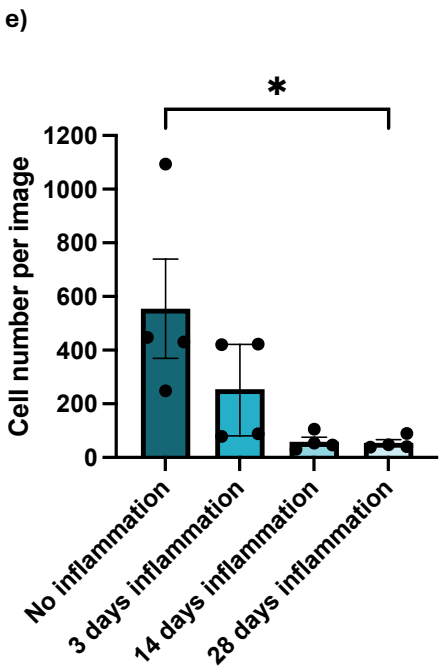

Figure 5-54: Cell numbers reduce significantly after 28 days grown in conditioned proinflammatory media. D28 cultured osteoblasts exposed to different durations of proinflammatory conditioned media. a-d) IF images in black and white showing DAPI nuclei staining of D28 cultures e) quantification of cell number. Each data point is an average of three images from a single well. The bars represent the median of four individual wells. All error bars are the interquartile range. Scale bars represent 500μm. Data were not normally distributed and so was analysed with a nonparametric Kruskal-Wallis test with Dunn's multiple comparisons test. P values = *p<0.05, **p<0.01, ***p<0.001, ****p<0.0001.

5.3.2.4 Cells that survive to D28 express osteoblast markers and upregulate MHCII

IF microscopy was used to analyse the cells at D28 of culture as previously, to ascertain if there was expression of osteoblast markers OCN and OPN, in cells grown in 0, 3, 14 and 28 days of conditioned proinflammatory media.

OPN expression, when shown for individual cells, was present across all the conditions, irrespective of exposure to proinflammation [Figure 5-55]. OCN expression by IF subjectively appeared to be less in conditions exposed to proinflammation compared with those grown in normal MSC culture media [Figure 5-56]. Imaging the cells was increasingly difficult for the D14 and D28 exposed groups, due to the significant reduction in cells within the cultures. This was not the case in the control no inflammation cultures or for those exposed to 3 days proinflammation only, when cells were clearly confluent.

IF microscopy was performed to detect MHCII for MSCs grown in 0, 3, 14 and 28 days proinflammation. MHCII expression was highest in the no inflammation control and appeared to reduce in the 14 days exposed group [Figure 5-57]. MHCII expression in the few remaining cells at D28 was largely comparable to normal conditions, but cell number was significantly reduced [Figure 5-54].

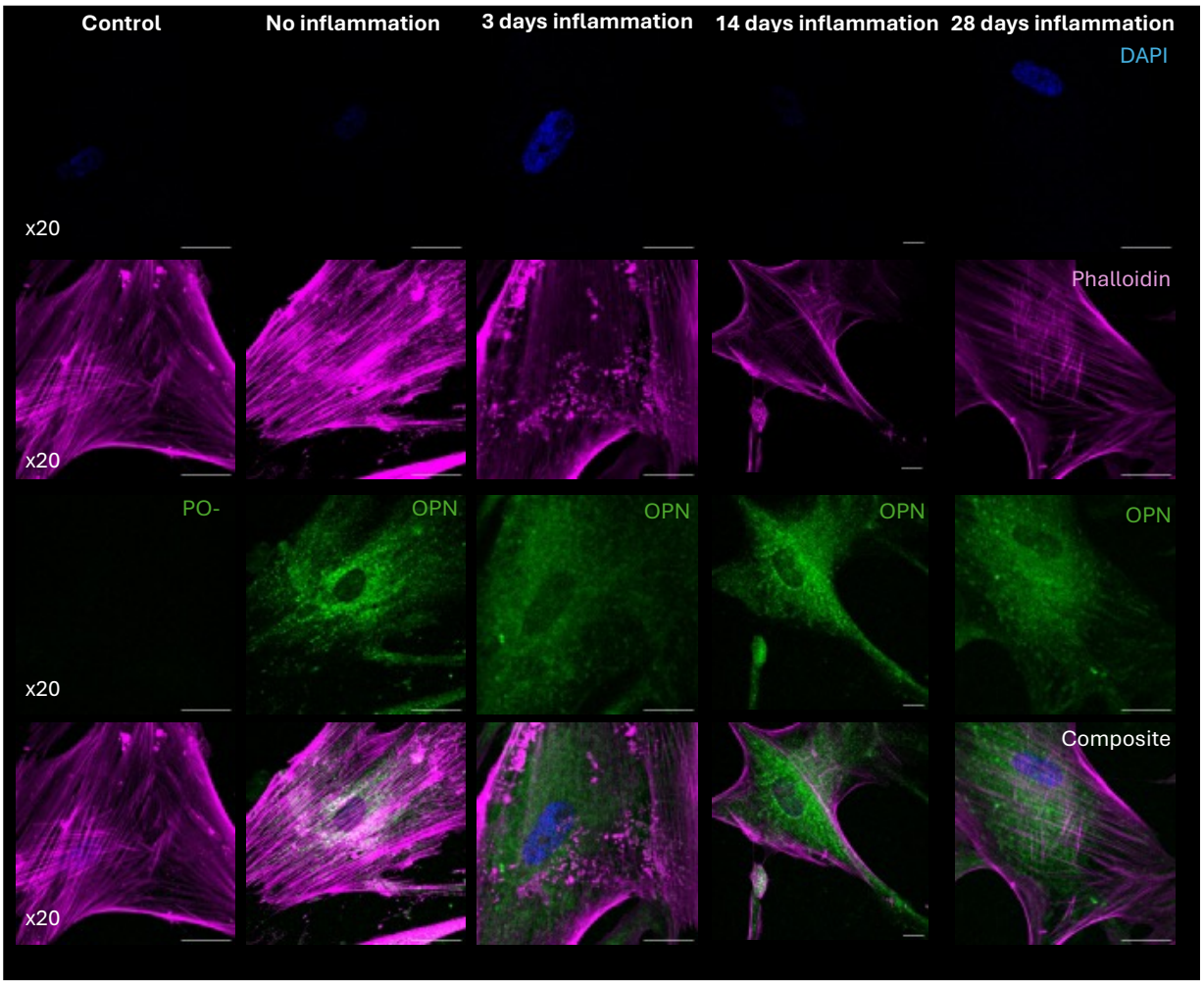

Figure 5-55: Expression of OPN in cells that survive to D28 culture irrespective of the presence of conditioned inflammatory media. Immunofluorescence microscopy images taken at D28 of fibronectin biomaterials cultured in proinflammatory conditioned media for 0, 3, 14 or 28 days. Cells were stained for DAPI (blue), phalloidin (magenta) and osteoblast differentiation marker osteopontin (OPN, green). Primary omission staining shown (PO-). Scale bars represent 50μm. All colour thresholds set the same to allow comparison between images, images are representative from 6 images per well and between 2 wells per condition.

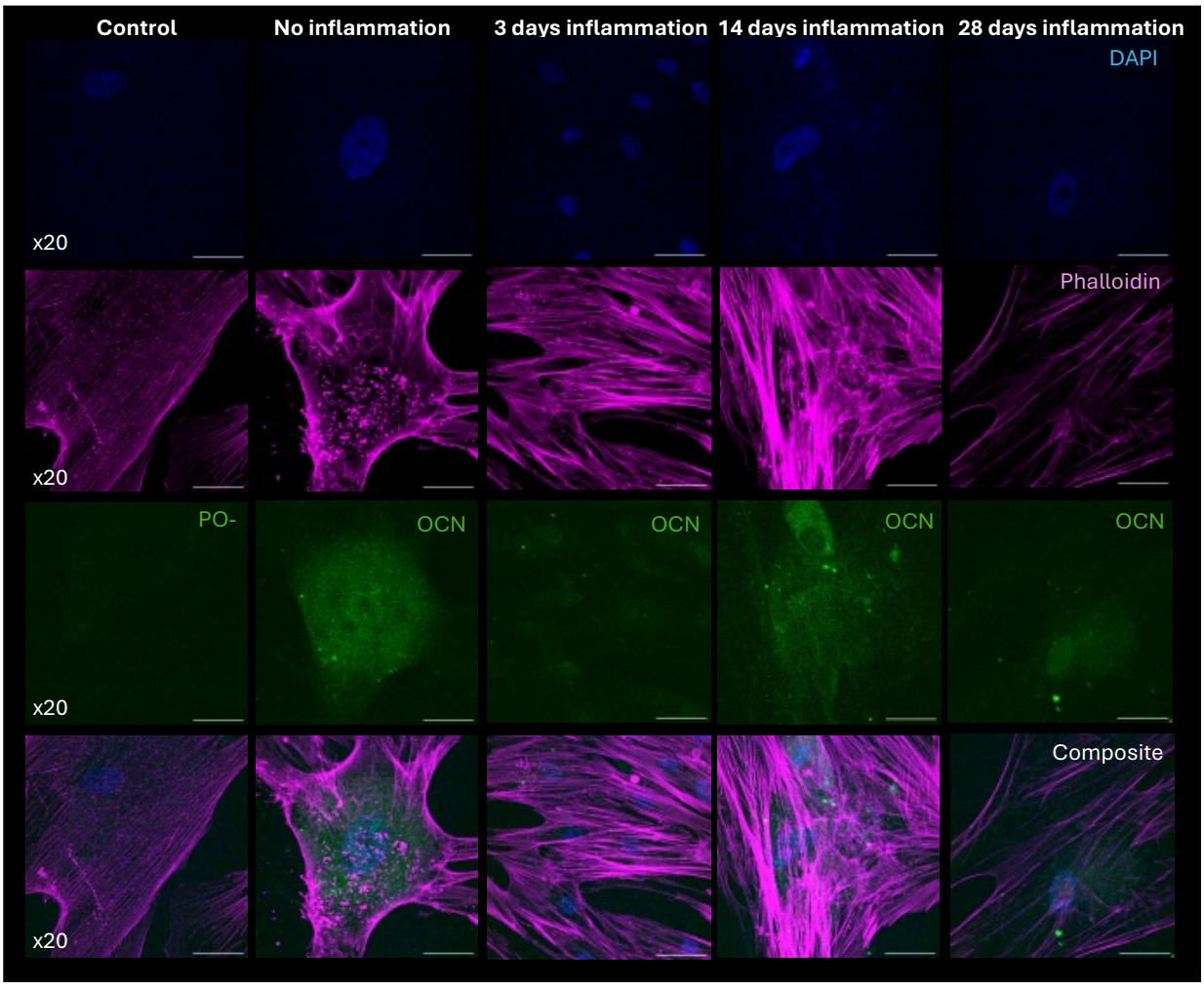

Figure 5-56: OCN expression highest in states of no inflammation by D28 culture. Immunofluorescence microscopy images taken at D28 of fibronectin biomaterials cultured in proinflammatory conditioned media for 0, 3, 14 or 28 days. Cells were stained for DAPI (blue), phalloidin (magenta) and osteoblast differentiation marker osteocalcin (OCN, green). Primary omission staining shown (PO-). Scale bars represent 50μm. All colour thresholds sets the same to allow comparison between images, images are representative from 6 images per well and between 2 wells per condition.

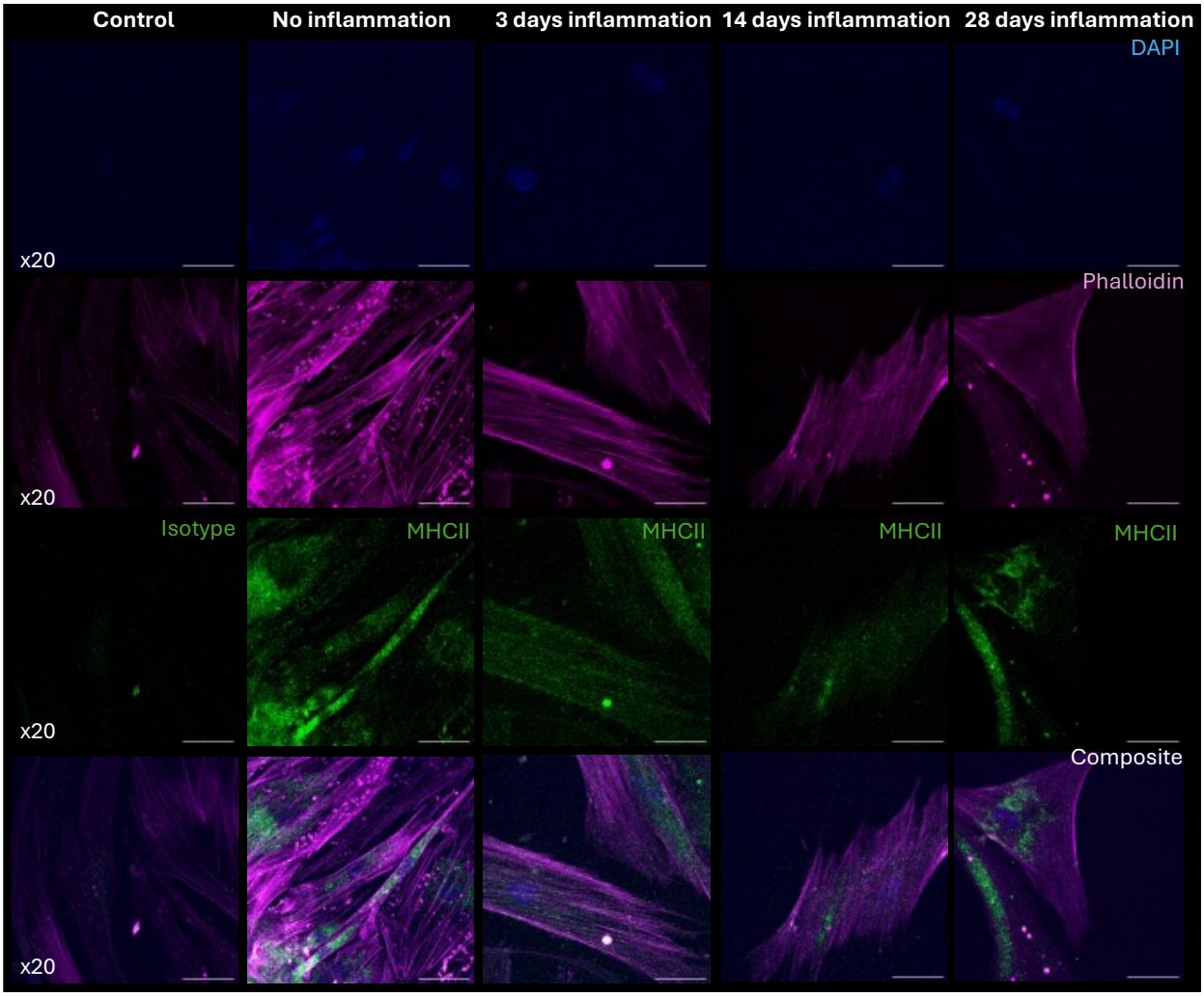

Figure 5-57: MHCII expression highest in D28 cells grown in either 3 days only or no inflammation. Immunofluorescence microscopy images taken at D28 of fibronectin biomaterials cultured in proinflammatory conditioned media for 0, 3, 14 or 28 days. Cells were stained for DAPI (blue), phalloidin (magenta) and MHC class II (MHCII, green). MHCII isotype control shown (Isotype). Scale bars represent 50μm. All colour thresholds set the same to allow comparison between images, images are representative from 6 images per well and between 1-3 wells per condition.

5.3.2.5 Significant decreases in T cell surface activation marker expression in co-culture with D28 cells grown in proinflammatory conditions

I had established that osteoblast differentiation had occurred by D28 in the normal (no inflammation controls), with evidence of some osteoblast differentiation in the various proinflammatory conditions but with significantly lower cell numbers. The presence of proinflammation had altered the conditions enough to disrupt the majority of the MSCs from either surviving or proliferating over their differentiation into osteoblasts. This is reflected in the D28 flow cytometry data after 5 days co-culture with the T cells. Unlike at the D3 timepoint, significant differences were found in the T cell responses to the cellularised biomaterials at D28 when comparing the different culture conditions.

In co-cultures with cellularised biomaterials exposed to 14 days of inflammatory media, CD4+ T cells had reduced expression of CD25, although a significant reduction was only found in comparisons with cultures exposed to 3 or 28 days of pro-inflammatory media. These CD4 T cells and those co-cultured with cellularised biomaterials exposed to 28 days of inflammatory media expressed less ICOS while PD1 was reduced on the CD4+ T cells in the day 28-inflamatory co-cultures compared to CD4 T cells in the day 3 inflammatory co-cultures.

There were no significant changes in CD8+ T cells expression of ICOS or CD25 between any of the co-culture conditions [Figure 5-58]. There was a small but significant reduction in PD1 expression in CD8+ T cells co-cultured with cellularised biomaterials exposed to 14 days compared to 3 days of inflammatory media.

There were some significant but very limited changes in the expression of FOXP3 and T-bet by CD4 T cells and no changes in GATA3 expression between control cellularised biomaterials and those grown in inflammatory media. There were more robust reductions in the percentages of CD4+ T cells expressing RoRγt in co-cultures with cellularised biomaterials cultured in the presence of the pro-inflammatory media [Figure 5-59].

CD8 T cell expression of the four Transcription Factors was generally unaffected by the addition of the inflammatory media to the cellularised biomaterials [Figure 5-59]. There were some significant differences, however given the small changes, these are unlikely to be biologically meaningful. There were also no changes in the proportion of CD4+ T cells that expressed both CD25 and FOXP3 [Figure 5-60].

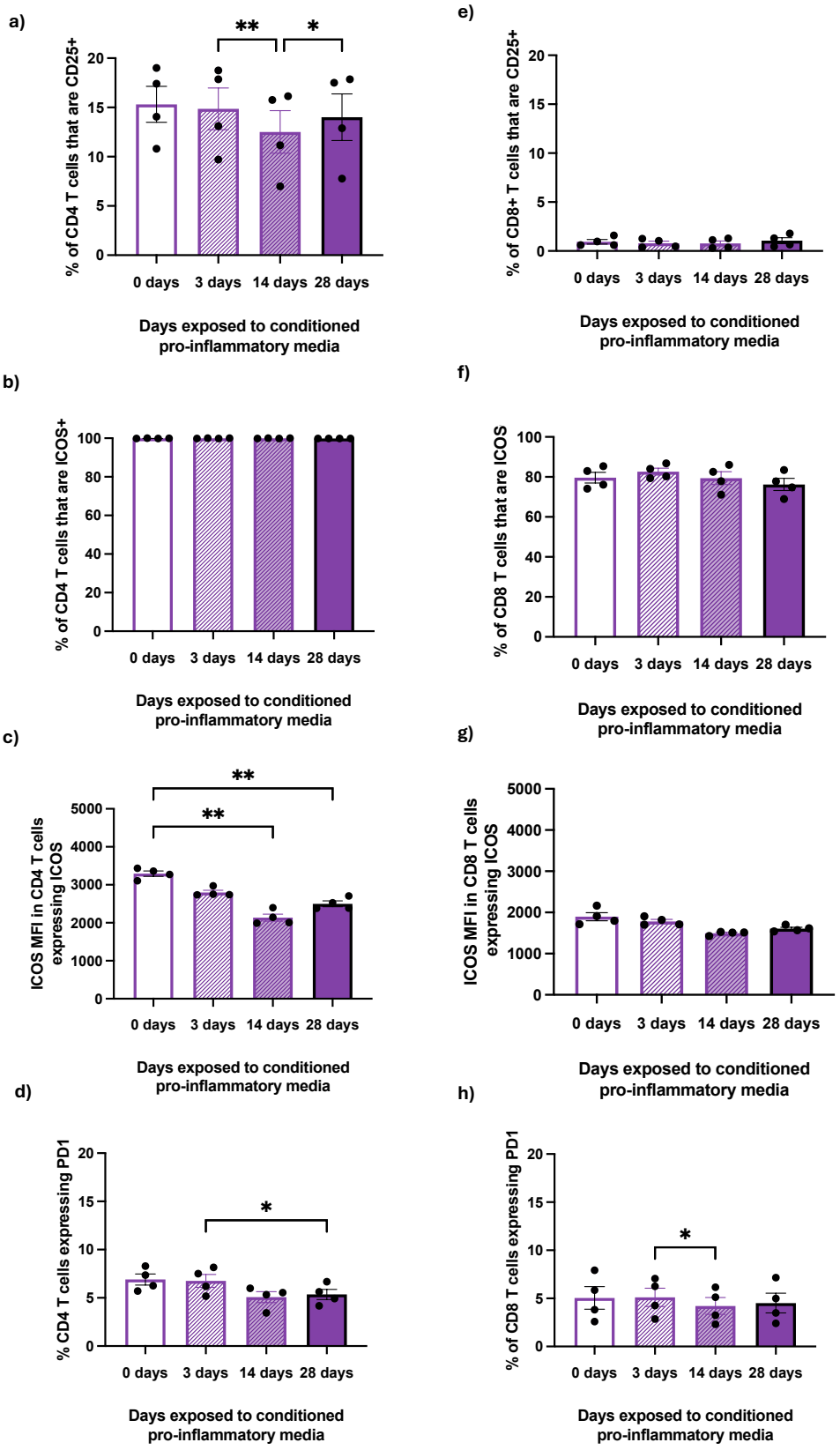

Figure 5-58: Late D28 osteoblast timepoint on fibronectin biomaterials in co-culture with the T cell model for 5 days either with control media for 28 days or 3, 14 or 28 days of conditioned proinflammatory media before switching to control media. Results shown for flow cytometry for surface marker expression on CD4+ (a-d) and CD8+ (e-h) T cells. Results shown for CD25+, ICOS+, ICOS MFI and PD1. Bars represent mean of 4 biological replicates plotted as mean of technical duplicates. Standard error of mean shown as error bars. Data were normally distributed and analysed by a one-way ANOVA with Šídák's multiple comparisons test, only significant results shown on the graphs. P values = *p<0.05, **p<0.01, ***p<0.001, ****p<0.0001.

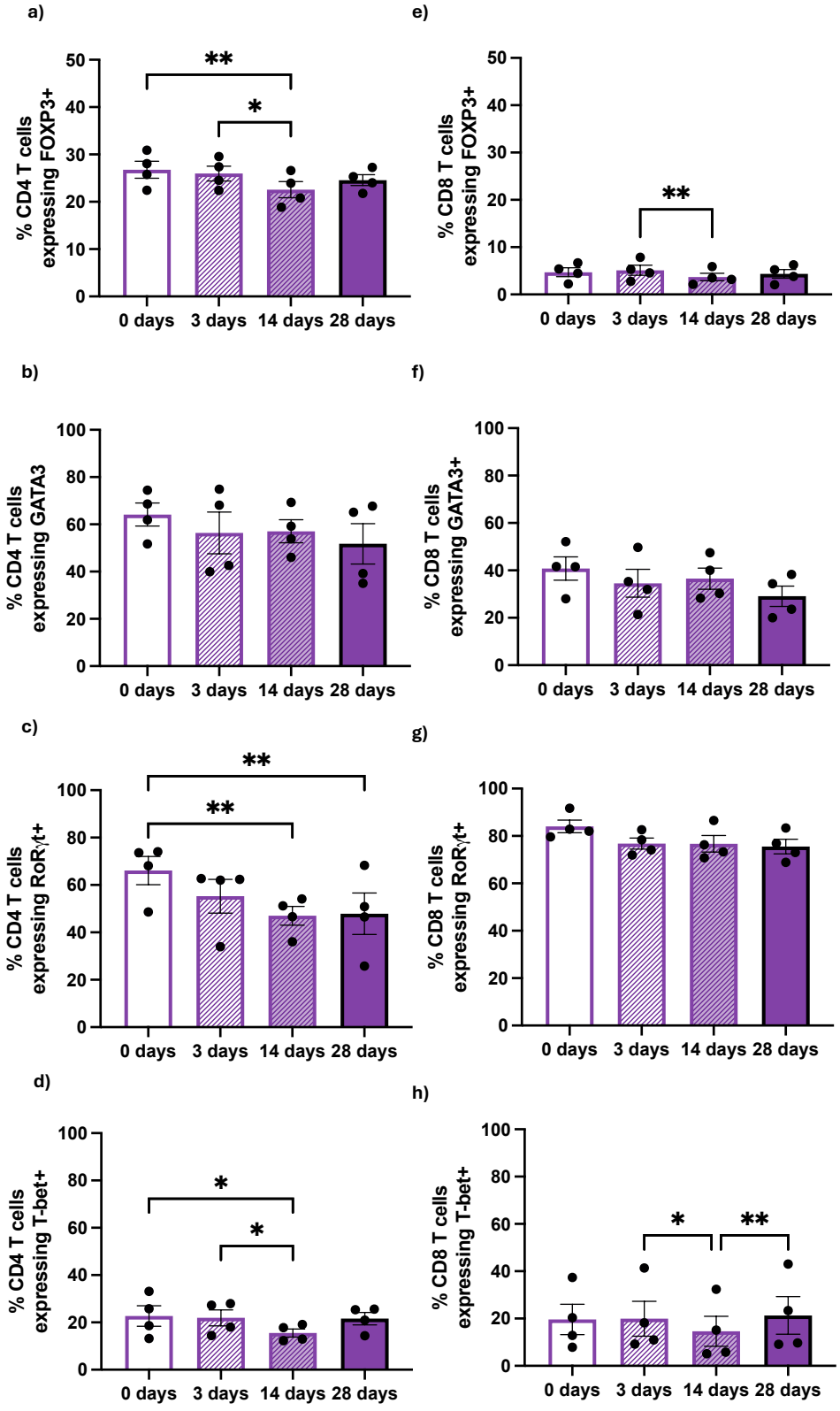

Figure 5-59: Late D28 osteoblast fibronectin biomaterials in co-culture with the T cell model for 5 days either with control media or conditioned proinflammatory media for 3, 14 or 28 days before switching to normal unconditioned media. Results shown for flow cytometry for transcription factor intranuclear marker expression on CD4+ (a-d) and CD8+ (e-h) T cells. Results shown for FOXP3+, GATA3+, RoRyt+ and T-bet+ cells. Bars represent the mean of 4 biological donors and each point is the average of technical replicates. Error bars show the standard error of the mean. Data were normally distributed and analysed by a one-way ANOVA with Šídák's multiple comparisons test, only significant results shown on the graphs. P values = *p<0.05, **p<0.01, ***p<0.001, ****p<0.0001.

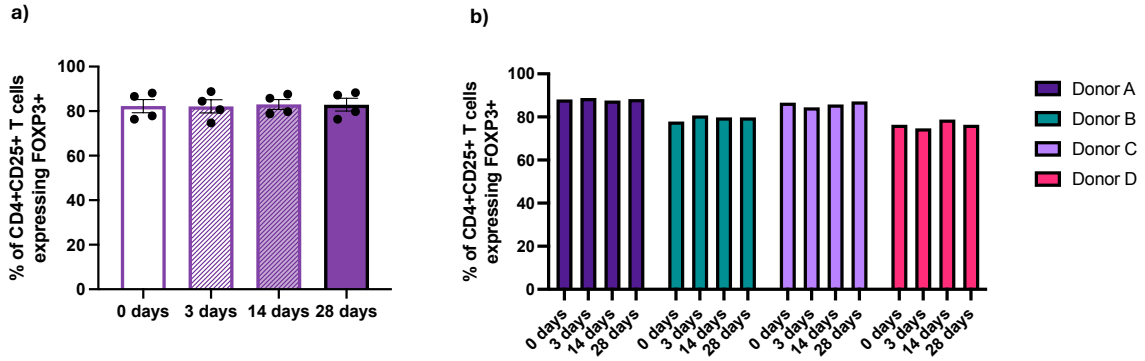

Figure 5-60: No difference in CD4+CD25+ T cell expression of transcription factor FOXP3. Flow cytometry data for D28 late timepoint osteoblast biomaterials in co-culture with the T cell model for 5 days either with control media or conditioned proinflammatory media for 3, 14 or 28 days before switching to normal unconditioned media. a) expression of FOXP3 by CD4+CD25+ T cells and b) proportions per donor of CD4+CD25+FOXP3+ T cells. Bars represent the mean of 4 biological donors and each point represent the average of two technical replicates. Error bars are the standards error of the mean. Data were normally distributed and analysed by a one-way ANOVA with Šídák's multiple comparisons test, only significant results shown on the graphs. P values = *p<0.05, **p<0.01, ***p<0.001, ****p<0.0001.

5.4 Discussion

5.4.1 Different biomaterial glycoproteins: equivalent T cell surface activation but distinct Teffector response?

Overall, the data do not suggest differences in T cell activation marker expression between laminin and fibronectin allogenic biomaterials. For both, the cellularised biomaterials induced a greater T cell response than the acellular biomaterial in terms of surface cell-marker expression. However, some differences in T cell functional responses to the different biomaterials were found and shall be discussed. It is possible these may be due to differences in the extent of MSC differentiation between the two types of biomaterials, with greater osteoblast differentiation on the fibronectin biomaterial condition.

5.4.1.1 Flow cytometry data reveals evidence of T cell activation responses to D3 MSC biomaterials

At the early MSC-D3 timepoint, after 5 days co-culture with allogenic T cells, there were significant increases in CD4+ and CD8+ T cell expression of CD25, ICOS and PD1 in co-culture with laminin MSC+ compared to acellular biomaterials. Comparatively, less overall T cell response was found for fibronectin MSC biomaterials as only CD25 was expressed at significantly higher levels by the CD4+ and CD8+ T cells co-cultured with MSC+ biomaterials.

Analysis of the transcription factors expressed by the T cells, showed that the majority of the CD4+CD25+ T cells were also positive for FOXP3, the defining transcription factor for Treg differentiation (365). This may seem unsurprising as MSCs have been shown to promote Treg proliferation and immunosuppressive activities (366). However, defining human Treg cells based on CD25 and FOXP3

may not be sufficient as CD25 and FOXP3 can be found on recently activated conventional CD4+ activated T cells (367-369). In addition to CD25, subsets of human Tregs would be expected to also express ICOS and/or PD1 (370). Li et *al*. argue that ICOS+ co-expression on T regs potentially endows Tregs with increased differentiation, proliferation and survival abilities and a superiority at immunotolerant activities due to the IL-10 induced by ICOS (371). Similarly, Strauss et *al.* found that ICOS+ Tregs were more suppressive than ICOS- Tregs (372, 373). PD1 is highly expressed alongside PD1 ligand (PD1L) on Tregs (374). Upregulation of isolated CD25+, in the absence of ICOS or PD1 co-expression, is therefore more likely to represent an activated T effector cell rather than a Treg, and approximately 35-40% of CD4+CD25+ cells at the early timepoint expressed CD25 in the absence of ICOS and PD1 [Figure 5-6](375). These data suggest that a mixed population of Treg and activated T effector cells are likely already within the co-cultures at this early MSC timepoint.

5.4.1.2 MSCs differentiated into osteoblasts *in vitro,* on functionalised biomaterials, express MHC II

Osteoblasts have been shown to express functional MHC class II molecules in both physiological and bacterial infection models (79, 355, 356, 376). As osteoblast differentiation has occurred by D28 within my cultures, this could possibly account for the increased expression of T cell activation surface markers if more MHC class II molecules were expressed. Increased MHCII expression may be increasing the pool of alloantigens that can be presented on MHCII to CD4+, or on MHCI to CD8+ T cells (377). Immunofluorescence microscopy demonstrated for the first time, evidence of MHCII upregulation in the *in vitro* biomaterial differentiated osteoblasts. *Ex vivo* primary human bone cells have been shown to express MHCII constitutively in 10-30% and a further 5-15% do so in long term

culture *in vitro* (378). However, historical reports suggest a failure of MSC differentiated osteoblasts to express MHCII after differentiation driven by osteogenic media (79). These data suggest a similar phenotype with regards to OCN, OPN and MHCII expression by the biomaterial-differentiated MSCs *in vitro* to *ex vivo* primary human bone cells.

5.4.1.3 T cell activation responses persist at D28, irrespective of biomaterial glycoprotein

At D28 after just 3 days co-culture with the fibronectin osteoblast biomaterials, significant increases were found in CD25, ICOS MFI and PD1 expression in CD4+ T cells over acellular matched controls. Similarly, for CD8+ T cells CD25, ICOS and PD1 expression increased. This response was largely comparable with the matched T cell response to laminin osteoblast biomaterials at this timepoint. With similar MHCII expression by osteoblasts differentiated in the presence of fibronectin or laminin, this could explain the matched responses.

CD4+ and CD8+ T cells co-cultured with day 28 cellularised fibronectin, but not laminin biomaterials, increased T-bet expression. However, this does not appear to be a higher percentage expression than found in the laminin cultures at this timepoint and likely non-biologically significant. The lack of significance for the T cells cultured with laminin biomaterials may be due to the spread of the data. As at the day 3-MSC timepoint, there were no significant differences found in CD4+CD25+FOXP3+ expression between osteoblast and acellular controls for either biomaterial.

5.4.1.4 Th1 responses were predominant in co-culture with both biomaterials and Th1-associated cytokines were increased by D28

At both the early MSC and late osteoblast biomaterial timepoint, LT-α and CCL2 were significantly increased compared to controls in both fibronectin and laminin biomaterials. Activated CD4 T cells are the main source of LT-α, which is a multifunctional cytokine that can be made by a number of cells (379). LT-α can induce apoptosis upon binding to TNFR1 or induce inflammatory responses by activating NF-κB upon binding to TNFR2 (380). LT-α is induced in an antigen-specific manner from CD4+ and CD8+ T cells and, furthermore, has been associated with promoting osteoclastogenesis, bone resorption and inhibition of bone collagen synthesis in vitro (381). CCL2 is responsible for the migration and infiltration of monocytes and macrophages to the site of injury (382).

For the laminin MSC biomaterial T cell co-cultures, significant increases in IL-18, IL-27, CXCL11 and IFNα were found at the D28 timepoint compared to the acellular control. IL-18 is a cytokine commonly found at sites of inflammation, it has a potent ability to induce IFNγ production and is associated with a number of pathologies associated with IFNγ-related systemic hyperinflammation (383). IL-18 is a mainly macrophage-derived cytokine that can also be produced by barrier epithelial cells. Interestingly, granzyme B found in cytotoxic granules can cleave IL-18 into an active form resulting in its downstream upregulation of IFNγ production and pro-inflammatory effects (383). However, IL-18 has been shown to also be released by osteoblasts and in this context, acts through M-CSF and not through IFNγ (384). This is likely due to the increased evidence for osteoblast differentiation at this timepoint and associated increased IL-18 production by these cells to limit osteoclast formation (384). Granzyme B was significantly elevated in

both the D28 biomaterial co-culture conditions compared to cultures of T cells with acellular biomaterial only.

IL-27 was significantly increased by D28 in both fibronectin and laminin osteoblast biomaterial T cell co-cultures and has roles in both innate and adaptive immunity. In adaptive immune responses, it promotes IFNγ production by CD4, CD8 and NKT cells (385, 386). IL-27 has also been classified as an early initiator of Th1 differentiation, as well as innate immunity responses through induction of IL-1, TNFα, IL-18 and IL-12 production by monocytes (387, 388). Significantly higher IL-27, IL-12 and TNFα were shown for D28 cellularised fibronectin co-cultures when compared to D28 cellularised laminin co-cultures implying less response to the allogenic cells on the laminin biomaterial. A role for IL-27 in inhibition of Th17 differentiation has recently been suggested in the literature but the precise mechanism of this is yet to be defined (389, 390). Finally, IL-27 has been shown to both inhibit LPS-induced osteolysis *in vivo* and significantly reduce RANKL-induced osteoclastogenesis, leading to less osteoclast differentiation, bone resorption and bone erosion (391). Increased expression of IL-27 in the supernatant co-cultures of the D28 biomaterials implies less of a bone-resorptive and, perhaps a Th17 suppressive state which would be both favourable to bone healing and allogenic cell tolerance, and IL-27 was found to be significantly increased for fibronectin over laminin biomaterials.

CXCL11 increased significantly in the D28 laminin biomaterial condition and is a potent chemoattractant for activated T cells. It causes intracellular calcium mobilisation and acts as an agonist for CXCR3 and CCR3 (392). However, whilst not significantly raised for fibronectin over acellular controls, it was significantly higher in cellularised D28 fibronectin than in cellularised D28 laminin conditions.

Finally, with regards to potent mediators of a Th1 response, IFNγ increased in the fibronectin osteoblast biomaterial and T cell co-culture, which was not the case for the D3 timepoint or the D28 laminin co-culture condition. IFNγ is a key cytokine due to its roles in inflammation, synergism with other cytokines (IL-1β and TNFα), and its ability to induce MHCI and II expression in many tissues (393). IFNγ has been shown *in vivo* to have contradictory roles in transplant responses. Early on, the absence of IFNγ is believed to cause allograft rejection due to failure of the graft microcirculation, whereas IFNγ has been shown to promote graft vessel disease later in the transplant timeline (393).

Overall, there were global increases in Th1 response-associated mediators by D28 for both biomaterials compared to fewer significant results at the early D3 MSC timepoint [Figure 5-14]. This could reflect a push towards more of a proinflammation response with increasing MSC differentiation into an osteoblast.

5.4.1.5 Th2 responses at D28 could inhibit bone resorption

Significantly increased Th2-associated analytes in the presence of fibronectin MSC and osteoblast biomaterials included: IL-4, IL-9 and eotaxin. IL-4 is the predominant cytokine of the Th2 response, helping to mediate Th2 immunity through activation of epithelial and myeloid cells (394). IL-4 and eotaxin increased significantly in both types of MSC biomaterial co-culture (laminin and fibronectin) compared to the T cell acellular control cultures. Eotaxin only increased significantly at the late timepoint in the fibronectin biomaterial, along with other Th2 mediators CCL17, IL-33 and IL-34. IL-4 is mainly secreted by activated T cells and has an antagonistic function on Th1 polarisation (395). Excess amounts of IL-4 and IL-13 are associated with an inhibition of neutrophil chemotaxis thus restricting excessive tissue damage during Th2 responses (396). IL-4 has a key role in

supporting Treg-mediated immune suppression through increased cell survival and granzyme expression by Tregs (395).

IL-9 is a cytokine that is predominantly produced by T cells and can be classified as Th2, Th17 or T regulatory in action (397). There are contradictions within the literature with regards to Treg cells ability to express IL-9. Data from mice showed FOXP3 and IL-9 co-expression in Treg cells found specifically in tolerant allografts *in vivo*, and in purified Treg populations *in vitro* (397). This however is contradicted in studies from healthy human donors in which FOXP3 expression was inhibited in Th9 conditions *in vitro* (398-400). This may reflect the known differences between human and mouse Tregs (117). Despite the inconsistencies, for all CD4+ T cell subsets, TGFβ is required to promote IL-9 production by T cells of any faction (397). Furthermore, natural killer T (NKT) cells can produce IL-9 following IL-2 stimulation, leading to NKT cells that expressed IL-4, IL-5, IL-13 and IL-9, but notably not IFNγ (397). The downstream effects of IL-9 are mainly to promote mast cell growth and production of IL-1β, IL-5, IL-6, IL-13 and TGFβ (397). At the D28 fibronectin timepoint, IL-1β, IL-6 and IL-9 were all significantly increased. IL-6 which was increased in all conditions. Other functions associated with IL-9 include; promotion of Treg immune suppressive function and induction of Th17 cell proliferation (397). The upregulation of IL-9 in fibronectin biomaterials and associated upregulation of some downstream cytokines may represent more of a Th17 response due to more of a mature osteoblast phenotype.

TSLP is pleotropic and can act on multiple cell lineages. Its predominant role is promoting Th2 immune response in allergic diseases and it is positively regulated by IL-4 and IL-13 (401). Other roles for TSLP include its ability to act directly on CD4+ T cells, and is a cytokine required for their full proliferation in response to

antigen (401). Eotaxin increased significantly in both biomaterial types at D3 and is a potent chemoattractant and induces the chemotaxis of IL-2 and IL-4 stimulated T cells. Furthermore, eotaxin upregulates ICAM-1, CD29, CD49a and CD49b on T cells resulting in T cell adhesiveness to the endothelium (402).

In addition to significant increases in IL-4 and eotaxin for the laminin MSC biomaterial and T cell co-cultures at D3, there were further increases, not seen in the fibronectin condition, for CCL17. CCL17 is categorised a T cell chemokine and has been implicated in a number of autoimmune and inflammatory diseases (403). CCL17 binds to CCR4 which is predominantly expressed by Th2 cells, but also made by Th17, Tregs, NKT cells and CD8+ T cells (403, 404). In the literature increased CCL17 has been associated with increased pain in both rheumatoid and osteoarthritis (405, 406). By D28, CCL17 was increased in both the laminin and fibronectin osteoblast and T cell co-cultures.

IL-5 appeared to trend to increased amounts in the laminin MSC and osteoblast biomaterial and T cell co-culture, as well as the osteoblast fibronectin biomaterial co-culture, however this did not reach statistical significance. This cytokine has been shown to have protective roles to prevent allograft rejection in transplant (407). An *in vitro* study demonstrated that CD4+CD25+ T cells were activated by alloantigen in combination with IL-4 to become Tregs that express the IL-5 receptor alpha (IL-5rα) and go on to express FOXP3, GATA3, interferon regulatory factor 3 (IRF3) and IL-5. Furthermore*, in vivo* IL-5 treatment was associated with cardiac graft survival in F344 rats, and this was reversable with the blocking of IL-4 and depletion of CD25+ cells (407). By D28, IL-33 had increased in both biomaterials and T cell co-cultures and was not seen at D3. IL-33 is an alarmin cytokine that is a member of the IL-1 family that can interact with a number of either Th1 or Th2 responsive cells (408). IL-33 is usually expressed by endothelial,

epithelial or stromal cells and is rapidly released in response to cellular damage or injury (408). Within my model at D28, the significant increase in IL-33 is likely from osteoblasts which are known to secrete it to reduce bone resorption (409).

Notably, no significant differences were found for any Th2 cytokine for cellularised D28 fibronectin and cellularised D28 laminin biomaterials, implying Th2 responses to allogenic cells remain the same irrespective of change in glycoprotein.

5.4.1.6 Predominant Th17 responses associated with co-culture with D28 osteoblast biomaterials irrespective of glycoprotein

Evidence of a Th17 response within the allogenic co-culture microenvironment was found at the early D3 timepoint. However, by D28, more Th17-associated cytokines were significantly increased for both biomaterials [Figure 5-14]. At all timepoints for both biomaterials, IL-6 was notably significantly increased. Similarly, CXCL1 increased significantly at all timepoints except D3 laminin biomaterials. In mice, early upregulation of CXCL1 within 3 days after transplantation of corneal allografts *in vivo* was shown to be crucial to the induction of T cell chemoattractants necessary to recruit allospecific CD4+ T cells into the graft leading to graft rejection (410). In humans, the multifunctional IL-6 has been identified as key to T cell activation, proliferation, survival and differentiation into Th17 effector cells (362). IL-6 has been shown to promote rejection and abrogate tolerance in many ways and was significantly increased in both laminin and fibronectin allogenic co-cultures, irrespective of timepoint. Firstly, IL-6 inhibits apoptosis of naïve and recently activated T cells (411, 412). Secondly, endothelial cell activation can promote a proinflammatory cytokine environment, including increased IL-6 expression which amplifies adaptive responses (362). Thirdly, IL-6 plays a pivotal role in commitment to a Th17 cell fate. Within my model, at the

early timepoint the IL-6 is likely made by both the T cells and the MSCs. IL-6 is known to be made by T cells, B cells, macrophages, dendritic cells, epithelial cells and stromal cells (413). MSCs have been shown to release IL-6 under exposure to inflammatory stimuli or interactions with immune cells (414). Furthermore, human MSCs have been found to release IL-6 leading to immunosuppression of activated T cell proliferation (415). By the later timepoints it is likely made by the osteoblasts which release it in response to bone resorption and remodelling (416).

TGFβ is crucial to both Th17 and peripheral Treg differentiation, with RORγt or FOXP3 transcription factor expression determining fate. TGFβ normally leads to predominantly peripheral Treg differentiation as FOXP3 binds directly to RORγt, inhibiting its transcriptional activation (362). However, in the presence of IL-6, this inhibition does not occur and the activated CD4+ T cells are more likely to differentiate into Th17 cells. A key inducer in humans for naïve T cell Th17 differentiation is IL-1β. IL-1β was significantly upregulated in both fibronectin and laminin biomaterials by the later D28 osteoblast timepoint in the T cell-biomaterial co-cultures compared to the relevant acellular controls. Furthermore, IL-6 can induce Th17 differentiation and was also significantly upregulated at both early and late timepoints. IL-6 in combination with IL-1β greatly enhances Th17 differentiation form naïve T cells (360).

Clinically, IL-6 has been associated with inflammation in the context of acute and chronic rejection of solid organ allotransplants (362, 417, 418). Furthermore, a decrease in IL-6 is often found following successful treatment for transplant rejection (419-421). The presence of IL-6 in PBMCs taken from renal biopsy samples has also been found to be 92% sensitive and 63% specific for predicting acute renal allograft transplant rejection (362). At the D28 later osteoblast

timepoint, key effector cytokines of a Th17 response that increased significantly were IL-21 and IL-22. Notably however, IL-17A, IL-17E and IL-17F were not elevated in the cultures with cellularised biomaterials as hallmarks of a classic Th17 response at D3. By D28 however, IL-17A and IL-17E had significantly increased in the laminin osteoblast and T cell co-cultures, only IL-17E had increased for the fibronectin D28 condition. When comparing D28 cellularised fibronectin biomaterial to D28 cellularised laminin biomaterial there were significant increases in IL-21.

In the D28 osteoblast laminin and fibronectin biomaterial T cell co-culture there were also increases in CXCL6. CXCL6 is a chemoattractant for neutrophilic granulocytes and interacts with CXCR1 and CXCR2 in humans, to promote repair and regeneration of tissues after ischaemia-reperfusion injury by regulating apoptosis (422).

Other analytes that increased in the T cell biomaterial co-culture compared to the T cell acellular cultures by D28 for both biomaterials were CXCL1 and IL-22. CXCL1 is implicated in a number of inflammatory diseases and primarily functions to increase the number of immune cells by activation of CXCR2 (423). Notably, CXCL1 was significantly higher for D28 cellularised fibronectin biomaterials versus laminin. IL-22 plays many key roles in tissue regeneration and altered IL-22 activity can lead to inflammatory diseases, poor wound healing and infections (424). The primary source of IL-22 production are CD4+ T cells and its main target of action are epithelial cells (425). Chung et *al*. demonstrated that IL-22 at both the protein and mRNA level is expressed by specific T cell subsets that produce IL-17 (Th17 cells) and Wolk et *al*. found increased IL-22 expression specifically with Th1 polarisation (426-428). The presence of this cytokine in the D28 biomaterial cultures and not the D3, suggests a greater Th1/Th17 response to the more

differentiated cells IL-22 production is usually triggered by increased IL-21, IL-12, IL-1β, IL-6 and TNFα, the majority of which were significantly elevated over controls by the D28 timepoint (425, 429).

These data support increasing Th17 responses to both biomaterials with increasing differentiation of the MSCs into osteoblasts. Classical Th17 cytokines IL-17E, IL-22, CXCL1, CXCL6 were increased at the D28 timepoint for both fibronectin and laminin conditions, with additional increases in IL-17A for laminin and IL-21 for fibronectin co-cultures at D28. IL-6 was significantly high in the presence of allogenic MSCs at D3 irrespective of glycoprotein and this persisted to D28.

5.4.1.7 Regulatory responses were low in the presence of MSC-biomaterials but more evident by D28

Tregs act to regulate tissue repair and regeneration through their interactions with both innate and adaptive immune cells following injury (139). Furthermore, Tregs undertake tissue-specific repair and notably do so in bone by limitation of osteoclastogenesis (365). Activated Tregs also exhibit perforin-granzyme cytolysis against a host of targets including CD4+ and CD8+ effector T cells in response to contact suppression (139). The only significant regulatory-associated chemokine upregulated at the early timepoint was CCL2 which is a macrophage-derived chemokine also produced by dendritic cells. CCL2 can recruit Tregs into tumour microenvironment (TME) sites and binds to CCR4 which is expressed primarily by T cells: it is found on Th2, Treg and Th17 effectors (430). The recruitment of Tregs to the TME enhances tumour immune evasion (430). Other notable Treg associated cytokines include high IL-10, high IL-35, with low IL-2. My data show that IL-10 and IL-2 were not significantly increased at D3, and IL-35 was

undetectable in the Luminex, across all experiment timepoint conditions. This therefore does not support the typical cytokine expression of a prominent Treg response. TGFβ was not included within the Luminex panels performed in this experiment, and as a key mediator of Treg differentiation, is notably absent. This was due to its incompatibility with the other three Luminex panels due to cross-reactivity between the antibodies and other analytes.

The D3 laminin MSC biomaterial and T cell co-culture had a different regulatory response with significant increases in only sCD137 compared with the acellular biomaterial. Activation of naïve CD4+ and CD8+ T cells after engagement of the TCR with its antigen on an APC also requires a second signal from a co-stimulatory molecule for full T cell activation. sCD137 acts as an inhibitory signal to CD137 signalling, which in turn is a costimulatory molecule for T cell activation and was found to be increased in patients after renal allograft versus healthy controls. Furthermore, along with sCD30, sPD1, sPD1L, sCD40 and sCD40L it was found to be predictive of poorer graft survival, if elevated at 3 months (431). Within the laminin biomaterials at D3, not only was sCD137 elevated, but sCD40L was increased and the flow cytometry data showed an increase in PD1. By D28, sCD137, sCD40L, CCL22 and IL-10 were significantly increased in both biomaterial osteoblast conditions. IL-10 encourages tolerance in T cells by selective inhibition of the CD28 co-stimulatory pathway (432). The function of IL-10 in transplant responses is not fully defined, however it is known to play an important role in maintaining peripheral immunotolerance and it was notably increased for all late timepoint co-cultures (433). An *in vivo* study in mice showed that depletion of IL-10 suppressed FOXP3+ T cells, reduced airway allograft microvasculature and propagated a proinflammatory phase (433). Increased IL-10 may prolong allograft survival and contribute to prevention of rejection responses

through suppression of T cell and antigen-mediated immune responses (434, 435).

5.4.1.8 Several activation-associated cytokines are increased in co-culture with D28 osteoblast biomaterials versus with acellular biomaterial cultures

Only one molecule, sFas, in the activation/cytotoxic category was increased in the T cell-MSC co-cultures with fibronectin biomaterials compared to acellular controls at the early time point [Figure 5-14]. sFas was also significantly higher in the laminin MSC co-cultures at the early timepoint, however, sFasL was not significantly increased. Allograft rejection in liver transplants is mediated by Fas/FasL triggered apoptotic cell-death. Higher expression of sFas was found in patients with acute allograft rejection and a reduction in sFas was reported after rejection treatment (436). Similarly, an increase in sFas levels was found in patients with clinically relevant acute GvHD post-allogenic bone marrow transplantation (BMT) (437). Conversely, a study of acute cardiac allograft rejection in humans implicated heightened expression of FasL and Fas in rejection responses but found no significant changes in sFas (438). FasL remained nonsignificant across both early and late timepoint co-culture results.

For laminin cellularised biomaterials, additional increases were found at D3 in sCD40L, as well as perforin. The CD40-CD40L costimulatory pathway leads to the production of IL-10 and IL-12 which can modulate T cell responses (439). sCD40L is shed by activated T cells and has been shown *in vitro* to promote the proliferation of myeloid-derived suppressor cells, inhibit autologous T cell proliferation and reduce their ability to secrete IFNγ (440).

By D28, there was evidence for more activation/cytotoxic-associated analytes with increases in sCD40L, granzyme B, sFas and perforin and CXCL13 for the fibronectin osteoblast co-cultures. In the D28 laminin osteoblast co-cultures, further significance was found for granzyme A. Perforin is a glycoprotein responsible for pore formation in cell membranes and facilitates target cell death by facilitating the transfer of granzymes to efficiently destroy the cell (441). The presence of perforin, granzyme A and B in the D28 laminin osteoblast co-culture does not support a favourable picture for ongoing cell survival in this co-culture condition. Granzyme B is an effector molecule associated with T cell responses, often co-expressed with IFNγ and perforin (442). During *in vitro* mixed lymphocyte reaction experiments of human alloresponses, it has been shown that proliferation responses are equivalent amongst CD4 and CD8 T cells but production of effector molecules, including granzyme B, was highest in CD8+ T cells, highlighting the threat that these cells pose to allografts (442). Granzyme-dependent killing is well established in the literature and defined as quick, efficient and mediated via intracellular, redundant cell-death pathways (443). Granzyme B leads to either direct activation of caspases 3 and 7 or indirect BID-dependent mitochondrial permeabilisation, ultimately causing caspase-mediated degradation leading to apoptosis of the cell (443-445). Notably, granzyme B has been shown to exhibit cytotoxic activity at even low concentrations (443).

An expanding role for granzymes as potential soluble mediators of inflammation has recently been raised. Patients with rheumatoid arthritis presenting with raised granzyme B levels had more severe erosive joint disease at an earlier point in the sequalae of the disease process (443, 446). Interestingly, granzyme B has been shown to cleave a multitude of ECM components, including fibronectin, vitronectin and laminin (447, 448). Cleaving of ECM proteins may promote detachment-

induced cell death or anoikis and the targeting of the ECM may explain the granzyme B-mediated increased joint erosion seen in rheumatoid arthritis (446). The increase in granzyme B within the D28 osteoblast biomaterial and T cell co-cultures is likely due to the activation of CD8+ T cells as shown in the flow data. The increase in extracellular granzyme B within these cultures may have deleterious effects on the biomaterial glycoprotein if granzyme B-mediated cleavage occurs.

5.4.1.9 Growth factor production is promoted in co-culture with D28 biomaterials

At D3 fibronectin MSC biomaterials in co-culture with T cells led to higher amounts of IL-2 and VEGF-A than T cell cultured with acellular biomaterials. IL-2 stimulates the proliferation of T cells, NK cells and B cells (449). For laminin, significant increases were seen in IL-3, VEGF-A and PDGF-AA/BB. By D28, both biomaterial glycoprotein conditions saw an increase in significantly expressed growth factors [Figure 5-14]. These include FGF2, M-CSF, IL-3, IL-11, IL-15, FLT3L, and EGF.

IL-2 is a potent T cell growth factor that has many roles that have been largely defined in mice. Conflicting literature proposes potential opposing roles, with T cell proliferation greatly expanded under IL-2 *in vitro* conditions but conversely, IL-2 deficient mice show enhanced T-cell mediated autoimmune diseases likely due to less Tregs as IL-2 is required for Treg survival (450-452). IL-2 is critical to the development of CD4+CD25+ regulatory T cells and thereby supports self-tolerance and reduces autoimmunity through suppression of T cell responses (453). Much less is known about IL-2 deficiency effects in humans, however a male child deficient in the IL-2Rα gene has been described and was immunocompromised with signs of T cell autoreactivity (454).

IL-11 is a member of the IL-6 family of cytokines and is secreted by bone marrow mesenchymal cells (455). VEGF-A is a well-studied mediator critical to vasculogenesis and repair (456, 457). It has been shown to be increased in human MSCs and is associated with promotion of angiogenesis and increased stimulation for mineralisation suggesting it acts as an autocrine factor promoting osteoblast differentiation (457).

5.4.1.10 Fibronectin biomaterials promote greater osteoblast differentiation by D28 than laminin biomaterials

Osteoprotegerin (OPG) is a member of the TNF receptor superfamily and functions as a soluble decoy receptor for receptor activator nuclear factor-κB ligand (RANKL), preventing osteoclastic bone resorption (458). OPG is produced by bone and stromal cells and was significantly increased in both the laminin and fibronectin MSC biomaterial co-cultures with the T cells at all timepoints. Osteotropic factors PTH, prostaglandin E2 and IL-11 induce the formation of osteoclasts by upregulating RANKL expression on stromal cells and immature osteoblasts (458). RANKL then binds to RANK on osteoclast precursors inducing their formation and survival (459). PTH was undetectable in the Luminex results, however already at the early timepoint increases in IL-11 were found in the co-cultures with the fibronectin MSC biomaterials. IL-11 continued to be significantly expressed at the D28 timepoint for both biomaterials. OPG blocks the RANK-RANKL interaction inhibiting osteoclastogenesis, promoting increased bone density and bone volume, and was significantly upregulated in all cultures (460).

Significant increases in expression of DKK1 were found in both laminin and fibronectin MSC biomaterial conditions compared to acellular controls at both timepoints. DKK1 is mainly expressed by bone-marrow derived MSCs to

antagonise the canonical Wnt/β-catenin signalling pathway, but the role of DKK1 in osteoblast function has not been fully defined. The Wnt/β-catenin signalling pathway regulates a host of cellular functions including proliferation, differentiation and survival (461, 462). Studies suggest DKK1, as a negative regulator of the Wnt signalling pathway, causes inhibition of cell proliferation and osteoblast maturation (461, 463, 464). Furthermore, DKK1 causes calcium influx and activation of the calcium/calmodulin dependent protein kinase II alpha (CAMK2A)-cAMP response. This leads to CREB1 phosphorylation, translocation into the nucleus, and action as a transcription factor to regulate expression of genes linked to osteoblast survival, proliferation and differentiation (465). In summary, interpretation of DKK1 is debated in the literature and whilst classically deemed to have a negative effect on osteoblast differentiation, contradictory reports highlight the importance of DKK1 on bone formation (466, 467).

SOST was found at low but significantly higher levels in both fibronectin and laminin biomaterials at all timepoints compared to the acellular biomaterial controls. SOST is a Wnt inhibitor produced largely by osteocytes, human hypertrophic chondrocytes and to a lesser extent osteoblasts, which inhibit BMP-induced bone formation as a protective mechanism to prevent excess bone mass (463, 468). SOST has been implicated in significant bone disease states, including high SOST levels in patients with pathological fractures (463). BMP-2, 4 and 6 induce SOST expression in mouse and human osteogenic cells, to prevent excessive exposure of skeletal cells to BMPs (468). SOST at levels of 0.5-1μg/ml was shown to increase adipogenic differentiation of primary mouse bone-marrow derived MSCs (469). A mean SOST level of 138.6pg/ml (laminin) and 110.7pg/ml (fibronectin) was found in my D3 co-culture, which is much lower than those reported to be functionally produced by osteocytes *in vitro* (469). By D28 these

remained non-biologically functional at 165.7pg/ml (laminin) and 170.18pg/ml (fibronectin) and not suggestive of osteocyte formation over osteoblasts. Furthermore, OCN and OPN, as markers of late osteoblast differentiation, prior to osteocyte formation, were not significantly raised in the fibronectin or laminin MSC culture at D3. At D28 conversely, significant increases in OPN and OCN were found for fibronectin osteoblast biomaterials supporting the immunofluorescence data and evidencing osteoblast differentiation in the presence of fibronectin. However, in D28 laminin conditions there was no significant increase in OPN compared to the acellular biomaterial control, implying potentially less osteoblast differentiation versus fibronectin. OPN is not exclusively made by osteoblasts, it is a multifunctional phosphoglycoprotein produced by T, B, NK osteoblasts, epithelial cells and neurons (470). Specifically, activated Th1 cells produce OPN which induces expression of IL-12 and inhibits IL-10 (353, 471). This is reflected in the laminin no MSC biomaterials with T cells co-culture at D3, in which significantly higher OPN was found in the absence of any MSCs.

Overall, these data support that osteoblast differentiation had occurred by D28 in the fibronectin biomaterials perhaps to a greater degree than on the laminin biomaterials, which supports the subtle differences shown on OCN and OPN IF microscopy. However, the presence of significantly increased DKK1, whose roles regarding osteogenic fate and function, to either inhibit osteoblast differentiation entirely or conversely support bone formation, raise concerns as to MSC fate under these conditions *in vivo*.

5.4.2 Biomaterial micro-environment modulation with conditioned proinflammatory media reduces cell proliferation and survival

Having manipulated the biomaterial with laminin and found some evidence for altered cytokine release profiles from the T cells at D3 versus D28 [Figure 5-14], I wanted to modulate the microenvironment to represent different durations of proinflammation and assess for any altered T cell response.

A fracture microenvironment is a proinflammatory one and the initial responding cells to trauma or surgical implantation are macrophages (345, 472, 473). I therefore used M1 macrophage supernatant supplemented with MSC media as proinflammation conditioned media and assessed the impact of this microenvironment on the T cells using my established modelling.

At the D3 timepoint, there were no differences between T cell activation surface marker expression to MSC fibronectin biomaterials grown for 3 days in proinflammation or normal conditions. Similarly, no significant differences were found in the transcription factor expression of the T cells at this timepoint. Furthermore, no obvious physical differences were found on inspection of the cell culture at this time point between conditions, and, by eye, the cells appeared to be growing as with all previous experimentation. Given the proinflammatory microenvironment of a fracture site, and the need for tolerogenic cells that can withstand that environment, this is reassuring for the potential use of MSC-based therapies. Human T cells within a M1 proinflammatory environment do not appear to increase their activation responses or differentiation fate in the presence of allogenic cells.

In contrast, by D28 significant differences were found in T cell responses to cellularised fibronectin biomaterials that had been exposed to 0, 3, 14 or 28 days of proinflammatory conditioned media. Firstly, it is important to highlight the cultures that were exposed to 14 or more days of proinflammatory media were less viable. The majority of cells within these cultures died and they were non-confluent in the 24 well plate. This was found to be significant in the 28 day inflammatory supernatant exposed group compared to the control (no inflammatory media) group. Of the cells that did survive, they had different cell morphology to the usual D28 osteoblast cultures with more spindle shaped cells that were more spread out, due the significant reduction in cell numbers. The surviving cells when imaged using IF microscopy did subjectively appear to express similar amounts of OPN, but potentially less OCN and MHCII at 14 days inflammation-exposed versus control.

The finding of less MHCII expression in the 14 days inflammation-exposed group combined with a lower cell number, is reflected in the flow cytometry findings at this timepoint. There were significantly fewer CD25+ CD4+ T cells in this group compared to control. Furthermore, CD4+ ICOS MFI was also reduced in the 14- and 28-days exposed groups. PD1+ expression was significantly lower in CD4+ T cells in the 28 days group and in the 14 days group for CD8+ T cells. With lower levels of MHCII within the co-cultures this would correlate with the results seen on flow cytometry at this timepoint. Notably, no group had increased expression of T cell surface activation markers above control levels, implying that the response to the allogenic cells is the driver and that this is not augmented by the presence of proinflammation. Supporting data from analysis of the T cell transcription factors showed reduced RoRγt, T-bet and FOXP3 expression in the 14 days inflammation exposed group and reduced RoRγt in the 28 days group. Again, less MHCII

expression and less allogenic cells would explain lower expression of Th1 or Th17 effectors and Tregs.

In conclusion, modulation of the immune microenvironment to a predominantly M1 proinflammatory state did not alter the T cell response to the allogenic MSC fibronectin biomaterials at the early D3 timepoint. However, the presence of extended proinflammation greatly affected the survival of the cultures by D28, leading to reduced allogenic cell burden and reduced T cell response compared to controls. Finally, the cells that did survive, were able to express OPN, OCN and MHCII but perhaps to a lesser amount than no inflammation controls. This implies that in proinflammatory microenvironments, such as a fracture, the MSCs within the biomaterial may struggle to proliferate and survive, reducing the number of cells available to differentiate into osteoblasts to rebuild bone. However, reassuringly, of the cells that do survive the proinflammation, they do show evidence for osteoblast differentiation and therefore the density of cell seeding within the biomaterial, would be an important consideration.

Chapter 6 Final Discussion

The aim of this PhD was to investigate human T cell immune responses to functionalised allogenic MSC biomaterials for bone regeneration, on the path towards clinical translation. To do this, firstly an *in vitro* model of human T cell immune responses was established and validated. Once established, the model was used to define T cell responses to fibronectin MSC biomaterials across their differentiation into osteoblasts. The model was then used to try to further understand the T cell response and function. This included a deeper examination of the T cells themselves, with analysis of their transcription factors to delineate Thelper subsets during the response to the biomaterial, as well as Luminex analysis of their cytokine release, as markers of the T cell function. Finally, the model was used to answer questions related to immunomodulation. First, can material modulation with laminin alter osteoblast differentiation and the associated T cell response? Second, does a proinflammatory environment, akin to that found in a fracture bone healing microenvironment, lead to altered differentiation and T cell responses?

This investigation has a tight clinical focus, namely the delivery of a bioengineered regenerative medicine solution for bone healing, reconstruction, and digital or limb lengthening possibilities. However, the potential impact of the human host immune response is of such translational significance and therapeutic potential, that its fundamental biology must first be understood, modelled, and adapted where necessary. Therefore, this thesis addresses *in vitro* modelling and fundamental biology, in response to highly promising bioengineered therapeutic products that are beginning to enter ‘first in human’ characterisation. Ultimately, the clinical utility of these regenerative strategies will rely on establishing factors to modulate the

biomaterial, or the local microenvironment, to promote repair phenotypes to improve biomaterial tolerance, functionality and patient outcomes. Control of the local immune response tailored to a specific biomaterial, in a specific tissue, for a specific local environment offers the potential to engineer biocompatible biomaterials.

Biomaterial tolerance is critical to facilitate use of ‘off the shelf’ biomaterials containing allogenic donor MSCs, for use at time of surgery. Use of donor and therefore allogenic MSCs has many advantages over using the patient’s own autologous MSCs. These include ready availability for immediate or high volume use, mitigating possible low bone marrow yield from certain individual donors or patient groups, and means they would be available even for patients contraindicated for bone marrow aspiration. There are also regulatory and pragmatic benefits for use of fully characterised, banked cell products. A greater understanding of the adaptive T cell immune response to allogenic MSC biomaterials, for bone regenerative therapies, is therefore critical to their clinical translation.

6.1 Modelling human T cell responses *in vitro*

The Engineering and Physical Sciences Research Council (EPSRC) funded LifETIME Centre for Doctoral Training, had the priority to replace, reduce and refine use of animal derived components and models, for improved clinical translation. Despite clear scientific and ethical imperative to move away from animal modelling, there remained a lack of T cell *in vitro,* animal-free modelling of human host responses to allogenic biomaterials, within the literature. Consequently, this body of work has developed and validated a novel, ethical model, that incorporates human T cells and APCs, for the broader investigation of host responses to regenerative medicine products and bioengineered constructs.

Furthermore, a strength of this work is that it is not solely reliant on an early timepoint modelling, and is instead, able to be undertaken at later, longer term timepoints, for the accurate assessment of T cell responses over MSC differentiation into more mature phenotypes.

The first results chapter [Chapter 3] established the methodology for ‘priming’ human T cells so that they may respond, in *in vitro* conditions, to subsequent antigen stimulus. Within *in vivo* conditions, naïve T cells are ‘primed’ in the lymph nodes, when APCs show them foreign antigen, after which they subsequently can re-enter the circulation and mount targeted antigen-specific responses. These data show that T cells can be efficiently ‘primed’ using an aCD3/aCD28 activator *in vitro,* rendering them capable of mounting subsequent activation responses (defined by increased CD25, ICOS and PD1 expression). These T cell activation responses occurred when the T cells were presented with either allogenic antigen or following further exposure to aCD3/aCD28 stimulus. Additionally, in the absence of further stimulus, there is no evidence of ongoing activation from the T cells (evidenced by low CD25 and PD1 expression). The model was established through a series of extensive, optimisation steps before subsequent validation through assessing response to allogenic macrophages. The T cells mounted increased activation responses to the allogenic macrophages over 5 days *in vitro* culture. The optimised methodology for the T cell ‘priming’ was then tested against different biomaterial constituent parts and showed no increased response to the inert components. These included PEA coating, glass, fibronectin or BMP-2 in various combinations. Responses to allogenic cells were detected by 5 days co-culture with the ‘primed’ T cells (7 days *ex-vivo*).

The novel, human T cell, *in vitro* model created is capable of being used with any biomaterial to measure firstly, the extent of the T cell activation response, and

secondly, the type of response, when used in combination with intracellular staining flow cytometry and Luminex analysis. This work has therefore created an *in vitro* tool through which immunomodulation may be modelled to assess the human T cell responses on the quest towards tuneable, tolerable biomaterials for bone regeneration. Furthermore, the model could be used to predict a patient-specific response to a proposed implant or regenerative cell product, allowing for *a priori* therapeutic modulation and deliverance of personalised medicine. Ultimately, this work delivers a functional *in vitro* model, capable of revealing extent and type of human T cell responses to any bioengineered construct. The scope for future applications is broad, for further acquisition of knowledge relating to T cell responses, but may also serve as a gatekeeper model for use in translational pipelines before first in human clinical trials.

6.2 Human T cell immune responses to MSCs on bioengineered biomaterials as they differentiate into osteoblasts

Having created the model for testing T cell activation, (via CD25, ICOS and PD1 expression), T cell responses to a specific functionalised allogenic MSC biomaterial were investigated. The Salmeron-Sanchez group at the University of Glasgow have established a PEA coating that can be functionalised with fibronectin, which adsorbs BMP-2, which directs MSCs to an osteogenic differentiation path over 28 days (67, 331). IF microscopy for OPN and OCN, ALP and alizarin red assays and RT-qPCR assessment, confirmed osteoblast differentiation by D28 up to D35 of *in vitro* culture. Utilisation of the *in vitro* model allowed for interrogation of T cell responses to the D3 MSC undifferentiated biomaterial, as well as the differentiated osteoblast D28 and D35 biomaterials.

These data support evidence of T cell activation responses to the D3 MSC biomaterials (increased CD25 expression), with evidence for a broader T cell response by D28 (increased CD25, ICOS MFI and PD1 expression) with increasing cell differentiation.

Further investigation of the T cells to characterise their Teffector differentiation was undertaken, using intracellular staining flow cytometry to analyse their transcription factors. These data demonstrate increased proportions of CD4+CD25+FOXP3+ cells in the presence of allogenic MSC and osteoblast biomaterials. However, as I have discussed previously, it is difficult to conclude whether all the FOXP3+ cells were Tregs and therefore likely to be immunosuppressive and induce a pro-tolerance environment around the functionalised biomaterial. An alternative explanation is that expression of FOXP3+ cells merely indicated recent TCR activation signals and these cells then could go on to form Teffector, rather than regulatory T cells (139, 141). Furthermore, if these cells were indeed Tregs, it is unclear whether they were surviving Tregs that were retained directly from the PBMC isolation and were subsequently just expanded within the *in vitro* cultures. Alternatively, they could be induced Tregs that differentiated within the model cultures, in response to the MSC biomaterial from naïve CD4 T cells, which would be more favourable suggesting a pro-tolerance effect of the MSC biomaterial.

Several approaches could be undertaken to clarify this distinction. Firstly, a cell sort of purified naïve T cells could be undertaken at the start of the experiment (as discussed in Chapter 3). To do this, T cells would be sorted based on expression of the IL-7 receptor (CD127) at high levels and exclude cells that express a Treg phenotype of CD127-low, CD25+ (474). Notably, this method would not involve measuring FOXP3 expression at this timepoint, due to the need to fix and

therefore kill the cells to be able to look for the transcription factor FOXP3, via an intranuclear stain. Secondly, a transcriptional analysis of the T cells could be undertaken from the model co-cultures, to provide a broader understanding of their function (475, 476). Thirdly, an option would be to sort the T cells after the co-cultures with the allogenic biomaterials and then add the sorted post-culture T cells to an *in vitro* assay, to test their ability to suppress other cells, as a hallmark of Treg function (477). This however has some caveats as the cells have already been ex-*vivo* for 7 days by the end of the existing model co-cultures and further co-cultures, without the addition of cytokines, would likely result in poor cell viability. Furthermore, addition of cytokines and growth factors alter Teffector cell differentiation, clouding ultimate conclusions on whether Tregs had differentiated within the original cultures.

6.3 Immunomodulation approaches

These data demonstrate that the model can be used to test changes to the biomaterial, and to the culture microenvironment, to investigate different approaches to immunomodulation that may impact on the biomaterial and T cell interactions.

The change of the biomaterial glycoprotein from fibronectin to laminin did not ultimately result in any biologically significant differences in T cell activation based on T cell surface marker upregulation. However, more subtle functional differences were detected through the analysis of the co-culture supernatants. Both laminin and fibronectin MSC biomaterials promoted a predominantly Th1 and Th17 response, however laminin biomaterials were associated with more evidence for cytotoxic responses, with upregulation of granzyme A, granzyme B and perforin by D28. When comparing allogenic D28 fibronectin biomaterials with allogenic D28

laminin biomaterials, there was some evidence for increased Th1 and Th17 responses to fibronectin, over laminin, cellularised biomaterials (significant increases in TNFα, CCL7, CXCL9 and CXCL11). Furthermore, laminin biomaterials revealed less evidence for successful osteoblast differentiation by D28 with significantly lower OPN expression. What can be concluded from these data is, that by changing the biomaterial glycoprotein to laminin, less osteoblast differentiation occurs and therefore the presence of fibronectin is clearly a key component for promoting bone regeneration within this construct. However, regarding the T cell responses to the two glycoprotein allogenic biomaterial configurations, no differences were found at surface activation marker expression level, with only subtle differences detected in the cytokine analysis. In summary, both fibronectin and laminin cellularised biomaterials led to a predominance for a significantly increased Th1 and Th17 response over acellular matched controls.

Growth of MSC biomaterials within a proinflammatory microenvironment, was deleterious to their proliferation, growth and survival as demonstrated with these data. The conditioned ‘proinflammatory’ media was designed to mimic the fracture microenvironment with high levels of IFNγ, TNFα, IL-6, IL-8, IL-10, IL-12 and various other cytokines associated with acute inflammation responses to trauma (478, 479) [Appendix 4, 7.4]. Of note, the ‘proinflammatory’ media will have contained a small proportion of other immune cells (beyond T cells) that may also contribute to the inflammatory mediators in the supernatant. This is because it came from a mixed population of PBMCs from which the monocytes were differentiated into macrophages over 8 days, but at no point were the monocytes isolated and purified. Arguably, this greater represents the fracture microenvironment cytokine milieu, as a mixed population of immune cells are present in response to the physiological trauma.

These data evidence a significant reduction in MSC cell number by D28 co-culture with proinflammatory media compared to normal culture media conditions. Of the MSCs that did survive till D28, most did differentiate into osteoblasts (shown by increased OCN and OPN levels) as well as immunofluorescence evidence of MHCII expression. In concordance with the reduced MSC cell numbers, a reduction in T cell responses was also found with increasing exposure to proinflammatory conditioned media. This raises concerns about cell engraftment and viability in a hostile immune fracture microenvironment in the acute phase of the immune response to injury. Bone regenerating MSC biomaterials will be implanted and used most likely within the first 48 hours after patient bone injury and therefore it is imperative that they can engraft, survive and differentiate within the bone injury immune microenvironment.

Issues with MSC engraftment with target tissues remain an ongoing challenge within the biomaterial literature (480, 481). Kean *et al.* in their review on the subject noted the ambiguity seen in the efficacy of MSC therapies in both animal studies and clinical trials, noting ineffectiveness or merely temporary efficacy, that the authors proposed was due to poor application of MSCs (480). They highlighted that very few studies quantified MSC engraftment and those that did, reported poor engraftment efficiency. Furthermore, quantification of MSC engraftment can be via a multitude of *in vivo* or *ex vivo* methods, and all the different approaches require consideration for feasibility, effect on MSC proliferation, and differentiation (482-485). *In vivo* human allogenic MSC studies are limited, but fewer than 1% of MSCs administered by intravenous (IV) injection into children with osteogenesis imperfecta were detected within the target organs by PCR, highlighting the need for local application and deliverance of MSC-based therapies (486, 487). This finding was replicated for IV MSC therapy administered for treatment of graft

versus host disease (488). Ultimately, the vast majority of MSC-based trials to date have been for safety and therefore, efficacy has been a secondary endpoint (489). The lack of successful long term MSC engraftment to date has been attributed to a raft of different reasons including, cell death, wash out, or rejection (mediated either immediately by the innate system, or later via becoming targets for adaptive immune responses after MSC differentiation) (480).

6.4 Future applications of the model

Future potential uses of the *in vitro* human T cell modelling include testing different immunomodulation approaches within engineered constructs, including means to enhance the immunomodulatory effect of MSCs. It is therefore pertinent to summarise the immunomodulatory characteristics of MSC behaviour that relate to MSC transplantation with biomaterials.

MSCs have been shown to release soluble factors capable of influencing local immune responses, these include indoleamine 2,3dioxygenase, nitric oxide, TGFβ and prostaglandin E2 (490-493). Further studies demonstrated that MSCs in isolation can inhibit allogenic human T cell expansion within *in vitro* co-culture but that this effect can be reversed with the addition of TGFβ and hepatocyte growth factor (248, 494). Finally, proinflammatory factors such as IFNγ and TNFα affect MSCs ability to release regulatory suppressive factors (495). The presence of soluble factors around the MSC biomaterial implantation site, will undoubtedly therefore affect the MSCs regulatory behaviour, and could be further investigated with this modelling.

The adsorption of anti-inflammatory, pro-repair cytokines, such as IL-10, could be incorporated within the biomaterial. These would then be tested over the

differentiation of the MSCs into osteoblasts over 28 days to assess for maintenance of osteoblast differentiation phenotype, a push to a more regulatory, tolerance response and an associated reduction in T cell activation markers detected by the modelling. The adsorption would need to be quantified and characterised on the biomaterial coating, it would then need to be assessed for its release over time and biological activity. A host of key cytokines could be tested in isolation or in combination to try to modulate the local microenvironment around the implantation site, through material-driven methods. However, effect on osteoblast differentiation and biomaterial efficacy would need to be re-characterised.

Alternative uses for the model would be to test different bioengineered materials, beyond the PEA fibronectin (or laminin) MSC biomaterials used within this thesis. Firstly, different biomaterial surfaces and topography are known to alter immune cell interactions. For example, Christo *et al*. demonstrated *in vitro* that different surface nanotopography leads to enhanced neutrophil production of matrix metalloproteinase-9, and a decrease in macrophage proinflammatory cytokine secretion (204). The effect of nanotopography, amongst other altered surface chemistries, could be further investigated, specific to T cell responses, using my model system.

Secondly, a different growth factor adsorption, such as VEGF for promotion of neovascularisation within the model, could be investigated to assess for any effect on T cell responses. Beyond human immune responses to bioengineered constructs, vascularisation remains an additional unmet challenge in regenerative research. Induction of angiogenesis at the biomaterial implantation site and subsequent neovascularisation of the biomaterial, can be guided by surface topography or modification with angiogenic substances (496). In a human *in vitro*

study, bone-marrow derived stem cells were found to express more VEGF after 21 days on surfaces with high roughness (497). *In vivo* animal models have demonstrated dose dependent angiogenic responses with VEGF and the ability to deliver bioactive VEGF through biomaterials (498-501). Notably, the literature lacks studies pertaining to subsequent effect on T cells of VEGF-loaded biomaterials, within the context of bone regeneration. However, VEGF is known to directly impact on effector T cells as *in vitro* activated T cells and tumour-infiltrating *in vivo* T cells express the VEGF receptor-2 (VEGFR-2)(502) . VEGF can directly suppress T cell proliferation and cytotoxic activity via this receptor and therefore, the effects on overall interaction of angiogenic biomaterials with the immune system, could yield fresh insight into improved biomaterial immune tolerance (502).

Thirdly, my modelling is based upon T cell interactions with the bioengineered coating with MSCs adsorbed in 2D cell culture. Future model applications could be to work within a 3D scaffold culture to try to better emulate the *in vivo* applicability of an implanted biomaterial within a 3D human bone, critical defect. Traditionally, 2D *in vitro* models or animal *in* vivo models have been employed to investigate bone regeneration and each approach has limitations that may affect clinical applicability (503, 504). 2D models are still widely used due to feasibility reasons and the simplicity of their design, however a major drawback is that they lack the physiological architecture of bone tissue. 3D cell models are therefore favoured, to better capitulate the 3D microenvironment and structure of bone, when modelling biophysical processes related to regeneration approaches (503, 505, 506). Animal *in vivo* models on the other hand do provide a complete biological system to investigate biomaterials within, but these carry the burden of high cost, low throughput, ethical considerations and poor clinical correlation to humans, due to

interspecies differences highlighted previously within this thesis (503). Ultimately, demand is high for robust, reliable evaluation methodology for modelling biomaterials and providing precise insight into their biocompatibility. Having optimised this T cell model within 2D culture, application of this to 3D culture using PEA/FN/BMP2+ coatings applied to various 3D scaffolds could be trialled. The described T cell modelling then could be repeated in culture with the 3D coated MSC biomaterial scaffolds and T cell responses understood and appreciated within a 3D microenvironment. Finally, modelling could be undertaken in 3D to better recapitulate the fracture site by using the bioengineered construct with bone within an *in vitro* culture (e.g. bone-construct-bone), with subsequent assessment of T cell response across a modelled critical bone gap.

6.5 Concluding remarks

The next frontier on the path to the clinical translation for bioengineered allogenic stem cell based regenerative therapies, will be promotion of short-term tolerance and successful incorporation of biomaterial with the host. With bone regeneration, the MSC biomaterials will act as a scaffold to bridge areas of critical bone defects and provide preliminary stromal cells to the area to form osteoblasts. Whilst ultimately, allogenic, the constant influx of the patient's own MSCs to the environment and ongoing osteoclastic resorption facilitating bone turnover, will enable the cells to ultimately be replaced long term by the patient's own autologous cells. These data support evidence for mixed human T cell responses to allogenic MSC biomaterials by D28, but poor survivability in the context of proinflammation. Therefore, further research is needed to better understand the responses to inflammation and facilitate the navigation of these extreme acute injury microenvironments, to enable the MSCs to proliferate and differentiate within a human host. Only with a better understanding of the human T cell responses to

the MSC biomaterials within these context-appropriate microenvironments, will we be closer to successful clinical trials and potential new therapeutic treatments for patients with critical bone loss.

6.6 Ethical approval

University of Glasgow Research Ethics was applied for and awarded in 2020 for 5 years under application ID: 300200112.

Chapter 7 Appendices

7.1 Appendix 1: Table of Reagents Used

Reagent	Company	Catalogue number	Added
DPBS (1x)	Gibco	Cat 14190-094	Without calcium or magnesium
Serum free RPMI	Gibco	Cat 31870-025	With pen/strep and L-glutamine added
T cell culture media	n/a	n/a	RPMI with 5mls pen/strep, 5mls L-glutamine and 10% FCS added
Foetal Calf Serum	Gibco	Cat 10270-106 Lot: 42F2190K	
MSC Growth Medium 2 (fast media)	Promocell	Cat C-28009	
DMEM with 4.5g glucose, L-glutamine, sodium pyruvate	Sigma-Aldrich	Cat D5796	5mls of pen/strep and 10% FCS
DMEM with 1g glucose, L-glutamine, sodium pyruvate	Gibco		5mls of pen/strep and 10% FCS
MSC media (normal media)	n/a	n/a	DMEM with 4.5g glucose, L-glutamine, sodium pyruvate, 5mls of non-essential amino acids, 10% FCS, 5mls pen/strep, 0.47ml of amphotericin B
MSC media (double concentration)	n/a	n/a	DMEM with 4.5g glucose, L-glutamine, sodium pyruvate. Add

			8.75ml of glucose solution (8g/L). Add 10mls of non-essential amino acids, 10% FCS, 10mls pen/strep, 0.94mls amphotericin B.
Trypsin-EDTA (1x)	Sigma	Cat T3924	
Amphotericin B	Gibco	Cat 15290-026	
Penicillin Streptomycin	Gibco	Cat 15140-122	
L-glutamine 200nM (100x)	Gibco	Cat 25030-024	
Non-essential amino acids	Gibco	Cat 11140-035	
Histopaque	Merck	Cat 10771	
FACs buffer	n/a	n/a	2% FCS, sodium azide 3.2ml (final 5mM), EDTA 4g, glucose 1g, KH2PO4 0.06g, Na2HPO4 0.19g, CaCl2 2H2O 0.19g, KCl 0.4g, NaCl 8g, MgCl2 0.2g, MgSO4 0.1g
4% Paraformaldehyde in PBS	Thermo Scientific	Cat J19943-K2	
True Nuclear Transcription Factor Buffer Set	Biolegend	Cat 424401	
T cell TransAct human	Miltenyi Biotech	Cat 130-128-758	
Human fibronectin protein carrier free	RND Systems	Cat 1918-FN-02M	
Biolaminin 322	Biolamina	Cat LN332-0502	

Recombinant Human/Mouse/Rat BMP-2 Protein with carrier	RND Systems	Cat 355-BM-010	
Dimethyl sulfoxide (DMSO)	Merck	Cat D2650	
Freezing media	n/a	n/a	10% DMSO added to 90% FCS
Lipopolysaccharides from E. coli (LPS)	Merck	Cat L2880	
Human GM-CSF	Miltenyi Biotech	Cat 130-093-862	
Human recombinant IFNy	Stemcell	Cat 78020.1	
Mesenchymal stem cells - female donor (2022)	Promocell	Cat C-12974	
		Lot no. 472Z023.1	
Mesenchymal stem cells - male donor (2023)	Promocell	Cat C-12974	
		Lot no. 465Z016	

7.2 Appendix 2: Luminex Plates

Plate name	Catalogue Number	Customisation
Human Cytokine/ Chemokine/ Growth Factor Panel A (48 Plex)	HCYTA-60K-PX48	None
Human Cytokine/ Chemokine/ Growth Factor Panel B (24 Plex)	HCYTB-60K-24C	BCA-1, sCD137, CTACK, CXCL6, CXCL16, ENA-78, sFASL, Granzyme A&B, HMGB1, I-309, IL-11, IL-21, IL-33, IL-34, IL-35, IFN, I-TAC, Perforin, TARC, TRAIL, TSLP
RANTES/CCL5 (Single Plex)	HYCTA-60K-01	None
Human Bone Panel (10 Plex)	HBNMAG-51K-10	ACTH, DKK1, FGF-23, Insulin, Leptin, Osteocalcin, Osteopontin, Osteoprotegerin, PTH, Sclerostin
MILLIPLEX Human RANKL (Single Plex)	HRNKLMAG-51K-01	None

7.3 Appendix 3: Shapiro-Wilks normality test results for Luminex analytes by data group

Luminex Data Set Analysed on Prism	Data detected as not normally distributed by Shapiro-Wilks normality test	
Fibronectin early D3 (13/66)	sCD40L IL-6 IL-10 IL-18 TNFα VEGF-A	IFNβ IL-11 IL-13 IL-33 TRAIL TSLP Granzyme A
Laminin early D3 (13/66)	Fractalkine IFNα IL-2 IL-13 MIP1α PDGF-AB/BB TGFα	VEGF-A I-309 IFNβ IL-33 IL-21 Perforin
Fibronectin Bone early D3 (3/7)	Insulin Leptin	Osteocalcin
Laminin Bone early D3 (3/7)	DKK1 Leptin	Osteocalcin
Fibronectin late D28 (20/66)	EGF FLT3L Gro-α IFNγ IL-1β IL-5 IL-6 IL-15 IL-22 IL-27	MIP-1α MIP-1β sFas sCD137 Granzyme A HMGB1 I-309 Granzyme B IL-33 TARC

Laminin late D28 (16/66)	sCD40L FGF2 IFNγ IL-1β IL-1RA IL-27 MIP-1α MIP-1β	TNFβ BCA-1 ENA-78 I-309 Granzyme B IFNβ TARC TSLP
Fibronectin Bone late D28 (4/7)	Insulin Leptin	Osteopontin Osteocalcin
Laminin Bone late D28 (4/7)	Leptin Osteopontin	Osteocalcin Sclerostin

7.4 Appendix 4: Characterisation of conditioned proinflammatory media by Luminex

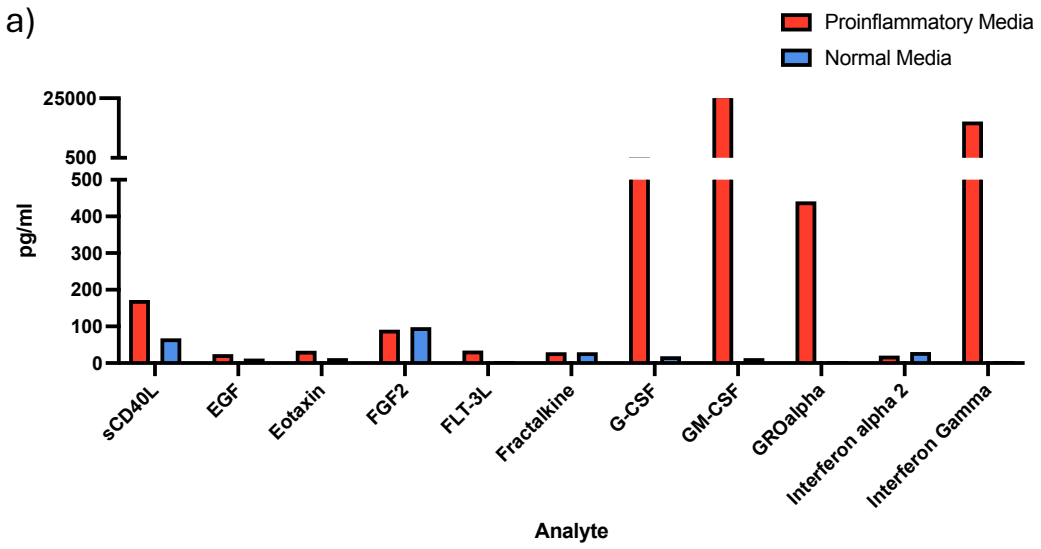

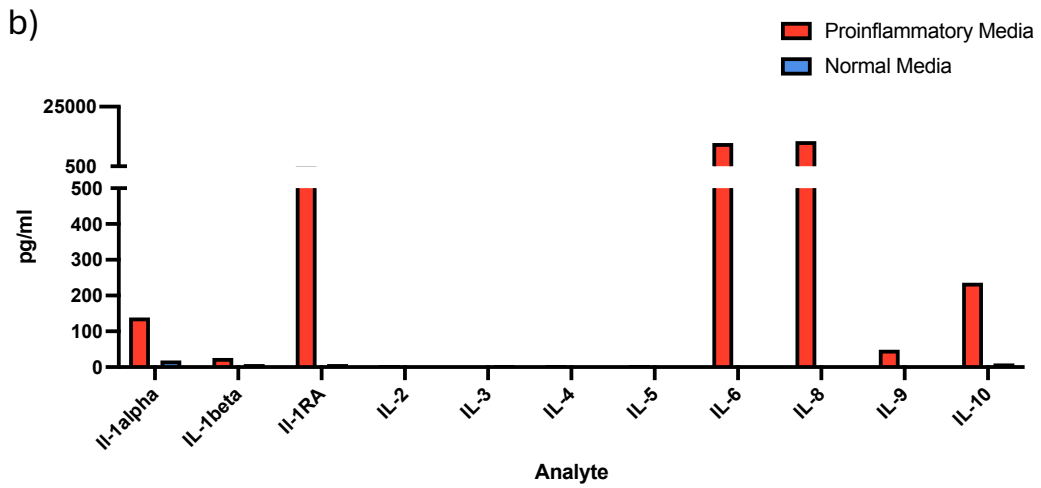

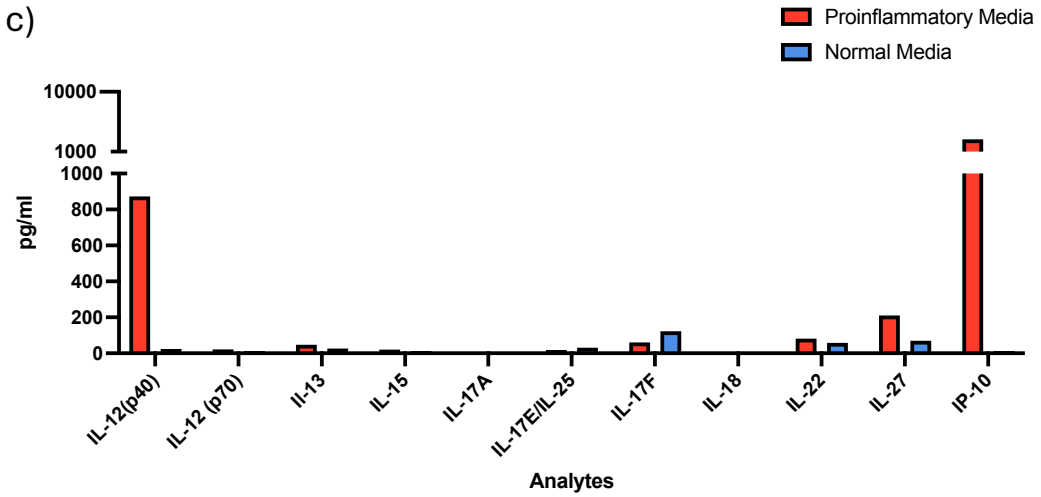

d)

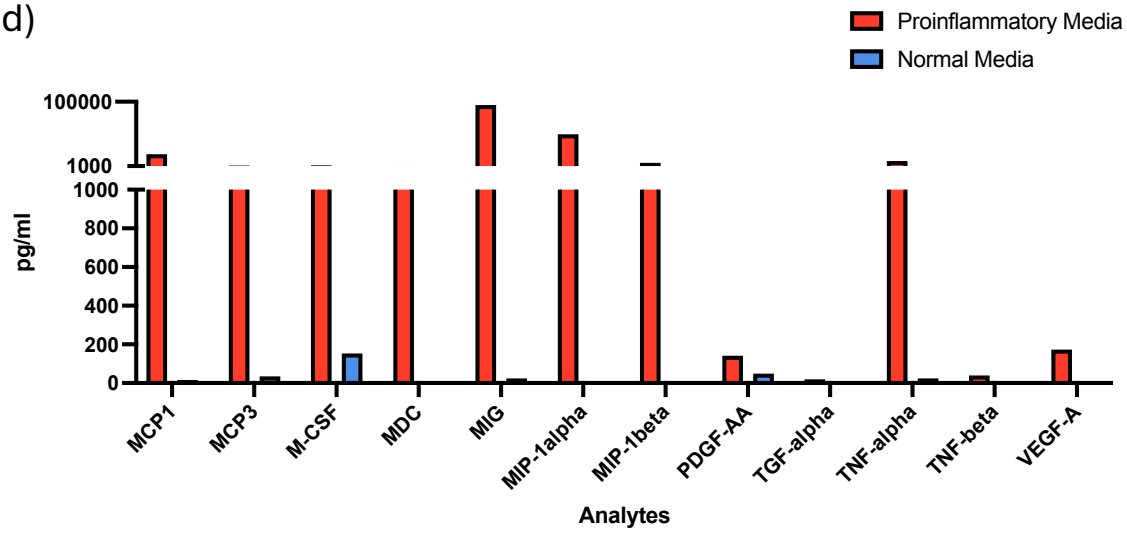
Proinflammatory Media
Normal Media
100000
1000
1000
800
600
400
200
0
pg/ml
MCP1
MCP3
M-CSF
MDC
MIG
MIP-1alpha
MIP-1beta
PDGF-AA
TGF-alpha
TNF-alpha
TNF-beta
VEGF-A
Analytes

e)

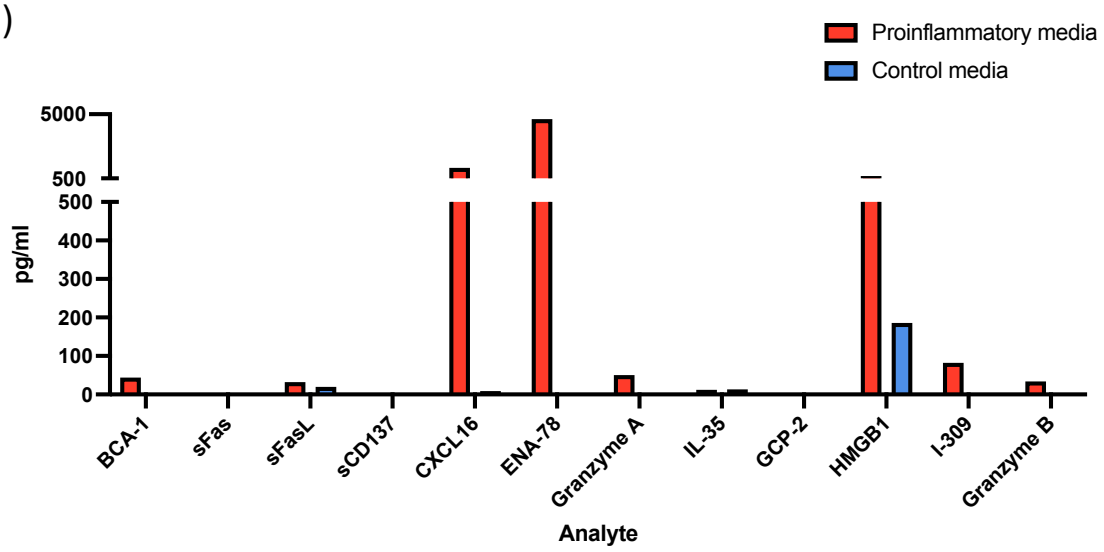
Proinflammatory media
Control media
5000
500
500
400
300
200
100
0
pg/ml
BCA-1
sFas
sFasL
sCD137
CXCL16
ENA-78
Granzyme A
IL-35
GCP-2
HMGB1
I-309
Granzyme B
Analyte

f)

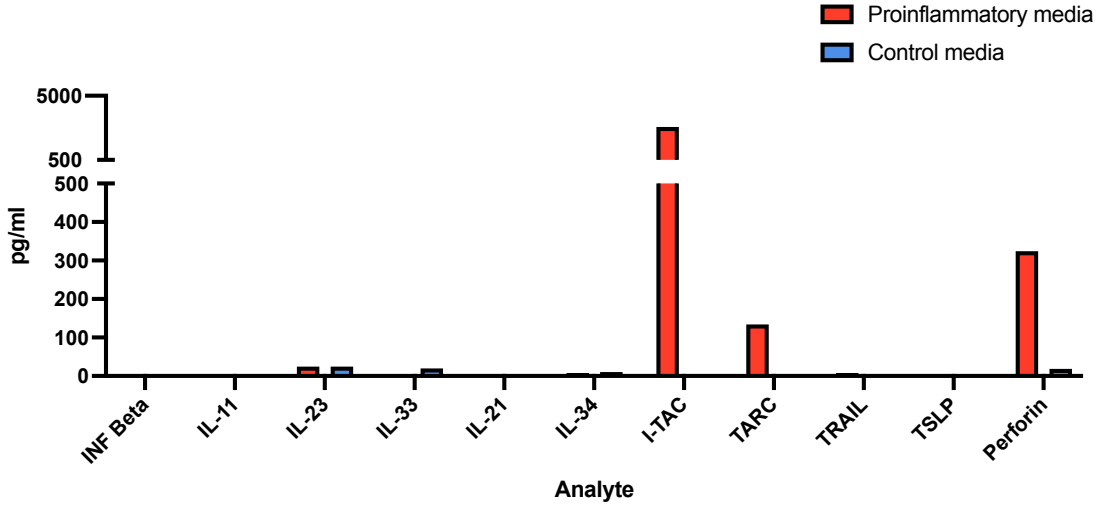
Proinflammatory media
Control media
5000
500
500
400
300
200
100
0
pg/ml
INF Beta
IL-11
IL-23
IL-33
IL-21
IL-34
I-TAC
TARC
TRAIL
TSLP
Perforin
Analyte

g)

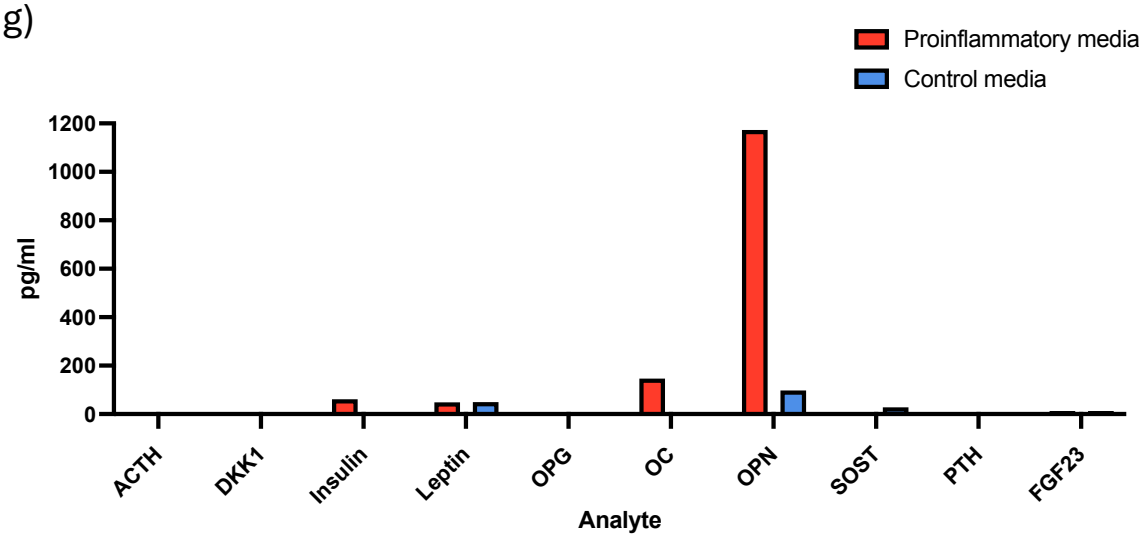
Proinflammatory media
Control media
1200
1000
800
600
400
200
0
pg/ml
ACTH
DKK1
Insulin
Leptin
OPG
OC
OPN
SOST
PTH
FGF23
Analyte

7.5 Appendix 5: RT-qPCR primers

	Reverse primer sequence	Forward primer sequence
OCN	5'-TCT GGA GTT TAT TTG GGA GCA G-3'	5'-CAG CGA GGT AGT GAA GAG ACC -3'
OPN	5'-TGA AAT TCA TGG CTG TGG AA-3'	5'-AGC TGG ATG ACC AGA GTG CT-3'
GAPDH	5'-TGG GTG GCA GTG ATG GCA-3'	5'-TCA AGG CTG AGA ACG GGA A-3'

References

1. Sallam AA, El-Deeb MS, Imam MA. Nerve transfer versus nerve graft for reconstruction of high ulnar nerve injuries. The Journal of hand surgery. 2017;42(4):265-73.

2. De Boer HH. The history of bone grafts. Clinical orthopaedics and related research. 1988(226):292-8.

3. Kornfeld T, Vogt PM, Radtke C. Nerve grafting for peripheral nerve injuries with extended defect sizes. Wiener Medizinische Wochenschrift. 2019;169(9):240-51.

4. Angeletti A, Cantarelli C, Cravedi P. Immune responses towards bioengineered tissues and strategies to control them. Current opinion in organ transplantation. 2019;24(5):582-9.

5. Webber MJ, Khan OF, Sydlik SA, Tang BC, Langer R. A perspective on the clinical translation of scaffolds for tissue engineering. Annals of biomedical engineering. 2015;43(3):641-56.

6. Sadtler K, Singh A, Wolf MT, Wang X, Pardoll DM, Elisseeff JH. Design, clinical translation and immunological response of biomaterials in regenerative medicine. Nature Reviews Materials. 2016;1(7).

7. Im GI. Biomaterials in orthopaedics: The past and future with immune modulation. Biomaterials Research. 2020;24(1):7-10.

8. Yoshikawa T, Ohgushi H, editors. Autogenous cultured bone graft--bone reconstruction using tissue engineering approach. Annales chirurgiae et gynaecologiae; 1999.

9. Franz S, Rammelt S, Scharnweber D, Simon JC. Immune responses to implants - A review of the implications for the design of immunomodulatory biomaterials. Biomaterials. 2011;32(28):6692-709.

10. Bracken MB. Why animal studies are often poor predictors of human reactions to exposure. Journal of the Royal Society of Medicine. 2009;102(3):120-2.

11. Fine B, Vunjak-Novakovic G. Shortcomings of Animal Models and the Rise of Engineered Human Cardiac Tissue. ACS Biomaterials Science & Engineering. 2017;3(9):1884-97.

12. Hu Y, Xiong Y, Tao R, Xue H, Chen L, Lin Z, et al. Advances and perspective on animal models and hydrogel biomaterials for diabetic wound healing. Biomater Transl. 2022;3(3):188-200.

13. Barakat M, DiPietro LA, Chen L. Limited Treatment Options for Diabetic Wounds: Barriers to Clinical Translation Despite Therapeutic Success in Murine Models. Advances in Wound Care. 2020;10(8):436-60.

14. Ahmed SM, Shivnaraine RV, Wu JC. FDA modernization act 2.0 paves the way to computational biology and clinical trials in a dish. Circulation. 2023;148(4):309-11.

15. Wancket LM, Schuh JCL, Drevon-Gaillot E. Chapter 11 - Biomedical Materials and Devices. In: Haschek WM, Rousseaux CG, Wallig MA, Bolon B, Bolon B, Heinz-Taheny KM, et al., editors. Haschek and Rousseaux' s Handbook of Toxicologic Pathology (Fourth Edition): Academic Press; 2023. p. 427-66.

16. MHRA UG. Medical device regulations: compliance and enforcement 2023 [Available from: https://www.gov.uk/government/publications/report-a-non-compliant-medical-device-enforcement-process.

17. Thomsen M, Yacoub‐Youssef H, Marcheix B. Reconstitution of a human immune system in immunodeficient mice: models of human alloreaction in vivo. Tissue antigens. 2005;66(2):73-82.

18. Del Rio NM, Huang L, Murphy L, Babu JS, Daffada CM, Haynes WJ, et al. Generation of the NeoThy mouse model for human immune system studies. Lab animal. 2023;52(7):149-68.

19. Legrand N, Weijer K, Spits H. Experimental models to study development and function of the human immune system in vivo. The Journal of Immunology. 2006;176(4):2053-8.

20. Tao L, Reese TA. Making mouse models that reflect human immune responses. Trends in immunology. 2017;38(3):181-93.

21. Mariani E, Lisignoli G, Borzì RM, Pulsatelli L. Biomaterials: Foreign bodies or tuners for the immune response? International Journal of Molecular Sciences. 2019;20(3).

22. Hed J, Johansson M, Lindroth M. Complement activation according to the alternate pathway by glass and plastic surfaces and its role in neutrophil adhesion. Immunology letters. 1984;8(6):295-9.

23. Jones KS. Effects of biomaterial-induced inflammation on fibrosis and rejection. Seminars in Immunology. 2008;20(2):130-6.

24. Nilsson B, Ekdahl KN, Mollnes TE, Lambris JD. The role of complement in biomaterial-induced inflammation. Molecular immunology. 2007;44(1-3):82-94.

25. Anderson JM, McNally AK. Biocompatibility of implants: lymphocyte/macrophage interactions. Seminars in Immunopathology. 2011;33(3):221-33.

26. Anderson JM, Rodriguez A, Chang DT. Foreign body reaction to biomaterials. Seminars in Immunology. 2008;20(2):86-100.

27. Andersson J, Ekdahl KN, Larsson R, Nilsson UR, Nilsson B. C3 Adsorbed to a Polymer Surface Can Form an Initiating Alternative Pathway Convertase. The Journal of Immunology. 2002;168(11):5786.

28. Miao X, Leng X, Zhang Q. The Current State of Nanoparticle-Induced Macrophage Polarization and Reprogramming Research. International Journal of Molecular Sciences. 2017;18(2):336.

29. Salthouse D, Novakovic K, Hilkens CMU, Ferreira AM. Interplay between biomaterials and the immune system: Challenges and opportunities in regenerative medicine. Acta Biomaterialia. 2023;155:1-18.

30. Wu A-M, Bisignano C, James SL, Abady GG, Abedi A, Abu-Gharbieh E, et al. Global, regional, and national burden of bone fractures in 204 countries and territories, 1990–2019: a systematic analysis from the Global Burden of Disease Study 2019. The Lancet Healthy Longevity. 2021;2(9):e580-e92.

31. Cheal EJ, Hayes WC, White AA, 3rd, Perren SM. Stress analysis of compression plate fixation and its effects on long bone remodeling. J Biomech. 1985;18(2):141-50.

32. Duan ZW, Lu H. Effect of Mechanical Strain on Cells Involved in Fracture Healing. Orthop Surg. 2021;13(2):369-75.

33. Aro HT, Chao EY. Biomechanics and biology of fracture repair under external fixation. Hand Clin. 1993;9(4):531-42.

34. Saunders MM, Lee JS. The influence of mechanical environment on bone healing and distraction osteogenesis. Atlas Oral Maxillofac Surg Clin North Am. 2008;16(2):147-58.

35. Sternlicht MD, Werb Z. How matrix metalloproteinases regulate cell behavior. Annu Rev Cell Dev Biol. 2001;17:463-516.

36. Chang C, Werb Z. The many faces of metalloproteases: cell growth, invasion, angiogenesis and metastasis. Trends Cell Biol. 2001;11(11):S37-43.

37. Ries C, Egea V, Karow M, Kolb H, Jochum M, Neth P. MMP-2, MT1-MMP, and TIMP-2 are essential for the invasive capacity of human mesenchymal stem cells: differential regulation by inflammatory cytokines. Blood. 2007;109(9):4055-63.

38. Sheen JR MA, Garla VV. . Fracture Healing Overview. : Treasure Island (FL): StatPearls Publishing Jan 2024.

39. Marsh DR, Li G. The biology of fracture healing: optimising outcome. Br Med Bull. 1999;55(4):856-69.

40. Dwek JR. The periosteum: what is it, where is it, and what mimics it in its absence? Skeletal Radiol. 2010;39(4):319-23.

41. Onishi T, Ishidou Y, Nagamine T, Yone K, Imamura T, Kato M, et al. Distinct and overlapping patterns of localization of bone morphogenetic protein (BMP) family members and a BMP type II receptor during fracture healing in rats. Bone. 1998;22(6):605-12.

42. Robinson D, Hasharoni A, Halperin N, Yayon A, Nevo Z. Mesenchymal cells and growth factors in bunions. Foot Ankle Int. 1999;20(11):727-32.

43. Go YY, Mun JY, Chae SW, Kim SH, Song H, Song JJ. Engineering functional BMP-2 expressing teratoma-derived fibroblasts for enhancing osteogenesis. Sci Rep. 2018;8(1):14581.

44. Hadjidakis DJ, Androulakis, II. Bone remodeling. Ann N Y Acad Sci. 2006;1092:385-96.

45. Rodan GA, Martin TJ. Role of osteoblasts in hormonal control of bone resorption - a hypothesis. Calcif Tissue Int. 1982;34(3):311.

46. Anderson DM, Maraskovsky E, Billingsley WL, Dougall WC, Tometsko ME, Roux ER, et al. A homologue of the TNF receptor and its ligand enhance T-cell growth and dendritic-cell function. Nature. 1997;390(6656):175-9.

47. Yasuda H, Shima N, Nakagawa N, Yamaguchi K, Kinosaki M, Mochizuki S, et al. Osteoclast differentiation factor is a ligand for osteoprotegerin/osteoclastogenesis-inhibitory factor and is identical to TRANCE/RANKL. Proc Natl Acad Sci U S A. 1998;95(7):3597-602.

48. Ghiasi MS, Chen J, Vaziri A, Rodriguez EK, Nazarian A. Bone fracture healing in mechanobiological modeling: A review of principles and methods. Bone Rep. 2017;6:87-100.

49. Lasanianos NG, Kanakaris NK, Giannoudis PV. Current management of long bone large segmental defects. Orthopaedics and Trauma. 2010;24(2):149-63.

50. Mauffrey C, Barlow BT, Smith W. Management of segmental bone defects. JAAOS-Journal of the American Academy of Orthopaedic Surgeons. 2015;23(3):143-53.

51. Keating JF, Simpson A, Robinson C. The management of fractures with bone loss. The Journal of Bone & Joint Surgery British Volume. 2005;87(2):142-50.

52. Tsang S-TJ, Ferreira N, Simpson AHRW. The reconstruction of critical bone loss. Bone & Joint Research. 2022;11(6):409-12.

53. Chimutengwende-Gordon M, Mbogo A, Khan W, Wilkes R. Limb reconstruction after traumatic bone loss. Injury. 2017;48(2):206-13.

54. Dalisson B, Charbonnier B, Aoude A, Gilardino M, Harvey E, Makhoul N, et al. Skeletal regeneration for segmental bone loss: Vascularised grafts, analogues and surrogates. Acta Biomaterialia. 2021;136:37-55.

55. Rigal S, Merloz P, Le Nen D, Mathevon H, Masquelet AC. Bone transport techniques in posttraumatic bone defects. Orthopaedics & Traumatology: Surgery & Research. 2012;98(1):103-8.

56. Pipitone PS, Rehman S. Management of traumatic bone loss in the lower extremity. Orthopedic Clinics. 2014;45(4):469-82.

57. Eccles S, Handley B, Khan U, McFadyen I, Nanchahal J, Nayagam S. Standards for the management of open fractures: Oxford University Press; 2020.

58. Taylor GI, MILLER GD, HAM FJ. The free vascularized bone graft: a clinical extension of microvascular techniques. Plastic and reconstructive surgery. 1975;55(5):533-44.

59. Scampa M, Mégevand V, Martineau J, Schaefer DJ, Kalbermatten DF, Oranges CM. Medial Femoral Condyle Free Flap: A Systematic Review and Proportional Meta-analysis of Applications and Surgical Outcomes. Plastic and Reconstructive Surgery – Global Open. 2024;12(4).

60. Foster RD, Anthony JP, Sharma A, Pogrel MA. Vascularized bone flaps versus nonvascularized bone grafts for mandibular reconstruction: an outcome analysis of primary bony union and endosseous implant success. Head & Neck: Journal for the Sciences and Specialties of the Head and Neck. 1999;21(1):66-71.

61. Pogrel M, Podlesh S, Anthony JP, Alexander J. A comparison of vascularized and nonvascularized bone grafts for reconstruction of mandibular continuity defects. Journal of oral and maxillofacial surgery. 1997;55(11):1200-6.

62. Hirche C, Xiong L, Heffinger C, Münzberg M, Fischer S, Kneser U, et al. Vascularized versus non-vascularized bone grafts in the treatment of scaphoid non-union: a clinical outcome study with therapeutic algorithm. Journal of Orthopaedic Surgery. 2017;25(1):2309499016684291.

63. Weiland AJ, Phillips TW, Randolph MA. Bone grafts: a radiologic, histologic, and biomechanical model comparing autografts, allografts, and free vascularized bone grafts. Plastic and reconstructive surgery. 1984;74(3):368-79.

64. Estrella EP, Wang EH. A comparison of vascularized free fibular flaps and nonvascularized fibular grafts for reconstruction of long bone defects after tumor resection. Journal of reconstructive microsurgery. 2017;33(03):194-205.

65. Penn-Barwell JG. Outcomes in lower limb amputation following trauma: A systematic review and meta-analysis. Injury. 2011;42(12):1474-9.

66. Ogasawara T, Kawaguchi H, Jinno S, Hoshi K, Itaka K, Takato T, et al. Bone morphogenetic protein 2-induced osteoblast differentiation requires Smad-mediated down-regulation of Cdk6. Mol Cell Biol. 2004;24(15):6560-8.

67. Cheng ZA, Alba-Perez A, Gonzalez-Garcia C, Donnelly H, Llopis-Hernandez V, Jayawarna V, et al. Nanoscale Coatings for Ultralow Dose BMP-2-Driven Regeneration of Critical-Sized Bone Defects. Advanced Science. 2019;6(2).

68. Lee SS, Huang BJ, Kaltz SR, Sur S, Newcomb CJ, Stock SR, et al. Bone regeneration with low dose BMP-2 amplified by biomimetic supramolecular nanofibers within collagen scaffolds. Biomaterials. 2013;34(2):452-9.

69. Ma C, Park MS, Alves do Monte F, Gokani V, Aruwajoye OO, Ren Y, et al. Local BMP2 hydrogel therapy for robust bone regeneration in a porcine model of Legg-Calvé-Perthes disease. npj Regenerative Medicine. 2023;8(1):50.

70. Lin H, Tang Y, Lozito TP, Oyster N, Wang B, Tuan RS. Efficient in vivo bone formation by BMP-2 engineered human mesenchymal stem cells encapsulated in a projection stereolithographically fabricated hydrogel scaffold. Stem Cell Research & Therapy. 2019;10(1):254.

71. Abbah S-A, Lam WMR, Hu T, Goh J, Wong H-K. Sequestration of rhBMP-2 into self-assembled polyelectrolyte complexes promotes anatomic localization of new bone in a porcine model of spinal reconstructive surgery. Tissue Engineering Part A. 2014;20(11-12):1679-88.

72. Chen B, Lin H, Wang J, Zhao Y, Wang B, Zhao W, et al. Homogeneous osteogenesis and bone regeneration by demineralized bone matrix loading with collagen-targeting bone morphogenetic protein-2. Biomaterials. 2007;28(6):1027-35.

73. Dmitriev AE, Lehman Jr RA, Symes AJ. Bone morphogenetic protein-2 and spinal arthrodesis: the basic science perspective on protein interaction with the nervous system. The Spine Journal. 2011;11(6):500-5.

74. Llopis-Hernández V, Cantini M, González-García C, Cheng ZA, Yang J, Tsimbouri PM, et al. Material-driven fibronectin assembly for high-efficiency presentation of growth factors. Science advances. 2016;2(8):e1600188.

75. Martino MM, Hubbell JA. The 12th–14th type III repeats of fibronectin function as a highly promiscuous growth factor‐binding domain. The FASEB Journal. 2010;24(12):4711-21.

76. Cantini M, Rico P, Moratal D, Salmerón-Sánchez M. Controlled wettability, same chemistry: biological activity of plasma-polymerized coatings. Soft Matter. 2012;8(20):5575-84.

77. Müllner M, Dodds SJ, Nguyen T-H, Senyschyn D, Porter CJ, Boyd BJ, et al. Size and rigidity of cylindrical polymer brushes dictate long circulating properties in vivo. ACS nano. 2015;9(2):1294-304.

78. Kreyling WG, Abdelmonem AM, Ali Z, Alves F, Geiser M, Haberl N, et al. In vivo integrity of polymer-coated gold nanoparticles. Nature nanotechnology. 2015;10(7):619-23.

79. Skjødt H, Møller T, Freiesleben SF. Human osteoblast-like cells expressing MHC class II determinants stimulate allogeneic and autologous peripheral blood mononuclear cells and function as antigen-presenting cells. Immunology. 1989;68(3):416-20.

80. Stanley KT, VanDort C, Motyl C, Endres J, Fox DA. Immunocompetent properties of human osteoblasts: interactions with T lymphocytes. Journal of Bone and Mineral Research. 2006;21(1):29-36.

81. Croes M, Öner FC, van Neerven D, Sabir E, Kruyt MC, Blokhuis TJ, et al. Proinflammatory T cells and IL-17 stimulate osteoblast differentiation. Bone. 2016;84:262-70.

82. Sun L, Su Y, Jiao A, Wang X, Zhang B. T cells in health and disease. Signal Transduction and Targeted Therapy. 2023;8(1):235.

83. Kumar BV, Connors TJ, Farber DL. Human T Cell Development, Localization, and Function throughout Life. Immunity. 2018;48(2):202-13.

84. Cohen IR. Activation of benign autoimmunity as both tumor and autoimmune disease immunotherapy: a comprehensive review. Journal of autoimmunity. 2014;54:112-7.

85. Rothenberg EV, Moore JE, Yui MA. Launching the T-cell-lineage developmental programme. Nature Reviews Immunology. 2008;8(1):9-21.

86. Rothenberg EV. Stepwise specification of lymphocyte developmental lineages. Current opinion in genetics & development. 2000;10(4):370-9.

87. Hosokawa H, Rothenberg EV. How transcription factors drive choice of the T cell fate. Nature Reviews Immunology. 2021;21(3):162-76.

88. Hosokawa H, Rothenberg EV. Cytokines, transcription factors, and the initiation of T-cell development. Cold Spring Harbor perspectives in biology. 2018;10(5):a028621.

89. Yui MA, Rothenberg EV. Developmental gene networks: a triathlon on the course to T cell identity. Nature Reviews Immunology. 2014;14(8):529-45.

90. Hosoya T, Kuroha T, Moriguchi T, Cummings D, Maillard I, Lim K-C, et al. GATA-3 is required for early T lineage progenitor development. Journal of Experimental Medicine. 2009;206(13):2987-3000.

91. Zhang JA, Mortazavi A, Williams BA, Wold BJ, Rothenberg EV. Dynamic transformations of genome-wide epigenetic marking and transcriptional control establish T cell identity. Cell. 2012;149(2):467-82.

92. Ikawa T, Hirose S, Masuda K, Kakugawa K, Satoh R, Shibano-Satoh A, et al. An Essential Developmental Checkpoint for Production of the T Cell Lineage. Science. 2010;329(5987):93-6.

93. Taghon T, Yui MA, Pant R, Diamond RA, Rothenberg EV. Developmental and molecular characterization of emerging β-and γδ-selected pre-T cells in the adult mouse thymus. Immunity. 2006;24(1):53-64.

94. Koncz B, Balogh GM, Papp BT, Asztalos L, Kemény L, Manczinger M. Self-mediated positive selection of T cells sets an obstacle to the recognition of nonself. Proceedings of the National Academy of Sciences. 2021;118(37):e2100542118.

95. Klein L, Kyewski B, Allen PM, Hogquist KA. Positive and negative selection of the T cell repertoire: what thymocytes see (and don't see). Nat Rev Immunol. 2014;14(6):377-91.

96. Weng NP. Numbers and odds: TCR repertoire size and its age changes impacting on T cell functions. Semin Immunol. 2023;69:101810.

97. Dustin ML, de Fougerolles AR. Reprograming T cells: the role of extracellular matrix in coordination of T cell activation and migration. Current Opinion in Immunology. 2001;13(3):286-90.

98. Cochran JR, Cameron TO, Stern LJ. The Relationship of MHC-Peptide Binding and T Cell Activation Probed Using Chemically Defined MHC Class II Oligomers. Immunity. 2000;12(3):241-50.

99. Hwang J-R, Byeon Y, Kim D, Park S-G. Recent insights of T cell receptor-mediated signaling pathways for T cell activation and development. Experimental & Molecular Medicine. 2020;52(5):750-61.

100. Malissen M, Minard K, Mjolsness S, Kronenberg M, Goverman J, Hunkapiller T, et al. Mouse T cell antigen receptor: structure and organization of constant and joining gene segments encoding the β polypeptide. Cell. 1984;37(3):1101-10.

101. Borst J, Coligan JE, Oettgen H, Pessano S, Malin R, Terhorst C. The δ-and ε-chains of the human T3/T-cell receptor complex are distinct polypeptides. Nature. 1984;312(5993):455-8.

102. Ullman KS, Northrop JP, Verweij CL, Crabtree GR. Transmission of signals from the T lymphocyte antigen receptor to the genes responsible for cell proliferation and immune function: the missing link. Annual review of immunology. 1990;8(1):421-52.

103. Glimcher LH, Singh H. Transcription factors in lymphocyte development—T and B cells get together. Cell. 1999;96(1):13-23.

104. Tai Y, Wang Q, Korner H, Zhang L, Wei W. Molecular Mechanisms of T Cells Activation by Dendritic Cells in Autoimmune Diseases. Frontiers in Pharmacology. 2018;9.

105. Jenkins MK, Taylor PS, Norton SD, Urdahl KB. CD28 delivers a costimulatory signal involved in antigen-specific IL-2 production by human T cells. Journal of immunology (Baltimore, Md: 1950). 1991;147(8):2461-6.

106. Wong HY, Schwarz H. CD137 / CD137 ligand signalling regulates the immune balance: A potential target for novel immunotherapy of autoimmune diseases. Journal of Autoimmunity. 2020;112:102499.

107. Reithofer M, Rosskopf S, Leitner J, Battin C, Bohle B, Steinberger P, et al. 4-1BB costimulation promotes bystander activation of human CD8 T cells. Eur J Immunol. 2021;51(3):721-33.

108. Zhang Z, Mateus J, Coelho CH, Dan JM, Moderbacher CR, Gálvez RI, et al. Humoral and cellular immune memory to four COVID-19 vaccines. Cell. 2022;185(14):2434-51.e17.

109. Croft M, So T, Duan W, Soroosh P. The significance of OX40 and OX40L to T-cell biology and immune disease. Immunol Rev. 2009;229(1):173-91.

110. Muntasell A, Ochoa MC, Cordeiro L, Berraondo P, López-Díaz de Cerio A, Cabo M, et al. Targeting NK-cell checkpoints for cancer immunotherapy. Current Opinion in Immunology. 2017;45:73-81.

111. Lakka Klement G, Shai E, Varon D. Chapter 24 - The Role of Platelets in Angiogenesis. In: Michelson AD, editor. Platelets (Third Edition): Academic Press; 2013. p. 487-502.

112. Simpson TR, Quezada SA, Allison JP. Regulation of CD4 T cell activation and effector function by inducible costimulator (ICOS). Current Opinion in Immunology. 2010;22(3):326-32.

113. McAdam AJ, Chang TT, Lumelsky AE, Greenfield EA, Boussiotis VA, Duke-Cohan JS, et al. Mouse inducible costimulatory molecule (ICOS) expression is enhanced by CD28 costimulation and regulates differentiation of CD4+ T cells. The Journal of Immunology. 2000;165(9):5035-40.

114. Liu R, Li H-F, Li S. PD-1-mediated inhibition of T cell activation: Mechanisms and strategies for cancer combination immunotherapy. Cell Insight. 2024;3(2):100146.

115. Boussiotis VA. Molecular and biochemical aspects of the PD-1 checkpoint pathway. New England Journal of Medicine. 2016;375(18):1767-78.

116. Adamczyk M, Bartosińska J, Raczkiewicz D, Kowal M, Surdacka A, Krasowska D, et al. The Expression of Activation Markers CD25 and CD69 Increases during Biologic Treatment of Psoriasis. J Clin Med. 2023;12(20).

117. Baecher-Allan C, Anderson DE. Regulatory cells and human cancer. Seminars in Cancer Biology. 2006;16(2):98-105.

118. Baecher-Allan C, Brown JA, Freeman GJ, Hafler DA. CD4+ CD25high regulatory cells in human peripheral blood. The Journal of Immunology. 2001;167(3):1245-53.

119. Roncador G, Brown PJ, Maestre L, Hue S, Martínez‐Torrecuadrada JL, Ling KL, et al. Analysis of FOXP3 protein expression in human CD4+ CD25+ regulatory T cells at the single‐cell level. European journal of immunology. 2005;35(6):1681-91.

120. Wing K, Larsson P, Sandström K, Lundin SB, Suri‐Payer E, Rudin A. CD4+ CD25+ FOXP3+ regulatory T cells from human thymus and cord blood suppress antigen‐specific T cell responses. Immunology. 2005;115(4):516-25.

121. Saito T, Germain RN. Predictable acquisition of a new MHC recognition specificity following expression of a transfected T-cell receptor β-chain gene. Nature. 1987;329(6136):256-9.

122. Bosteels V, Janssens S. Striking a balance: new perspectives on homeostatic dendritic cell maturation. Nature Reviews Immunology. 2024.

123. Schlitzer A, Sivakamasundari V, Chen J, Sumatoh HRB, Schreuder J, Lum J, et al. Identification of cDC1-and cDC2-committed DC progenitors reveals early lineage priming at the common DC progenitor stage in the bone marrow. Nature immunology. 2015;16(7):718-28.

124. Feng J, Pucella JN, Jang G, Alcántara-Hernández M, Upadhaya S, Adams NM, et al. Clonal lineage tracing reveals shared origin of conventional and plasmacytoid dendritic cells. Immunity. 2022;55(3):405-22. e11.

125. Cabeza-Cabrerizo M, Cardoso A, Minutti CM, Pereira da Costa M, Reis e Sousa C. Dendritic cells revisited. Annual review of immunology. 2021;39(1):131-66.

126. Mellman I, Steinman RM. Dendritic cells: specialized and regulated antigen processing machines. Cell. 2001;106(3):255-8.

127. Cenerenti M, Saillard M, Romero P, Jandus C. The era of cytotoxic CD4 T cells. Frontiers in Immunology. 2022;13:867189.

128. Dobrzanski MJ. Expanding roles for CD4 T cells and their subpopulations in tumor immunity and therapy. Frontiers in oncology. 2013;3:63.

129. Zhu J. T helper cell differentiation, heterogeneity, and plasticity. Cold Spring Harbor perspectives in biology. 2018;10(10):a030338.

130. Walker JA, McKenzie AN. TH2 cell development and function. Nature Reviews Immunology. 2018;18(2):121-33.

131. Jeong J, Lee HK. The role of CD4+ T cells and microbiota in the pathogenesis of asthma. International Journal of Molecular Sciences. 2021;22(21):11822.

132. Korn T, Bettelli E, Oukka M, Kuchroo VK. IL-17 and Th17 Cells. Annual review of immunology. 2009;27(1):485-517.

133. Mangan PR, Harrington LE, O'Quinn DB, Helms WS, Bullard DC, Elson CO, et al. Transforming growth factor-β induces development of the TH17 lineage. Nature. 2006;441(7090):231-4.

134. Ivanov II, McKenzie BS, Zhou L, Tadokoro CE, Lepelley A, Lafaille JJ, et al. The orphan nuclear receptor RORγt directs the differentiation program of proinflammatory IL-17+ T helper cells. Cell. 2006;126(6):1121-33.

135. Korn T, Bettelli E, Gao W, Awasthi A, Jäger A, Strom TB, et al. IL-21 initiates an alternative pathway to induce proinflammatory TH17 cells. Nature. 2007;448(7152):484-7.

136. Ghoreschi K, Laurence A, Yang X-P, Tato CM, McGeachy MJ, Konkel JE, et al. Generation of pathogenic TH17 cells in the absence of TGF-β signalling. Nature. 2010;467(7318):967-71.

137. Mufazalov IA, Schelmbauer C, Regen T, Kuschmann J, Wanke F, Gabriel LA, et al. IL‐1 signaling is critical for expansion but not generation of autoreactive GM‐CSF+ Th17 cells. The EMBO journal. 2017;36(1):102-15.

138. Akdis M, Palomares O, van de Veen W, van Splunter M, Akdis CA. TH17 and TH22 cells: a confusion of antimicrobial response with tissue inflammation versus protection. Journal of Allergy and Clinical Immunology. 2012;129(6):1438-49.

139. Shevyrev D, Tereshchenko V. Treg Heterogeneity, Function, and Homeostasis. Frontiers in Immunology. 2020;10.

140. Plitas G, Rudensky AY. Regulatory T cells: differentiation and function. Cancer immunology research. 2016;4(9):721-5.

141. Hori S. FOXP3 as a master regulator of Treg cells. Nature Reviews Immunology. 2021;21(10):618-9.

142. Koh C-H, Lee S, Kwak M, Kim B-S, Chung Y. CD8 T-cell subsets: heterogeneity, functions, and therapeutic potential. Experimental & Molecular Medicine. 2023;55(11):2287-99.

143. Shoukry NH, Grakoui A, Houghton M, Chien DY, Ghrayeb J, Reimann KA, et al. Memory CD8+ T cells are required for protection from persistent hepatitis C virus infection. The Journal of experimental medicine. 2003;197(12):1645-55.

144. Griffin DE, Lin W-H, Pan C-H. Measles virus, immune control, and persistence. FEMS microbiology reviews. 2012;36(3):649-62.

145. Schmitz JE, Kuroda MJ, Santra S, Sasseville VG, Simon MA, Lifton MA, et al. Control of viremia in simian immunodeficiency virus infection by CD8+ lymphocytes. Science. 1999;283(5403):857-60.

146. Jiang H, Zhang S-l, Pernis B. Role of CD8+ T cells in murine experimental allergic encephalomyelitis. Science. 1992;256(5060):1213-5.

147. Koh D-R, Fung-Leung W-P, Ho A, Gray D, Acha-Orbea H, Mak T-W. Less mortality but more relapses in experimental allergic encephalomyelitis in CD8-/-mice. Science. 1992;256(5060):1210-3.

148. Kim H-J, Wang X, Radfar S, Sproule TJ, Roopenian DC, Cantor H. CD8+ T regulatory cells express the Ly49 Class I MHC receptor and are defective in autoimmune prone B6-Yaa mice. Proceedings of the National Academy of Sciences. 2011;108(5):2010-5.

149. Andorko JI, Jewell CM. Designing biomaterials with immunomodulatory properties for tissue engineering and regenerative medicine. Bioengineering & Translational Medicine. 2017;2(2):139-55.

150. Xu Z, Chen X, Tan R, She Z, Chen Z, Xia Z. Preparation and characterization of a gallium-loaded antimicrobial artificial dermal scaffold. Mater Sci Eng C Mater Biol Appl. 2019;105:110063.

151. Zindel J, Kubes P. DAMPs, PAMPs, and LAMPs in Immunity and Sterile Inflammation. Annu Rev Pathol. 2020;15:493-518.

152. Deppermann C, Kubes P. Start a fire, kill the bug: The role of platelets in inflammation and infection. Innate Immun. 2018;24(6):335-48.

153. Maruyama M, Rhee C, Utsunomiya T, Zhang N, Ueno M, Yao Z, et al. Modulation of the Inflammatory Response and Bone Healing. Front Endocrinol (Lausanne). 2020;11:386.

154. Bianchi ME. DAMPs, PAMPs and alarmins: all we need to know about danger. Journal of leukocyte biology. 2007;81(1):1-5.

155. Liu X, Zhou Z, Zeng W-N, Zeng Q, Zhang X. The role of toll-like receptors in orchestrating osteogenic differentiation of mesenchymal stromal cells and osteoimmunology. Frontiers in Cell and Developmental Biology. 2023;11.

156. Zhou T, Yuan Z, Weng J, Pei D, Du X, He C, et al. Challenges and advances in clinical applications of mesenchymal stromal cells. Journal of hematology & oncology. 2021;14:1-24.

157. Nilsson U. Deposition of C3b/iC3b leads to the concealment of antigens, immunoglobulins and bound C1q in complement-activating immune complexes. Molecular Immunology. 2001;38(2-3):151-60.

158. Tengvall P, Askendal A, Lundström I. Ellipsometric in vitro studies on the activation of complement by human immunoglobulins M and G after adsorption to methylated silicon. Colloids and Surfaces B: Biointerfaces. 2001;20(1):51-62.

159. Andersson J, Ekdahl KN, Lambris JD, Nilsson B. Binding of C3 fragments on top of adsorbed plasma proteins during complement activation on a model biomaterial surface. Biomaterials. 2005;26(13):1477-85.

160. Tengvall P, Askendal A, Lundström II. Ellipsometric in vitro studies on the activation of complement by human immunoglobulins M and G after adsorption to methylated silicon. Colloids Surf B Biointerfaces. 2001;20(1):51-62.

161. Thiele L, Diederichs JE, Reszka R, Merkle HP, Walter E. Competitive adsorption of serum proteins at microparticles affects phagocytosis by dendritic cells. Biomaterials. 2003;24(8):1409-18.

162. Oppenheim JJ. Cytokine Reference: a compendium of cytokines and other mediators of host defense. 1.[Ligands]: Academic Press; 2001.

163. Castro PR, Marques SM, Campos PP, Cardoso CC, Sampaio FP, Ferreira MAND, et al. Kinetics of implant-induced inflammatory angiogenesis in abdominal muscle wall in mice. Microvascular research. 2012;84(1):9-15.

164. Oviedo-Socarrás T, Vasconcelos AC, Barbosa IX, Pereira NB, Campos PP, Andrade SP. Diabetes alters inflammation, angiogenesis, and fibrogenesis in intraperitoneal implants in rats. Microvascular research. 2014;93:23-9.

165. Ratner BD. Reducing capsular thickness and enhancing angiogenesis around implant drug release systems. Journal of controlled release : official journal of the Controlled Release Society. 2002;78(1-3):211-8.

166. Martinez FO. Regulators of macrophage activation. European Journal of Immunology. 2011;41(6):1531-4.

167. Sadowska JM, Ginebra MP. Inflammation and biomaterials: Role of the immune response in bone regeneration by inorganic scaffolds. Journal of Materials Chemistry B. 2020;8(41):9404-27.

168. Shen EC, Chou T-C, Gau C-H, Tu H-P, Chen Y-T, Fu E. Releasing growth factors from activated human platelets after chitosan stimulation: a possible bio-material for platelet-rich plasma preparation. Clinical oral implants research. 2006;17(5):572-8.

169. Bao P, Kodra A, Tomic-Canic M, Golinko MS, Ehrlich HP, Brem H. The role of vascular endothelial growth factor in wound healing. The Journal of surgical research. 2009;153(2):347-58.

170. Garg K, Sell SA, Madurantakam P, Bowlin GL. Angiogenic potential of human macrophages on electrospun bioresorbable vascular grafts. Biomedical materials (Bristol, England). 2009;4(3):31001-.

171. Luckheeram RV, Zhou R, Verma AD, Xia B. CD4 T Cells: Differentiation and Functions. Clinical and Developmental Immunology. 2012;2012:925135.

172. Rowley AT, Nagalla RR, Wang S-W, Liu WF. Extracellular Matrix-Based Strategies for Immunomodulatory Biomaterials Engineering. Advanced Healthcare Materials. 2019;8(8):1801578.

173. Moore EM, Maestas DR, Cherry CC, Garcia JA, Comeau HY, Davenport Huyer L, et al. Biomaterials direct functional B cell response in a material-specific manner. Science Advances. 2021;7(49):eabj5830.

174. Sîrbulescu RF, Boehm CK, Soon E, Wilks MQ, Ilieş I, Yuan H, et al. Mature B cells accelerate wound healing after acute and chronic diabetic skin lesions. Wound Repair and Regeneration. 2017;25(5):774-91.

175. Doloff JC, Veiseh O, Vegas AJ, Tam HH, Farah S, Ma M, et al. Colony stimulating factor-1 receptor is a central component of the foreign body response to biomaterial implants in rodents and non-human primates. Nature Materials. 2017;16(6):671-80.

176. Mora-Solano C, Collier JH. Engaging adaptive immunity with biomaterials. Journal of Materials Chemistry B. 2014;2(17):2409-21.

177. Babensee JE. Interaction of dendritic cells with biomaterials. Seminars in immunology. 2008;20(2):101-8.

178. Hunt JA, Flanagan BF, McLaughlin PJ, Strickland I, Williams DF. Effect of biomaterial surface charge on the inflammatory reponse: Evaluation of cellular infiltration and TNFα production. Journal of Biomedical Materials Research. 1996;31(1):139-44.

179. Gill R, editor The role of direct and indirect antigen presentation in the response to islet xenografts. Transplantation proceedings; 1992.

180. Zhao Z, Zhao Q, Gu B, Yin C, Shen K, Tang H, et al. Minimally invasive implantation and decreased inflammation reduce osteoinduction of biomaterial. Theranostics. 2020;10(8):3533-45.

181. Cai X, Lin Y, Ou G, Luo E, Man Y, Yuan Q, et al. Ectopic osteogenesis and chondrogenesis of bone marrow stromal stem cells in alginate system. Cell Biology International. 2007;31(8):776-83.

182. Llopis-Hernández V, Cantini M, González-García C, Cheng ZA, Yang J, Tsimbouri PM, et al. Material-driven fibronectin assembly for high-efficiency presentation of growth factors. Science Advances. 2016;2(8):1-11.

183. Peng H, Usas A, Olshanski A, Ho AM, Gearhart B, Cooper GM, et al. VEGF Improves, Whereas sFlt1 Inhibits, BMP2-Induced Bone Formation and Bone Healing Through Modulation of Angiogenesis. Journal of Bone and Mineral Research. 2005;20(11):2017-27.

184. Ren G, Zhao X, Zhang L, Zhang J, L'Huillier A, Ling W, et al. Inflammatory Cytokine-Induced Intercellular Adhesion Molecule-1 and Vascular Cell Adhesion Molecule-1 in Mesenchymal Stem Cells Are Critical for Immunosuppression. The Journal of Immunology. 2010;184(5):2321-8.

185. Avery D, Morandini L, Gabriec M, Sheakley L, Peralta M, Donahue HJ, et al. Contribution of αβ T cells to macrophage polarization and MSC recruitment and proliferation on titanium implants. Acta Biomaterialia. 2023.

186. Al-Maawi S, Orlowska A, Sader R, James Kirkpatrick C, Ghanaati S. In vivo cellular reactions to different biomaterials—Physiological and pathological aspects and their consequences. Seminars in Immunology. 2017;29:49-61.

187. Browning MB, Cereceres SN, Luong PT, Cosgriff-Hernandez EM. Determination of the in vivo degradation mechanism of PEGDA hydrogels. Journal of Biomedical Materials Research Part A. 2014;102(12):4244-51.

188. Reid B, Gibson M, Singh A, Taube J, Furlong C, Murcia M, et al. PEG hydrogel degradation and the role of the surrounding tissue environment. Journal of tissue engineering and regenerative medicine. 2015;9(3):315-8.

189. Sadtler K, Estrellas K, Allen BW, Wolf MT, Fan H, Tam AJ, et al. Developing a pro-regenerative biomaterial scaffold microenvironment requires T helper 2 cells. Science. 2016;352(6283):366-70.

190. Burmeister DM, Gómez B, Chao T, Cancio LC, Dubick MA. 402 Enteral Resuscitation Shows Similar Efficacy to IV Resuscitation in a Porcine 40%TBSA Contact Model. Journal of Burn Care & Research. 2018;39(suppl_1):S172-S.

191. Ramelli G, Fuertes S, Narayan S, Busso N, Acha-Orbea H, So A. Protease-activated receptor 2 signalling promotes dendritic cell antigen transport and T-cell activation in vivo. IMMUNOLOGY. 2010;129(1):20-7.

192. Da Silva CA, Chalouni C, Williams A, Hartl D, Lee CG, Elias JA. Chitin is a size-dependent regulator of macrophage TNF and IL-10 production. The Journal of immunology. 2009;182(6):3573-82.

193. Fernández TD, Pearson JR, Leal MP, Torres MJ, Blanca M, Mayorga C, et al. Intracellular accumulation and immunological properties of fluorescent gold nanoclusters in human dendritic cells. Biomaterials. 2015;43:1-12.

194. Huang J, Fan C, Chen Y, Ye J, Yang Y, Tang C, et al. Single-cell RNA-seq reveals functionally distinct biomaterial degradation-related macrophage populations. Biomaterials. 2021;277:121116.

195. Echeverria Molina MI, Malollari KG, Komvopoulos K. Design Challenges in Polymeric Scaffolds for Tissue Engineering. Frontiers in Bioengineering and Biotechnology. 2021;9.

196. Kohli N, Ho S, Brown SJ, Sawadkar P, Sharma V, Snow M, et al. Bone remodelling in vitro: Where are we headed?:-A review on the current understanding of physiological bone remodelling and inflammation and the strategies for testing biomaterials in vitro. Bone. 2018;110:38-46.

197. Gross O, Thomas CJ, Guarda G, Tschopp J. The inflammasome: an integrated view. Immunological reviews. 2011;243(1):136-51.

198. Niikura K, Matsunaga T, Suzuki T, Kobayashi S, Yamaguchi H, Orba Y, et al. Gold nanoparticles as a vaccine platform: influence of size and shape on immunological responses in vitro and in vivo. ACS nano. 2013;7(5):3926-38.

199. Bartneck M, Keul HA, Singh S, Czaja K, Bornemann J, Bockstaller M, et al. Rapid uptake of gold nanorods by primary human blood phagocytes and immunomodulatory effects of surface chemistry. ACS nano. 2010;4(6):3073-86.

200. Schanen BC, Karakoti AS, Seal S, Drake DR, 3rd, Warren WL, Self WT. Exposure to titanium dioxide nanomaterials provokes inflammation of an in vitro human immune construct. ACS Nano. 2009;3(9):2523-32.

201. Sunshine JC, Perica K, Schneck JP, Green JJ. Particle shape dependence of CD8+ T cell activation by artificial antigen presenting cells. Biomaterials. 2014;35(1):269-77.

202. Padmore T, Stark C, Turkevich LA, Champion JA. Quantitative analysis of the role of fiber length on phagocytosis and inflammatory response by alveolar macrophages. Biochimica et Biophysica Acta (BBA)-General Subjects. 2017;1861(2):58-67.

203. Vaine CA, Patel MK, Zhu J, Lee E, Finberg RW, Hayward RC, et al. Tuning innate immune activation by surface texturing of polymer microparticles: the role of shape in inflammasome activation. The Journal of Immunology. 2013;190(7):3525-32.

204. Christo SN, Bachhuka A, Diener KR, Mierczynska A, Hayball JD, Vasilev K. The Role of Surface Nanotopography and Chemistry on Primary Neutrophil and Macrophage Cellular Responses. Advanced Healthcare Materials. 2016;5.

205. Hotchkiss KM, Clark NM, Olivares-Navarrete R. Macrophage response to hydrophilic biomaterials regulates MSC recruitment and T-helper cell populations. Biomaterials. 2018;182:202-15.

206. Mendonça G, Mendonça DBS, Aragão FJL, Cooper LF. Advancing dental implant surface technology – From micron- to nanotopography. Biomaterials. 2008;29(28):3822-35.

207. Ross EA, Turner L-A, Donnelly H, Saeed A, Tsimbouri MP, Burgess KV, et al. Nanotopography reveals metabolites that maintain the immunomodulatory phenotype of mesenchymal stromal cells. Nature Communications. 2023;14(1):753.

208. Sokolowska M, Chen L-Y, Eberlein M, Martinez-Anton A, Liu Y, Alsaaty S, et al. Low Molecular Weight Hyaluronan Activates Cytosolic Phospholipase A2α and Eicosanoid Production in Monocytes and Macrophages*♦. Journal of Biological Chemistry. 2014;289(7):4470-88.

209. Rayahin JE, Buhrman JS, Zhang Y, Koh TJ, Gemeinhart RA. High and low molecular weight hyaluronic acid differentially influence macrophage activation. ACS biomaterials science & engineering. 2015;1(7):481-93.

210. Hotaling NA, Tang L, Irvine DJ, Babensee JE. Biomaterial Strategies for Immunomodulation. Annual review of biomedical engineering. 2015;17:317-49.

211. Moyano DF, Goldsmith M, Solfiell DJ, Landesman-Milo D, Miranda OR, Peer D, et al. Nanoparticle hydrophobicity dictates immune response. Journal of the American Chemical Society. 2012;134(9):3965-7.

212. Seong S-Y, Matzinger P. Hydrophobicity: an ancient damage-associated molecular pattern that initiates innate immune responses. Nature Reviews Immunology. 2004;4(6):469-78.

213. Tiller JC, Bonner G, Pan LC, Klibanov AM. Improving biomaterial properties of collagen films by chemical modification. Biotechnology and bioengineering. 2001;73(3):246-52.

214. Peppas NA, Hilt JZ, Khademhosseini A, Langer R. Hydrogels in biology and medicine: from molecular principles to bionanotechnology. Advanced materials. 2006;18(11):1345-60.

215. Drury JL, Mooney DJ. Hydrogels for tissue engineering: scaffold design variables and applications. Biomaterials. 2003;24(24):4337-51.

216. Chun YW, Wang W, Choi J, Nam T-H, Lee Y-H, Cho K-K, et al. Control of macrophage responses on hydrophobic and hydrophilic carbon nanostructures. Carbon. 2011;49(6):2092-103.

217. Yuan DJ, Shi L, Kam LC. Biphasic response of T cell activation to substrate stiffness. Biomaterials. 2021;273:120797.

218. Lambert LH, Goebrecht GK, De Leo SE, O'Connor RS, Nunez-Cruz S, Li T-D, et al. Improving T cell expansion with a soft touch. Nano letters. 2017;17(2):821-6.

219. Dang AP, De Leo S, Bogdanowicz DR, Yuan DJ, Fernandes SM, Brown JR, et al. Enhanced activation and expansion of T cells using mechanically soft elastomer fibers. Advanced biosystems. 2018;2(2):1700167.

220. Judokusumo E, Tabdanov E, Kumari S, Dustin ML, Kam LC. Mechanosensing in T lymphocyte activation. Biophysical journal. 2012;102(2):L5-L7.

221. Saitakis M, Dogniaux S, Goudot C, Bufi N, Asnacios S, Maurin M, et al. Different TCR-induced T lymphocyte responses are potentiated by stiffness with variable sensitivity. Elife. 2017;6:e23190.

222. Shi L, Lim JY, Kam LC. Substrate stiffness enhances human regulatory T cell induction and metabolism. Biomaterials. 2023;292:121928.

223. Neumann S, Burkert K, Kemp R, Rades T, Rod Dunbar P, Hook S. Activation of the NLRP3 inflammasome is not a feature of all particulate vaccine adjuvants. Immunology and cell biology. 2014;92(6):535-42.

224. Getts DR, Terry RL, Getts MT, Deffrasnes C, Müller M, van Vreden C, et al. Therapeutic inflammatory monocyte modulation using immune-modifying microparticles. Science translational medicine. 2014;6(219):219ra7-ra7.

225. Morris AH, Stamer DK, Kyriakides TR. The host response to naturally-derived extracellular matrix biomaterials. Seminars in immunology. 2017;29:72-91.

226. Navarro M, Michiardi A, Castano O, Planell J. Biomaterials in orthopaedics. Journal of the royal society interface. 2008;5(27):1137-58.

227. Vasconcelos DM, Gonçalves RM, Almeida CR, Pereira IO, Oliveira MI, Neves N, et al. Fibrinogen scaffolds with immunomodulatory properties promote in vivo bone regeneration. Biomaterials. 2016;111:163-78.

228. Garg K, Pullen NA, Oskeritzian CA, Ryan JJ, Bowlin GL. Macrophage functional polarization (M1/M2) in response to varying fiber and pore dimensions of electrospun scaffolds. Biomaterials. 2013;34(18):4439-51.

229. Kuboki Y, Jin Q, Takita H. Geometry of carriers controlling phenotypic expression in BMP-induced osteogenesis and chondrogenesis. JBJS. 2001;83(1_suppl_2):S105-S15.

230. Kim HJ, Kim U-J, Vunjak-Novakovic G, Min B-H, Kaplan DL. Influence of macroporous protein scaffolds on bone tissue engineering from bone marrow stem cells. Biomaterials. 2005;26(21):4442-52.

231. Chen Z, Klein T, Murray RZ, Crawford R, Chang J, Wu C, et al. Osteoimmunomodulation for the development of advanced bone biomaterials. Materials Today. 2016;19(6):304-21.

232. Wright HL, McCarthy HS, Middleton J, Marshall MJ. RANK, RANKL and osteoprotegerin in bone biology and disease. Current Reviews in Musculoskeletal Medicine. 2009;2(1):56-64.

233. Li Y, Toraldo G, Li A, Yang X, Zhang H, Qian W-P, et al. B cells and T cells are critical for the preservation of bone homeostasis and attainment of peak bone mass in vivo. Blood. 2007;109(9):3839-48.

234. J C-L, H C, J.E F. Osteoimmunology — The hidden immune regulation of bone. Autoimmunity Reviews. 2009;8(3):250-5.

235. Hess K, Ushmorov A, Fiedler J, Brenner RE, Wirth T. TNFα promotes osteogenic differentiation of human mesenchymal stem cells by triggering the NF-κB signaling pathway. Bone. 2009;45(2):367-76.

236. Yang X, Ricciardi BF, Hernandez-Soria A, Shi Y, Camacho NP, Bostrom MP. Callus mineralization and maturation are delayed during fracture healing in interleukin-6 knockout mice. Bone. 2007;41(6):928-36.

237. Guihard P, Boutet M-A, Brounais-Le Royer B, Gamblin A-L, Amiaud J, Renaud A, et al. Oncostatin m, an inflammatory cytokine produced by macrophages, supports intramembranous bone healing in a mouse model of tibia injury. The American journal of pathology. 2015;185(3):765-75.

238. Feldmann M, Maini RN. Anti-TNF Therapy, from Rationale to Standard of Care: What Lessons Has It Taught Us? The Journal of Immunology. 2010;185(2):791-4.

239. Chang MK, Raggatt L-J, Alexander KA, Kuliwaba JS, Fazzalari NL, Schroder K, et al. Osteal Tissue Macrophages Are Intercalated throughout Human and Mouse Bone Lining Tissues and Regulate Osteoblast Function In Vitro and In Vivo1. The Journal of Immunology. 2008;181(2):1232-44.

240. Toben D, Schroeder I, El Khassawna T, Mehta M, Hoffmann J-E, Frisch J-T, et al. Fracture healing is accelerated in the absence of the adaptive immune system. Journal of Bone and Mineral Research. 2011;26(1):113-24.

241. Reinke S, Geissler S, Taylor WR, Schmidt-Bleek K, Juelke K, Schwachmeyer V, et al. Terminally differentiated $CD8^+$ T cells negatively affect bone regeneration in humans. Sci Transl Med. 2013;5(177):177ra36.

242. Madden LR, Mortisen DJ, Sussman EM, Dupras SK, Fugate JA, Cuy JL, et al. Proangiogenic scaffolds as functional templates for cardiac tissue engineering. Proceedings of the National Academy of Sciences. 2010;107(34):15211-6.

243. Li P, Ou Q, Shi S, Shao C. Immunomodulatory properties of mesenchymal stem cells/dental stem cells and their therapeutic applications. Cellular & Molecular Immunology. 2023;20(6):558-69.

244. Galipeau J, Sensébé L. Mesenchymal Stromal Cells: Clinical Challenges and Therapeutic Opportunities. Cell Stem Cell. 2018;22(6):824-33.

245. Margiana R, Markov A, Zekiy AO, Hamza MU, Al-Dabbagh KA, Al-Zubaidi SH, et al. Clinical application of mesenchymal stem cell in regenerative medicine: a narrative review. Stem Cell Research & Therapy. 2022;13(1):366.

246. Koç ON, Gerson SL, Cooper BW, Dyhouse SM, Haynesworth SE, Caplan AI, et al. Rapid hematopoietic recovery after coinfusion of autologous-blood stem cells and culture-expanded marrow mesenchymal stem cells in advanced breast cancer patients receiving high-dose chemotherapy. Journal of clinical oncology. 2000;18(2):307-.

247. Le Blanc K, Frassoni F, Ball L, Locatelli F, Roelofs H, Lewis I, et al. Mesenchymal stem cells for treatment of steroid-resistant, severe, acute graft-versus-host disease: a phase II study. The Lancet. 2008;371(9624):1579-86.

248. Di Nicola M, Carlo-Stella C, Magni M, Milanesi M, Longoni PD, Matteucci P, et al. Human bone marrow stromal cells suppress T-lymphocyte proliferation induced by cellular or nonspecific mitogenic stimuli. Blood, The Journal of the American Society of Hematology. 2002;99(10):3838-43.

249. Bartholomew A, Sturgeon C, Siatskas M, Ferrer K, McIntosh K, Patil S, et al. Mesenchymal stem cells suppress lymphocyte proliferation in vitro and prolong skin graft survival in vivo. Experimental hematology. 2002;30(1):42-8.

250. Djouad F, Plence P, Bony C, Tropel P, Apparailly F, Sany J, et al. Immunosuppressive effect of mesenchymal stem cells favors tumor growth in allogeneic animals. Blood. 2003;102(10):3837-44.

251. Djouad F, Fritz V, Apparailly F, Louis‐Plence P, Bony C, Sany J, et al. Reversal of the immunosuppressive properties of mesenchymal stem cells by tumor necrosis factor α in collagen‐induced arthritis. Arthritis & Rheumatism. 2005;52(5):1595-603.

252. Ge W, Jiang J, Baroja M, Arp J, Zassoko R, Liu W, et al. Infusion of mesenchymal stem cells and rapamycin synergize to attenuate alloimmune responses and promote cardiac allograft tolerance. American journal of transplantation. 2009;9(8):1760-72.

253. Waterman RS, Tomchuck SL, Henkle SL, Betancourt AM. A new mesenchymal stem cell (MSC) paradigm: polarization into a pro-inflammatory MSC1 or an Immunosuppressive MSC2 phenotype. PloS one. 2010;5(4):e10088.

254. Barberini DJ, Freitas NPP, Magnoni MS, Maia L, Listoni AJ, Heckler MC, et al. Equine mesenchymal stem cells from bone marrow, adipose tissue and umbilical cord: immunophenotypic characterization and differentiation potential. Stem cell research & therapy. 2014;5:1-11.

255. Abbaszadeh H, Ghorbani F, Abbaspour-Aghdam S, Kamrani A, Valizadeh H, Nadiri M, et al. Chronic obstructive pulmonary disease and asthma: mesenchymal stem cells and their extracellular vesicles as potential therapeutic tools. Stem Cell Research & Therapy. 2022;13(1):262.

256. Ankrum JA, Ong JF, Karp JM. Mesenchymal stem cells: immune evasive, not immune privileged. Nature biotechnology. 2014;32(3):252-60.

257. Reinders ME, Dreyer GJ, Bank JR, Roelofs H, Heidt S, Roelen DL, et al. Safety of allogeneic bone marrow derived mesenchymal stromal cell therapy in renal transplant recipients: the neptune study. Journal of translational medicine. 2015;13:1-8.

258. Singh A, Peppas NA. Hydrogels and scaffolds for immunomodulation. Advanced materials. 2014;26(38):6530-41.

259. Keshavarz R, Olsen S, Almeida B. Using biomaterials to improve mesenchymal stem cell therapies for chronic, nonhealing wounds. Bioeng Transl Med. 2024;9(1):e10598.

260. Rosset P, Deschaseaux F, Layrolle P. Cell therapy for bone repair. Orthopaedics & Traumatology: Surgery & Research. 2014;100(1, Supplement):S107-S12.

261. Yousefpour P, Ni K, Irvine DJ. Targeted modulation of immune cells and tissues using engineered biomaterials. Nature Reviews Bioengineering. 2023;1(2):107-24.

262. Meyer RA, Sunshine JC, Perica K, Kosmides AK, Aje K, Schneck JP, et al. Biodegradable nanoellipsoidal artificial antigen presenting cells for antigen specific T-cell activation. Small. 2015;11(13):1519-25.

263. Kakizawa Y, Lee JS, Bell B, Fahmy TM. Precise manipulation of biophysical particle parameters enables control of proinflammatory cytokine production in presence of TLR 3 and 4 ligands. Acta biomaterialia. 2017;57:136-45.

264. Peppas NA, Bures P, Leobandung WS, Ichikawa H. Hydrogels in pharmaceutical formulations. European journal of pharmaceutics and biopharmaceutics. 2000;50(1):27-46.

265. Kim JJ, Park K. Modulated insulin delivery from glucose-sensitive hydrogel dosage forms. Journal of Controlled Release. 2001;77(1-2):39-47.

266. Šťastný M, Plocova D, Etrych T, Ulbrich K, Říhová B. HPMA-hydrogels result in prolonged delivery of anticancer drugs and are a promising tool for the treatment of sensitive and multidrug resistant leukaemia. European Journal of Cancer. 2002;38(4):602-8.

267. Tiller JC. Increasing the local concentration of drugs by hydrogel formation. Angewandte Chemie International Edition. 2003;42(27):3072-5.

268. Kim DH, Martin DC. Sustained release of dexamethasone from hydrophilic matrices using PLGA nanoparticles for neural drug delivery. Biomaterials. 2006;27(15):3031-7.

269. Norton LW, Koschwanez HE, Wisniewski NA, Klitzman B, Reichert WM. Vascular endothelial growth factor and dexamethasone release from nonfouling sensor coatings affect the foreign body response. J Biomed Mater Res A. 2007;81(4):858-69.

270. Zhong Y, Bellamkonda RV. Dexamethasone-coated neural probes elicit attenuated inflammatory response and neuronal loss compared to uncoated neural probes. Brain Res. 2007;1148:15-27.

271. Patil SD, Papadmitrakopoulos F, Burgess DJ. Concurrent delivery of dexamethasone and VEGF for localized inflammation control and angiogenesis. J Control Release. 2007;117(1):68-79.

272. Benkirane-Jessel N, Lavalle P, Meyer F, Audouin F, Frisch B, Schaaf P, et al. Control of Monocyte Morphology on and Response to Model Surfaces for Implants Equipped with Anti-Inflammatory Agent. Advanced Materials. 2004;16(17):1507-11.

273. Schultz P, Vautier D, Richert L, Jessel N, Haikel Y, Schaaf P, et al. Polyelectrolyte multilayers functionalized by a synthetic analogue of an anti-inflammatory peptide, alpha-MSH, for coating a tracheal prosthesis. Biomaterials. 2005;26(15):2621-30.

274. Zhong Y, Bellamkonda RV. Controlled release of anti-inflammatory agent alpha-MSH from neural implants. J Control Release. 2005;106(3):309-18.

275. Nguyen KT, Shaikh N, Shukla KP, Su SH, Eberhart RC, Tang L. Molecular responses of vascular smooth muscle cells and phagocytes to curcumin-eluting bioresorbable stent materials. Biomaterials. 2004;25(23):5333-46.

276. Su SH, Nguyen KT, Satasiya P, Greilich PE, Tang L, Eberhart RC. Curcumin impregnation improves the mechanical properties and reduces the inflammatory response associated with poly(L-lactic acid) fiber. J Biomater Sci Polym Ed. 2005;16(3):353-70.

277. Hahn SK, Jelacic S, Maier RV, Stayton PS, Hoffman AS. Anti-inflammatory drug delivery from hyaluronic acid hydrogels. J Biomater Sci Polym Ed. 2004;15(9):1111-9.

278. Rele SM, Cui W, Wang L, Hou S, Barr-Zarse G, Tatton D, et al. Dendrimer-like PEO glycopolymers exhibit anti-inflammatory properties. J Am Chem Soc. 2005;127(29):10132-3.

279. Tseng PY, Rele SS, Sun XL, Chaikof EL. Membrane-mimetic films containing thrombomodulin and heparin inhibit tissue factor-induced thrombin generation in a flow model. Biomaterials. 2006;27(12):2637-50.

280. Bridges AW, García AJ. Anti-inflammatory polymeric coatings for implantable biomaterials and devices. J Diabetes Sci Technol. 2008;2(6):984-94.

281. Shen M, Martinson L, Wagner MS, Castner DG, Ratner BD, Horbett TA. PEO-like plasma polymerized tetraglyme surface interactions with leukocytes and proteins: in vitro and in vivo studies. J Biomater Sci Polym Ed. 2002;13(4):367-90.

282. Hyung Park J, Bae YH. Hydrogels based on poly(ethylene oxide) and poly(tetramethylene oxide) or poly(dimethyl siloxane). III. In vivo biocompatibility and biostability. J Biomed Mater Res A. 2003;64(2):309-19.

283. Li M, Wei F, Yin X, Xiao L, Yang L, Su J, et al. Synergistic regulation of osteoimmune microenvironment by IL-4 and RGD to accelerate osteogenesis. Materials Science and Engineering: C. 2020;109:110508.

284. Wang Y, Qi H, Miron RJ, Zhang Y. Modulating macrophage polarization on titanium implant surface by poly(dopamine)-assisted immobilization of IL4. Clinical Implant Dentistry and Related Research. 2019;21(5):977-86.

285. Shamskhou EA, Kratochvil MJ, Orcholski ME, Nagy N, Kaber G, Steen E, et al. Hydrogel-based delivery of Il-10 improves treatment of bleomycin-induced lung fibrosis in mice. Biomaterials. 2019;203:52-62.

286. Shen H, Xu B, Yang C, Xue W, You Z, Wu X, et al. A DAMP-scavenging, IL-10-releasing hydrogel promotes neural regeneration and motor function recovery after spinal cord injury. Biomaterials. 2022;280:121279.

287. Hume PS, He J, Haskins K, Anseth KS. Strategies to reduce dendritic cell activation through functional biomaterial design. Biomaterials. 2012;33(14):3615-25.

288. Gu L, Mooney DJ. Biomaterials and emerging anticancer therapeutics: engineering the microenvironment. Nature Reviews Cancer. 2016;16(1):56-66.

289. Zhan Q, Shen B, Fang Y, Deng X, Chen H, Jin J, et al. Drug-eluting scaffold inhibited in vivo pancreatic tumorigenesis by engaging murine CCR4+ CD8+ T cells. Colloids and Surfaces B: Biointerfaces. 2017;158:469-73.

290. Wen Y, Kolonich HR, Kruszewski KM, Giannoukakis N, Gawalt ES, Meng WS. Retaining antibodies in tumors with a self-assembling injectable system. Molecular pharmaceutics. 2013;10(3):1035-44.

291. Zhang C, Liu J, Zhong JF, Zhang X. Engineering CAR-T cells. Biomarker Research. 2017;5(1):22.

292. Maude SL, Frey N, Shaw PA, Aplenc R, Barrett DM, Bunin NJ, et al. Chimeric antigen receptor T cells for sustained remissions in leukemia. New England Journal of Medicine. 2014;371(16):1507-17.

293. Kalos M, Levine BL, Porter DL, Katz S, Grupp SA, Bagg A, et al. T cells with chimeric antigen receptors have potent antitumor effects and can establish memory in patients with advanced leukemia. Science translational medicine. 2011;3(95):95ra73-95ra73.

294. Dunn ZS, Mac J, Wang P. T cell immunotherapy enhanced by designer biomaterials. Biomaterials. 2019;217:119265.

295. Markley JC, Sadelain M. IL-7 and IL-21 are superior to IL-2 and IL-15 in promoting human T cell–mediated rejection of systemic lymphoma in immunodeficient mice. Blood, The Journal of the American Society of Hematology. 2010;115(17):3508-19.

296. Adachi K, Kano Y, Nagai T, Okuyama N, Sakoda Y, Tamada K. IL-7 and CCL19 expression in CAR-T cells improves immune cell infiltration and CAR-T cell survival in the tumor. Nature biotechnology. 2018;36(4):346-51.

297. Hoyos V, Savoldo B, Quintarelli C, Mahendravada A, Zhang M, Vera J, et al. Engineering CD19-specific T lymphocytes with interleukin-15 and a suicide gene to enhance their anti-lymphoma/leukemia effects and safety. Leukemia. 2010;24(6):1160-70.

298. Avanzi MP, Yeku O, Li X, Wijewarnasuriya DP, van Leeuwen DG, Cheung K, et al. Engineered tumor-targeted T cells mediate enhanced anti-tumor efficacy both directly and through activation of the endogenous immune system. Cell reports. 2018;23(7):2130-41.

299. Gómez‐Barrena E, Rosset P, Müller I, Giordano R, Bunu C, Layrolle P, et al. Bone regeneration: stem cell therapies and clinical studies in orthopaedics and traumatology. Journal of cellular and molecular medicine. 2011;15(6):1266-86.

300. Ryan JM, Barry FP, Murphy JM, Mahon BP. Mesenchymal stem cells avoid allogeneic rejection. J Inflamm (Lond). 2005;2:8.

301. Klyushnenkova E, Mosca JD, Zernetkina V, Majumdar MK, Beggs KJ, Simonetti DW, et al. T cell responses to allogeneic human mesenchymal stem cells: immunogenicity, tolerance, and suppression. Journal of biomedical science. 2005;12(1):47-57.

302. Asari S, Itakura S, Ferreri K, Liu C-P, Kuroda Y, Kandeel F, et al. Mesenchymal stem cells suppress B-cell terminal differentiation. Experimental hematology. 2009;37(5):604-15.

303. Schindelin J, Arganda-Carreras I, Frise E, Kaynig V, Longair M, Pietzsch T, et al. Fiji: an open-source platform for biological-image analysis. Nature Methods. 2012;9(7):676-82.

304. Girón J, Kerstner E, Medeiros T, Oliveira L, Machado GM, Malfatti CF, et al. Biomaterials for bone regeneration: an orthopedic and dentistry overview. Braz J Med Biol Res. 2021;54(9):e11055.

305. Ibrahim Y, Jamal S, Akhtar K. The evidence base for 2017 BOAST-4 guidance on open fracture management: Are we due an update? Journal of Clinical Orthopaedics and Trauma. 2021;17:233-8.

306. Kannan S, Gokul Krishna S, Gupta PK, Kolkundkar UK. Advantages of pooling of human bone marrow-derived mesenchymal stromal cells from different donors versus single-donor MSCs. Scientific Reports. 2024;14(1):12654.

307. Afzali B, Lechler RI, Hernandez-Fuentes MP. Allorecognition and the alloresponse: clinical implications. Tissue Antigens. 2007;69(6):545-56.

308. Ankrum JA, Ong JF, Karp JM. Mesenchymal stem cells: immune evasive, not immune privileged. Nat Biotechnol. 2014;32(3):252-60.

309. Theodosaki AM, Tzemi M, Galanis N, Bakopoulou A, Kotsiomiti E, Aggelidou E, et al. Bone Regeneration with Mesenchymal Stem Cells in Scaffolds: Systematic Review of Human Clinical Trials. Stem Cell Reviews and Reports. 2024;20(4):938-66.

310. Morrison DA, Kop AM, Nilasaroya A, Sturm M, Shaw K, Honeybul S. Cranial reconstruction using allogeneic mesenchymal stromal cells: A phase 1 first-in-human trial. Journal of Tissue Engineering and Regenerative Medicine. 2018;12(2):341-8.

311. Frangogiannis NG. Why animal model studies are lost in translation. J Cardiovasc Aging. 2022;2(2).

312. Mak IW, Evaniew N, Ghert M. Lost in translation: animal models and clinical trials in cancer treatment. Am J Transl Res. 2014;6(2):114-8.

313. Cook N, Jodrell DI, Tuveson DA. Predictive in vivo animal models and translation to clinical trials. Drug Discovery Today. 2012;17(5):253-60.

314. Ritskes-Hoitinga M, Leenaars C, Beumer W, Coenen-de Roo T, Stafleu F, Meijboom FLB. Improving Translation by Identifying Evidence for More Human-Relevant Preclinical Strategies. Animals. 2020;10(7):1170.

315. Zushin PH, Mukherjee S, Wu JC. FDA Modernization Act 2.0: transitioning beyond animal models with human cells, organoids, and AI/ML-based approaches. J Clin Invest. 2023;133(21).

316. Piatnitskaia S, Rafikova G, Bilyalov A, Chugunov S, Akhatov I, Pavlov V, et al. Modelling of macrophage responses to biomaterials in vitro: state-of-the-art and the need for the improvement. Frontiers in Immunology. 2024;15.

317. Luque-Martin R, Mander PK, Leenen PJM, Winther MPJ. Classic and new mediators for in vitro modelling of human macrophages. Journal of Leukocyte Biology. 2021;109(3):549-60.

318. Sapudom J, Karaman S, Mohamed WKE, Garcia-Sabaté A, Quartey BC, Teo JCM. 3D in vitro M2 macrophage model to mimic modulation of tissue repair. npj Regenerative Medicine. 2021;6(1):83.

319. Saleh LS, Bryant SJ. In Vitro and In Vivo Models for Assessing the Host Response to Biomaterials. Drug Discov Today Dis Models. 2017;24:13-21.

320. Bogle G, Dunbar PR. T cell responses in lymph nodes. WIREs Systems Biology and Medicine. 2010;2(1):107-16.

321. Obst R. The Timing of T Cell Priming and Cycling. Front Immunol. 2015;6:563.

322. Alba-Perez A, Jayawarna V, Childs PG, Dalby MJ, Salmeron-Sanchez M. Plasma polymerised nanoscale coatings of controlled thickness for efficient solid-phase presentation of growth factors. Materials Science and Engineering C. 2020;113(April):110966-.

323. Weiss ARR, Dahlke MH. Immunomodulation by Mesenchymal Stem Cells (MSCs): Mechanisms of Action of Living, Apoptotic, and Dead MSCs. Frontiers in Immunology. 2019;10.

324. Liu H, Rhodes M, Wiest DL, Vignali DAA. On the Dynamics of TCR:CD3 Complex Cell Surface Expression and Downmodulation. Immunity. 2000;13(5):665-75.

325. Kleiveland CR. Peripheral blood mononuclear cells. The Impact of Food Bioactives on Health: in vitro and ex vivo models. 2015:161-7.

326. Bispo DSC, Jesus CSH, Correia M, Ferreira F, Bonifazio G, Goodfellow BJ, et al. NMR Metabolomics Assessment of Osteogenic Differentiation of Adipose-Tissue-Derived Mesenchymal Stem Cells. J Proteome Res. 2022;21(3):654-70.

327. Mollentze J, Durandt C, Pepper MS. An In Vitro and In Vivo Comparison of Osteogenic Differentiation of Human Mesenchymal Stromal/Stem Cells. Stem Cells Int. 2021;2021:9919361.

328. Zoch ML, Clemens TL, Riddle RC. New insights into the biology of osteocalcin. Bone. 2016;82:42-9.

329. Mazzali M, Kipari T, Ophascharoensuk V, Wesson JA, Johnson R, Hughes J. Osteopontin—a molecule for all seasons. QJM: An International Journal of Medicine. 2002;95(1):3-13.

330. Sodek J, Ganss B, McKee MD. Osteopontin. Crit Rev Oral Biol Med. 2000;11(3):279-303.

331. Llopis-Hernández V, Cantini M, González-García C, Cheng ZA, Yang J, Tsimbouri PM, et al. Material-driven fibronectin assembly for high-efficiency presentation of growth factors. Science Advances.2(8):e1600188.

332. Chen Q, Shou P, Zhang L, Xu C, Zheng C, Han Y, et al. An osteopontin-integrin interaction plays a critical role in directing adipogenesis and osteogenesis by mesenchymal stem cells. Stem Cells. 2014;32(2):327-37.

333. Upmanyu V, Sapra L, Srivastava RK. Chapter 5 - Employment of selective pharmacologically active natural compounds in treatment and management of osteoporosis. In: Atta ur R, editor. Studies in Natural Products Chemistry. 75: Elsevier; 2022. p. 161-241.

334. Rucci N. Molecular biology of bone remodelling. Clinical cases in mineral and bone metabolism. 2008;5(1):49.

335. Greenbaum A, Hsu Y-MS, Day RB, Schuettpelz LG, Christopher MJ, Borgerding JN, et al. CXCL12 in early mesenchymal progenitors is required for haematopoietic stem-cell maintenance. Nature. 2013;495(7440):227-30.

336. Huang W, Yang S, Shao J, Li Y-P. Signaling and transcriptional regulation in osteoblast commitment and differentiation. Frontiers in bioscience: a journal and virtual library. 2007;12:3068.

337. Pino AM, Rosen CJ, Rodríguez JP. In osteoporosis, differentiation of mesenchymal stem cells (MSCs) improves bone marrow adipogenesis. Biological research. 2012;45(3):279-87.

338. Zhu S, Chen W, Masson A, Li Y-P. Cell signaling and transcriptional regulation of osteoblast lineage commitment, differentiation, bone formation, and homeostasis. Cell Discovery. 2024;10(1):71.

339. Anh DJ, Dimai HP, Hall SL, Farley JR. Skeletal alkaline phosphatase activity is primarily released from human osteoblasts in an insoluble form, and the net release is inhibited by calcium and skeletal growth factors. Calcif Tissue Int. 1998;62(4):332-40.

340. Simon T, Bromberg JS. Regulation of the Immune System by Laminins. Trends Immunol. 2017;38(11):858-71.

341. Uehara N, Kukita A, Kyumoto-Nakamura Y, Yamaza T, Yasuda H, Kukita T. Osteoblast-derived Laminin-332 is a novel negative regulator of osteoclastogenesis in bone microenvironments. Laboratory Investigation. 2017;97(10):1235-44.

342. Dobre O, Oliva MAG, Ciccone G, Trujillo S, Rodrigo-Navarro A, Venters DC, et al. Hydrogel Platforms: A Hydrogel Platform that Incorporates Laminin Isoforms for Efficient Presentation of Growth Factors – Neural Growth and Osteogenesis (Adv. Funct. Mater. 21/2021). Advanced Functional Materials. 2021;31(21):2170150.

343. McCauley J, Bitsaktsis C, Cottrell J. Macrophage subtype and cytokine expression characterization during the acute inflammatory phase of mouse bone fracture repair. Journal of Orthopaedic Research. 2020;38(8):1693-702.

344. Chow SK-H, Wong CH-W, Cui C, Li MM-C, Wong RMY, Cheung W-H. Modulating macrophage polarization for the enhancement of fracture healing, a systematic review. Journal of Orthopaedic Translation. 2022;36:83-90.

345. Schell H, Duda GN, Peters A, Tsitsilonis S, Johnson KA, Schmidt-Bleek K. The haematoma and its role in bone healing. Journal of Experimental Orthopaedics. 2017;4(1):5.

346. Kolar P, Schmidt-Bleek K, Schell H, Gaber T, Toben D, Schmidmaier G, et al. The early fracture hematoma and its potential role in fracture healing. Tissue Engineering Part B: Reviews. 2010;16(4):427-34.

347. Mizuno K, Mineo K, Tachibana T, Sumi M, Matsubara T, Hirohata K. The osteogenetic potential of fracture haematoma. Subperiosteal and intramuscular transplantation of the haematoma. The Journal of Bone & Joint Surgery British Volume. 1990;72(5):822-9.

348. Lienau J, Schmidt-Bleek K, Peters A, Weber H, Bail HJ, Duda GN, et al. Insight into the molecular pathophysiology of delayed bone healing in a sheep model. Tissue Engineering Part A. 2010;16(1):191-9.

349. Brighton CT. The biology of fracture repair. Instructional course lectures. 1984;33:60-82.

350. Gaber T, Dziurla R, Tripmacher R, Burmester GR, Buttgereit F. Hypoxia inducible factor (HIF) in rheumatology: low O2! See what HIF can do! Annals of the rheumatic diseases. 2005;64(7):971-80.

351. Gaber T, Häupl T, Sandig G, Tykwinska K, Fangradt M, Tschirschmann M, et al. Adaptation of human CD4+ T cells to pathophysiological hypoxia: a transcriptome analysis. The Journal of rheumatology. 2009;36(12):2655-69.

352. Hoff P, Maschmeyer P, Gaber T, Schütze T, Raue T, Schmidt-Bleek K, et al. Human immune cells' behavior and survival under bioenergetically restricted conditions in an in vitro fracture hematoma model. Cellular & molecular immunology. 2013;10(2):151-8.

353. Shinohara ML, Jansson M, Hwang ES, Werneck MB, Glimcher LH, Cantor H. T-bet-dependent expression of osteopontin contributes to T cell polarization. Proceedings of the National Academy of Sciences. 2005;102(47):17101-6.

354. Sansom DM, Manzotti CN, Zheng Y. What's the difference between CD80 and CD86? Trends in Immunology. 2003;24(6):313-8.

355. Reyes-Botella C, Montes MJ, Vallecillo-Capilla MF, Olivares EG, Ruiz Rodriguez C. Expression of molecules involved in antigen presentation and T cell activation (HLA-DR, CD80, CD86, CD44 and CD54) by cultured human osteoblasts. Journal of Periodontology. 2000;71(4):614-7.

356. Reyes-Botella C, Montes M, Vallecillo-Capilla M, Olivares E, Ruiz C. Antigenic phenotype of cultured human osteoblast-like cells. Cellular Physiology and Biochemistry. 2002;12(5-6):359-64.

357. Krzywinski M, Altman N. Nonparametric tests. Nature Methods. 2014;11(5):467-8.

358. Berger A. Th1 and Th2 responses: what are they? Bmj. 2000;321(7258):424.

359. Xu H, Yusuf N, Elmets CA. 23 - Immunology of the Skin. In: Rich RR, Fleisher TA, Schroeder HW, Weyand CM, Corry DB, Puck JM, editors. Clinical Immunology (Sixth Edition). New Delhi: Elsevier; 2023. p. 295-305.

360. Tesmer LA, Lundy SK, Sarkar S, Fox DA. Th17 cells in human disease. Immunol Rev. 2008;223:87-113.

361. Heidt S, Segundo DS, Chadha R, Wood KJ. The impact of Th17 cells on transplant rejection and the induction of tolerance. Curr Opin Organ Transplant. 2010;15(4):456-61.

362. Chandran S, Tang Q. Impact of interleukin-6 on T cells in kidney transplant recipients. American Journal of Transplantation. 2022;22:18-27.

363. Sun J, Tang DN, Fu T, Sharma P. Identification of human regulatory T cells in the setting of T-cell activation and anti-CTLA-4 immunotherapy on the basis of expression of latency-associated peptide. Cancer Discov. 2012;2(2):122-30.

364. Klune JR, Dhupar R, Cardinal J, Billiar TR, Tsung A. HMGB1: endogenous danger signaling. Mol Med. 2008;14(7-8):476-84.

365. Li J, Tan J, Martino MM, Lui KO. Regulatory T-Cells: Potential Regulator of Tissue Repair and Regeneration. Frontiers in Immunology. 2018;9.

366. Negi N, Griffin MD. Effects of mesenchymal stromal cells on regulatory T cells: Current understanding and clinical relevance. Stem Cells. 2020;38(5):596-605.

367. Kmieciak M, Gowda M, Graham L, Godder K, Bear HD, Marincola FM, et al. Human T cells express CD25 and Foxp3 upon activation and exhibit effector/memory phenotypes without any regulatory/suppressor function. J Transl Med. 2009;7:89.

368. Allan SE, Crome SQ, Crellin NK, Passerini L, Steiner TS, Bacchetta R, et al. Activation-induced FOXP3 in human T effector cells does not suppress proliferation or cytokine production. International Immunology. 2007;19(4):345-54.

369. Wang J, Ioan-Facsinay A, van der Voort EIH, Huizinga TWJ, Toes REM. Transient expression of FOXP3 in human activated nonregulatory CD4+ T cells. European Journal of Immunology. 2007;37(1):129-38.

370. Wegrzyn AS, Kedzierska AE, Obojski A. Identification and classification of distinct surface markers of T regulatory cells. Frontiers in Immunology. 2023;13.

371. Li DY, Xiong XZ. ICOS(+) Tregs: A Functional Subset of Tregs in Immune Diseases. Front Immunol. 2020;11:2104.

372. Strauss L, Bergmann C, Szczepanski MJ, Lang S, Kirkwood JM, Whiteside TL. Expression of ICOS on human melanoma-infiltrating CD4+ CD25highFoxp3+ T regulatory cells: implications and impact on tumor-mediated immune suppression. The Journal of Immunology. 2008;180(5):2967-80.

373. Kornete M, Sgouroudis E, Piccirillo CA. ICOS-dependent homeostasis and function of Foxp3+ regulatory T cells in islets of nonobese diabetic mice. The Journal of Immunology. 2012;188(3):1064-74.

374. Francisco LM, Sage PT, Sharpe AH. The PD‐1 pathway in tolerance and autoimmunity. Immunological reviews. 2010;236(1):219-42.

375. Poloni C, Schonhofer C, Ivison S, Levings MK, Steiner TS, Cook L. T-cell activation–induced marker assays in health and disease. Immunology & Cell Biology. 2023;101(6):491-503.

376. Schrum LW, Bost KL, Hudson MC, Marriott I. Bacterial infection induces expression of functional MHC class II molecules in murine and human osteoblasts. Bone. 2003;33(5):812-21.

377. Benichou G, Thomson AW. Direct versus indirect allorecognition pathways: on the right track. Am J Transplant. 2009;9(4):655-6.

378. Skjødt H, Hughes DE, Dobson PR, Russell RG. Constitutive and inducible expression of HLA class II determinants by human osteoblast-like cells in vitro. J Clin Invest. 1990;85(5):1421-6.

379. Upadhyay V, Fu Y-X. Lymphotoxin signalling in immune homeostasis and the control of microorganisms. Nature Reviews Immunology. 2013;13(4):270-9.

380. Laddha NC, Dwivedi M, Gani AR, Mansuri MS, Begum R. Tumor necrosis factor B (TNFB) genetic variants and its increased expression are associated with vitiligo susceptibility. PLoS One. 2013;8(11):e81736.

381. Bertolini DR, Nedwin GE, Bringman TS, Smith DD, Mundy GR. Stimulation of bone resorption and inhibition of bone formation in vitro by human tumour necrosis factors. Nature. 1986;319(6053):516-8.

382. Cranford TL, Enos RT, Velázquez KT, McClellan JL, Davis JM, Singh UP, et al. Role of MCP-1 on inflammatory processes and metabolic dysfunction following high-fat feedings in the FVB/N strain. International Journal of Obesity. 2016;40(5):844-51.

383. Landy E, Carol H, Ring A, Canna S. Biological and clinical roles of IL-18 in inflammatory diseases. Nature Reviews Rheumatology. 2024;20(1):33-47.

384. Udagawa N, Horwood NJ, Elliott J, Mackay A, Owens J, Okamura H, et al. Interleukin-18 (interferon-gamma-inducing factor) is produced by osteoblasts and acts via granulocyte/macrophage colony-stimulating factor and not via interferon-gamma to inhibit osteoclast formation. J Exp Med. 1997;185(6):1005-12.

385. Yoshida H, Hamano S, Senaldi G, Covey T, Faggioni R, Mu S, et al. WSX-1 is required for the initiation of Th1 responses and resistance to L. major infection. Immunity. 2001;15(4):569-78.

386. Chen Q, Ghilardi N, Wang H, Baker T, Xie M-H, Gurney A, et al. Development of Th1-type immune responses requires the type I cytokine receptor TCCR. Nature. 2000;407(6806):916-20.

387. Owaki T, Asakawa M, Morishima N, Hata K, Fukai F, Matsui M, et al. A role for IL-27 in early regulation of Th1 differentiation. The Journal of Immunology. 2005;175(4):2191-200.

388. Artis D, Villarino A, Silverman M, He W, Thornton EM, Mu S, et al. The IL-27 receptor (WSX-1) is an inhibitor of innate and adaptive elements of type 2 immunity. The Journal of Immunology. 2004;173(9):5626-34.

389. Stumhofer JS, Laurence A, Wilson EH, Huang E, Tato CM, Johnson LM, et al. Interleukin 27 negatively regulates the development of interleukin 17–producing T helper cells during chronic inflammation of the central nervous system. Nature immunology. 2006;7(9):937-45.

390. Colgan J, Rothman P. All in the family: IL-27 suppression of TH-17 cells. Nature immunology. 2006;7(9):899-901.

391. Li X, Luo W, Hu J, Chen Y, Yu T, Yang J, et al. Interleukin-27 prevents LPS-induced inflammatory osteolysis by inhibiting osteoclast formation and function. Am J Transl Res. 2019;11(3):1154-69.

392. Nomiyama H, Osada N, Yoshie O. The evolution of mammalian chemokine genes. Cytokine & Growth Factor Reviews. 2010;21(4):253-62.

393. Hidalgo LG, Halloran PF. Role of IFN-gamma in allograft rejection. Crit Rev Immunol. 2002;22(4):317-49.

394. Gadani SP, Cronk JC, Norris GT, Kipnis J. IL-4 in the brain: a cytokine to remember. J Immunol. 2012;189(9):4213-9.

395. Yang W-C, Hwang Y-S, Chen Y-Y, Liu C-L, Shen C-N, Hong W-H, et al. Interleukin-4 Supports the Suppressive Immune Responses Elicited by Regulatory T Cells. Frontiers in Immunology. 2017;8.

396. Heeb LEM, Egholm C, Boyman O. Evolution and function of interleukin-4 receptor signaling in adaptive immunity and neutrophils. Genes & Immunity. 2020;21(3):143-9.

397. Noelle RJ, Nowak EC. Cellular sources and immune functions of interleukin-9. Nature Reviews Immunology. 2010;10(10):683-7.

398. Wong MT, Ye JJ, Alonso MN, Landrigan A, Cheung RK, Engleman E, et al. Regulation of human Th9 differentiation by type I interferons and IL‐21. Immunology and cell biology. 2010;88(6):624-31.

399. Beriou G, Bradshaw EM, Lozano E, Costantino CM, Hastings WD, Orban T, et al. TGF-β Induces IL-9 Production from human Th17 Cells. The Journal of Immunology. 2010;185(1):46-54.

400. Putheti P, Awasthi A, Popoola J, Gao W, Strom TB. Human CD4+ memory T cells can become CD4+ IL-9+ T cells. PloS one. 2010;5(1):e8706.

401. Ebina-Shibuya R, Leonard WJ. Role of thymic stromal lymphopoietin in allergy and beyond. Nature Reviews Immunology. 2023;23(1):24-37.

402. Jinquan T, Quan S, Feili G, Larsen CG, Thestrup-Pedersen K. Eotaxin Activates T Cells to Chemotaxis and Adhesion Only if Induced to Express CCR3 by IL-2 Together with IL-41. The Journal of Immunology. 1999;162(7):4285-92.

403. Lupancu TJ, Eivazitork M, Hamilton JA, Achuthan AA, Lee KMC. CCL17/TARC in autoimmunity and inflammation—not just a T-cell chemokine. Immunology & Cell Biology. 2023;101(7):600-9.

404. Yoshie O, Matsushima K. CCR4 and its ligands: from bench to bedside. International immunology. 2015;27(1):11-20.

405. Lee KM-C, Jarnicki A, Achuthan A, Fleetwood AJ, Anderson GP, Ellson C, et al. CCL17 in Inflammation and Pain. The Journal of Immunology. 2020;205(1):213-22.

406. Palada V, Siddiqah Ahmed A, Hugo A, Radojčić MR, Svensson CI, Kosek E. Expression of mitochondrial TSPO and FAM173B is associated with inflammation and symptoms in patients with painful knee osteoarthritis. Rheumatology. 2021;60(4):1724-33.

407. Hall BM, Hall RM, Tran GT, Robinson CM, Wilcox PL, Rakesh PK, et al. Interleukin-5 (IL-5) Therapy Prevents Allograft Rejection by Promoting CD4(+)CD25(+) Ts2 Regulatory Cells That Are Antigen-Specific and Express IL-5 Receptor. Front Immunol. 2021;12:714838.

408. Cayrol C, Girard J-P. Interleukin-33 (IL-33): A critical review of its biology and the mechanisms involved in its release as a potent extracellular cytokine. Cytokine. 2022;156:155891.

409. Ohori F, Kitaura H, Ogawa S, Shen WR, Qi J, Noguchi T, et al. IL-33 Inhibits TNF-α-Induced Osteoclastogenesis and Bone Resorption. Int J Mol Sci. 2020;21(3).

410. Amescua G, Collings F, Sidani A, Bonfield TL, Rodriguez JP, Galor A, et al. Effect of CXCL-1/KC production in high risk vascularized corneal allografts on T cell recruitment and graft rejection. Transplantation. 2008;85(4):615-25.

411. Teague TK, Schaefer BC, Hildeman D, Bender J, Mitchell T, Kappler JW, et al. Activation-induced inhibition of interleukin 6–mediated T cell survival and signal transducer and activator of transcription 1 signaling. The Journal of experimental medicine. 2000;191(6):915.

412. Ayroldi E, Zollo O, Cannarile L, D'Adamio F, Grohmann U, Delfino DV, et al. Interleukin-6 (IL-6) prevents activation-induced cell death: IL-2–independent inhibition of Fas/fasL expression and cell death. Blood, The Journal of the American Society of Hematology. 1998;92(11):4212-9.

413. Mihara M, Hashizume M, Yoshida H, Suzuki M, Shiina M. IL-6/IL-6 receptor system and its role in physiological and pathological conditions. Clinical science. 2012;122(4):143-59.

414. Kerkis I, Silva ÁPd, Araldi RP. The impact of interleukin-6 (IL-6) and mesenchymal stem cell-derived IL-6 on neurological conditions. Frontiers in Immunology. 2024;15.

415. Dorronsoro A, Lang V, Ferrin I, Fernández-Rueda J, Zabaleta L, Pérez-Ruiz E, et al. Intracellular role of IL-6 in mesenchymal stromal cell immunosuppression and proliferation. Scientific Reports. 2020;10(1):21853.

416. Ishimi Y, Miyaura C, Jin CH, Akatsu T, Abe E, Nakamura Y, et al. IL-6 is produced by osteoblasts and induces bone resorption. J Immunol. 1990;145(10):3297-303.

417. Di Paolo S, Gesualdo L, Stallone G, Ranieri E, Schena FP. Renal expression and urinary concentration of EGF and IL-6 in acutely dysfunctioning kidney transplanted patients. Nephrology, dialysis, transplantation: official publication of the European Dialysis and Transplant Association-European Renal Association. 1997;12(12):2687-93.

418. Sadeghi M, Daniel V, Wiesel M, Hergesell O, Opelz G. High urine sIL-6R as a predictor of late graft failure in renal transplant recipients. Transplantation. 2003;76(8):1190-4.

419. Van Oers M, Van der Heyden AA, Aarden L. Interleukin 6 (IL-6) in serum and urine of renal transplant recipients. Clinical and experimental immunology. 1988;71(2):314.

420. VANDENBRoECKE C, CAILLAT-ZUCMAN S, LEGENDRE C, NOEL L-H, KREIS H, WooDRow D, et al. Differential in situ expression of cytokines in renal allograft rejection. Transplantation. 1991;51(3):602-9.

421. YOSHIMURA N, OKA T, KAHAN BD. Sequential determinations of serum interleukin 6 levels as an immunodiagnostic tool to differentiate rejection from nephrotoxicity in renal allograft recipients. Transplantation. 1991;51(1):172-5.

422. Wang X, Dai Y, Zhang X, Pan K, Deng Y, Wang J, et al. CXCL6 regulates cell permeability, proliferation, and apoptosis after ischemia-reperfusion injury by modulating Sirt3 expression via AKT/FOXO3a activation. Cancer Biol Ther. 2021;22(1):30-9.

423. Jiang S, Liang J, Li W, Wang L, Song M, Xu S, et al. The role of CXCL1/CXCR2 axis in neurological diseases. International Immunopharmacology. 2023;120:110330.

424. Arshad T, Mansur F, Palek R, Manzoor S, Liska V. A Double Edged Sword Role of Interleukin-22 in Wound Healing and Tissue Regeneration. Frontiers in Immunology. 2020;11.

425. Basu R, O'Quinn DB, Silberger DJ, Schoeb TR, Fouser L, Ouyang W, et al. Th22 cells are an important source of IL-22 for host protection against enteropathogenic bacteria. Immunity. 2012;37(6):1061-75.

426. Liang SC, Tan X-Y, Luxenberg DP, Karim R, Dunussi-Joannopoulos K, Collins M, et al. Interleukin (IL)-22 and IL-17 are coexpressed by Th17 cells and cooperatively enhance expression of antimicrobial peptides. The Journal of experimental medicine. 2006;203(10):2271.

427. Chung Y, Yang X, Chang SH, Ma L, Tian Q, Dong C. Expression and regulation of IL-22 in the IL-17-producing CD4+ T lymphocytes. Cell research. 2006;16(11):902-7.

428. Wolk K, Kunz S, Asadullah K, Sabat R. Cutting edge: immune cells as sources and targets of the IL-10 family members? The Journal of Immunology. 2002;168(11):5397-402.

429. Abikhair M, Mitsui H, Yanofsky V, Roudiani N, Ovits C, Bryan T, et al. Cyclosporine A immunosuppression drives catastrophic squamous cell carcinoma through IL-22. JCI insight. 2016;1(8).

430. Cheng D, Wang J, Wang Y, Xue Y, Yang Q, Yang Q, et al. Chemokines: Function and therapeutic potential in bone metastasis of lung cancer. Cytokine. 2023;172:156403.

431. Melendreras SG, Martínez-Camblor P, Menéndez A, Bravo-Mendoza C, González-Vidal A, Coto E, et al. Soluble co-signaling molecules predict long-term graft outcome in kidney-transplanted patients. PLoS One. 2014;9(12):e113396.

432. Akdis CA, Blaser K. Mechanisms of interleukin-10-mediated immune suppression. Immunology. 2001;103(2):131-6.

433. Khan MA, Ashoor GA, Shamma T, Alanazi F, Altuhami A, Kazmi S, et al. IL-10 Mediated Immunomodulation Limits Subepithelial Fibrosis and Repairs Airway Epithelium in Rejecting Airway Allografts. Cells. 2021;10(5).

434. Bromberg JS. IL-10 immunosuppression in transplantation. Current Opinion in Immunology. 1995;7(5):639-43.

435. Carlini V, Noonan DM, Abdalalem E, Goletti D, Sansone C, Calabrone L, et al. The multifaceted nature of IL-10: regulation, role in immunological homeostasis and its relevance to cancer, COVID-19 and post-COVID conditions. Frontiers in Immunology. 2023;14.

436. Rivero M, Crespo J, Mayorga M, Fábrega E, Casafont F, Pons-Romero F. Involvement of the Fas system in liver allograft rejection. The American Journal of Gastroenterology. 2002;97(6):1501-6.

437. Liem LM, van Lopik T, van Nieuwenhuijze AEM, van Houwelingen HC, Aarden L, Goulmy E. Soluble Fas Levels in Sera of Bone Marrow Transplantation Recipients Are Increased During Acute Graft-Versus-Host Disease But Not During Infections. Blood. 1998;91(4):1464-8.

438. Pérez EC, Shulzhenko N, Morgun A, Diniz RVZ, Almeida DR, Musatti CC, et al. Expression of Fas, FasL, and Soluble Fas mRNA in Endomyocardial Biopsies of Human Cardiac Allografts. Human Immunology. 2006;67(1):22-6.

439. Schlom J, Jochems C, Gulley JL, Huang J. The role of soluble CD40L in immunosuppression. Oncoimmunology. 2013;2(1):e22546.

440. Huang J, Jochems C, Talaie T, Anderson A, Jales A, Tsang KY, et al. Elevated serum soluble CD40 ligand in cancer patients may play an immunosuppressive role. Blood, The Journal of the American Society of Hematology. 2012;120(15):3030-8.

441. Voskoboinik I, Whisstock JC, Trapani JA. Perforin and granzymes: function, dysfunction and human pathology. Nature Reviews Immunology. 2015;15(6):388-400.

442. Macedo C, Orkis EA, Popescu I, Elinoff BD, Zeevi A, Shapiro R, et al. Contribution of naïve and memory T-cell populations to the human alloimmune response. Am J Transplant. 2009;9(9):2057-66.

443. Cullen SP, Brunet M, Martin SJ. Granzymes in cancer and immunity. Cell Death & Differentiation. 2010;17(4):616-23.

444. Cullen S, Martin S. Mechanisms of granule-dependent killing. Cell Death & Differentiation. 2008;15(2):251-62.

445. Adrain C, Murphy BM, Martin SJ. Molecular ordering of the caspase activation cascade initiated by the cytotoxic T lymphocyte/natural killer (CTL/NK) protease granzyme B. Journal of Biological Chemistry. 2005;280(6):4663-73.

446. Goldbach-Mansky R, Suson S, Wesley R, Hack C, El-Gabalawy H, Tak P. Raised granzyme B levels are associated with erosions in patients with early rheumatoid factor positive rheumatoid arthritis. Annals of the rheumatic diseases. 2005;64(5):715-21.

447. Buzza MS, Zamurs L, Sun J, Bird CH, Smith AI, Trapani JA, et al. Extracellular matrix remodeling by human granzyme B via cleavage of vitronectin, fibronectin, and laminin. Journal of Biological Chemistry. 2005;280(25):23549-58.

448. Froelich CJ, Zhang X, Turbov J, Hudig D, Winkler U, Hanna WL. Human granzyme B degrades aggrecan proteoglycan in matrix synthesized by chondrocytes. Journal of immunology (Baltimore, Md: 1950). 1993;151(12):7161-71.

449. McCann SM, Milenkovic L, Gonzalez MC, Lyson K, Karanth S, Rettori V. [11] - Endocrine Aspects of Neuroimmunomodulation: Methods and Overview. In: De Souza EB, editor. Methods in Neurosciences. 16: Academic Press; 1993. p. 187-210.

450. Willerford DM, Chen J, Ferry JA, Davidson L, Ma A, Alt FW. Interleukin-2 receptor alpha chain regulates the size and content of the peripheral lymphoid compartment. Immunity. 1995;3(4):521-30.

451. Schorle H, Holtschke T, Hünig T, Schimpl A, Horak I. Development and function of T cells in mice rendered interleukin-2 deficient by gene targeting. Nature. 1991;352(6336):621-4.

452. Sadlack B, Merz H, Schorle H, Schimpl A, Feller AC, Horak I. Ulcerative colitis-like disease in mice with a disrupted interleukin-2 gene. Cell. 1993;75(2):253-61.

453. Nelson BH. IL-2, Regulatory T Cells, and Tolerance. The Journal of Immunology. 2004;172(7):3983-8.

454. Sharfe N, Dadi HK, Shahar M, Roifman CM. Human immune disorder arising from mutation of the alpha chain of the interleukin-2 receptor. Proc Natl Acad Sci U S A. 1997;94(7):3168-71.

455. Harwood JL, Alexander JH, Mayerson JL, Scharschmidt TJ. Targeted Chemotherapy in Bone and Soft-Tissue Sarcoma. Orthopedic Clinics of North America. 2015;46(4):587-608.

456. Gilfillan M, Bhandari V. Chapter 13 - Genetic Basis of Bronchopulmonary Dysplasia. In: Ohls RK, Maheshwari A, Christensen RD, editors. Hematology, Immunology and Genetics (Third Edition). Philadelphia: Elsevier; 2019. p. 149-64.

457. Mayer H, Bertram H, Lindenmaier W, Korff T, Weber H, Weich H. Vascular endothelial growth factor (VEGF-A) expression in human mesenchymal stem cells: Autocrine and paracrine role on osteoblastic and endothelial differentiation. Journal of Cellular Biochemistry. 2005;95(4):827-39.

458. Fili S, Karalaki M, Schaller B. Mechanism of bone metastasis: The role of osteoprotegerin and of the host-tissue microenvironment-related survival factors. Cancer Letters. 2009;283(1):10-9.

459. Roodman GD. Mechanisms of bone metastasis. New England journal of medicine. 2004;350(16):1655-64.

460. Schoppet M, Preissner KT, Hofbauer LC. RANK ligand and osteoprotegerin: paracrine regulators of bone metabolism and vascular function. Arteriosclerosis, thrombosis, and vascular biology. 2002;22(4):549-53.

461. Park H, Jo S, Jang MA, Choi SH, Kim TH. Dikkopf-1 promotes matrix mineralization of osteoblasts by regulating Ca(+)-CAMK2A- CREB1 pathway. BMB Rep. 2022;55(12):627-32.

462. Yang CM, Ji S, Li Y, Fu LY, Jiang T, Meng FD. β-Catenin promotes cell proliferation, migration, and invasion but induces apoptosis in renal cell carcinoma. Onco Targets Ther. 2017;10:711-24.

463. Terpos E, Gavriatopoulou M. Multiple Myeloma Bone Disease. In: Huhtaniemi I, Martini L, editors. Encyclopedia of Endocrine Diseases (Second Edition). Oxford: Academic Press; 2019. p. 329-40.

464. Zhu Y, Sun Z, Han Q, Liao L, Wang J, Bian C, et al. Human mesenchymal stem cells inhibit cancer cell proliferation by secreting DKK-1. Leukemia. 2009;23(5):925-33.

465. Sheng M, Thompson MA, Greenberg ME. CREB: a Ca²⁺-Regulated Transcription Factor Phosphorylated by Calmodulin-Dependent Kinases. Science. 1991;252(5011):1427-30.

466. Jo S, Yoon S, Lee SY, Kim SY, Park H, Han J, et al. DKK1 Induced by 1,25D3 Is Required for the Mineralization of Osteoblasts. Cells. 2020;9(1).

467. Lin L, Qiu Q, Zhou N, Dong W, Shen J, Jiang W, et al. Dickkopf-1 is involved in BMP9-induced osteoblast differentiation of C3H10T1/2 mesenchymal stem cells. BMB Rep. 2016;49(3):179-84.

468. Bezooijen RLv, Dijke Pt, Papapoulos SE, G.M. Löwik CW. SOST/sclerostin, an osteocyte-derived negative regulator of bone formation. Cytokine & Growth Factor Reviews. 2005;16(3):319-27.

469. Fairfield H, Falank C, Harris E, Demambro V, McDonald M, Pettitt JA, et al. The skeletal cell-derived molecule sclerostin drives bone marrow adipogenesis. Journal of Cellular Physiology. 2018;233(2):1156-67.

470. Shurin MR. Osteopontin controls immunosuppression in the tumor microenvironment. J Clin Invest. 2018;128(12):5209-12.

471. Ashkar S, Weber GF, Panoutsakopoulou V, Sanchirico ME, Jansson M, Zawaideh S, et al. Eta-1 (osteopontin): an early component of type-1 (cell-mediated) immunity. Science. 2000;287(5454):860-4.

472. Hoteit L, Loughran P, Haldeman S, Reiser D, Alsaadi N, Andraska E, et al. MACROPHAGE SWITCHING: POLARIZATION AND MOBILIZATION AFTER TRAUMA. Shock. 2023;59(2):232-8.

473. Vi L, Baht GS, Whetstone H, Ng A, Wei Q, Poon R, et al. Macrophages promote osteoblastic differentiation in vivo: implications in fracture repair and bone homeostasis. Journal of Bone and Mineral Research. 2015;30(6):1090-102.

474. Milward K, Hester J, Wood KJ. Isolation of Human Regulatory T Lymphocytes by Fluorescence-Activated Cell Sorting. Methods Mol Biol. 2019;1899:43-54.

475. Thornton AM, Lu J, Korty PE, Kim YC, Martens C, Sun PD, et al. Helios(+) and Helios(-) Treg subpopulations are phenotypically and functionally distinct and express dissimilar TCR repertoires. Eur J Immunol. 2019;49(3):398-412.

476. Luo Y, Xu C, Wang B, Niu Q, Su X, Bai Y, et al. Single-cell transcriptomic analysis reveals disparate effector differentiation pathways in human T(reg) compartment. Nat Commun. 2021;12(1):3913.

477. Long AE, Tatum M, Mikacenic C, Buckner JH. A novel and rapid method to quantify Treg mediated suppression of CD4 T cells. J Immunol Methods. 2017;449:15-22.

478. Walters G, Pountos I, Giannoudis PV. The cytokines and micro-environment of fracture haematoma: Current evidence. Journal of Tissue Engineering and Regenerative Medicine. 2018;12(3):e1662-e77.

479. Pountos I, Walters G, Panteli M, Einhorn TA, Giannoudis PV. Inflammatory Profile and Osteogenic Potential of Fracture Haematoma in Humans. J Clin Med. 2019;9(1).

480. Kean TJ, Lin P, Caplan AI, Dennis JE. MSCs: Delivery Routes and Engraftment, Cell-Targeting Strategies, and Immune Modulation. Stem Cells Int. 2013;2013:732742.

481. Ezquer FE, Ezquer ME, Vicencio JM, Calligaris SD. Two complementary strategies to improve cell engraftment in mesenchymal stem cell-based therapy: Increasing transplanted cell resistance and increasing tissue receptivity. Cell Adh Migr. 2017;11(1):110-9.

482. Karp JM, Teo GSL. Mesenchymal stem cell homing: the devil is in the details. Cell stem cell. 2009;4(3):206-16.

483. Kostura L, Kraitchman DL, Mackay AM, Pittenger MF, Bulte JW. Feridex labeling of mesenchymal stem cells inhibits chondrogenesis but not adipogenesis or osteogenesis. NMR in Biomedicine: An International Journal Devoted to the Development and Application of Magnetic Resonance In Vivo. 2004;17(7):513-7.

484. Lin P, Lin Y, Lennon DP, Correa D, Schluchter M, Caplan AI. Efficient lentiviral transduction of human mesenchymal stem cells that preserves proliferation and differentiation capabilities. Stem cells translational medicine. 2012;1(12):886-97.

485. Srinivas M, Aarntzen E, Bulte J, Oyen W, Heerschap A, De Vries I, et al. Imaging of cellular therapies. Advanced drug delivery reviews. 2010;62(11):1080-93.

486. Horwitz EM, Gordon PL, Koo WK, Marx JC, Neel MD, McNall RY, et al. Isolated allogeneic bone marrow-derived mesenchymal cells engraft and stimulate growth in children with osteogenesis imperfecta: Implications for cell therapy of bone. Proceedings of the National Academy of Sciences. 2002;99(13):8932-7.

487. Horwitz EM, Prockop DJ, Fitzpatrick LA, Koo WW, Gordon PL, Neel M, et al. Transplantability and therapeutic effects of bone marrow-derived mesenchymal cells in children with osteogenesis imperfecta. Nature medicine. 1999;5(3):309-13.

488. Von Bahr L, Batsis I, Moll G, Hägg M, Szakos A, Sundberg B, et al. Analysis of tissues following mesenchymal stromal cell therapy in humans indicates limited long-term engraftment and no ectopic tissue formation. Stem cells. 2012;30(7):1575-8.

489. Ankrum J, Karp JM. Mesenchymal stem cell therapy: Two steps forward, one step back. Trends in molecular medicine. 2010;16(5):203-9.

490. Krampera M, Cosmi L, Angeli R, Pasini A, Liotta F, Andreini A, et al. Role for interferon-γ in the immunomodulatory activity of human bone marrow mesenchymal stem cells. Stem cells. 2006;24(2):386-98.

491. Ren G, Zhang L, Zhao X, Xu G, Zhang Y, Roberts AI, et al. Mesenchymal stem cell-mediated immunosuppression occurs via concerted action of chemokines and nitric oxide. Cell stem cell. 2008;2(2):141-50.

492. English K, Barry FP, Field-Corbett CP, Mahon BP. IFN-γ and TNF-α differentially regulate immunomodulation by murine mesenchymal stem cells. Immunology letters. 2007;110(2):91-100.

493. Ryan J, Barry F, Murphy J, Mahon BP. Interferon-γ does not break, but promotes the immunosuppressive capacity of adult human mesenchymal stem cells. Clinical & Experimental Immunology. 2007;149(2):353-63.

494. Tse W, Pendleton J, Beyer W, Egalka M, Guinan E. Suppression of allogeneic T-cell proliferation by human marrow stromal cells: Implications in transplantation, Transplantation. 2003.

495. Krampera M, Cosmi L, Angeli R, Pasini A, Liotta F, Andreini A, et al. Role for Interferon-γ in the Immunomodulatory Activity of Human Bone Marrow Mesenchymal Stem Cells. Stem Cells. 2005;24(2):386-98.

496. Sorg H, Tilkorn DJ, Hauser J, Ring A. Improving Vascularization of Biomaterials for Skin and Bone Regeneration by Surface Modification: A Narrative Review on Experimental Research. Bioengineering (Basel). 2022;9(7).

497. Milan PB, Khamseh S, Zarrintaj P, Ramezanzadeh B, Badawi M, Morisset S, et al. Copper-enriched diamond-like carbon coatings promote regeneration at the bone–implant interface. Heliyon. 2020;6(4).

498. Singh S, Wu BM, Dunn JCY. The enhancement of VEGF-mediated angiogenesis by polycaprolactone scaffolds with surface cross-linked heparin. Biomaterials. 2011;32(8):2059-69.

499. Rocha LA, Sousa RA, Learmonth DA, Salgado AJ. The Role of Biomaterials as Angiogenic Modulators of Spinal Cord Injury: Mimetics of the Spinal Cord, Cell and Angiogenic Factor Delivery Agents. Frontiers in Pharmacology. 2018;9.

500. Li B, Wang H, Zhou G, Zhang J, Su X, Huang Z, et al. VEGF-loaded biomimetic scaffolds: a promising approach to improve angiogenesis and osteogenesis in an ischemic environment. RSC Advances. 2017;7(8):4253-9.

501. Moulisová V, Gonzalez-García C, Cantini M, Rodrigo-Navarro A, Weaver J, Costell M, et al. Engineered microenvironments for synergistic VEGF - Integrin signalling during vascularization. Biomaterials. 2017;126:61-74.

502. Bourhis M, Palle J, Galy-Fauroux I, Terme M. Direct and Indirect Modulation of T Cells by VEGF-A Counteracted by Anti-Angiogenic Treatment. Frontiers in Immunology. 2021;12.

503. Hao M, Xue L, Wen X, Sun L, Zhang L, Xing K, et al. Advancing bone regeneration: Unveiling the potential of 3D cell models in the evaluation of bone regenerative materials. Acta Biomaterialia. 2024;183:1-29.

504. Koons GL, Diba M, Mikos AG. Materials design for bone-tissue engineering. Nature Reviews Materials. 2020;5(8):584-603.

505. Duval K, Grover H, Han L-H, Mou Y, Pegoraro AF, Fredberg J, et al. Modeling physiological events in 2D vs. 3D cell culture. Physiology. 2017;32(4):266-77.

506. Kapałczyńska M, Kolenda T, Przybyła W, Zajączkowska M, Teresiak A, Filas V, et al. 2D and 3D cell cultures–a comparison of different types of cancer cell cultures. Archives of medical science. 2018;14(4):910-9.